



HAL
open science

Modeling and imaging of attenuation in biological media.

Abdul Wahab

► **To cite this version:**

Abdul Wahab. Modeling and imaging of attenuation in biological media.. Analysis of PDEs [math.AP]. Ecole Polytechnique X, 2011. English. NNT: . tel-00674109

HAL Id: tel-00674109

<https://theses.hal.science/tel-00674109>

Submitted on 25 Feb 2012

HAL is a multi-disciplinary open access archive for the deposit and dissemination of scientific research documents, whether they are published or not. The documents may come from teaching and research institutions in France or abroad, or from public or private research centers.

L'archive ouverte pluridisciplinaire **HAL**, est destinée au dépôt et à la diffusion de documents scientifiques de niveau recherche, publiés ou non, émanant des établissements d'enseignement et de recherche français ou étrangers, des laboratoires publics ou privés.



Thesis submitted in partial fulfillment of the requirements to obtain the title of

Doctor of École Polytechnique
in
Applied Mathematics

by

ABDUL WAHAB

**MODELING AND IMAGING OF ATTENUATION IN
BIOLOGICAL MEDIA**

prepared at
Centre de Mathématiques Appliquées,
École Polytechnique, France,
under the supervision of

PROF. HABIB AMMARI,

defended publicly on Friday, November 25, 2011 in front of the jury composed of:

<i>President</i>	Eric BONNETIER	University Joseph Fourier, Grenoble.
<i>Advisor</i>	Habib AMMARI	École Normale Supérieure, Paris.
<i>Reviewers</i>	Maïtine BERGOUNIOUX	University of Orléans.
	Otmar SCHERZER	University of Vienna.
<i>Examiners</i>	Elie BRETIN	INSA of Lyon.
	Josselin GARNIER	University Paris Diderot, Paris VII.

Modeling and Imaging of Attenuation in Biological Media*

©ABDUL WAHAB

Centre de Mathématiques Appliquées, École Polytechnique,
91128 Palaiseau, France.

wahab@cmap.polytechnique.fr

*This thesis is financially supported by *Higher Education Commission of Pakistan* under the fellowship program *N&BS-France*.

To My Parents

$\mathcal{T}_o \nu_i \{ \alpha, \zeta, \mu(\alpha) \}, \kappa [\nu_\psi, \mu_\psi], \omega_s(\sqrt{-1}), 2^{-1} \alpha \sim \mu$

Millions saw the apple fall, but Newton asked why

Bernard Baruch

کچھ اوزہمی نظر آتا ہے کا رو پارِ جہاں
نگاہِ شوق اگر ہو شریکِ بینائی
نگاہِ شوق میسر نہیں اگر تجھ کو
ترا وجود ہے قلب و نظر کی رسوائی

"The course of world appears somewhat different, if vision is accompanied by an eager glance. If you do not possess an eager glance, your being is a source of shame on heart and sight."

*Dr. Muhammad Iqbal from *Harb e Kaleem**

ACKNOWLEDGEMENTS

Finally the time for a last and a personal word! While I was working on the thesis, I often dreamt of this moment when the manuscript would be written, the final stress would be gone and I would look back at this period of my life with pleasure, nostalgia and gratitude. Finally, the moment has come and I can see many wonderful people, from inside and outside the work-sphere, I met during these years, contributing to this thesis in assorted ways. They made this adventure possible and even enjoyable. It is indeed a pleasure to convey my gratitude to them all in my humble acknowledgement.

The journey started on November 13, 2006, with an e-mail reply:

“ Many thanks for your interest. I would be
happy to have you in Paris ”,

from Habib Ammari to my request for a PhD studentship and it wasn't long after that, that I was actually in Paris. After toiling through two years of course work in MS, I was finally able to start an internship and subsequently a PhD with Habib Ammari. From the day he wrote a recommendation letter for me till this moment, Habib has always been there to provide me unflinching encouragement, support and guidance in different ways. I am profoundly impressed by his understanding of mathematics and his technical thoroughness. His truly scientist intuition has made him as a constant oasis of ideas and passion in science, which exceptionally inspired and enriched my growth as a student. He proved to be an excellent example of a brilliant mathematician, a successful professor, a thoughtful friend and a generous man, all in one. I am indebted to him more than he knows and I am always looking forward to learning more from him.

I am very grateful to Maitine Bergounioux, Eric Bonnetier, Elie Bretin, Joselin Garnier and Otmar Scherzer, who, besides their busy schedule, accepted to

be members of my oral defense committee. I am particularly thankful to Maitine Bergounioux and Otmar Scherzer for their valuable and devoted time to review this thesis.

It's a pleasure to pay a tribute to all my collaborators, Elie Bretin, Josselin Garnier, Lili Gaudarrama-Bustos and Vincent Jugnon. I would like to offer a special thank you to Elie for his friendship, contagious enthusiasm and energetic support. Our long discussions were very fruitful for shaping up my ideas and research. Moreover, a large part of my thesis and the fancy numerical illustrations contained in this dissertation would not have been there without him. I am proud of the fact that I had several opportunities to work with these brilliant scientists.

I keep a good memory of the lunch and coffee breaks at CMAP. The discussions and exchanges there added a lot to my knowledge of French culture and traditions and also helped me improve my French linguistic skills. Surely, CMAP would be a very different place without my fellow PhD students. I would like to express my gratitude to my officemates Jean-Baptiste Bellet, Yosra Boukari, Meisam Sharify and Denis Villemonais and also to Harsha Hutridurga-Ramaiah and Zixian Jiang for being very nice, friendly and supportive. They made my time spent at CMAP very interesting and memorable.

This thesis was financially supported by Higher Education Commission of Pakistan through a doctoral fellowship under the scheme -N& BS France- for which I am grateful to all the tax-payers of Pakistan. The facilities and grants provided by CMAP, École Polytechnique, especially the travel grants for the workshop -Doctorial- at Fréjus, France (2010) and conference -RAMMMA- at Lahore University of Management Sciences, Pakistan (2011), are highly acknowledged. The staff at CMAP deserves massive thanks for their help with the administrative and bureaucratic matters during my stay. I would especially like to mention Nasséra Naar at CMAP for her indispensable help. I truly admire the assistant director Alexandra Belus and the former director Michel Rosso of the doctoral school, for all their help during my PhD.

The warm support of all my friends in Paris enabled me to complete this thesis and have a wonderful time along the way. I enjoyed the hospitality of Mubeen, Qasim Malik, Fazli, Anzar, Qamar, Qasim Raza, Adeel Ahmad and Iftikhar Ahmad at numerous occasions. Sohail and Khashif Muhammad deserve my special mention for their helping hands to arrange a wonderful reception at my PhD defense. Playing Badminton and Cricket with Adnan, Amir, Ata, Farasat, Jam Rafique, Kashif Zahoor, Khurum, Mehmood and Yousuf, was fun. Finally, the discussions about research with Ayaz, Ibrar and Saad were quite inspiring. I must say I was lucky enough to have the company of these caring friends along the way. I thank you everybody.

From my early days in France, Azba, Adeel Mehmood, Babar, Inam, Tauqeer,

Liaqat, Umar and later on Nida Babar have shared so many special moments with me, contributing to a common story whose colorful pages now lead me towards a new chapter. Thank you all for the priceless memories. I am especially grateful to Azba, Nida and Babar for their hospitality and the great time we spent together.

Words fail me to express my gratitude and appreciation to my family for their unconditional support, love and prayers. I am forever grateful to my parents for their dedication and conscientious efforts in educating me. I am thankful to my siblings, brother and sisters in law for being supportive and caring. I cannot pen down this acknowledgement note without according my deep love and affection to my lovely nieces, Nihal, Mahnoor, Arfa, Zainab, Ezzah and my nephew Abdullah.

At last, someone special deserves my thanks for making the ending more colorful, charming and exciting.

Abdul Wahab,
Palaiseau.

CONTENTS

ACKNOWLEDGEMENT	I
CONTENTS	V
LIST OF FIGURES	IX
GENERAL INTRODUCTION	1
I Imaging in Attenuating Acoustic Media	9
1 PHOTO-ACOUSTIC IMAGING IN ATTENUATING MEDIA	11
1.1 Introduction	11
1.2 Photo-acoustic imaging in free space	12
1.2.1 Mathematical formulation	12
1.2.2 Limited-view data	14
1.2.3 Compensation of the effect of acoustic attenuation	16
1.2.4 Relationship between p and p_a	18
1.2.5 A singular value decomposition approach	19
1.2.6 Asymptotics of \mathcal{L}	20
1.2.6.1 Thermo-viscous case: $\kappa(\omega) \simeq \omega/c_0 + ia\omega^2/2$	20
1.2.6.2 General case: $\kappa(\omega) = \omega/c_0 + ia \omega ^\zeta$	24
1.2.7 Iterative shrinkage-thresholding algorithm with correction	25
1.3 Photo-acoustic imaging with imposed boundary conditions	25
1.3.1 Mathematical formulation	26
1.3.2 Inversion algorithms	27
1.3.3 Compensation of the effect of acoustic attenuation	30
1.3.4 Case of a spherical wave as a probe function	30

1.3.5	Case of a plane wave as a probe function	31
1.4	Conclusion	34
	Appendices	34
1.A	Stationary phase theorem and proofs	34
1.A.1	Stationary phase theorem	34
1.A.2	Proof of approximation (1.8)	35
1.A.3	Proof of approximation (1.29)	36
2	TIME REVERSAL ALGORITHMS FOR ATTENUATING ACOUSTIC MEDIA	39
2.1	Introduction	39
2.2	Time reversal in homogeneous media without attenuation	40
2.2.1	Ideal time reversal imaging technique	41
2.2.2	Modified time-reversal imaging technique	41
2.3	Time reversal algorithm for an attenuating acoustic medium	43
2.3.1	Analysis of regularized time reversal functional	45
2.4	Reconstruction alternative for higher order attenuation correction	48
2.5	Numerical illustrations	48
2.5.1	Description of the algorithm	48
2.5.2	Experiments	49
2.6	Discussion and conclusion	50
3	NOISE SOURCE LOCALIZATION IN ATTENUATING MEDIA	55
3.1	Introduction	55
3.2	Media without attenuation	56
3.3	Source localization	58
3.3.1	Two- and three-dimensional homogeneous media	59
3.3.2	Back-propagation in a two-dimensional medium	62
3.3.3	Numerical simulations	63
3.4	Localization of sources in an attenuating medium	66
3.4.1	Helmholtz-Kirchhoff identity	68
3.4.2	Three-dimensional homogeneous medium	69
3.4.3	Back-propagation in a two-dimensional medium	70
3.4.4	Back-propagation of pre-processed data	72
3.4.5	Numerical experiments	73
3.5	Localization of correlated sources	74
3.5.1	Spatially correlated sources	74
3.5.2	Extended distributions of locally correlated sources	75
3.5.3	A collection of correlated point sources	76
3.5.4	Numerical experiments for correlated source localization	77
3.6	Conclusion	78

II	Imaging in Viscoelastic Media	81
4	IMAGING IN ISOTROPIC VISCOELASTIC MEDIA	83
4.1	Introduction	83
4.2	General viscoelastic wave equation	84
4.3	Green function	86
4.3.1	Solution of (4.4) with a concentrated force.	87
4.3.2	Viscoelastic Green function	90
4.4	Ideal Green function retrieval and imaging procedure	91
4.4.1	Asymptotics of attenuation operator for Voigt model	92
4.4.2	Imaging procedure	95
4.5	Numerical illustrations	96
4.5.1	Profile of the Green function	96
4.5.2	Approximation of attenuation operator \mathcal{L}	98
4.6	Conclusion	99
	Appendices	99
4.A	Stationary phase method	99
5	TIME REVERSAL ALGORITHMS FOR VISCOELASTIC MEDIA	103
5.1	Introduction	103
5.2	Time reversal in homogeneous elastic media without viscosity	104
5.2.1	Time-reversal imaging analysis	105
5.2.1.1	Integral formulation	105
5.2.1.2	Helmholtz-Kirchhoff identity	107
5.2.1.3	Approximation of the co-normal derivative	110
5.2.1.4	Analysis of the imaging functional $\tilde{\mathcal{I}}$	112
5.2.2	Numerical simulations	114
5.2.2.1	Description of the algorithm	114
5.2.2.2	Experiments	115
5.3	Time-reversal algorithm for a viscoelastic medium	116
5.3.1	Green tensor in viscoelastic media	121
5.3.2	Attenuation operator and its asymptotics	122
5.3.3	Helmholtz-Kirchhoff identity in viscoelastic media	123
5.3.4	Analysis of the regularized time-reversal algorithm	125
5.3.5	Numerical simulations	127
5.3.5.1	Description of the algorithm	128
5.3.5.2	Experiments	128
6	SOME ANISOTROPIC VISCOELASTIC GREEN FUNCTIONS	133
6.1	Introduction	133
6.2	Mathematical context and chapter outlines	135
6.2.1	Viscoelastic wave equation	135

6.2.2	Spectral decomposition using Christoffel tensors	136
6.2.3	Chapter outline	137
6.3	Some simple anisotropic viscoelastic media	138
6.3.1	Medium I	138
6.3.2	Medium II	139
6.3.3	Medium III	140
6.3.4	Properties of the media and main assumptions	140
6.3.4.1	Properties	140
6.3.4.2	Assumptions	141
6.4	Resolution of the model wave problem	141
6.5	Resolution of the model potential problem	143
6.5.1	The potential problem	143
6.5.2	Derivatives of the potential field	145
6.6	Elastodynamic Green function	146
6.6.1	Medium I	146
6.6.2	Medium II	147
6.6.3	Medium III	149
6.6.4	Isotropic medium	151
	Appendices	152
6.A	Decomposition of the Green function	152
6.B	Derivative of potential: case I	153
6.C	Derivative of potential: case II	154
	CONCLUSION AND PERSPECTIVES	155
	BIBLIOGRAPHY	159
	INDEX	171

LIST OF FIGURES

0.1	Image reconstruction using elastic time reversal algorithm	2
0.2	Image reconstruction using acoustic time reversal algorithm	2
0.3	Reconstruction of acoustic sources using Radon transform	3
1.1	Numerical inversion using (1.3)	14
1.2	Numerical inversion with truncated (1.3)	15
1.3	Iterative shrinkage-thresholding solution and error analysis	16
1.4	Limited angle tests with Beck and Teboulle IST algorithm	17
1.5	Numerical inversion of attenuated wave equation	19
1.6	Compensation of acoustic attenuation with SVD regularization	21
1.7	Compensation of acoustic attenuation with formula (1.10)	23
1.8	Iterative shrinkage-thresholding algorithm with $\eta = 0.001$ & $a = 0.0025$	26
1.9	Reconstruction with homogeneous Dirichlet boundary conditions	28
1.10	Numerical inversion with Dirichlet boundary conditions	29
1.11	Attenuation compensation using (1.29) with Dirichlet conditions	33
2.1	Comparison between \mathcal{S}_1 and \mathcal{S}_2 without attenuation	50
2.2	Reconstruction using \mathcal{S}_2 from attenuated data g_a	50
2.3	Reconstruction using $\mathcal{S}_{2,a,\rho}$ from attenuated data g_a	51
2.4	Cut-off frequency for different values of attenuation coefficients	52
2.5	Reconstruction by preprocessing data with the filter $\mathcal{L}_{a,k}^{-1}$	53
2.6	Reconstruction of the attenuation coefficient	54
3.1	Point source reconstruction in ideal media	66
3.2	Estimations of the power spectral density with and without averaging	67
3.3	Localization of point sources in attenuating medium	73
3.4	Localization of correlated point sources	79
3.5	Localization of correlated extended sources	79

4.1	Plot of $A = \left(\frac{1}{\sqrt{2}}r, \frac{1}{\sqrt{2}}r, 0\right)$ and plane $P = \{\mathbf{x} \in \mathbb{R}^3, x_3 = \frac{r}{2}\}$	96
4.2	Temporal response of elastic Green function	97
4.3	2D spatial response of the elastic Green function	98
4.4	Comparison between $u_{1,v_s}(x, t)$ and $\mathcal{L}u_{1,ideal}$ observed at $x = A$	100
4.5	Approximation of operator \mathcal{L} : Error plot in logarithmic scale	101
5.1	Comparison between \mathcal{F} and $\tilde{\mathcal{F}}$ with Lamé constants $(\lambda, \mu) = (1, 1)$	117
5.2	Comparison between \mathcal{F} and $\tilde{\mathcal{F}}$ with Lamé coefficients $(\lambda, \mu) = (10, 1)$	118
5.3	Less localized source reconstruction using \mathcal{F} and $\tilde{\mathcal{F}}$ with $(\lambda, \mu) = (1, 1)$	119
5.4	$\tilde{\mathcal{F}}$ and $\tilde{\mathcal{F}}_{a,\rho}$ with $(\lambda, \mu) = (1, 1)$, $\left(\frac{v_s^2}{c_s^2}, \frac{v_p^2}{c_p^2}\right) = (2 \times 10^4, 2 \times 10^4)$, $\rho = 15, 20, 25$	129
5.5	$\tilde{\mathcal{F}}$ and $\tilde{\mathcal{F}}_{a,\rho}$ with $(\lambda, \mu) = (1, 1)$, $\left(\frac{v_s^2}{c_s^2}, \frac{v_p^2}{c_p^2}\right) = (5 \times 10^5, 5 \times 10^5)$, $\rho = 15, 20, 25$	130
5.6	$\tilde{\mathcal{F}}$ and $\tilde{\mathcal{F}}_{a,\rho}$ with $(\lambda, \mu) = (1, 1)$, $(\eta_\lambda, \eta_\mu) = (5 \times 10^5, 5 \times 10^5)$, $\rho = 25, 30, 35$	131

GENERAL INTRODUCTION

MOTIVATIONS

The rise of mathematical imaging over the past few decades is an extraordinary story of accomplishments [114]. Imaging modalities are revolutionized with technological advances and the use of computer-based mathematical methods [7, 59, 115, 116, 149]. Mature techniques are markedly improved and several new techniques have emerged, empowering practitioners with profound understanding [7, 8, 9].

The quest for new and improved imaging techniques still continues in order to overcome the intrinsic deficiencies of the existing techniques [36, 66, 71, 113, 126, 139]. The issues envisaged by researchers are mainly related to image quality, data acquisition time, sensitivity, portability and feature detection abilities of the imaging techniques. Cost and safety are also among major concerns [8, 9, 93, 114, 120].

An interesting problem in imaging is to model and compensate for the effects of wave attenuation on image quality. Most imaging techniques either emphasize a non-attenuating medium or do not adequately incorporate underlying phenomenon in reconstruction algorithms. As a consequence, one retrieves erroneous or less accurate wave synthetics which produce serious blurring in reconstructed images (see, for example, Figures 0.1, 0.2 and 0.3) and result in loss of important information [86, 109, 132, 134].

The envisaged problem is indeed challenging and has received considerably less attention because of its inherent mathematical difficulty. In fact, only recently, some efforts have been made to establish realistic models for wave propagation in attenuating media and a handful of imaging algorithms are proposed which compensate for attenuation effects. (See for instance, survey articles [82, 133]. See also [41, 86, 104, 132, 134] and references therein). This sub-

stantiates a real need to investigate attenuation effect on image quality and to propose its remedies for image reconstruction.

This thesis is devoted to study attenuation and to develop stable and robust algorithms for reconstructing acoustic and elastic sources in attenuating media. The source localization problems have been of significant interest in recent years and find numerous applications in different fields, particularly in biomedical imaging [11, 19, 67, 79, 106, 117, 122, 130]. Our main motivation is the recent advances on hybrid ensemble methods making use of elastic and acoustic properties of soft tissues [11, 19, 20, 71, 113]. We also address the problem of locating ambient noise sources in attenuating media [29, 67, 68, 69, 112].

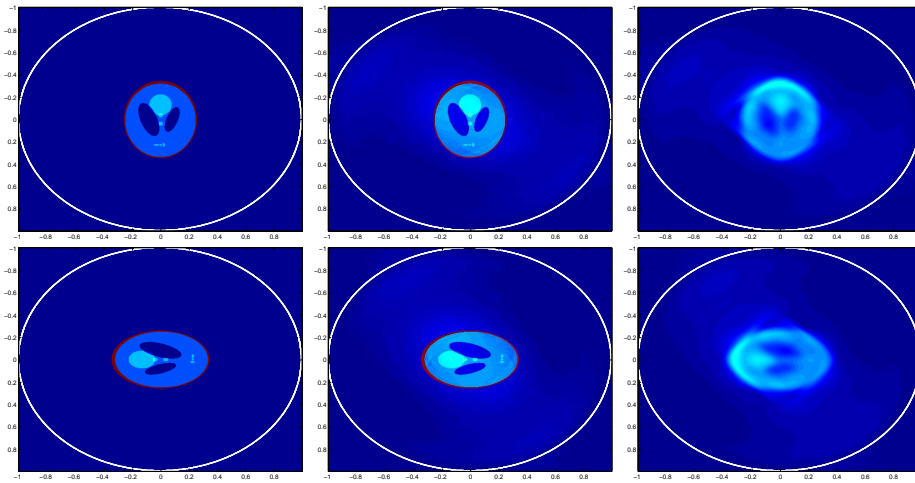


FIGURE 0.1. Image reconstruction using elastic time reversal algorithm: First row: Pressure Component; Second Row: Shear Component. Left to right: initial sources, reconstruction in a loss-less medium, reconstruction in an attenuating medium.

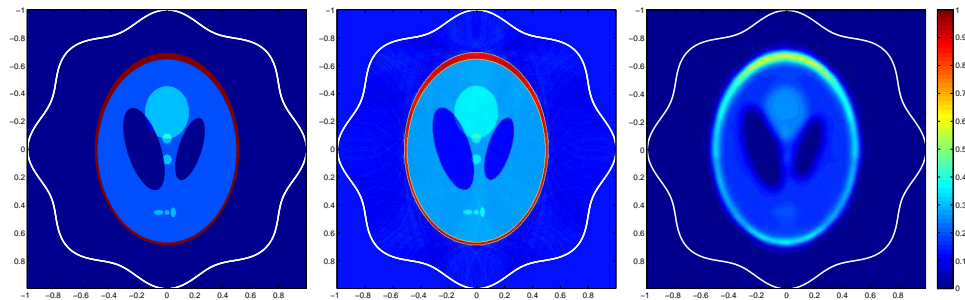


FIGURE 0.2. Image reconstruction using acoustic time reversal algorithm: Left to right: initial source; reconstruction in a loss-less medium; reconstruction in an attenuating medium.

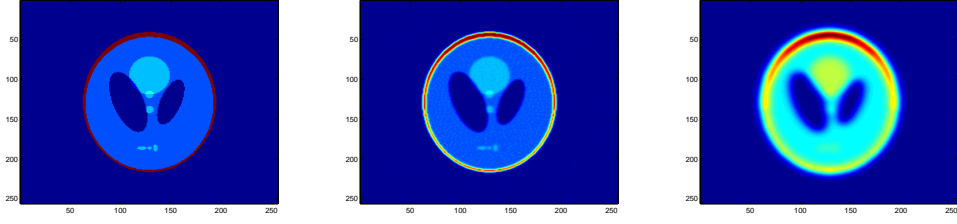


FIGURE 0.3. Reconstruction of acoustic sources using Radon transform: Left to right: initial source; reconstruction in a loss-less medium; reconstruction in an attenuating medium.

MATHEMATICAL CONTEXT AND MAIN CONTRIBUTIONS

In this section, we briefly introduce the set of problems under consideration in mathematical context and summarize important results of the thesis.

STATEMENT OF THE PROBLEMS STUDIED

Let p be the solution of the wave equation

$$\begin{cases} \frac{1}{c^2} \frac{\partial^2 p}{\partial t^2}(x, t) - \Delta p(x, t) = 0, & (x, t) \in \mathbb{R}^d \times \mathbb{R}^+, \\ p(x, 0) = p_0(x) \quad \text{and} \quad \frac{\partial p}{\partial t}(x, 0) = 0, \end{cases} \quad (1)$$

where c is the phase velocity and the support, $\text{supp}\{p_0(x)\}$, of $p_0(x)$ is strictly contained in a bounded domain $\Omega \subset \mathbb{R}^d$ with $d = 2, 3$. Then, the problem (\mathcal{P}_{ideal}) , defined as

$$(\mathcal{P}_{ideal}) \quad \left\{ \begin{array}{l} \text{reconstruct } p_0(x) \text{ given the measurements} \\ \left\{ g(y, t) := p(y, t), \quad \forall (y, t) \in \partial\Omega \times (0, T) \right\} \text{ for } T \text{ sufficiently large,} \end{array} \right.$$

is tractable. Indeed, (\mathcal{P}_{ideal}) can be related to the spherical Radon transform

$$\mathcal{R}[f](y, r) = \int_{S^{d-1}} r^{d-1} f(y + r\xi) d\sigma(\xi) \quad (2)$$

where $d\sigma$ is the standard surface measure on the unit sphere S^{d-1} in \mathbb{R}^d . A large class of retro-projection inversion formulae exists for \mathcal{R} . Several other techniques such as time reversal, spectral decomposition and optimal control can also be applied [37, 60, 61, 73, 74, 85, 99].

A major drawback of problem (\mathcal{P}_{ideal}) is that it does not take into account the inevitable frequency dependent wave attenuation severely affecting high frequency components in measured data. This proves to be an impediment to imaging sharp edges and small structures, which correspond to the short wavelengths and therefore to the high frequencies, thereby introducing blur in images and causing loss of information.

In order to account for wave attenuation, we consider the problem (\mathcal{P}_{att}) defined as

$$(\mathcal{P}_{att}) \quad \left| \begin{array}{l} \text{reconstruct } p_0(x) \text{ given the measurements} \\ \left\{ g_a(y, t) := p_a(y, t), \quad \forall (y, t) \in \partial\Omega \times (0, T) \right\} \text{ for } T \text{ sufficiently large,} \end{array} \right.$$

where p_a is the solution of the attenuated wave equation:

$$\frac{1}{c^2} \frac{\partial^2 p_a}{\partial t^2}(x, t) - \Delta p_a(x, t) - L_a[p_a](x, t) = 0, \quad (x, t) \in \mathbb{R}^d \times \mathbb{R}^+ \quad (3)$$

with loss operator L_a . In contrast with (\mathcal{P}_{ideal}) , the problem (\mathcal{P}_{att}) is more involved and intricate. Indeed, it is quite troublesome to adopt ideal reconstruction algorithms to solve (\mathcal{P}_{att}) because attenuation induces instability. On the other hand, some of the algorithms even fail as their underlying assumptions are no more valid. For example, the ideal time reversal technique does not work because attenuation breaks down the time reversibility of waves. A further problematic situation is when we have to impose boundary condition on p_a or have access to only partial boundary data g_a .

The viscoelastic counterpart of (\mathcal{P}_{att}) , that is,

$$(\mathcal{P}_{ve}) \quad \left| \begin{array}{l} \text{reconstruct } \mathbf{u}_0(x) \text{ given the measurements} \\ \left\{ \mathbf{g}_a(y, t) := \mathbf{u}_a(y, t), \quad \forall (y, t) \in \partial\Omega \times (0, T) \right\} \text{ for } T \text{ sufficiently large,} \end{array} \right.$$

is even more challenging and hard-won where \mathbf{u} satisfies viscoelastic wave equation:

$$\left(\rho \frac{\partial^2}{\partial t^2} - \mathcal{L}_{\lambda, \mu} - \frac{\partial}{\partial t} \mathcal{L}_{\eta_\lambda, \eta_\mu} \right) \mathbf{u}_a(x, t) = \frac{\partial \delta_0(t)}{\partial t} \mathbf{u}_0(x), \quad (x, t) \in \mathbb{R}^d \times \mathbb{R}^+, \quad (4)$$

with Lamé parameters (λ, μ) , viscoelastic moduli (η_λ, η_μ) and

$$\mathcal{L}_{a,b} \mathbf{v} = (a + b) \nabla(\nabla \cdot \mathbf{v}) - b \Delta \mathbf{v}.$$

The additional difficulty in (\mathcal{P}_{ve}) stems from the fact that the measured data is a combination of both shear and pressure waves having different phase velocities and polarization directions.

In this thesis, we aim to present stable and robust algorithms in order to solve (\mathcal{P}_{att}) , (\mathcal{P}_{ve}) and the allied problems. We also address their applications to biomedical imaging and ambient noise imaging.

SUMMARY OF THE MAIN RESULTS

First of all, we consider Radon transform based algorithms to solve (\mathcal{P}_{att}) . For simplicity, we let p_a satisfy thermo-viscous wave equation:

$$\frac{1}{c^2} \frac{\partial^2 p_a}{\partial t^2}(x, t) - \Delta p_a(x, t) - a \frac{\partial}{\partial t} (\Delta p_a)(x, t) = 0, \quad (x, t) \in \mathbb{R}^d \times \mathbb{R}^+ \quad (5)$$

where a represents attenuation coefficient. When a is constant, we relate non-attenuated wave p to p_a via an attenuation operator \mathcal{L} as

$$p_a = \mathcal{L}[p],$$

where

$$\mathcal{L}[\phi](x, t) = \frac{1}{\sqrt{2\pi}} \int_{\mathbb{R}} \int_{\mathbb{R}^+} \frac{1}{\sqrt{1+ia\omega}} \phi(x, s) \exp\left\{\frac{i\omega s}{\sqrt{1+ia\omega}}\right\} \exp\{i\omega t\} ds d\omega. \quad (6)$$

The attenuation correction can be achieved by inverting \mathcal{L} . However, \mathcal{L} is ill-conditioned. Therefore, by using stationary phase theorem, we present an asymptotic development of \mathcal{L} with respect to a small attenuation coefficient a of the form

$$\mathcal{L}[\phi] = \sum_{j=0}^k a^j \mathcal{L}_k[\phi] + o(a^k).$$

This permits us to find an approximate inverse \mathcal{L}_k^{-1} of the attenuation operator and therefore the ideal Radon transform of the initial conditions. Subsequently we find $p_0(x)$ using retro-projection inverse Radon transform formulae [60, 61]. We compare our results with a singular value decomposition approach for approximating \mathcal{L}^{-1} , as taken in [86, 95]. Our results appear to be more stable and accurate. The partial boundary data problems are treated with *TV-Tikhonov* regularization techniques [72]. We study three different iterative algorithms and present special preconditioning weights in order to increase convergence speed. Finally, in the case of imposed boundary conditions, we use a duality approach originally proposed in [11], whereas stationary phase theorem is used to rectify attenuation artifacts. We also explain the case of power-law attenuation correction [82, 127].

Motivated by their simplicity and robustness, we then study the time reversal techniques to solve (\mathcal{P}_{att}) and (\mathcal{P}_{ve}) [46, 62]. As the attenuating waves are not time invariant, we test the idea of using adjoint attenuated waves for time reversal, as suggested by [41, 134]. For (\mathcal{P}_{att}) , we justify mathematically using attenuation operator \mathcal{L} previously defined, that this technique provides an approximation of p_0 correct up to first order of attenuation, but it is not quite stable. As an alternative we propose a preprocessing technique consisting of two steps: use asymptotically obtained filter \mathcal{L}_k^{-1} to pre-process measured data and afterward an ideal time reversal algorithm. We establish that the new technique is more stable and is accurate up to order k .

The elastic time reversal is studied for both elastic and viscoelastic media. In elastic media, the boundary data

$$\{\mathbf{g}(y, t) := \mathbf{u}(y, t), \quad (y, t) \in \mathbb{R}^d \times (0, T)\}$$

is a combination of the pressure and the shear waves propagating with different phase velocities and polarization directions. Consequently, we observe additional artefacts when we time reverse the displacement field. Therefore, we first

address these artefacts by proposing an original technique based on a weighted Helmholtz decomposition. Then, we solve (\mathcal{P}_{ve}) using a regularized version of adjoint viscoelastic wave together with modified time reversal functional. We prove that our results are of order $(v_s^2/c_s^2 + v_p^2/c_p^2)$, where (v_s, v_p) are the shear and bulk viscosities and (c_s, c_p) are the shear and pressure wave speeds respectively.

As an application of the inverse source problems, we aim to locate noise sources from boundary measurements over an interval of time. More precisely, we consider the following problem:

$$(\mathcal{P}_{noise}) \quad \left| \begin{array}{l} \text{reconstruct spatial support } K(\mathbf{x}) \text{ of noise source } n(\mathbf{x}, t) \text{ given} \\ \left\{ g(\mathbf{y}, t) := p(\mathbf{y}, t), \quad \forall (\mathbf{y}, t) \in \partial\Omega \times (0, T) \right\} \text{ for } T \text{ sufficiently large,} \end{array} \right.$$

where p is the solution of the wave equation (1) (respectively (3) for attenuating media) with source $n(\mathbf{x}, t)$ being a stationary Gaussian process with mean zero and covariance function

$$\langle n(t, \mathbf{x}) n(s, \mathbf{y}) \rangle = F(t - s) K(\mathbf{x}) \delta(\mathbf{x} - \mathbf{y}).$$

Here F is the time covariance of the noise signals and $\langle \cdot \rangle$ stands for the statistical average. By using statistical cross correlation of the noise signals, we propose efficient weighted functionals to solve (\mathcal{P}_{noise}) , with and without attenuation. In attenuating media, we use a regularized version of the back-propagator to locate sources. We also discuss the impact of spatial correlation between the noise sources and derive functionals capable of first locating such sources and then estimating their correlation matrix.

In another study, we adopt the ideal anomaly detection algorithms to the case of a quasi-incompressible viscoelastic medium. For doing so, we first derive a closed form expression of the viscoelastic Green function in a homogeneous isotropic medium. We show that when the compressional modulus $\lambda \rightarrow \infty$ the ideal elastic Green function, \mathbb{G}_{ideal} , can be approximated from the viscoelastic Green function, \mathbb{G}_{att} , by solving an ordinary differential equation. This result is also based on the asymptotic development of an attenuation operator using stationary phase theorem.

Finally, we provide some anisotropic viscoelastic Green functions with an aim to enhance our results to the case of anisotropic media. We follow an approach proposed by Burridge *et al.* [42]. We write Green function in terms of three functions, ϕ_i , satisfying the scalar wave equation in attenuating media. The problem of finding the Green function is then related to resolve the wave equations in order to find ϕ_i 's and three subsequent potential equations of the form

$$\Delta_{\mathcal{E}} \psi_i = \phi_i,$$

where $\Delta_{\mathcal{E}}$ is the Laplacian in ellipsoidal coordinates. The potential equation is finally solved using an argument of potential theory in ellipsoidal coordinates [50, 80].

THESIS OUTLINES

The thesis consists of six chapters, essentially divided into two parts.

PART I deals with imaging techniques in acoustic media and their applications to biomedical imaging and noise source imaging. It consists of CHAPTERS 1, 2 and 3.

CHAPTER 1 is devoted to the reconstruction algorithms based on Radon transform and their applications to Photoacoustic imaging in attenuating media. We detail results related to attenuation correction, imposed boundary conditions and partial data problems.

CHAPTER 2 presents time reversal methods to find acoustic sources. We recall time reversal techniques for ideal acoustic media and analyze the technique based on an adjoint attenuated wave. Finally, we provide an algorithm based on pre-processing of the measured data.

CHAPTER 3 deals with the problems of locating ambient noise sources in acoustic media. We present algorithms to locate point as well as extended sources in both attenuating and non-attenuating media. The case of spatially correlated sources is also discussed.

PART II deals with imaging in elastic media and consists of CHAPTERS 4, 5 and 6.

CHAPTER 4 addresses the imaging problems in isotropic viscoelastic media in a quasi-incompressible regime. We first present an expression for viscoelastic Green function and then provide a stable technique for attenuation correction.

CHAPTER 5 aims to present and justify the time reversal techniques for viscoelastic media. We discuss a modified time reversal functional in a purely elastic regime to tackle imaging artefacts. Then, we extend this technique to viscoelastic media.

CHAPTER 6 deals with visco-elastic anisotropy in order to extend results presented in Chapter 4 and 5.

Finally, we sum up the thesis in CONCLUSION AND PERSPECTIVES, where we also discuss some open questions related to the subject matter.

All the chapters of the thesis are self-contained and can be read independently. Thesis mainly contains the results presented in [14, 15, 16, 17, 39, 40].

Part I

Imaging in Attenuating Acoustic Media

PHOTO-ACOUSTIC IMAGING IN ATTENUATING MEDIA

1.1 INTRODUCTION

In photo-acoustic imaging, optical energy absorption causes thermo-elastic expansion of the tissue, which leads to the propagation of a pressure wave. This signal is measured by transducers distributed on the boundary of the object, which in turn is used for imaging optical properties of the object. The major contribution of photo-acoustic imaging is to provide images of optical contrasts (based on the optical absorption) with the resolution of ultrasound [145].

If the medium is acoustically homogeneous and has the same acoustic properties as the free space, then the boundary of the object plays no role and the optical properties of the medium can be extracted from measurements of the pressure wave by inverting a spherical Radon transform [73, 74, 84].

If a boundary condition has to be imposed on the pressure field, then an explicit inversion formula no longer exists. However, using a quite simple duality approach, one can still reconstruct the optical absorption coefficient. In fact, in the recent works [11, 12], Ammari *et al.* investigated quantitative photoacoustic imaging in the case of a bounded medium with imposed boundary conditions. In a further study [10], they proposed a geometric-control approach to deal with the case of limited view measurements. In both cases, they focused on a situation with small optical absorbers in a non-absorbing background and proposed adapted algorithms to locate the absorbers and estimate their absorbed energy.

A second challenging problem in photo-acoustic imaging is to take into account the issue of modeling the acoustic attenuation and its compensation. This subject is addressed in [41, 81, 83, 86, 92, 104, 124, 132].

In this chapter, we propose a new approach to image extended optical sources from photo-acoustic data and to correct the effect of acoustic attenuation. By testing our measurements against an appropriate family of functions, we show that we can access the Radon transform of the initial condition, and thus recover quantitatively any initial condition for the photoacoustic problem. We also show

how to compensate the effect of acoustic attenuation on image quality by using the stationary phase theorem. We use a frequency power-law model for the attenuation losses.

The chapter is organized as follows. In Section 1.2 we consider the photo-acoustic imaging problem in free space. We first propose three algorithms to recover the absorbing energy density from limited-view and compare their speeds of convergence. We then present two approaches to correct the effect of acoustic attenuation. We use a power-law model for the attenuation. We test the singular value decomposition approach proposed in [86] and provide a new technique based on the stationary phase theorem. Section 1.3 is devoted to correct the effect of imposed boundary conditions. By testing our measurements against an appropriate family of functions, we show how to obtain the Radon transform of the initial condition in the acoustic wave equation, and thus recover quantitatively the absorbing energy density. We also show how to compensate for the effect of acoustic attenuation on image quality by once again using the stationary phase theorem. The chapter ends with a discussion.

1.2 PHOTO-ACOUSTIC IMAGING IN FREE SPACE

In this section, we first formulate the imaging problem in free space and present a simulation for the reconstruction of the absorbing energy density using the spherical Radon transform. Then, we provide a total variation regularization to find a satisfactory solution of the imaging problem with limited-view data. Finally, we present two deconvolution strategies to compensate for the effect of acoustic attenuation and compare their performance. The first strategy is based on a singular value decomposition while the second one uses the stationary phase theorem.

1.2.1 MATHEMATICAL FORMULATION

We consider the wave equation in \mathbb{R}^d ,

$$\frac{1}{c_0^2} \frac{\partial^2 p}{\partial t^2}(x, t) - \Delta p(x, t) = 0 \quad \text{in } \mathbb{R}^d \times (0, T),$$

with

$$p(x, 0) = p_0 \quad \text{and} \quad \frac{\partial p}{\partial t}(x, 0) = 0.$$

Here c_0 is the phase velocity in a non-attenuating medium.

Assume that the support of p_0 , the absorbing energy density, is contained in a bounded set Ω of \mathbb{R}^d . Our objective in this part is to reconstruct p_0 from the measurements

$$\left\{ g(y, t) := p(y, t), \quad \forall (y, t) \in \partial\Omega \times (0, T) \right\},$$

where $\partial\Omega$ denotes the boundary of Ω .

The problem of reconstructing p_0 is related to the inversion of the spherical Radon transform given by

$$\mathcal{R}_\Omega[f](y, r) = \int_S r f(y + r\xi) d\sigma(\xi), \quad (y, r) \in \partial\Omega \times \mathbb{R}^+,$$

where S denotes the unit sphere. It is known that in dimension 2, Kirchoff's formula implies that [61]

$$\begin{cases} p(y, t) = \frac{1}{2\pi} \frac{\partial}{\partial t} \int_0^t \frac{\mathcal{R}_\Omega[p_0](y, c_0 r)}{\sqrt{t^2 - r^2}} dr, \\ \mathcal{R}_\Omega[p_0](y, r) = 4r \int_0^r \frac{p(y, t/c_0)}{\sqrt{r^2 - t^2}} dt. \end{cases}$$

Let the operator \mathcal{W} be defined by

$$\mathcal{W}[g](y, r) = 4r \int_0^r \frac{g(y, t/c_0)}{\sqrt{r^2 - t^2}} dt \quad \text{for all } g: \partial\Omega \times \mathbb{R}^+ \rightarrow \mathbb{R}. \quad (1.1)$$

Then, it follows that

$$\mathcal{R}_\Omega[p_0](y, r) = \mathcal{W}[p](y, r). \quad (1.2)$$

In recent works, a large class of inversion retro-projection formulae for the spherical Radon transform have been obtained in even and odd dimensions when Ω is a ball; see for instance [60, 61, 85, 99]. In dimension 2, when Ω is the unit ball, it turns out that

$$p_0(x) = \frac{1}{(4\pi^2)} \int_{\partial\Omega} \int_0^2 \left[\frac{d^2}{dr^2} \mathcal{R}_\Omega[p_0](y, r) \right] \ln|r^2 - (y-x)^2| dr d\sigma(y). \quad (1.3)$$

This formula can be rewritten as follows:

$$p_0(x) = \frac{1}{4\pi^2} \mathcal{R}_\Omega^* \mathcal{B} \mathcal{R}_\Omega[p_0](x),$$

where \mathcal{R}_Ω^* is the adjoint of \mathcal{R}_Ω ,

$$\mathcal{R}_\Omega^*[g](x) = \int_{\partial\Omega} g(y, |y-x|) d\sigma(y),$$

and \mathcal{B} is defined by

$$\mathcal{B}[g](x, t) = \int_0^2 \frac{d^2 g}{dr^2}(y, r) \ln|r^2 - t^2| dr$$

for $g: \Omega \times \mathbb{R}^+ \rightarrow \mathbb{R}$.

In Figure 1.1, we give a numerical illustration for the reconstruction of p_0 using the spherical Radon transform. We adopt the same approach as in [60] for the discretization of formulae (1.1) and (1.3).

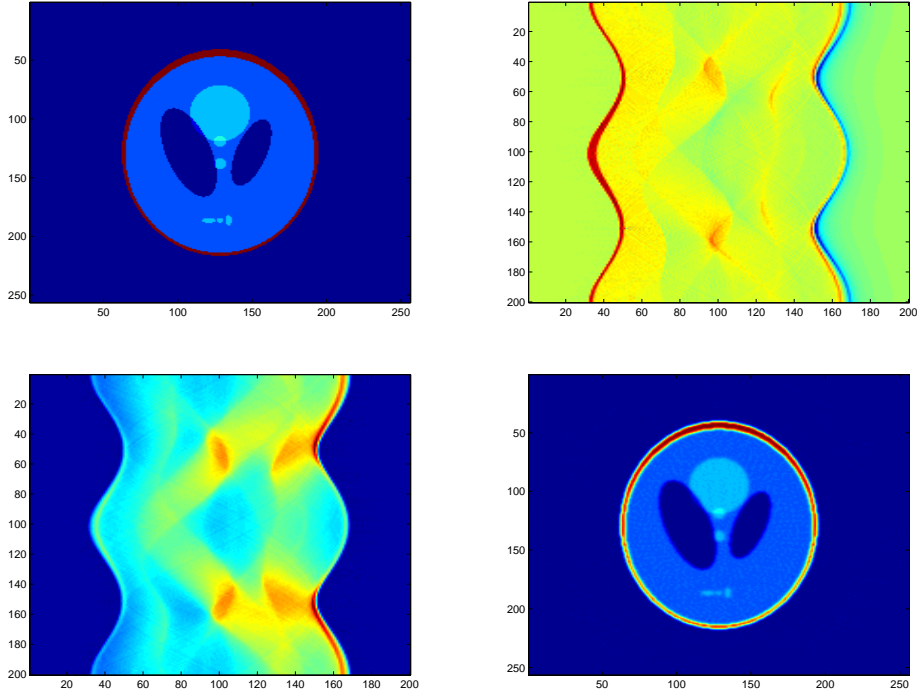


FIGURE 1.1. Numerical inversion using (1.3) with $N = 256$, $N_R = 200$ and $N_\theta = 200$. Top left: p_0 ; Top right: $p(y, t)$ with $(y, t) \in \partial\Omega \times (0, 2)$; Bottom left: $\mathcal{R}_\Omega[p_0](y, t)$ with $(y, t) \in \partial\Omega \times (0, 2)$; Bottom right: $\frac{1}{4\pi^2} \mathcal{R}_\Omega^* \mathcal{B} \mathcal{R}_\Omega[p_0]$.

1.2.2 LIMITED-VIEW DATA

In many situations, we have only at our disposal data on $\Gamma \times (0, T)$, where $\Gamma \subset \partial\Omega$. As illustrated in Figure 1.2, restricting the integration in formula (1.3) to Γ as follows:

$$p_0(x) \simeq \frac{1}{(4\pi^2)} \int_\Gamma \int_0^2 \left[\frac{d^2}{dr^2} \mathcal{R}_\Omega[p_0](y, r) \right] \ln|r^2 - (y-x)^2| dr d\sigma(y), \quad (1.4)$$

is not stable enough to give a correct reconstruction of p_0 .

The inverse problem becomes severely ill-posed and needs to be regularized; see for instance [72, 146]. We apply here a Tikhonov regularization with a total variation term, which is well adapted to the reconstruction of smooth solutions with front discontinuities. We then introduce the function $p_{0,\eta}$ as the minimizer of

$$J[f] = \left\| Q[\mathcal{R}_\Omega[f] - g] \right\|_{L^2(\partial\Omega \times (0,2))} + \eta \|\nabla f\|_{L^1(\Omega)},$$

where Q is a positive weight operator.

Direct computation of $p_{0,\eta}$ can be complicated as the TV term is not smooth (not of class \mathcal{C}^1). Here, we obtain an approximation of $p_{0,\eta}$ via an iterative

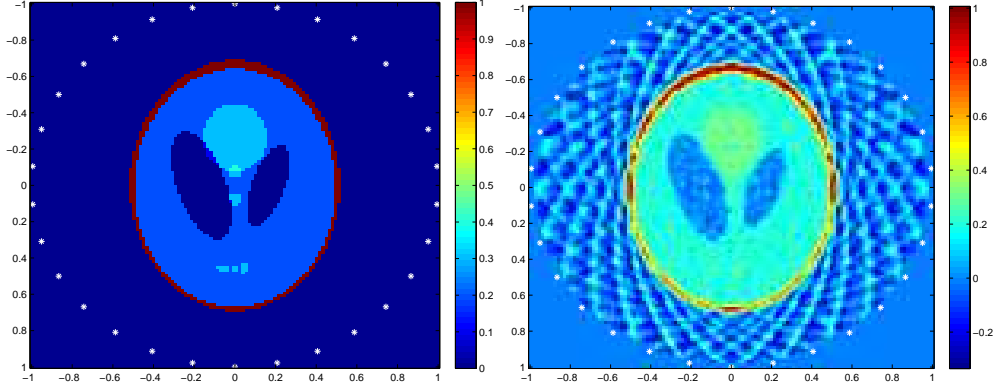


FIGURE 1.2. Numerical inversion with truncated (1.3) formula. $N = 128$, $N_R = 128$, and $N_\theta = 30$. Left: p_0 ; Right: $\frac{1}{4\pi^2} \mathcal{R}_\Omega^* \mathcal{B} \mathcal{R}_\Omega [p_0]$.

shrinkage-thresholding algorithm [52, 55]. This algorithm can be seen as a split, gradient-descent, iterative scheme:

- Data g , initial solution $f_0 = 0$;
- (1) Data link step: $f_{k+1/2} = f_k - \gamma \mathcal{R}_\Omega^* Q^* Q [\mathcal{R}_\Omega [f_k] - g]$;
- (2) Regularization step: $f_k = T_{\gamma\eta} [f_{k+1/2}]$,

where γ is a virtual descent time step and the operator T_η is defined by

$$T_\eta[y] = \arg \min_x \left\{ \|y - x\|_{L^2} + \eta \|\nabla x\|_{L^1} \right\}.$$

One advantage of the algorithm is to minimize implicitly the TV term using the duality algorithm of Chambolle [49]. This algorithm converges [52, 55] under the assumption $\gamma \|\mathcal{R}_\Omega^* Q^* Q \mathcal{R}_\Omega\| \leq 1$, but its rate of convergence is known to be slow. Thus, in order to accelerate the convergence rate, we will also consider a variant algorithm of Beck and Teboulle [34] defined as

- Data g , initial set: $f_0 = x_0 = 0$, $t_1 = 1$;
- (1) $x_k = T_{\gamma\eta} (f_k - \gamma \mathcal{R}_\Omega^* Q^* Q [\mathcal{R}_\Omega [f_k] - g])$;
- (2) $f_{k+1} = x_k + \frac{t_k - 1}{t_{k+1}} (x_k - x_{k-1})$ with $t_{k+1} = \frac{1 + \sqrt{1 + 4t_k^2}}{2}$.

The standard choice of Q is the identity, Id , and then it is easy to see that $\|\mathcal{R}_\Omega \mathcal{R}_\Omega^*\| \simeq 2\pi$. It will be also interesting to use $Q = \frac{1}{2\pi} \mathcal{B}^{1/2}$, which is well defined since \mathcal{B} is symmetric and positive. In this case, $\mathcal{R}_\Omega^* Q^* Q \simeq \mathcal{R}_\Omega^{-1}$ and we can hope to improve the convergence rate of the regularized algorithm.

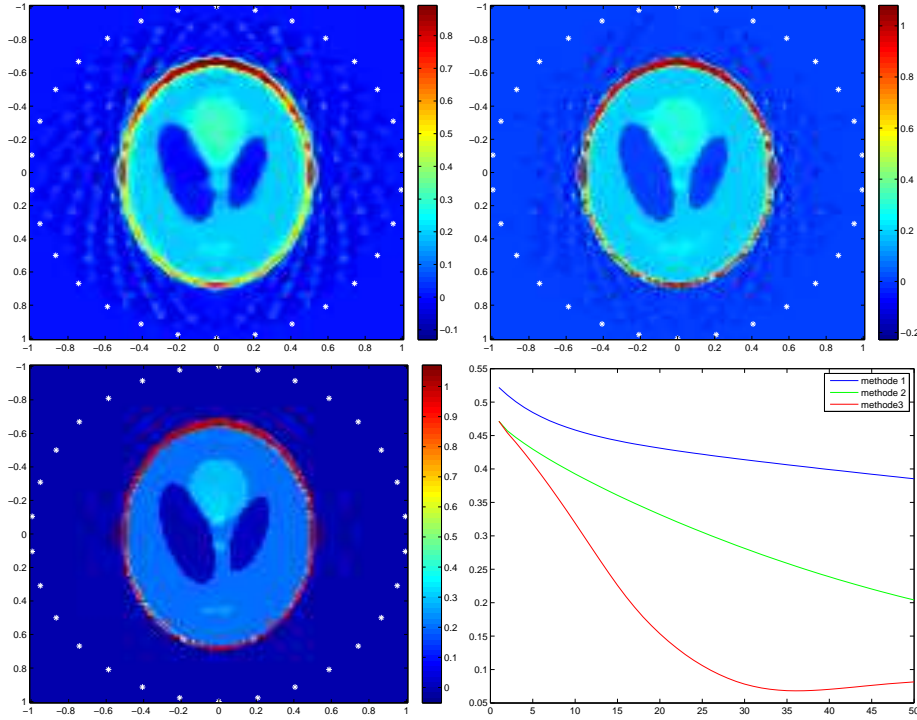


FIGURE 1.3. Iterative shrinkage-thresholding solution after 30 iterations with $\eta = 0.01$, $N = 128$, $N_R = 128$, and $N_\theta = 30$. Top left: simplest algorithm with $Q = \text{Id}$ and $\mu = 1/(2\pi)$; Top right: simplest algorithm with $Q = \frac{1}{2\pi}\mathcal{B}^{1/2}$ and $\mu = 0.5$; Bottom left: Beck and Teboulle variant with $Q = \frac{1}{2\pi}\mathcal{B}^{1/2}$ and $\mu = 0.5$; Bottom right: error $k \rightarrow \|f_k - p_0\|_\infty$ for each of the previous situations.

We compare three algorithms of this kind in Figure 1.3. The first and the second one correspond to the simplest algorithm with $Q = \text{Id}$ and $Q = \frac{1}{2\pi}\mathcal{B}^{1/2}$ respectively. The last method uses the variant of Beck and Teboulle with $Q = \frac{1}{2\pi}\mathcal{B}^{1/2}$. The speed of convergence for each one of these algorithms is presented in Figure 1.3. Clearly, the third method is the best and after 30 iterations, a very good approximation of p_0 is reconstructed.

Two limited-angle experiments are presented in Figure 1.4 using the third algorithm.

1.2.3 COMPENSATION OF THE EFFECT OF ACOUSTIC ATTENUATION

Our aim in this section is to compensate for the effect of acoustic attenuation. The pressures $p(x, t)$ and $p_a(x, t)$ are respectively solutions of the following wave equations:

$$\frac{1}{c_0^2} \frac{\partial^2 p}{\partial t^2}(x, t) - \Delta p(x, t) = \frac{1}{c_0^2} \frac{\partial}{\partial t} \delta_{t=0} p_0(x),$$

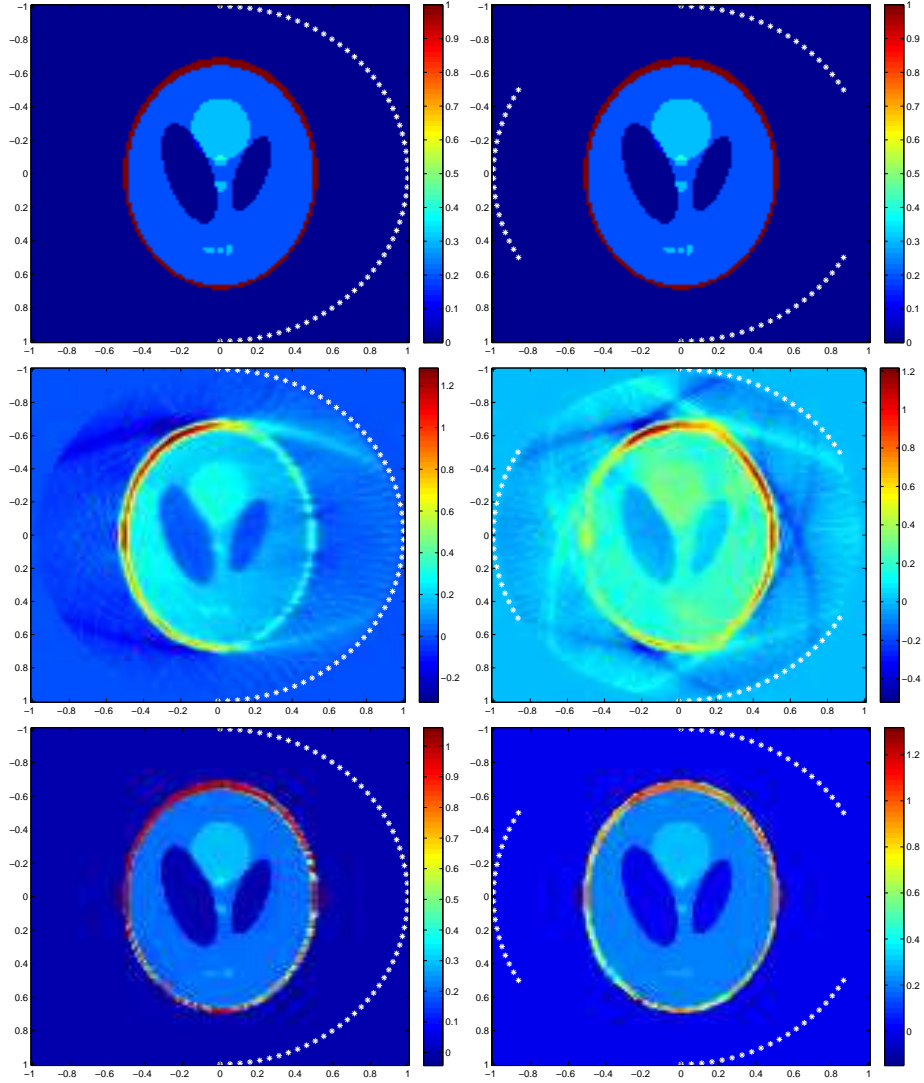


FIGURE 1.4. Limited angle case with Beck and Teboulle iterative shrinkage-thresholding after 50 iterations, with parameters: $\eta = 0.01$, $N = 128$, $N_R = 128$, $N_\theta = 64$ and $Q = \frac{1}{2\pi} \mathcal{B}^{1/2}$. Top to Bottom: p_0 ; $\frac{1}{4\pi^2} \mathcal{R}_\Omega^* \mathcal{B} \mathcal{R}_\Omega [p_0]$; f_{50} . Left: Configuration 1, Right: Configuration 2.

and

$$\frac{1}{c_0^2} \frac{\partial^2 p_a}{\partial t^2}(x, t) - \Delta p_a(x, t) - L(t) * p_a(x, t) = \frac{1}{c_0^2} \frac{\partial}{\partial t} \delta_{t=0} p_0(x),$$

where L is defined by

$$L(t) = \frac{1}{\sqrt{2\pi}} \int_{\mathbb{R}} \left(\kappa^2(\omega) - \frac{\omega^2}{c_0^2} \right) e^{i\omega t} d\omega. \quad (1.5)$$

Many models exist for $\kappa(\omega)$ [82]. Here we use the power-law model. Then $\kappa(\omega)$ is the complex wave number, defined by

$$\kappa(\omega) = \frac{\omega}{c(\omega)} + ia|\omega|^\zeta, \quad (1.6)$$

where ω is the frequency, $c(\omega)$ is the frequency dependent phase velocity and $1 \leq \zeta \leq 2$ is the power-law exponent; see [83, 125]. A common model, known as the thermo-viscous model, is given by $\kappa(\omega) = \frac{\omega}{c_0 \sqrt{1 - ia\omega c_0}}$ and corresponds approximately to $\zeta = 2$ with $c(\omega) = c_0$.

Our strategy is now to:

- Estimate $p(y, t)$ from $p_a(y, t)$ for all $(y, t) \in \partial\Omega \times \mathbb{R}^+$.
- Apply the inverse formula for the spherical Radon transform to reconstruct p_0 from the non-attenuated data.

A natural definition of an attenuated spherical Radon transform $\mathcal{R}_{\Omega, a}$ is

$$\mathcal{R}_{\Omega, a} [p_0] = \mathcal{W} [p_a].$$

1.2.4 RELATIONSHIP BETWEEN p AND p_a

Recall that the Fourier transforms of p and p_a satisfy

$$\left(\Delta + \left(\frac{\omega}{c_0} \right)^2 \right) \widehat{p}(x, \omega) = \frac{i\omega}{\sqrt{2\pi} c_0^2} p_0(x)$$

and

$$(\Delta + \kappa(\omega)^2) \widehat{p}_a(x, \omega) = \frac{i\omega}{\sqrt{2\pi} c_0^2} p_0(x),$$

which implies that

$$\widehat{p}(x, c_0 \kappa(\omega)) = \frac{c_0 \kappa(\omega)}{\omega} \widehat{p}_a(x, \omega).$$

The issue is to estimate p from p_a using the relationship $p_a = \mathcal{L} [p]$, where \mathcal{L} is defined by

$$\mathcal{L} [\phi] (s) = \frac{1}{2\pi} \int_{\mathbb{R}} \frac{\omega}{c_0 \kappa(\omega)} e^{-i\omega s} \int_0^\infty \phi(t) \exp \{ i c_0 \kappa(\omega) t \} dt d\omega.$$

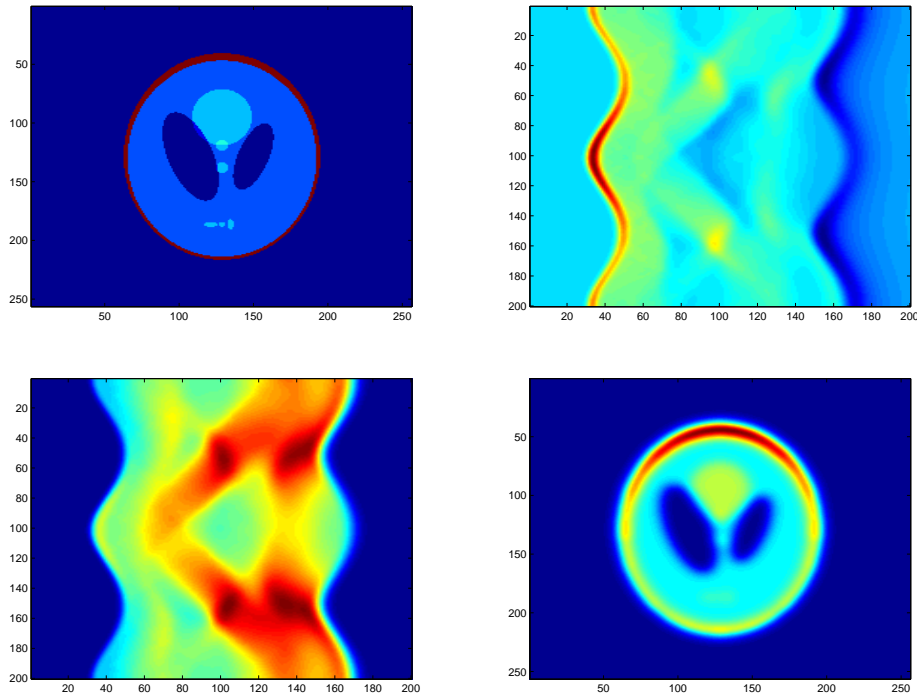


FIGURE 1.5. Numerical inversion of attenuated wave equation with $\kappa(\omega) = \frac{\omega}{c_0} + ia\frac{\omega^2}{2}$ and $a = 0.001$. Here $N = 256$, $N_R = 200$ and $N_\theta = 200$. Top left: p_0 ; Top right: $p_a(y, t)$ with $(y, t) \in \partial\Omega \times (0, 2)$; Bottom left: $\mathcal{W}[p_a](y, t)$ with $(y, t) \in \partial\Omega \times (0, 2)$; Bottom right: $\frac{1}{4\pi^2} \mathcal{R}_\Omega^* \mathcal{B}(\mathcal{W}[p_a](y, t))$.

The main difficulty is that \mathcal{L} is not well conditioned. We will compare two approaches. The first one uses a regularized inverse of \mathcal{L} via a singular value decomposition (SVD), which has been recently introduced in [86]. The second one is based on the asymptotic behavior of \mathcal{L} as the attenuation coefficient a tends to zero.

Figure 1.5 gives some numerical illustrations of the inversion of the attenuated spherical Radon transform without a correction of the attenuation effect, where a thermo-viscous attenuation model is used with $c_0 = 1$.

1.2.5 A SINGULAR VALUE DECOMPOSITION APPROACH

La Rivière, Zhang and Anastasio have recently proposed in [86] to use a regularized inverse of the operator \mathcal{L} obtained by a standard SVD approach:

$$\mathcal{L}[\phi] = \sum_l \sigma_l \langle \phi, \tilde{\psi}_l \rangle \psi_l,$$

where $(\tilde{\psi}_l)$ and (ψ_l) are two orthonormal bases of $L^2(0, T)$ and σ_l are positives eigenvalues such that

$$\begin{cases} \mathcal{L}^*[\phi] &= \sum_l \sigma_l \langle \phi, \psi_l \rangle \tilde{\psi}_l, \\ \mathcal{L}^* \mathcal{L}[\phi] &= \sum_l \sigma_l^2 \langle \phi, \tilde{\psi}_l \rangle \tilde{\psi}_l, \\ \mathcal{L} \mathcal{L}^*[\phi] &= \sum_l \sigma_l^2 \langle \phi, \psi_l \rangle \psi_l. \end{cases}$$

An ϵ -approximation inverse of \mathcal{L} is then given by

$$\mathcal{L}_{1,\epsilon}^{-1}[\phi] = \sum_l \frac{\sigma_l}{\sigma_l^2 + \epsilon^2} \langle \phi, \psi_l \rangle \tilde{\psi}_l,$$

where $\epsilon > 0$.

In Figure 1.6 we present some numerical inversions of the thermo-viscous wave equation with $a = 0.0005$ and $a = 0.0025$. We first obtain the ideal measurements from the attenuated ones and then apply the inverse formula for the spherical Radon transform to reconstruct p_0 from the ideal data. We take ϵ respectively equal to 0.01, 0.001 and 0.0001. As expected, this algorithm corrects a part of the attenuation effect but is unstable when ϵ tends to zero.

1.2.6 ASYMPTOTICS OF \mathcal{L}

In physical situations, the coefficient of attenuation a is very small. We will take this phenomenon into account and introduce an approximation of \mathcal{L} and \mathcal{L}^{-1} as a goes to zero:

$$\mathcal{L}_k[\phi] = \mathcal{L}[\phi] + o(a^{k+1}) \quad \text{and} \quad \mathcal{L}_{2,k}^{-1}[\phi] = \mathcal{L}^{-1}[\phi] + o(a^{k+1}),$$

where k represents an order of approximation.

1.2.6.1 THERMO-VISCOUS CASE: $\kappa(\omega) \simeq \frac{\omega}{c_0} + ia \frac{\omega^2}{2}$

Let us consider in this section the attenuation model $\kappa(\omega) \simeq \frac{\omega}{c_0} + ia \frac{\omega^2}{2}$ at low frequencies $\omega \ll \frac{1}{a}$, such that

$$\frac{1}{1 + ia c_0 \omega / 2} \simeq 1 - i \frac{a c_0}{2} \omega.$$

The operator \mathcal{L} is approximated as follows

$$\mathcal{L}[\phi](s) \simeq \frac{1}{2\pi} \int_0^\infty \phi(t) \int_{\mathbb{R}} \left(1 - i \frac{a c_0}{2} \omega\right) \exp\left\{-\frac{1}{2} c_0 a \omega^2 t\right\} \exp\{i\omega(t-s)\} d\omega dt.$$

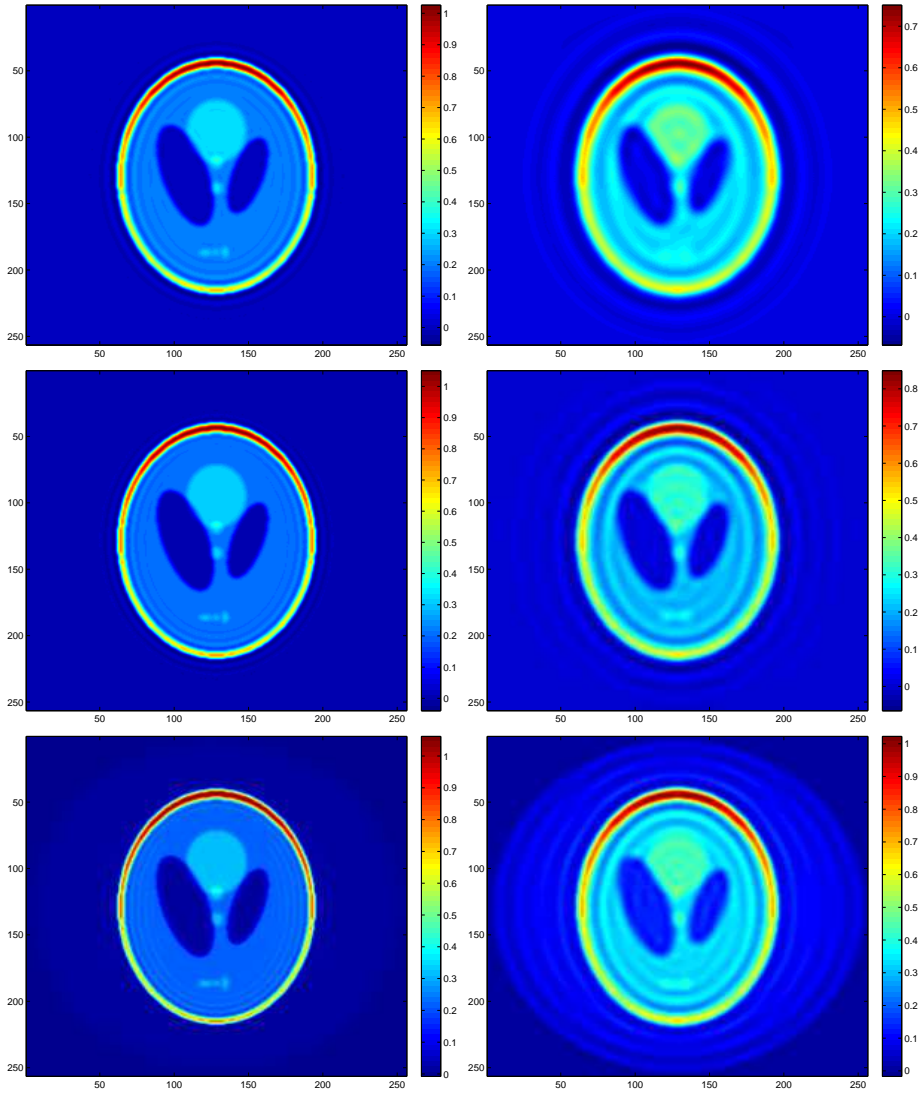


FIGURE 1.6. Compensation of acoustic attenuation with SVD regularization: $N = 256$, $N_R = 200$ and $N_\theta = 200$. Left: $a = 0.0005$; Right: $a = 0.0025$. Top to bottom: $\mathcal{L}_{1,\epsilon}^{-1}$ with $\epsilon = 0.01$, $\epsilon = 0.001$ and $\epsilon = 0.0001$ respectively.

Since

$$\frac{1}{\sqrt{2\pi}} \int_{\mathbb{R}} \exp\left\{-\frac{1}{2}c_0 a \omega^2 t\right\} \exp\{i\omega(t-s)\} d\omega = \frac{1}{\sqrt{c_0 a t}} \exp\left\{-\frac{1}{2} \frac{(s-t)^2}{c_0 a t}\right\},$$

and

$$\frac{1}{\sqrt{2\pi}} \int_{\mathbb{R}} \frac{-i a c_0 \omega}{2} \exp\left\{-\frac{1}{2}c_0 a \omega^2 t\right\} \exp\{i\omega(t-s)\} d\omega = \frac{a c_0}{2} \frac{\partial}{\partial s} \left(\frac{1}{\sqrt{c_0 a t}} \exp\left\{-\frac{1}{2} \frac{(s-t)^2}{c_0 a t}\right\} \right),$$

it follows that

$$\mathcal{L}[\phi] \simeq \left(1 + \frac{a c_0}{2} \frac{\partial}{\partial s}\right) \left(\frac{1}{\sqrt{2\pi}} \int_0^{+\infty} \phi(t) \frac{1}{\sqrt{c_0 a t}} \exp\left\{-\frac{1}{2} \frac{(s-t)^2}{c_0 a t}\right\} dt \right).$$

We then investigate the asymptotic behavior of $\widetilde{\mathcal{L}}$ defined by

$$\widetilde{\mathcal{L}}[\phi] = \frac{1}{\sqrt{2\pi}} \int_0^{+\infty} \phi(t) \frac{1}{\sqrt{c_0 a t}} \exp\left\{-\frac{1}{2} \frac{(s-t)^2}{c_0 a t}\right\} dt. \quad (1.7)$$

Since the phase in (1.7) is quadratic and a is small, by the stationary phase theorem we can prove that

$$\widetilde{\mathcal{L}}[\phi](s) = \sum_{i=0}^k \frac{(c_0 a)^i}{2^i i!} D_i[\phi](s) + o(a^k), \quad (1.8)$$

where the differential operators D_i satisfy $D_i[\phi](s) = (t^i \phi(t))^{(2i)}(s)$; see Appendix 1.A.2. We can also deduce the following approximation of order k of $\widetilde{\mathcal{L}}^{-1}$

$$\widetilde{\mathcal{L}}_k^{-1}[\psi] = \sum_{j=0}^k a^j \psi_{k,j}, \quad (1.9)$$

where $\psi_{k,j}$ are defined recursively by

$$\psi_{k,0} = \psi \quad \text{and} \quad \psi_{k,j} = - \sum_{i=1}^j \frac{c_0^i}{2^i i!} D_i[\psi_{k,j-i}], \quad \text{for all } j \leq k.$$

Finally, we define

$$\mathcal{L}_k = \left(1 + \frac{a c_0}{2} \frac{\partial}{\partial s}\right) \widetilde{\mathcal{L}}_k \quad \text{and} \quad \mathcal{L}_{2,k}^{-1} = \widetilde{\mathcal{L}}_k^{-1} \left(1 + \frac{a c_0}{2} \frac{\partial}{\partial t}\right)^{-1}. \quad (1.10)$$

We present in Figure 1.7 some numerical reconstructions of p_0 using a thermo-viscous wave equation with $a = 0.0005$ and $a = 0.0025$. We take respectively: $k = 0$, $k = 1$ and $k = 8$. These reconstructions seem to be as good as those obtained by the SVD regularization approach. Moreover, this new algorithm has better stability properties.

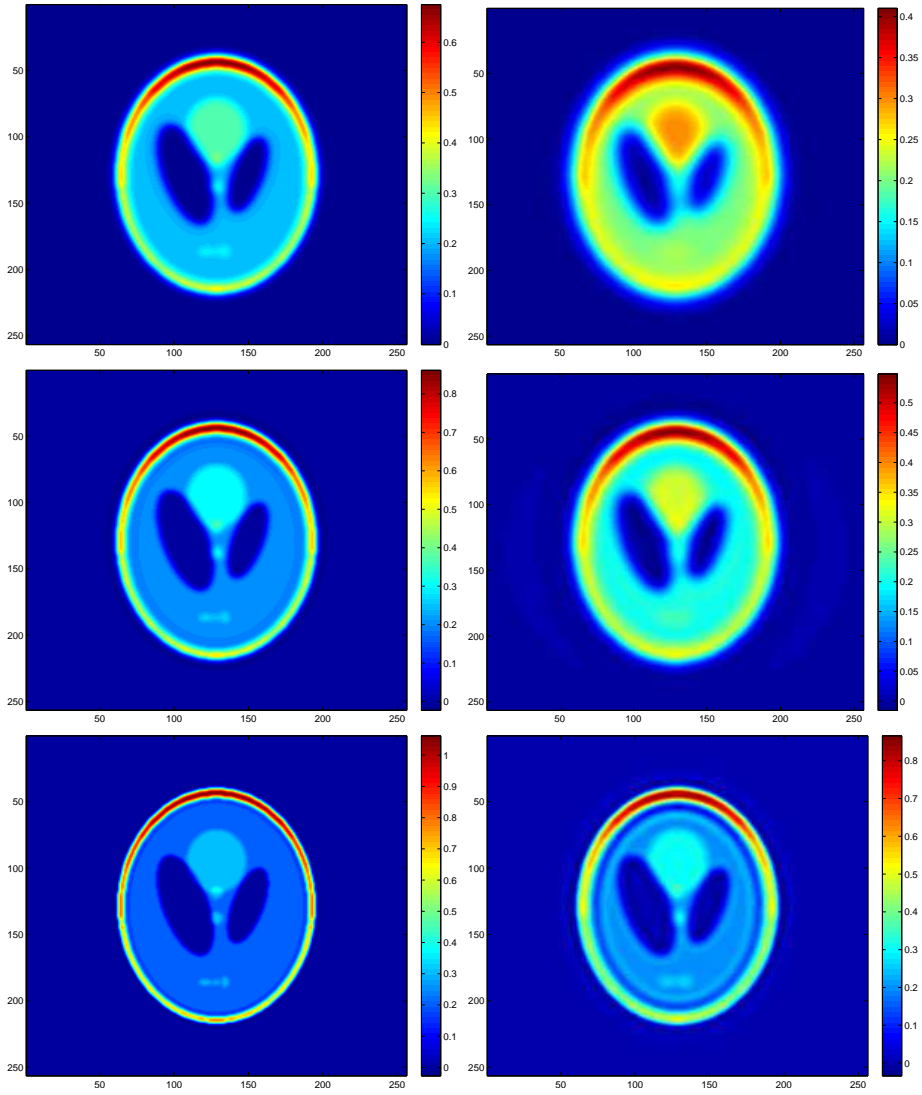


FIGURE 1.7. Compensation of acoustic attenuation with formula (1.10): $N = 256$, $N_R = 200$ and $N_\theta = 200$. Left: $a = 0.0005$; Right: $a = 0.0025$. Top to Bottom: \mathcal{L}_k^{-1} with $k = 0$; $k = 1$ and $k = 8$.

1.2.6.2 GENERAL CASE: $\kappa(\omega) = \frac{\omega}{c_0} + ia|\omega|^\zeta$ WITH $1 \leq \zeta < 2$

We now consider the attenuation model $\kappa(\omega) = \frac{\omega}{c_0} + ia|\omega|^\zeta$ with $1 \leq \zeta < 2$. As before, this problem can be reduced to the approximation of the operator $\widetilde{\mathcal{L}}$ defined by

$$\widetilde{\mathcal{L}}[\phi](s) = \int_0^\infty \phi(t) \int_{\mathbb{R}} \exp\{i\omega(t-s)\} \exp\{-|\omega|^\zeta c_0 a t\} d\omega dt.$$

It is also interesting to see that its adjoint $\widetilde{\mathcal{L}}^*$ satisfies

$$\widetilde{\mathcal{L}}^*[\phi](s) = \int_0^\infty \phi(t) \int_{\mathbb{R}} \exp\{i\omega(s-t)\} \exp\{-|\omega|^\zeta c_0 a s\} d\omega dt.$$

Suppose for the moment that $\zeta = 1$, and working with the adjoint operator \mathcal{L}^* , we see that

$$\widetilde{\mathcal{L}}^*[\phi](s) = \frac{1}{\pi} \int_0^\infty \frac{c_0 a s}{(c_0 a s)^2 + (s-t)^2} \phi(t) dt.$$

Invoking the dominated convergence theorem, we have

$$\begin{aligned} \lim_{a \rightarrow 0} \widetilde{\mathcal{L}}^*[\phi](s) &= \lim_{a \rightarrow 0} \frac{1}{\pi} \int_{-\frac{1}{ac_0}}^\infty \frac{1}{1+y^2} \phi(s+c_0 a y s) dy \\ &= \frac{1}{\pi} \int_{-\infty}^\infty \frac{1}{1+y^2} \phi(s) dy \\ &= \phi(s). \end{aligned}$$

More precisely, introducing the fractional Laplacien $\Delta^{1/2}$ as follows

$$\Delta^{1/2} \phi(s) = \frac{1}{\pi} \text{p.v.} \int_{-\infty}^{+\infty} \frac{\phi(t) - \phi(s)}{(t-s)^2} dt,$$

where p.v. stands for the Cauchy principal value, we get

$$\begin{aligned} \frac{1}{a} (\widetilde{\mathcal{L}}^*[\phi](s) - \phi(s)) &= \frac{1}{a} \int_{-\infty}^\infty \frac{1}{\pi c_0 a s} \frac{1}{1 + \left(\frac{s-t}{c_0 a s}\right)^2} (\phi(t) - \phi(s)) dt \\ &= \int_{-\infty}^\infty \frac{1}{\pi} \frac{c_0 s}{(c_0 a s)^2 + (s-t)^2} (\phi(t) - \phi(s)) dt \\ &= \lim_{\epsilon \rightarrow 0} \int_{\mathbb{R} \setminus [s-\epsilon, s+\epsilon]} \frac{1}{\pi} \frac{c_0 s}{(c_0 a s)^2 + (s-t)^2} (\phi(t) - \phi(s)) dt \\ &\rightarrow \lim_{\epsilon \rightarrow 0} \int_{\mathbb{R} \setminus [s-\epsilon, s+\epsilon]} \frac{1}{\pi} \frac{c_0 s}{(s-t)^2} (\phi(t) - \phi(s)) dt \\ &= c_0 s \Delta^{1/2} \phi(s), \end{aligned}$$

as a tends to zero. We therefore deduce that

$$\widetilde{\mathcal{L}}^*[\phi](s) = \phi(s) + c_0 a s \Delta^{1/2} \phi(s) + o(a)$$

and

$$\widetilde{\mathcal{L}}[\phi](s) = \phi(s) + c_0 a \Delta^{1/2} (s\phi(s)) + o(a).$$

Applying exactly the same argument for $1 < \zeta < 2$, we obtain that

$$\widetilde{\mathcal{L}}^\zeta[\phi](s) = \phi(s) + C c_0 a \Delta^{\zeta/2} (s\phi(s)) + o(a),$$

where C is a constant, depending only on ζ and $\Delta^{\zeta/2}$ is defined by

$$\Delta^{\zeta/2} \phi(s) = \frac{1}{\pi} \text{p.v.} \int_{-\infty}^{+\infty} \frac{\phi(t) - \phi(s)}{(t-s)^{1+\zeta}} dt.$$

1.2.7 AN ITERATIVE SHRINKAGE-THRESHOLDING ALGORITHM WITH CORRECTION OF ATTENUATION

The previous correction of attenuation is not so efficient for a large attenuation coefficient a . In this case, to further enhance the resolution of the reconstruction, we may use again a Tikhonov regularization. Let $\mathcal{R}_{\Omega,a,k}^{-1}$ be an approximate inverse of the attenuated spherical Radon transform $\mathcal{R}_{\Omega,a}$:

$$\mathcal{R}_{\Omega,a,k}^{-1} = \mathcal{R}_{\Omega^{-1}} \mathcal{W} \mathcal{L}_{2,k}^{-1} \mathcal{W}^{-1}.$$

Although its convergence is not clear, we will now consider the following iterative shrinkage-thresholding algorithm:

- Data g , initial set: $f_0 = x_0 = 0$, $t_1 = 1$;
- (1) $x_j = T_{\gamma\eta} \left(f_j - \gamma \mathcal{R}_{\Omega,a,k}^{-1} (\mathcal{R}_{\Omega,a} f_j - g) \right)$;
- (2) $f_{j+1} = x_j + \frac{t_j - 1}{t_{j+1}} (x_j - x_{j-1})$ with $t_{j+1} = \frac{1 + \sqrt{1 + 4t_j^2}}{2}$.

Figure 1.8 shows the efficiency of this algorithm.

1.3 PHOTO-ACOUSTIC IMAGING WITH IMPOSED BOUNDARY CONDITIONS

In this section, we consider the case where a boundary condition has to be imposed on the pressure field. We first formulate the photo-acoustic imaging problem in a bounded domain before reviewing the reconstruction procedures. We refer the reader to [140] where the half-space problem has been considered. We then introduce a new algorithm which reduces the reconstruction problem to the

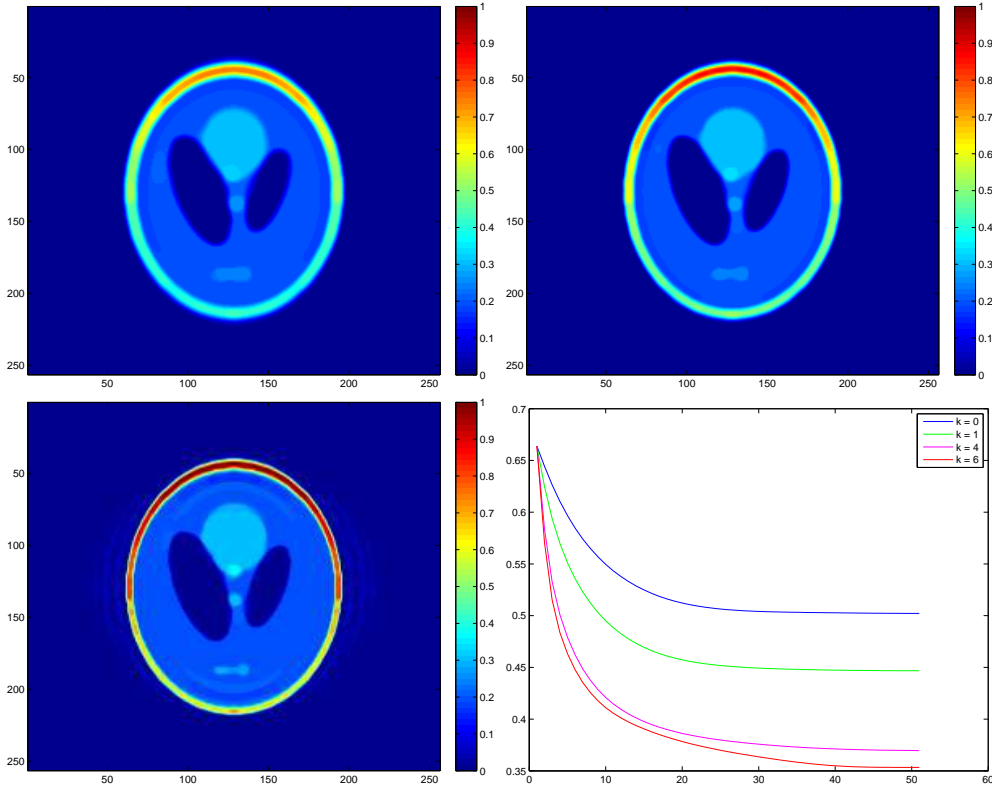


FIGURE 1.8. Numerical results for iterative shrinkage-thresholding algorithm with $\eta = 0.001$ and $a = 0.0025$. Left up: f_{50} with $k = 0$; Top right: f_{50} with $k = 1$; Bottom left: f_{50} with $k = 6$; Bottom right: error $j \rightarrow \|f_j - p_0\|$ for different values of k .

inversion of a Radon transform. This procedure is particularly well-suited for extended absorbers. Finally, we discuss the issue of correcting the attenuation effect and propose an algorithm analogous to the one described in the previous section.

1.3.1 MATHEMATICAL FORMULATION

Let Ω be a bounded domain. We consider the wave equation in the domain Ω :

$$\begin{cases} \frac{1}{c_0^2} \frac{\partial^2 p}{\partial t^2}(x, t) - \Delta p(x, t) = 0 & \text{in } \Omega \times (0, T), \\ p(x, 0) = p_0(x) & \text{in } \Omega, \\ \frac{\partial p}{\partial t}(x, 0) = 0 & \text{in } \Omega, \end{cases} \quad (1.11)$$

with the Dirichlet (resp. the Neumann) imposed boundary conditions:

$$p(x, t) = 0 \quad \left(\text{resp. } \frac{\partial p}{\partial \nu}(x, t) = 0 \right) \quad \text{on } \partial\Omega \times (0, T). \quad (1.12)$$

Our objective in the next subsection is to reconstruct $p_0(x)$ from the measurements of $\frac{\partial p}{\partial \nu}(x, t)$ (resp. $p(x, t)$) on the boundary $\partial\Omega \times (0, T)$.

1.3.2 INVERSION ALGORITHMS

Consider probe functions satisfying

$$\begin{cases} \frac{1}{c_0^2} \frac{\partial^2 v}{\partial t^2}(x, t) - \Delta v(x, t) = 0 & \text{in } \Omega \times (0, T), \\ v(x, T) = 0 & \text{in } \Omega, \\ \frac{\partial v}{\partial t}(x, T) = 0 & \text{in } \Omega. \end{cases} \quad (1.13)$$

Multiplying (1.11) by v and integrating by parts yields (in the case of Dirichlet boundary conditions):

$$\int_0^T \int_{\partial\Omega} \frac{\partial p}{\partial \nu}(x, t) v(x, t) d\sigma(x) dt = \int_{\Omega} p_0(x) \frac{\partial v}{\partial t}(x, 0) dx. \quad (1.14)$$

Choosing a probe function v with proper initial time derivative allows us to infer information on p_0 (right-hand side in (1.14)) from our boundary measurements (left-hand side in (1.14)).

In [11], considering a full view setting, Ammari *et al.* used a 2-parameter travelling plane wave given by

$$v_{\tau, \theta}^{(1)}(x, t) = \delta\left(\frac{x \cdot \theta}{c_0} + t - \tau\right), \quad (1.15)$$

and determined the inclusion's characteristic functions by varying (θ, τ) . They also used in three dimensions the spherical waves given by

$$w_{\tau, y}(x, t) = \frac{\delta\left(t + \tau - \frac{|x-y|}{c_0}\right)}{4\pi|x-y|}, \quad (1.16)$$

for $y \in \mathbb{R}^3 \setminus \Omega$, to probe the medium.

In [10], Ammari *et al.* assumed that the measurements are only made on a part of the boundary $\Gamma \subset \partial\Omega$. Using geometric control, one could choose the form of $\frac{\partial v}{\partial t}(x, 0)$ and design a probe function v satisfying (1.13) together with

$$v(x, t) = 0 \quad \text{on } \partial\Omega \setminus \bar{\Gamma},$$

so that

$$\int_0^T \int_{\Gamma} \frac{\partial p}{\partial \nu}(x, t) v(x, t) d\sigma(x) dt = \int_{\Omega} p_0(x) \frac{\partial v}{\partial t}(x, 0) dx. \quad (1.17)$$

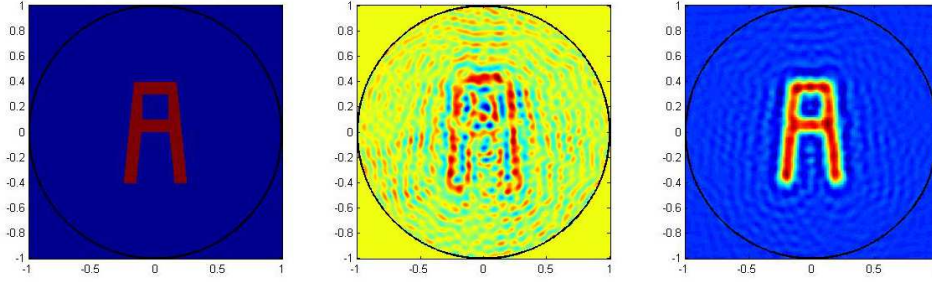


FIGURE 1.9. Reconstruction in the case of homogeneous Dirichlet boundary conditions. Left: initial condition p_0 ; Center: reconstruction using spherical Radon transform; Right: reconstruction using probe functions algorithm.

Varying the choice of $\frac{\partial v}{\partial t}(x, 0)$, one could adapt classical imaging algorithms (MUSIC, back-propagation, Kirchhoff migration, arrival-time) to the case of limited view data.

Now simply consider the 2-parameter family of probe functions:

$$v_{\tau, \theta}^{(2)}(x, t) = 1 - H\left(\frac{x \cdot \theta}{c_0} + t - \tau\right), \quad (1.18)$$

where H is the Heaviside function. The probe function $v_{\tau, \theta}^{(2)}(x, t)$ is an incoming plane wavefront. Its equivalent, still denoted by $v_{\tau, \theta}^{(2)}$ in the limited-view setting satisfies the initial conditions

$$v_{\tau, \theta}^{(2)}(x, 0) = 0 \quad \text{and} \quad \frac{\partial v_{\tau, \theta}^{(2)}}{\partial t}(x, 0) = \delta\left(\frac{x \cdot \theta}{c_0} - \tau\right), \quad (1.19)$$

together with the boundary condition $v_{\tau, \theta}^{(2)} = 0$ on $\partial\Omega \setminus \Gamma \times (0, T)$. In both the full- and the limited-view cases, we get

$$\int_0^T \int_{\partial\Omega \text{ or } \Gamma} \frac{\partial p}{\partial v}(x, t) v_{\tau, \theta}^{(2)}(x, t) d\sigma(x) dt = R[p_0](\theta, \tau), \quad (1.20)$$

where $R[f]$ is the (line) Radon transform of f . Applying a classical filtered back-projection algorithm to the data (1.20), one can reconstruct $p_0(x)$.

To illustrate the need of this approach, we present in Figure 1.9 the reconstructions from data with homogeneous Dirichlet boundary conditions. We compare the reconstruction using the inverse spherical Radon transform with the duality approach presented above. It appears that if we do not take boundary conditions into account, it leads to huge errors in the reconstruction.

We then tested this approach on the Shepp-Logan phantom, using the family of probe functions $v_{\tau, \theta}^{(2)}$. The reconstructions are given in Figure 1.10. We notice numerical noise due to the use of discontinuous (Heaviside) test functions against discrete measurements.

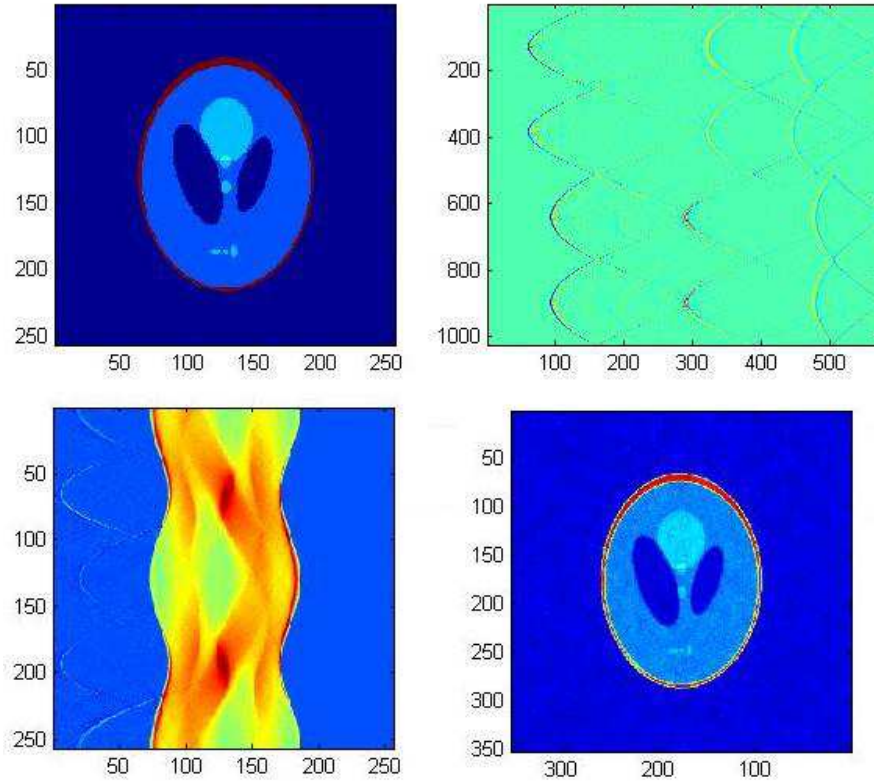


FIGURE 1.10. Numerical inversion in the case of homogeneous Dirichlet boundary conditions. Here, $N = 256$, $N_R = 200$ and $N_\theta = 200$. Top left: p_0 ; Top right: $p(y, t)$ with $(y, t) \in \partial\Omega \times (0, 3)$; Bottom left: $R[p_0]$; Bottom right: reconstruction using probe functions algorithm.

The numerical tests were conducted using MATLAB. Three different forward solvers have been used for the wave equation:

- a FDTD solver, with Newmark scheme for time differentiation;
- a space-Fourier solver, with Crank-Nicholson finite difference scheme in time;
- a space-(P1) FEM-time finite difference solver.

Measurements were supposed to be obtained on equi-distributed captors on a circle or a square. The use of integral transforms (line or spherical Radon transform) avoids inverse crime since such transforms are computed on a different class of parameters (center and radius for spherical Radon transform, direction and shift for line Radon transform). Indeed, their numerical inversion (achieved using formula (1.3) or the iradon function of MATLAB) are not computed on the same grid as the one for the forward solvers.

1.3.3 COMPENSATION OF THE EFFECT OF ACOUSTIC ATTENUATION

Our aim in this section is to compensate for the effect of acoustic attenuation. Let $p_a(x, t)$ be the solution of the wave equation in an attenuating medium:

$$\frac{1}{c_0^2} \frac{\partial^2 p_a}{\partial t^2}(x, t) - \Delta p_a(x, t) - L(t) * p_a(x, t) = \frac{1}{c_0^2} \frac{\partial}{\partial t} \delta_{t=0} p_0(x) \quad \text{in } \Omega \times \mathbb{R}, \quad (1.21)$$

with the Dirichlet (resp. the Neumann) imposed boundary conditions:

$$p_a(x, t) = 0 \quad \left(\text{resp. } \frac{\partial p_a}{\partial \nu}(x, t) = 0 \right) \quad \text{on } \partial\Omega \times \mathbb{R}, \quad (1.22)$$

where L is defined by (1.5).

We want to recover $p_0(x)$ from boundary measurements of $\frac{\partial p_a}{\partial \nu}(x, t)$ (resp. $p_a(x, t)$). Again, we assume that a is small.

Taking the Fourier transform of (1.21), we obtain

$$\begin{cases} (\Delta + \kappa^2(\omega)) \hat{p}_a(x, \omega) = \frac{i\omega}{\sqrt{2\pi}c_0^2} p_0(x) & x \in \Omega, \\ \hat{p}_a(x, \omega) = 0 \quad \left(\text{resp. } \frac{\partial \hat{p}_a}{\partial \nu}(x, \omega) = 0 \right) & x \in \partial\Omega, \end{cases} \quad (1.23)$$

where \hat{p}_a denotes the Fourier transform of p_a .

1.3.4 CASE OF A SPHERICAL WAVE AS A PROBE FUNCTION

By multiplying (1.23) by the Fourier transform, $\hat{w}_{0,y}(x, \omega)$, of $w_{\tau=0,y}$ given by (1.16), we arrive at, for any τ ,

$$\frac{i}{\sqrt{2\pi}} \int_{\Omega} p_0(x) \left(\int_{\mathbb{R}} \omega e^{i\omega\tau} \hat{w}_{0,y}(x, \kappa(\omega)) d\omega \right) dx = \int_{\mathbb{R}} e^{i\omega\tau} \int_{\partial\Omega} \frac{\partial \hat{p}_a}{\partial \nu}(x, \omega) \hat{w}_{0,y}(x, \kappa(\omega)) d\omega, \quad (1.24)$$

for the Dirichlet problem and

$$\frac{i}{\sqrt{2\pi}} \int_{\Omega} p_0(x) \left(\int_{\mathbb{R}} \omega e^{i\omega\tau} \hat{w}_{0,y}(x, \kappa(\omega)) d\omega \right) dx = - \int_{\mathbb{R}} e^{i\omega\tau} \int_{\partial\Omega} \hat{p}_a(x, \omega) \frac{\partial \hat{w}_{0,y}}{\partial \nu}(x, \kappa(\omega)) d\omega, \quad (1.25)$$

for the Neumann problem.

Next, we compute $\int_{\mathbb{R}} \omega e^{i\omega\tau} \hat{w}_{0,y}(x, \kappa(\omega)) d\omega$ for the thermo-viscous model. Recall that in this case,

$$\kappa(\omega) \simeq \frac{\omega}{c_0} + \frac{ia\omega^2}{2}.$$

We have

$$\int_{\mathbb{R}} \omega e^{i\omega\tau} \hat{w}_{0,y}(x, \kappa(\omega)) d\omega \simeq \frac{1}{4\pi|x-y|} \int_{\mathbb{R}} \omega \exp \left\{ i\omega \left(\tau - \frac{|x-y|}{c_0} \right) \right\} \exp \left\{ -a\omega^2 \frac{|x-y|}{c_0} \right\} d\omega, \quad (1.26)$$

and again, the stationary phase theorem can be applied to approximate the inversion procedure for $p_0(x)$.

Note that if we use the Fourier transform \widehat{v} of (1.15) or (1.18) as a test function then we have to truncate the integral in (1.24) since $\widehat{v}(x, \kappa(\omega))$ is exponentially growing in some regions of Ω .

1.3.5 CASE OF A PLANE WAVE AS A PROBE FUNCTION

Let us first introduce the function $\tilde{\kappa}(\omega)$ defined by $\tilde{\kappa}(\omega) = \sqrt{\kappa(\omega)^2}$ and consider a solution of the Helmholtz equation

$$(\Delta + \tilde{\kappa}^2(\omega)) \widehat{v}_a(x, \omega) = 0$$

of the form

$$\widehat{v}_a(x, \omega) = \exp\{-i\omega(x \cdot \theta - c_0\tau)\} g(\omega), \quad (1.27)$$

where $g(\omega)$ decays sufficiently fast.

Multiplying (1.23) by $\overline{\widehat{v}_a(x, \omega)}$, we obtain

$$\frac{i}{\sqrt{2\pi}} \int_{\Omega} p_0(x) \left(\int_{\mathbb{R}} \omega \overline{\widehat{v}_a(x, \omega)} d\omega \right) dx = \int_{\mathbb{R}} \int_{\partial\Omega} \frac{\partial \widehat{p}_a}{\partial \nu}(x, \omega) \overline{\widehat{v}_a(x, \omega)} d\sigma(x) d\omega. \quad (1.28)$$

Since $\tilde{\kappa}(\omega) \simeq \frac{\omega}{c_0} - \frac{ia\omega^2}{2}$, then by taking in formula (1.27)

$$g(\omega) = \exp\left\{-\frac{1}{2}\omega^2 ac_0 T\right\} \quad \text{and} \quad g(\omega) = \frac{1}{i\omega} \exp\left\{-\frac{1}{2}\omega^2 ac_0 T\right\},$$

we can use the plane waves $\widehat{v}_a^{(1)}$ and $\widehat{v}_a^{(2)}$ given by

$$\begin{aligned} \widehat{v}_a^{(1)}(x, \omega) &= \exp\{-i\omega(x \cdot \theta - c_0\tau)\} \exp\left\{-\frac{1}{2}\omega^2 ac_0 \left(T + \frac{x \cdot \theta}{c_0} - \tau\right)\right\}, \\ \widehat{v}_a^{(2)}(x, \omega) &= \frac{1}{i\omega} \exp\{-i\omega(x \cdot \theta - c_0\tau)\} \exp\left\{-\frac{1}{2}\omega^2 ac_0 \left(T + \frac{x \cdot \theta}{c_0} - \tau\right)\right\}, \end{aligned}$$

as approximate probe functions.

Take T sufficiently large such that $\left(T + \frac{x \cdot \theta}{c_0} - \tau\right)$ stays positive for all $x \in \Omega$. Thus,

$$v_a^{(1)}(x, t) \simeq \frac{1}{\sqrt{ac_0 \left(T + \frac{x \cdot \theta}{c_0} - \tau\right)}} \exp\left\{-\frac{(x \cdot \theta - c_0\tau + t)^2}{2ac_0 \left(T + \frac{x \cdot \theta}{c_0} - \tau\right)}\right\},$$

and

$$v_a^{(2)}(x, t) \simeq \operatorname{erf}\left(\frac{x \cdot \theta - c_0\tau + t}{\sqrt{ac_0 \left(T + \frac{x \cdot \theta}{c_0} - \tau\right)}}\right).$$

Now using $v_a^{(2)}$ in formula (1.28) leads to the convolution of the Radon transform of p_0 with a quasi-Gaussian kernel. Indeed, the left hand-side of (1.28) satisfies

$$\begin{aligned} & \frac{i}{\sqrt{2\pi}} \int_{\Omega} p_0(x) \left(\int_{\mathbb{R}} \overline{\omega \widehat{v}_a^{(2)}(x, \omega)} d\omega \right) dx \\ & \simeq \int_{\Omega} p_0(x) \frac{1}{\sqrt{ac_0 \left(T + \frac{x \cdot \theta}{c_0} - \tau \right)}} \exp \left\{ -\frac{(x \cdot \theta - c_0 \tau)^2}{2ac_0 \left(T + \frac{x \cdot \theta}{c_0} - \tau \right)} \right\} dx \\ & = \int_{s_{min}}^{s_{max}} R[p_0](\theta, s) \frac{1}{\sqrt{ac_0 \left(T + \frac{s}{c_0} - \tau \right)}} \exp \left\{ -\frac{(s - c_0 \tau)^2}{2ac_0 \left(T + \frac{s}{c_0} - \tau \right)} \right\} ds, \end{aligned}$$

and the right hand-side is explicitly estimated by

$$\int_{\mathbb{R}} \int_{\partial\Omega} \frac{\partial \widehat{p}_a}{\partial \nu}(x, \omega) \overline{\widehat{v}_a^{(2)}(x, \omega)} d\sigma(x) d\omega \simeq \int_0^T \int_{\partial\Omega} \frac{\partial p_a}{\partial \nu}(x, t) \cdot \operatorname{erf} \left(\frac{x \cdot \theta - c_0 \tau + t}{\sqrt{ac_0 \left(T + \frac{x \cdot \theta}{c_0} - \tau \right)}} \right) d\sigma(x) dt.$$

As previously, we can compensate the effect of attenuation using the stationary phase theorem on the operator $\widetilde{\mathcal{L}}$,

$$\widetilde{\mathcal{L}}[\phi](\tau) = \int_{s_{min}}^{s_{max}} \phi(s) \frac{1}{\sqrt{ac_0 \left(T + \frac{s}{c_0} - \tau \right)}} \exp \left\{ -\frac{(s - c_0 \tau)^2}{2ac_0 \left(T + \frac{s}{c_0} - \tau \right)} \right\} ds,$$

which reads

$$\widetilde{\mathcal{L}}[\phi](\tau) \simeq \phi(c_0 \tau) + \frac{ac_0 T}{2} \left(\phi''(c_0 \tau) + \frac{2\phi'(c_0 \tau)}{c_0 T} \right); \quad (1.29)$$

see appendix 1.A.3. More generally,

$$\widetilde{\mathcal{L}}[\phi](\tau) = \sum_{i=0}^k \frac{(c_0 a)^i}{2^i i!} D_i[\phi] + o(a^k), \quad (1.30)$$

where the differential operators D_i satisfy

$$D_i[\phi] = \left[\left(\left(T + \frac{s}{c_0} - \tau \right)^i [\phi](s) \right)^{(2i)} \right]_{s=c_0 \tau}.$$

Define $\widetilde{\mathcal{L}}_k^{-1}$ as in (1.9). Using (1.30), we reconstruct the line Radon transform of p_0 correcting the effect of attenuation. We then apply a standard filtered back-projection algorithm to inverse the Radon transform. Results are presented in Figure 1.11.

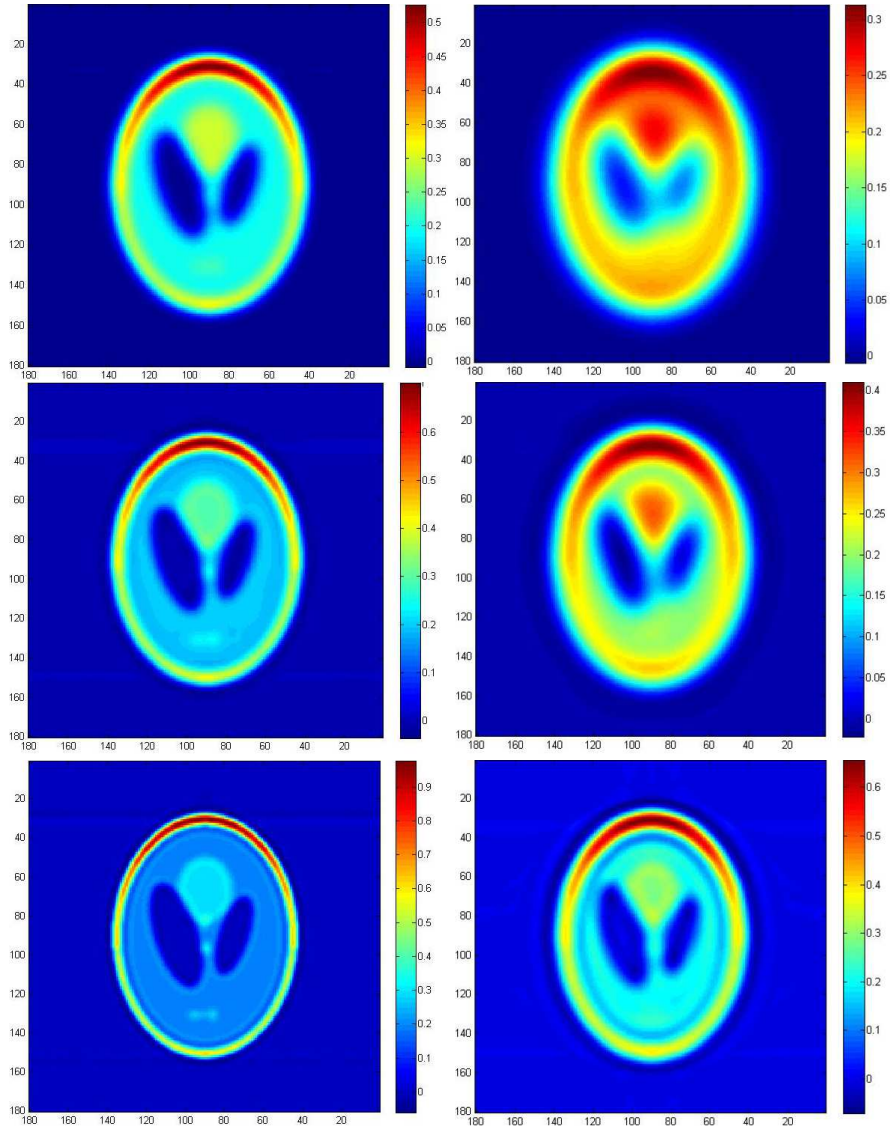


FIGURE 1.11. Compensation of acoustic attenuation with formula (1.29) in the case of homogeneous Dirichlet boundary conditions. Here, $N = 256$, $N_R = 200$ and $N_\theta = 200$. Left: $a = 0.0005$; Right: $a = 0.0025$. Top to Bottom: $\tilde{\mathcal{L}}_k^{-1}$ with $k = 0$; $k = 1$ and $k = 8$.

1.4 CONCLUSION

In this chapter we have provided new approaches to correct the effect of imposed boundary conditions as well as the effect of acoustic attenuation. It is interesting to analytically investigate their robustness with respect to measurement noise and medium noise. In this connection, we refer to [13] for a coherent interferometric strategy for photo-acoustic imaging in the presence of microscopic random fluctuations of the speed of sound.

Finally, it is worth emphasizing that it is the absorption coefficient, not the absorbed energy, that is a fundamental physiological parameter. The absorbed energy density is in fact the product of the optical absorption coefficient and the light fluence which depends on the distribution of scattering and absorption within the domain, as well as the light sources. In [12], methods for reconstructing the normalized optical absorption coefficient of small absorbers from the absorbed density are proposed. Multi-wavelength acoustic measurements are combined with diffusing light measurements to separate the product of absorption coefficient and optical fluence. In the case of extended absorbers, multi-wavelength photo-acoustic imaging is also expected to lead to a satisfactory solution [54].

1.A STATIONARY PHASE THEOREM AND PROOFS

1.A.1 STATIONARY PHASE THEOREM

THEOREM 1.A.1. (*Stationary Phase [78]*)

Let $K \subset [0, \infty)$ be a compact set, X an open neighbourhood of K and k a positive integer. If $\psi \in \mathcal{C}_0^{2k}(K)$, $f \in \mathcal{C}^{3k+1}(X)$ such that

$$\Im m\{f\} \geq 0 \text{ in } X, \quad \Im m\{f(t_0)\} = 0, \quad f'(t_0) = 0, \quad f''(t_0) \neq 0, \quad f' \neq 0 \text{ in } K \setminus \{t_0\}$$

then for $\epsilon > 0$

$$\left| \int_K \psi(t) e^{if(t)/\epsilon} dt - e^{if(t_0)/\epsilon} (\epsilon^{-1} f''(t_0)/2\pi i)^{-1/2} \sum_{j < k} \epsilon^j L_j[\psi] \right| \leq C \epsilon^k \sum_{\alpha \leq 2k} \sup_x |\psi^{(\alpha)}(x)|.$$

Here C is bounded when f stays in a bounded set in $\mathcal{C}^{3k+1}(X)$ and $\left| \frac{t-t_0}{f'(t)} \right|$ has a uniform bound. With,

$$g_{t_0}(t) = f(t) - f(t_0) - \frac{1}{2} f''(t_0)(t-t_0)^2,$$

which vanishes up to third order at t_0 , and

$$L_j[\psi] = \sum_{\nu-\mu=j} \sum_{2\nu \geq 3\mu} i^{-j} \frac{2^{-\nu}}{\nu! \mu!} (-1)^\nu f''(t_0)^{-\nu} \left(g_{t_0}^\mu \psi \right)^{(2\nu)}(t_0).$$

We will use this theorem with $k = 2$. Note that L_1 can be expressed as the sum

$$L_1[\psi] = L_1^{(1)}[\psi] + L_1^{(2)}[\psi] + L_1^{(3)}[\psi],$$

where $L_1^{(j)}$ is respectively associated to the couple $(\nu_j, \mu_j) = (1, 0), (2, 1), (3, 2)$ and is identified as

$$\left\{ \begin{array}{l} L_1^{(1)}[\psi] = -\frac{1}{2i} f''(t_0)^{-1} \psi^{(2)}(t_0), \\ L_1^{(2)}[\psi] = \frac{1}{2^2 2! i} f''(t_0)^{-2} (g_{t_0} \psi)^{(4)}(t_0) \\ \quad = \frac{1}{8i} f''(t_0)^{-2} \left(g_{t_0}^{(4)}(t_0) \psi(t_0) + 4g_{t_0}^{(3)}(t_0) \psi'(t_0) \right), \\ L_1^{(3)}[\psi] = \frac{-1}{2^3 2! 3! i} f''(t_0)^{-3} \left(g_{t_0}^2 \psi \right)^{(6)}(t_0) \\ \quad = \frac{-1}{2^3 2! 3! i} f''(t_0)^{-3} \left(g_{t_0}^2 \right)^{(6)}(t_0) \psi(t_0). \end{array} \right.$$

1.A.2 PROOF OF APPROXIMATION (1.8)

Let us now apply the stationary phase theorem to the operator $\widetilde{\mathcal{L}}$

$$\widetilde{\mathcal{L}}[\phi] = \frac{1}{\sqrt{2\pi}} \int_0^{+\infty} \phi(t) \frac{1}{\sqrt{c_0 a t}} \exp\left\{-\frac{1}{2} \frac{(s-t)^2}{c_0 a t}\right\} dt.$$

Note that the integral

$$J(s) = \int_0^{\infty} \psi(t) e^{if(t)/\epsilon} dt,$$

with

$$\psi(t) = \frac{\phi(t)}{\sqrt{t}}, \quad \epsilon = c_0 a, \quad f(t) = i \frac{(t-s)^2}{2t},$$

satisfies $J(s) = \sqrt{2c_0 a \pi} \widetilde{\mathcal{L}}[\phi]$. The phase f vanishes at $t = s$ and satisfies

$$f'(t) = i \frac{1}{2} \left(1 - \frac{s^2}{t^2} \right), \quad f''(t) = i \frac{s^2}{t^3}, \quad f''(s) = i \frac{1}{s}.$$

The function $g_s(t)$ is given by

$$g_s(t) = i \frac{1}{2} \frac{(t-s)^2}{t} - i \frac{1}{2} \frac{(t-s)^2}{s} = i \frac{(s-t)^3}{2ts}.$$

We can deduce that

$$\left\{ \begin{array}{l} (g_s \psi)^{(4)}(s) = \left(g_{x_0}^{(4)}(s) \psi(s) + 4g_{x_0}^{(3)}(s) \psi'(s) \right) \\ \quad = i \frac{1}{2} \left(\frac{24}{s^3} \psi(s) - \frac{24}{s^2} \psi'(s) \right), \\ (g_s^2 \psi)^{(6)}(s) = \left(g_{x_0}^2 \right)^{(6)}(s) \psi(s) \\ \quad = -\frac{1}{4} \frac{6!}{s^4} \psi(s), \end{array} \right.$$

and then, with the same notation as in Theorem 1.A.1,

$$\left\{ \begin{array}{l} L_1^{(1)}[\psi] = -\frac{1}{i} \left(\frac{1}{2} (f''(s))^{-1} \psi''(s) \right) \\ \quad = \frac{1}{2} s \left(\frac{\phi}{\sqrt{s}} \right)'' \\ \quad = \frac{1}{2} \left(\sqrt{s} \phi''(s) - \frac{\phi'(s)}{\sqrt{s}} + \frac{3}{4} \frac{\phi}{s^{3/2}} \right), \\ L_1^{(2)}[\psi] = \frac{1}{8i} f''(s)^{-2} (g_s^{(4)}(s) \psi(s) + 4g_s^{(3)}(s) \psi'(s)) \\ \quad = \frac{1}{2} \left(3 \left(\frac{\phi(s)}{\sqrt{s}} \right)' - 3 \frac{\phi(s)}{s^{3/2}} \right) \\ \quad = \frac{1}{2} \left(3 \frac{\phi'(s)}{\sqrt{s}} - \frac{9}{2} \frac{\phi(s)}{s^{3/2}} \right), \\ L_1^{(3)}[\psi] = \frac{-1}{2^3 2! 3! i} f''(s)^{-3} (g_s^{(2)})^{(6)}(s) \psi(s) \\ \quad = \frac{1}{2} \left(\frac{15}{4} \frac{\phi(s)}{s^{3/2}} \right). \end{array} \right.$$

The operator L_1 is given by

$$\begin{aligned} L_1[\psi] &= L_1^{(1)}[\psi] + L_1^{(2)}[\psi] + L_1^{(3)}[\psi] \\ &= \frac{1}{2} \left(\sqrt{s} \phi''(s) + (3-1) \frac{\phi'(s)}{\sqrt{s}} + \left(\frac{3}{4} - \frac{9}{2} + \frac{15}{4} \right) \frac{\phi(s)}{s^{3/2}} \right) \\ &= \frac{1}{2\sqrt{s}} (s\phi(s))'', \end{aligned}$$

and so,

$$\left| J(s) - \sqrt{2\pi a c_0 s} \left(\frac{\phi(s)}{\sqrt{s}} + a \frac{1}{2\sqrt{s}} (s\phi(s))'' \right) \right| \leq C a^2 \sum_{\alpha \leq 4} \sup |\phi^{(\alpha)}(x)|.$$

Finally, we arrive at

$$\left| \frac{1}{\sqrt{2\pi}} \int_0^\infty \phi(t) \frac{1}{\sqrt{a c_0 t}} \exp \left\{ -\frac{(t-s)^2}{2 a c_0 t} \right\} dt - \left(\phi(s) + \frac{a}{2} (s\phi(s))'' \right) \right| \leq C a^{3/2} \sum_{\alpha \leq 4} \sup |\phi^{(\alpha)}(t)|.$$

1.A.3 PROOF OF APPROXIMATION (1.29)

Let us now apply the stationary phase theorem to the operator \mathcal{L} defined by

$$\begin{aligned} \widetilde{\mathcal{L}}[\phi](\tau) &= \frac{1}{\sqrt{2\pi}} \int_{s_{min}}^{s_{max}} \left[\phi(s) [a(c_0 T + s - c_0 \tau)]^{-\frac{1}{2}} \exp \left\{ -\frac{(s - c_0 \tau)^2}{2a(c_0 T + s - c_0 \tau)} \right\} \right] ds \\ &= \frac{1}{\sqrt{2\pi}} \int_{s_{min} - c_0 \tau}^{s_{max} - c_0 \tau} \left[\phi(t + c_0 \tau) [a(\widetilde{T} + t)]^{-\frac{1}{2}} \exp \left\{ -\frac{t^2}{2a(\widetilde{T} + t)} \right\} \right] dt, \end{aligned}$$

where $\tilde{T} = c_0 T$. Note that the integral

$$J(\tau) = \int_{s_{\min} - c_0 \tau}^{s_{\max} - c_0 \tau} \psi(t) e^{if(t)/\epsilon} dt,$$

with

$$\psi(t) = \frac{\phi(t + c_0 \tau)}{\sqrt{\tilde{T} + t}} \quad \epsilon = a \quad f(t) = i \frac{t^2}{2(\tilde{T} + t)},$$

satisfies $J(\tau) = \sqrt{a2\pi} \tilde{\mathcal{L}}[\phi]$.

The phase f vanishes at $t = 0$ and satisfies

$$f'(t) = i \frac{1}{2} \frac{t(t + 2\tilde{T})}{(t + \tilde{T})^2}, \quad f''(t) = i \frac{\tilde{T}^2}{(t + \tilde{T})^3}, \quad f''(0) = i \frac{1}{\tilde{T}}.$$

The function $g_0(t)$ is identified as

$$g_0(t) = -i \frac{1}{2} \frac{t^3}{\tilde{T}(\tilde{T} + t)}.$$

We have

$$\left\{ \begin{array}{l} (g_0 \psi)^{(4)}(0) = (g_0^{(4)}(0) \psi(0) + 4g_0^{(3)}(0) \psi'(0)) \\ \quad = i \frac{1}{2} \left(\frac{24}{\tilde{T}^3} \psi(0) - \frac{24}{\tilde{T}^2} \psi'(0) \right), \\ (g_0^2 \psi)^{(6)}(0) = (g_0^2)^{(6)}(0) \psi(0) \\ \quad = -\frac{1}{4} \frac{6!}{\tilde{T}^4} \psi(0), \end{array} \right.$$

and

$$\psi(0) = \frac{\phi(c_0 \tau)}{\tilde{T}^{1/2}}, \quad \psi'(0) = \frac{\phi'(c_0 \tau)}{\tilde{T}^{1/2}} - \frac{1}{2} \frac{\phi(c_0 \tau)}{\tilde{T}^{3/2}}, \quad \psi''(0) = \frac{\phi''(c_0 \tau)}{\tilde{T}^{1/2}} - \frac{\phi'(c_0 \tau)}{\tilde{T}^{3/2}} + \frac{3}{4} \frac{\phi(c_0 \tau)}{\tilde{T}^{5/2}}.$$

Therefore, again with the same notation as in Theorem 1.A.1,

$$\left\{ \begin{array}{l} L_1^{(1)}[\psi] = -\frac{1}{i} \left(\frac{1}{2} (f''(0))^{-1} \psi''(0) \right) \\ \quad = \frac{1}{2} \left(\sqrt{\tilde{T}} \phi''(c_0 \tau) - \frac{\phi'(c_0 \tau)}{\tilde{T}^{1/2}} + \frac{3}{4} \frac{\phi(c_0 \tau)}{\tilde{T}^{3/2}} \right), \\ L_1^{(2)}[\psi] = \frac{1}{8i} f''(0)^{-2} \left(g_0^{(4)}(0) \psi(0) + 4g_0^{(3)}(0) \psi'(0) \right) \\ \quad = \frac{1}{2} \left(3\psi'(0) - 3 \frac{\psi(0)}{\tilde{T}} \right) \\ \quad = \frac{1}{2} \left(3 \frac{\phi'(c_0 \tau)}{\tilde{T}^{1/2}} - \frac{9}{2} \frac{\phi(c_0 \tau)}{\tilde{T}^{3/2}} \right), \\ L_1^{(3)}[\psi] = -\frac{1}{2^3 2! 3! i} f''(0)^{-3} (g_0^2)^{(6)}(0) \psi(0) \\ \quad = \frac{1}{2} \left(\frac{15}{4} \frac{\phi(c_0 \tau)}{\tilde{T}^{3/2}} \right), \end{array} \right.$$

and L_1 is given by

$$\begin{aligned} L_1[\psi] &= L_1^{(1)}[\psi] + L_1^{(2)}[\psi] + L_1^{(3)}[\psi] \\ &= \frac{1}{2\sqrt{\tilde{T}}} \left(\tilde{T}\phi''(c_0\tau) + 2\phi'(c_0\tau) \right) \\ &= \frac{1}{2\sqrt{\tilde{T}}} \left[\left((s - c_0\tau + \tilde{T})\phi'(s) \right)' \right]_{s=c_0\tau}, \end{aligned}$$

which yields

$$\left| J(\tau) - \sqrt{2\pi a} \left(\phi(c_0\tau) + a/2 \left[\left((s - c_0\tau + c_0T)\phi'(s) \right)' \right]_{s=c_0\tau} \right) \right| \leq Ca^2 \sum_{\alpha \leq 4} \sup |\phi^{(\alpha)}(x)|.$$

Hence,

$$\left| \tilde{\mathcal{L}}[\phi] - \left[\phi(c_0\tau) + \frac{ac_0T}{2} \left(\phi''(c_0\tau) + \frac{2\phi'(c_0\tau)}{c_0T} \right) \right] \right| \leq Ca^{3/2} \sum_{\alpha \leq 4} \sup |\phi^{(\alpha)}(t)|.$$

2.1 INTRODUCTION

Many inverse problems in biomedical imaging are concerned with the determination of strength and location of sources causing fluctuations in the medium properties [7, 11, 12, 19, 65]. Given the measurements on a detection surface, these problems are equivalent to find the *initial conditions* on the wavefield, provided that the sources are temporally localized. The goal of finding such initial conditions, can be achieved by using the so called *time reversibility* of the wave equations in non-dissipative media. It is possible to reverse a wave from a *final state* in such a way that it retraces its original path back through the medium and refocuses on the source location. This provides the basis of the time-reversal technique. See for instance [7, 30, 31, 38, 56, 62, 63, 65, 129] and references therein for comprehensive details. See also [20, 25, 147] for applications of time reversal techniques in biomedical imaging.

In acoustic imaging, a challenging problem is to model the acoustic attenuation and to compensate for its effect in image reconstruction [82, 86, 109, 132, 134]. In this chapter, we consider the problem of reconstructing sources in attenuating acoustic media using a time-reversal technique. It is motivated by the recent works on hybrid imaging using acoustics such as photoacoustic imaging [10, 11, 12], magneto-acoustic imaging [19], and radiation force imaging [20]. Classical time-reversal methods, without taking account of the attenuation effect, produce blurring in reconstructing source terms. Indeed attenuation is a key issue as it breaks down the time reversibility of the wave equation. Some recent works propose to modify the time-reversal process by using the adjoint of the attenuated wave operator instead of the ideal one [41, 134]. In this chapter, we aim to justify this technique as a first order correction of the attenuation effect. At the same time, we also present a modified approach for higher order corrections. We use a thermo-viscous law model for the attenuation losses. However, our analysis can be extended to more general power law attenuation

models with fractional exponents.

The rest of this chapter is organized as follows. In Section 2.2, we recall two classical time reversal methods for the acoustic wave equation in an ideal acoustic medium. In Section 2.3, we propose and analyze a time reversal method for attenuating acoustic media. In Section 2.4, we present an alternative approach which consists of pre-processing the data before applying the classical time reversal algorithm. In Section 2.5, we present the numerical illustrations to compare different variants of the time reversal and to highlight the potential of our approach. Finally, the chapter ends with a short discussion and a conclusion in Section 2.6.

2.2 TIME REVERSAL IN HOMOGENEOUS MEDIA WITHOUT ATTENUATION

Let Ω be a smooth bounded domain in \mathbb{R}^d , $d = 2$ or 3 . Consider the acoustic wave equation

$$\begin{cases} \frac{\partial^2}{\partial t^2} p(x, t) - \Delta p(x, t) = \frac{\partial \delta_0}{\partial t}(t) f(x), & (x, t) \in \mathbb{R}^d \times [0, \infty[, \\ p(x, t) = 0 \quad \text{and} \quad \frac{\partial p(x, t)}{\partial t} = 0, & t \ll 0. \end{cases} \quad (2.1)$$

where δ_0 is the Dirac mass at $t = 0$ and the source f is smooth and has a smooth support $K \subset\subset \Omega$. We assume that f is a real-valued function. Equation (2.1) models photoacoustic imaging with f being the absorbed optical energy density [11].

Let $g(y, t)$ be defined as $g(y, t) := p(y, t)$ for all $y \in \partial\Omega$ and $t \in [0, T]$, where T is supposed to be sufficiently large such that $p(x, t) = 0 = \frac{\partial p(x, t)}{\partial t}$ for $t \geq T$ and $x \in \Omega$. Our aim in this section is to reconstruct an approximation of the source f from g on $\partial\Omega \times [0, T]$.

In the sequel, \mathcal{F} denotes the Fourier transform, that is

$$\mathcal{F}[v](x, \omega) = \frac{1}{\sqrt{2\pi}} \int_{\mathbb{R}} v(x, t) e^{i\omega t} dt.$$

We also introduce

$$\begin{aligned} \Gamma(x, y, \tau, t) &= \mathcal{F}^{-1}[\Gamma_\omega(x, y)](t - \tau) \\ &= \frac{1}{\sqrt{2\pi}} \int_{\mathbb{R}} \Gamma_\omega(x, y) \exp\{-i\omega(t - \tau)\} d\omega. \end{aligned}$$

where $\Gamma_\omega(x, y)$ is the outgoing fundamental solution to the Helmholtz equation $-(\Delta + \omega^2)$ in \mathbb{R}^d *i.e.*

$$(\Delta_y + \omega^2)\Gamma_\omega(x, y) = -\delta_x(y) \quad \forall y \in \mathbb{R}^d,$$

subject to the outgoing radiation condition.

2.2.1 IDEAL TIME REVERSAL IMAGING TECHNIQUE

Introduce the solution v of the following wave problem

$$\begin{cases} \frac{\partial^2 v}{\partial t^2}(x, t) - \Delta v(x, t) = 0, & (x, t) \in \Omega \times [0, T], \\ v(x, 0) = 0 = \frac{\partial v}{\partial t}(x, 0), & x \in \Omega, \\ v(x, t) = g(x, T - t), & (x, t) \in \partial\Omega \times [0, T]. \end{cases}$$

The time-reversal imaging functional $\mathcal{I}_1(x)$ reads

$$\mathcal{I}_1(x) = v(x, T), \quad x \in \Omega.$$

In order to study $\mathcal{I}_1(x)$, we introduce the Dirichlet Green Function $G(x, y, \tau, t)$ defined as the solution of the following wave equation

$$\begin{cases} \frac{\partial^2 G}{\partial t^2}(x, y, \tau, t) - \Delta_y G(x, y, \tau, t) = \delta_x \delta_\tau, & (y, t) \in \Omega \times \mathbb{R}, \\ G(x, y, \tau, t) = 0, \quad \frac{\partial G}{\partial t}(x, y, \tau, t) = 0, & t \ll \tau, \\ G(x, y, \tau, t) = 0, & (y, t) \in \partial\Omega \times \mathbb{R}, \end{cases}$$

where δ_x and δ_τ are the Dirac masses at x and at τ respectively.

Using the reversibility of the wave equation, we arrive at

$$\mathcal{I}_1(x) = v(x, T) = \int_0^T \int_{\partial\Omega} \frac{\partial G}{\partial \nu_y}(x, y, \tau, t) g(y, T - t) d\sigma(y) dt. \quad (2.2)$$

where $\frac{\partial}{\partial \nu_y}$ denotes the normal derivative at $y \in \partial\Omega$. In identity (2.2), the dependence of the time-reversal functional \mathcal{I}_1 on the boundary data g is explicitly shown. Moreover, since

$$g(y, s) = \int_{\Omega} \frac{\partial \Gamma}{\partial t}(z, y, 0, s) f(z) dz \Big|_{y \in \partial\Omega},$$

it follows that

$$\mathcal{I}_1(x) = \int_{\Omega} f(z) \int_0^T \int_{\partial\Omega} \frac{\partial G}{\partial \nu_y}(x, y, T, t) \frac{\partial \Gamma}{\partial t}(z, y, 0, T - t) d\sigma(y) dt dz.$$

2.2.2 MODIFIED TIME-REVERSAL IMAGING TECHNIQUE

In this section, we present a modified approach to the time-reversal concept using *free boundary conditions*. Introduce a function v_s as the solution to the wave

problem

$$\begin{cases} \frac{\partial^2 v_s}{\partial t^2}(x, t) - \Delta v_s(x, t) = \frac{\partial \delta_s}{\partial t}(t)g(x, T-s)\delta_{\partial\Omega}(x), & (x, t) \in \mathbb{R}^d \times \mathbb{R}, \\ v_s(x, t) = 0, & x \in \mathbb{R}^d, t \ll s, \\ \frac{\partial v_s}{\partial t}(x, t) = 0, & x \in \mathbb{R}^d, t \ll s. \end{cases}$$

Here, $\delta_{\partial\Omega}$ is the surface Dirac mass on $\partial\Omega$ and g is the measured data.

We define a modified time-reversal imaging functional by

$$\mathcal{I}_2(x) = \int_0^T v_s(x, T) ds, \quad x \in \Omega.$$

Note that

$$v_s(x, t) = \int_{\partial\Omega} \frac{\partial \Gamma}{\partial t}(x, y, s, t)g(y, T-s)d\sigma(y).$$

Consequently, the functional \mathcal{I}_2 can be expressed in terms of the free-space Green function Γ as follows

$$\mathcal{I}_2(x) = \int_0^T \int_{\partial\Omega} \frac{\partial \Gamma}{\partial t}(x, y, s, T)g(y, T-s)d\sigma(y) ds, \quad x \in \Omega.$$

Note that \mathcal{I}_2 is not exactly equivalent to \mathcal{I}_1 but is an approximation. Indeed, with

$$g_\omega(y) = \mathcal{F}[g](y, \omega) = -i\omega \int_{\Omega} \Gamma_\omega(z, y)f(z)dz, \quad \forall y \in \partial\Omega,$$

Parseval's relation gives

$$\begin{aligned} \mathcal{I}_2(x) &= \int_0^T \int_{\partial\Omega} \frac{\partial \Gamma}{\partial t}(x, y, s, T)g(y, T-s)d\sigma(y) ds \\ &= -\frac{1}{2\pi} \int_{\mathbb{R}} \int_{\partial\Omega} i\omega \Gamma_\omega(x, y)\bar{g}_\omega(y)d\sigma(y) d\omega \\ &= \frac{1}{2\pi} \int_{\mathbb{R}^d} f(z) \int_{\mathbb{R}} \int_{\partial\Omega} \omega^2 \Gamma_\omega(x, y)\bar{\Gamma}_\omega(z, y)d\sigma(y) d\omega dz. \end{aligned}$$

Using the Helmholtz-Kirchhoff identity [7]

$$\int_{\partial\Omega} \Gamma_\omega(x, y)\bar{\Gamma}_\omega(z, y)d\sigma(y) \simeq \frac{1}{\omega} \Im m\{\Gamma_\omega(x, z)\},$$

which is valid when Ω is a sphere with a large radius in \mathbb{R}^d , we find

$$\mathcal{I}_2(x) \simeq \frac{1}{2\pi} \int_{\mathbb{R}^d} f(z) \int_{\mathbb{R}} \omega \Im m\{\Gamma_\omega(x, z)\} d\omega dz.$$

Using the identity

$$\frac{1}{2\pi} \int_{\mathbb{R}} \omega \Im m\{\Gamma_\omega(x, z)\} d\omega = \delta_x(z),$$

which follows from the fact that $\frac{\partial \Gamma}{\partial t}(x, z, 0, 0) = \delta_x(z)$, we finally find that

$$\mathcal{I}_2(x) \simeq f(x).$$

REMARK 2.2.1. *Our interest in this new time reversal imaging functional is due to its usefulness for viscous media. Moreover, numerical reconstructions of sources using \mathcal{I}_1 or \mathcal{I}_2 are quite similar; see for instance the numerical illustrations in Figure 2.1. In fact, formally, if we let $G_\omega = \mathcal{F}[G]$, then by Parseval's relation*

$$\mathcal{I}_1(x) = -\frac{i}{2\pi} \int_{\Omega} f(z) \int_{\mathbb{R}} \omega \int_{\partial\Omega} \frac{\partial G_\omega}{\partial \nu_y}(x, y) \bar{\Gamma}_\omega(z, y) d\sigma(y) dz d\omega.$$

But by integration by parts over Ω and recalling that G_ω is real-valued, we have

$$\Im m \left\{ \int_{\partial\Omega} \frac{\partial G_\omega}{\partial \nu_y}(x, y) \bar{\Gamma}_\omega(z, y) d\sigma(y) \right\} = \Im m \left\{ \Gamma_\omega(x, z) \right\},$$

and therefore,

$$\mathcal{I}_1(x) = f(x),$$

which yields

$$\mathcal{I}_2(x) \simeq \mathcal{I}_1(x).$$

REMARK 2.2.2. *Note also that the operator $\mathcal{T} : f \rightarrow g$ can be expressed in the form*

$$\mathcal{T}[f](y, t) = g(y, t) = - \int_{\mathbb{R}^d} \frac{\partial \Gamma}{\partial t}(x, y, 0, t) f(x) dx, \quad (y, t) \in \partial\Omega \times [0, T].$$

Then its adjoint \mathcal{T}^* satisfies

$$\mathcal{T}^*[g](x) = - \int_0^T \int_{\partial\Omega} \frac{\partial \Gamma}{\partial t}(x, y, t, T) g(y, T-t) d\sigma(y) dt,$$

which can clearly be identified as the time reversal functional \mathcal{I}_2 .

2.3 TIME REVERSAL ALGORITHM FOR AN ATTENUATING ACOUSTIC MEDIUM

In this section, we present and analyze the concept of time reversal in attenuating acoustic media. We consider the thermo-viscous wave model to incorporate viscosity effect in wave propagation. Let p_a be the solution of the problem

$$\begin{cases} \frac{\partial^2 p_a}{\partial t^2}(x, t) - \Delta p_a(x, t) - a \frac{\partial}{\partial t} \Delta p_a(x, t) = \frac{\partial \delta_0}{\partial t} f(x), & (x, t) \in \mathbb{R}^d \times \mathbb{R} \\ p_a(x, t) = 0, & t \ll 0, \\ \frac{\partial p_a}{\partial t}(x, t) = 0, & t \ll 0, \end{cases}$$

and let

$$g_a(y, t) := p_a(y, t), \quad \forall (y, t) \in \partial\Omega \times [0, +\infty[.$$

Again, the problem is to reconstruct the source f from measured data g_a . The strategy of time-reversal is to consider the functional

$$\mathcal{I}_{2,a}(x) = \int_0^T v_{s,a}(x, T) ds, \quad x \in \Omega,$$

where $v_{s,a}$ should now be the *solution* of the time-reverted attenuated wave equation

$$\begin{cases} \frac{\partial^2 v_{s,a}}{\partial t^2}(x, t) - \Delta v_{s,a}(x, t) + a \frac{\partial}{\partial t} \Delta v_{s,a}(x, t) = \frac{\partial \delta_s}{\partial t} (g_a(y, T-s) \delta_{\partial\Omega}), & x \in \Omega, \\ v_{s,a}(x, t) = 0, & x \in \mathbb{R}^d, t \ll s, \\ \frac{\partial v_{s,a}}{\partial t}(x, t) = 0, & x \in \mathbb{R}^d, t \ll s. \end{cases}$$

Unfortunately, this problem is ill-posed. Indeed, the term $+a \frac{\partial}{\partial t} \Delta v_{s,a}(x, t)$ allows frequency component to increase exponentially. Therefore, we need to regularize the time-reverted attenuated wave equation, for instance, by truncating the high frequencies in time or in space.

Let us introduce the free space fundamental solution $\tilde{\Gamma}_{a,\omega}$ of the Helmholtz equation

$$\omega^2 \tilde{\Gamma}_{a,\omega}(x, y) + (1 + ia\omega) \Delta_y \tilde{\Gamma}_{a,\omega}(x, y) = -\delta_x \quad \text{in } \mathbb{R}^d. \quad (2.3)$$

Then, we have

$$v_{s,a}(x, t) = -\frac{1}{2\pi} \int_{\mathbb{R}} \left\{ \int_{\partial\Omega} i\omega \tilde{\Gamma}_{a,\omega}(x, y) g_a(y, T-s) d\sigma(y) \right\} \exp\{-i\omega(t-s)\} d\omega,$$

and we can define an approximation $v_{s,a,\rho}$ of the function $v_{s,a}$ as follows

$$v_{s,a,\rho}(x, t) = -\frac{1}{2\pi} \int_{|\omega| \leq \rho} \left\{ \int_{\partial\Omega} i\omega \tilde{\Gamma}_{a,\omega}(x, y) g_a(y, T-s) d\sigma(y) \right\} \exp\{-i\omega(t-s)\} d\omega,$$

where ρ is a cut off parameter. A *regularized* time reversal imaging functional is then defined by

$$\mathcal{I}_{2,a,\rho}(x) = \int_0^T v_{s,a,\rho}(x, T) ds, \quad (2.4)$$

that can equivalently be given by

$$\mathcal{I}_{2,a,\rho}(x) = \int_{\partial\Omega} \int_0^T \frac{\partial \tilde{\Gamma}_{a,\rho}}{\partial t}(x, y, s, T) g_a(y, T-s) d\sigma(y) ds,$$

where

$$\tilde{\Gamma}_{a,\rho}(x, y, s, t) = \frac{1}{2\pi} \int_{|\omega| \leq \rho} \tilde{\Gamma}_{a,\omega}(x, y) \exp\{-i\omega(t-s)\} d\omega.$$

We will precise how to calibrate the cut off parameter ρ in Remark 2.3.6 in order to get a stable imaging functional.

REMARK 2.3.1. Let \mathcal{S}' be the space of tempered distributions, i.e., the dual of the Schwartz space \mathcal{S} of rapidly decreasing functions (see for instance [78]). The function $v_{s,a,\rho}(x, t)$ can be identified as the solution of the following wave equation:

$$\frac{\partial^2 v_{s,a,\rho}}{\partial t^2}(x, t) - \Delta v_{s,a,\rho}(x, t) + a \frac{\partial}{\partial t} \Delta v_{s,a,\rho}(x, t) = S_\rho \left[\frac{\partial \delta_s}{\partial t} \right] (g_a(y, T-s) \delta_{\partial\Omega}),$$

where S_ρ is the operator defined on the space \mathcal{S}' by

$$S_\rho[\psi](t) = \frac{1}{2\pi} \int_{|\omega| \leq \rho} e^{-i\omega t} \mathcal{F}[\psi](\omega) d\omega.$$

2.3.1 ANALYSIS OF REGULARIZED TIME REVERSAL FUNCTIONAL

Recall that $p_a(x, t)$ and $p(x, t)$ are respectively solutions of the wave equations

$$\frac{\partial^2 p_a}{\partial t^2}(x, t) - \Delta p_a(x, t) - a \frac{\partial}{\partial t} \Delta p_a(x, t) = \frac{\partial \delta_0}{\partial t} f(x),$$

and

$$\frac{\partial^2 p}{\partial t^2}(x, t) - \Delta p(x, t) = \frac{\partial \delta_0}{\partial t} f(x),$$

and the functions $p_{a,\omega} := \mathcal{F}[p_a](x, \omega)$ and $p_\omega := \mathcal{F}[p](x, \omega)$ are solutions of the Helmholtz equations

$$(\kappa(\omega)^2 + \Delta) p_{a,\omega}(x) = i \frac{\kappa(\omega)^2}{\omega} f(x), \quad \text{and} \quad (\omega^2 + \Delta) p_\omega(x) = i\omega f(x),$$

respectively, where $\kappa(\omega) = \frac{\omega}{\sqrt{1 - ia\omega}}$. It can be seen that

$$p_{\omega,a}(x) = \frac{\kappa(\omega)}{\omega} p_{\kappa(\omega)}(x), \quad \text{or} \quad p_a(x, t) = \mathcal{L}_a[p(x, \cdot)](t),$$

where

$$\mathcal{L}_a[\phi](t) = \frac{1}{2\pi} \int_{\mathbb{R}} \frac{\kappa(\omega)}{\omega} \left\{ \int_{\mathbb{R}} \phi(s) \exp\{i\kappa(\omega)s\} ds \right\} \exp\{-i\omega t\} d\omega.$$

The following result holds.

PROPOSITION 2.3.2. Let $\phi(t) \in \mathcal{S}([0, \infty])$ (where \mathcal{S} is the Schwartz space). Then,

$$\mathcal{L}_a[\phi](t) = \phi(t) + \frac{a}{2} (t\phi)'(t) + o(a).$$

Proof. Formally, it follows that

$$\begin{aligned} \mathcal{L}_a[\phi](t) &= \frac{1}{2\pi} \int_{\mathbb{R}} \left[1 + i \frac{a}{2} \omega \right] \left\{ \int_0^\infty \left[1 - \omega^2 \frac{a}{2} s \right] \phi(s) \exp\{i\omega s\} ds \right\} \exp\{-i\omega t\} d\omega \\ &\quad + o(a) \\ &= \phi(t) + \frac{a}{2} (-\phi'(t) + (t\phi)''(t)) + o(a) \\ &= \phi(t) + \frac{a}{2} (t\phi)'(t) + o(a). \end{aligned}$$

This result can be rigorously justified using the stationary phase theorem (See Appendix 1.A.2, Chapter 1). \square

Similarly, introduce the operator $\widetilde{\mathcal{L}}_{a,\rho}$ defined by

$$\widetilde{\mathcal{L}}_{a,\rho}[\phi](t) = \frac{1}{2\pi} \int_0^\infty \phi(s) \left\{ \int_{|\omega| \leq \rho} \frac{\widetilde{\kappa}(\omega)}{\omega} \exp\{i\widetilde{\kappa}(\omega)s\} \exp\{-i\omega t\} d\omega \right\} ds,$$

where $\widetilde{\kappa}(\omega) = \frac{\omega}{\sqrt{1+i a \omega}}$. By definition, we have

$$\frac{\partial \widetilde{\Gamma}_{a,\rho}}{\partial t} = \widetilde{\mathcal{L}}_{a,\rho} \left[\frac{\partial \Gamma}{\partial t} \right]. \quad (2.5)$$

Moreover, the adjoint operator of $\widetilde{\mathcal{L}}_{a,\rho}$ reads

$$\widetilde{\mathcal{L}}_{a,\rho}^*[\phi](t) = \frac{1}{2\pi} \int_{|\omega| \leq \rho} \frac{\widetilde{\kappa}(\omega)}{\omega} \exp\{i\widetilde{\kappa}(\omega)t\} \left\{ \int_0^\infty \phi(s) \exp\{-i\omega s\} ds \right\} d\omega.$$

Then we have:

PROPOSITION 2.3.3. *Let $\phi(t) \in \mathcal{D}([0, \infty[)$ where $\mathcal{D}([0, \infty[)$ is the space of C^∞ -functions of compact support in $[0, \infty[$. Then for all $\rho > 0$,*

$$\widetilde{\mathcal{L}}_{a,\rho}^*[\phi](t) = S_\rho[\phi](t) - \frac{a}{2} S_\rho[(t\phi)'](t) + o(a) \quad \text{as } a \rightarrow 0.$$

Proof. Note that, as $\phi(t) \in \mathcal{D}([0, \infty[)$, the support of $\phi \subset [0, T_{max}]$,

$$\begin{aligned} \widetilde{\mathcal{L}}_{a,\rho}^*[\phi](t) &= \frac{1}{2\pi} \int_{|\omega| \leq \rho} \frac{\widetilde{\kappa}(\omega)}{\omega} \exp\{i\widetilde{\kappa}(\omega)t\} \left\{ \int_0^{T_{max}} \phi(s) \exp\{-i\omega s\} ds \right\} d\omega \\ &= \frac{1}{2\pi} \int_{|\omega| \leq \rho} \int_0^{T_{max}} \left[1 - i\frac{a}{2}\omega \right] \left[1 + \omega^2 \frac{a}{2}t \right] \phi(s) \exp\{-i\omega(s-t)\} ds d\omega \\ &\quad + o(a) \\ &= S_\rho[\phi(t)] - \frac{a}{2} S_\rho[(t\phi)'](t) + o(a). \end{aligned}$$

\square

As an immediate consequence of Proposition 2.3.2 and 2.3.3, the following result holds.

PROPOSITION 2.3.4. *Let $\phi(t) \in \mathcal{D}([0, \infty[)$, then*

$$\widetilde{\mathcal{L}}_{a,\rho}^* \mathcal{L}_a[\phi](t) = S_\rho[\phi](t) + o(a) \quad \text{as } a \rightarrow 0.$$

We also have the following proposition which indicates that the use of the adjoint attenuated wave operator instead of the ideal one gives a first order correction to the attenuation effect.

PROPOSITION 2.3.5. *The regularized time-reversal imaging functional defined by (2.4) satisfies*

$$\mathcal{I}_{2,a,\rho}(x) = - \int_{\partial\Omega} \int_0^T \frac{\partial\Gamma}{\partial t}(x, y, T-s, T) S_\rho [g(y, \cdot)](s) ds d\sigma(y) + o(a),$$

for a small enough.

Proof. By virtue of (2.5), $\mathcal{I}_{2,a,\rho}$ can be rewritten in the form

$$\mathcal{I}_{2,a,\rho}(x) = - \int_{\partial\Omega} \int_0^T \frac{\partial\Gamma}{\partial t}(x, y, T-s, T) \widetilde{\mathcal{L}}_{a,\rho}^* [g_a(y, \cdot)](s) ds d\sigma(y).$$

Recall as well that $g_a = \mathcal{L}[g]$, so that

$$\begin{aligned} \mathcal{I}_{2,a,\rho}(x) &= - \int_{\partial\Omega} \int_0^T \frac{\partial\Gamma}{\partial t}(x, y, T-s, T) \widetilde{\mathcal{L}}_{a,\rho}^* \mathcal{L}[g(y, \cdot)](s) ds d\sigma(y) \\ &= - \int_{\partial\Omega} \int_0^T \frac{\partial\Gamma}{\partial t}(x, y, T-s, T) S_\rho [g(y, \cdot)](s) ds d\sigma(y) + o(a), \end{aligned}$$

by using Proposition 2.3.4. □

Finally, observe that the function $\delta_{\rho,x}(z)$ defined by

$$\delta_{\rho,x}(z) = \int_{|\omega| \leq \rho} \omega \Im m \{ \Gamma_\omega(x, z) \} d\omega, \quad (2.6)$$

is an approximation of the Dirac delta distribution, that is, $\delta_{\rho,x} \rightarrow \delta_x$ as $\rho \rightarrow +\infty$. It implies

$$\begin{aligned} - \int_{\partial\Omega} \int_0^T \frac{\partial\Gamma}{\partial t}(x, y, T-s, T) S_\rho [g(y, \cdot)](s) d\sigma(y) ds &\simeq \delta_{\rho,x} * f, \\ &\xrightarrow{\rho \rightarrow \infty} f(x) \end{aligned}$$

when x is far away from the boundary $\partial\Omega$.

REMARK 2.3.6. *The function $\delta_{\rho,x}$ defined in (2.6) gives a peak at a source point x with a width of order ρ^{-1} . Therefore, ρ must be taken sufficiently large for a good resolution. On the other hand, $\mathcal{I}_{2,a,\rho}$ uses the fundamental solution $\widetilde{\Gamma}_{a,\omega}(x, y)$ of (2.3) that grows exponentially as $\exp\{\Im m\{\tilde{\kappa}(\omega)\}|x-y|\}$. In order to ensure stability of $\mathcal{I}_{2,a,\rho}$, this term must not be greater than one. Since $\tilde{\kappa}(\omega)$ grows like $a\omega^2/2$ for $a|\omega| < 1$, (and as $\sqrt{|\omega|/(2a)}$ for $a|\omega| > 1$), one should not use frequency components larger than $(a \text{diam}(\Omega))^{-1/2}$, that is $\rho \simeq (a \text{diam}(\Omega))^{-1/2}$ is a threshold for stability of the imaging functional, where diam represents the diameter. It implies that the imaging functional can be stable at the expense of a loss in resolution. In Figure 2.4, we present some numerical results where we chose ρ slightly less than the threshold $(a \text{diam}(\Omega))^{-1/2}$.*

2.4 RECONSTRUCTION ALTERNATIVE FOR HIGHER ORDER ATTENUATION CORRECTION

In the previous section, we have shown that the time reversal method using the adjoint of attenuated wave operator can be justified as a first order correction to attenuation effect. The algorithm $\mathcal{S}_{2,a,\rho}$ can be seen as a classical time reversal method applied to *preprocessed* data $\widetilde{\mathcal{L}}_{a,\rho}^*[g_a]$. Moreover, Proposition 2.3.4 indicates that the operator $\widetilde{\mathcal{L}}_{a,\rho}^*$ is an order one approximation of the inverse of attenuation operator \mathcal{L}_a . A higher order correction to attenuation effect can be given using a preprocessed data $\mathcal{L}_{a,k}^{-1}[g_a]$ instead of using time reversal method with adjoint of attenuated wave operator. Here, the filter $\mathcal{L}_{a,k}^{-1}$ can be defined as an order k approximation of the inverse of operator \mathcal{L}_a .

As in Chapter 1, the idea is to use an approximation of operator \mathcal{L}_a obtained by a classical argument of stationary phase theorem. More precisely, in the simplified case where $\kappa(\omega) \simeq \omega + i\frac{a}{2}\omega^2$, we have for integer $k > 0$

$$\mathcal{L}_a[\phi](t) = \sum_{m=0}^k \frac{a^m}{m! 2^m} (t^m \phi')^{(2m-1)}(t) + o(a^k).$$

An approximation of order k of the inverse of operator \mathcal{L}_a can then be given by

$$\mathcal{L}_{a,k}^{-1}[\phi](t) = \sum_{m=0}^k a^m \phi_{k,m}(t),$$

where $\phi_{k,m}$ are recursively defined by

$$\begin{cases} \phi_{k,0} &= \phi \\ \phi_{k,m} &= -\sum_{l=1}^m \mathbf{D}_l[\phi_{k,m-l}], \end{cases} \quad \text{with} \quad \mathbf{D}_m[\phi](t) = \frac{1}{m! 2^m} (t^m \phi')^{(2m-1)}(t).$$

Thus, a higher order reconstruction alternative can finally be described as

1. Pre-process the measured data g_a using the filter $\mathcal{L}_{a,k}^{-1}$,
2. Use classical time-reversal functional \mathcal{S}_1 or \mathcal{S}_2 for the reconstruction of the source f .

2.5 NUMERICAL ILLUSTRATIONS

2.5.1 DESCRIPTION OF THE ALGORITHM

All the wave equations are solved in the box $[-L/2, L/2]^2$ with periodic boundary conditions, where L is supposed to be sufficiently large to prevent any reflection on the boundary. Numerical integrations of each equation are then performed exactly in the Fourier space.

As the solution $v_{s,a,\rho}(x, t)$ is very difficult to obtain numerically, we regularize the problem by truncating high frequency components in space. This can be seen as an approximation $\tilde{v}_{s,a,\rho}$ of $v_{s,a,\rho}$, defined as the solution of

$$\frac{\partial^2 \tilde{v}_{s,a,\rho}}{\partial t^2}(x, t) - \Delta \tilde{v}_{s,a,\rho}(x, t) + a \frac{\partial}{\partial t} \Delta \tilde{v}_{s,a,\rho}(x, t) = \frac{\partial \delta_0}{\partial t} \chi_\rho [(g_a(y, T - s) \delta_{\partial\Omega})],$$

where the operator χ_ρ is given by

$$\chi_\rho [f](x) = \frac{1}{L^2} \sum_{|j| \leq \rho} \int_{[-L/2, L/2]^2} f(z) \exp \left\{ i \frac{2\pi}{L} (z - x) \cdot j \right\} dz.$$

The numerical approximation of $p_a(x, t)$ is obtained by using its spatial Fourier decomposition. Indeed, recall that $p_a(x, t)$ is the solution of wave equation

$$\frac{\partial^2 p_a}{\partial t^2}(x, t) - \Delta p_a(x, t) - a \frac{\partial}{\partial t} \Delta p_a(x, t) = \frac{\partial \delta_0}{\partial t} f(x).$$

Therefore, when $f = \sum_{j \in \mathbb{Z}^2} f_j \exp \left(-i \frac{2\pi}{L} j \cdot x \right)$, the function $p_a(x, t)$ can be expanded as

$$p_a(x, t) = \sum_{j \in \mathbb{Z}^2} p_j(t) \exp \left(-i \frac{2\pi}{L} j \cdot x \right)$$

with

$$p_j(t) = \exp \left(-\frac{a}{2} \left(\frac{2\pi}{L} \right)^2 |j|^2 t \right) \cos \left(t \sqrt{\left(\frac{2\pi}{L} \right)^2 |j|^2 - \frac{a^2}{4} \left(\frac{2\pi}{L} \right)^4 |j|^4} \right) f_j.$$

The function $\tilde{v}_{s,a,\rho}$ can similarly be approximated numerically.

2.5.2 EXPERIMENTS

In the sequel, for numerical illustrations, Ω is defined in polar coordinates by

$$\Omega = \left\{ (r, \theta) \in [0, \infty[\times [0, 2\pi[; r \leq 0.95 + 0.05 \cos(8\theta) \right\},$$

and its boundary is discretized by 1024 sensors. The solutions p and $\tilde{v}_{s,a,\rho}$ are also calculated over $(x, t) \in [-L/2, L/2]^2 \times [0, T]$ with $L = 4$ and $T = 2$, and we use a step of discretization given by $dt = T/2^{10}$ and $dx = L/2^9$.

Figure 2.1 presents a comparison between the two time reversal imaging functionals \mathcal{I}_1 and \mathcal{I}_2 for a non attenuating acoustic medium. One can observe that the two reconstructions are almost identical.

Figure 2.2 shows reconstructions using \mathcal{I}_2 for an attenuating medium. As expected, the two images obtained with attenuation coefficient $a = 0.0005$ and $a = 0.001$ appear blurry.

Figure 2.3 presents reconstructions using $\mathcal{I}_{2,a,\rho}$ for an attenuating medium. The images corresponding to $\mathcal{I}_{2,a,\rho}$ are computed for three different values of ρ .

It appears that $\mathcal{I}_{2,a,\rho}$ gives a better reconstruction of f than the functional \mathcal{I}_2 , provided that the regularization parameter ρ is chosen sufficiently large for better resolution. However, when ρ is larger than the threshold, $\mathcal{I}_{2,a,\rho}$ is unstable.

Figure 2.4, highlights numerical results for an appropriate choice of the cut-off parameter for different attenuation coefficients. The values of ρ are chosen slightly less than the threshold $(\text{diam}(\Omega))^{-1/2}$. We can observe that the image resolution is improved with a barely minimum instability.

Figure 2.5 gives some reconstructions obtained by preprocessing the data with the filter $\mathcal{L}_{a,k}^{-1}$ followed by the time-reversal using the imaging functional \mathcal{I}_2 , in an attenuating medium. This approach is tested by varying the approximation order k . It clearly provides a better reconstruction of f than by using functional \mathcal{I}_2 . Moreover, this approach has, apparently, no instability issues.

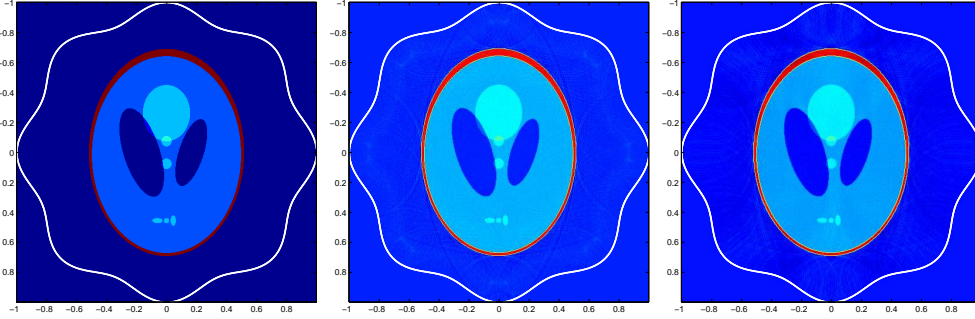


FIGURE 2.1. Comparison between \mathcal{I}_1 and \mathcal{I}_2 without attenuation (i.e. $a = 0$): Left: source $f(x)$; middle: reconstruction using \mathcal{I}_1 ; Right: reconstruction using \mathcal{I}_2 .

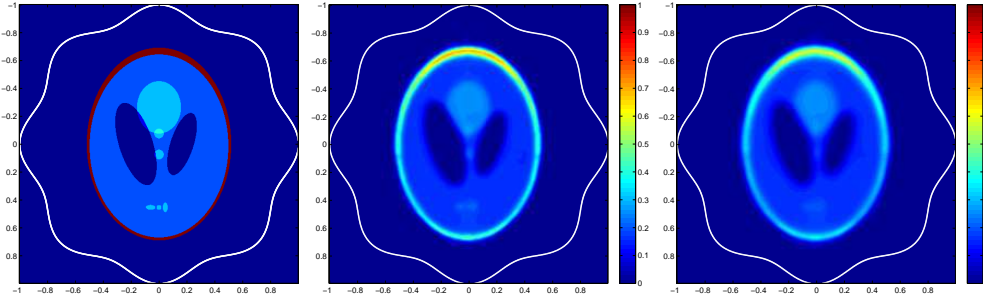


FIGURE 2.2. Reconstruction using \mathcal{I}_2 from attenuated data g_a : Left ; source $f(x)$; middle: reconstruction using \mathcal{I}_2 with $a = 0.0005$; Right : reconstruction using \mathcal{I}_2 with $a = 0.001$

2.6 DISCUSSION AND CONCLUSION

In this work, the attenuation coefficient is assumed to be homogeneous and known a priori. However, in practical situations, this is not always the case and an estimation of the attenuation coefficient is sometimes necessary. This can

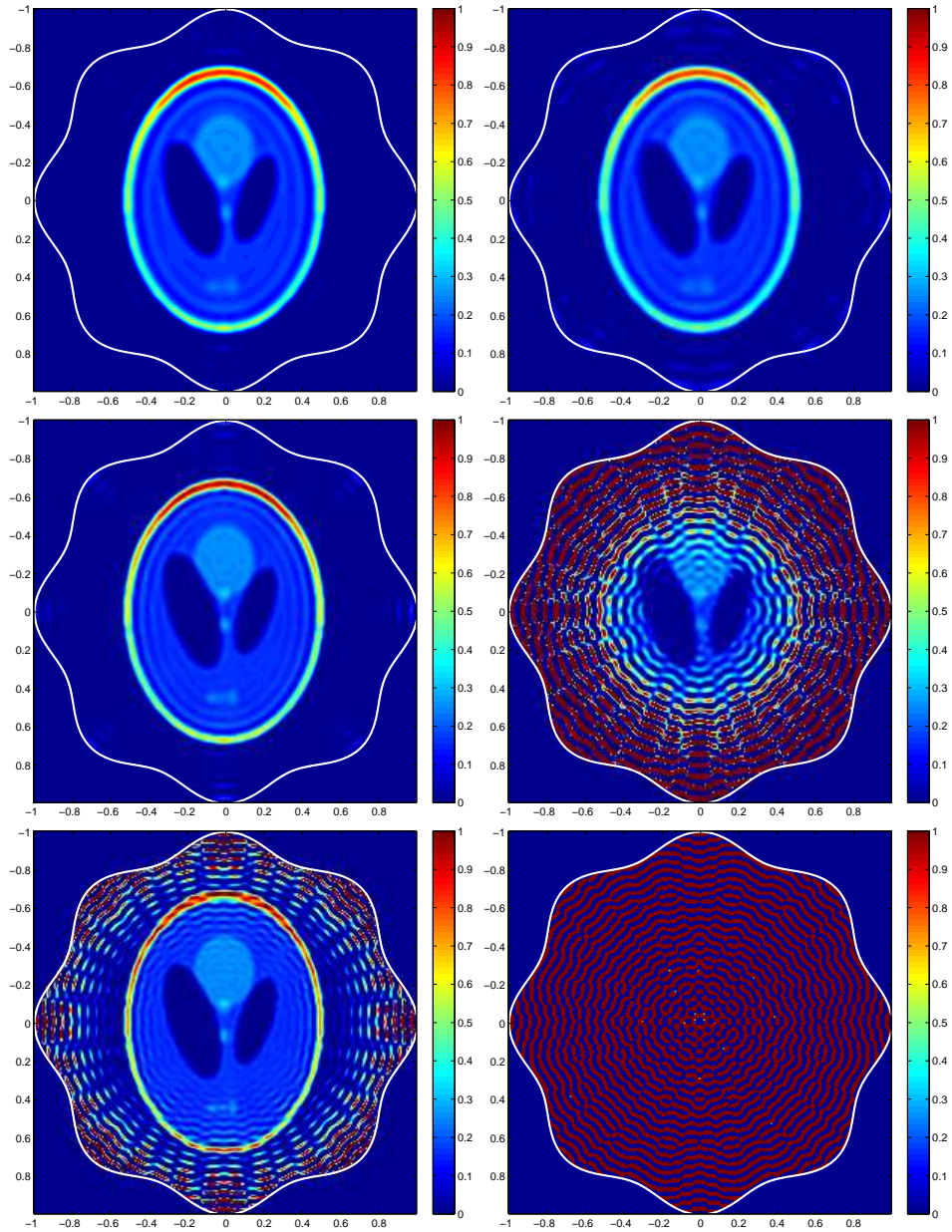


FIGURE 2.3. Reconstruction using $\mathcal{F}_{2,a,\rho}$ from attenuated data g_a . Left: $a = 0.0005$; Right: $a = 0.001$; Top to Bottom: $\rho = 15$, $\rho = 20$, $\rho = 25$.

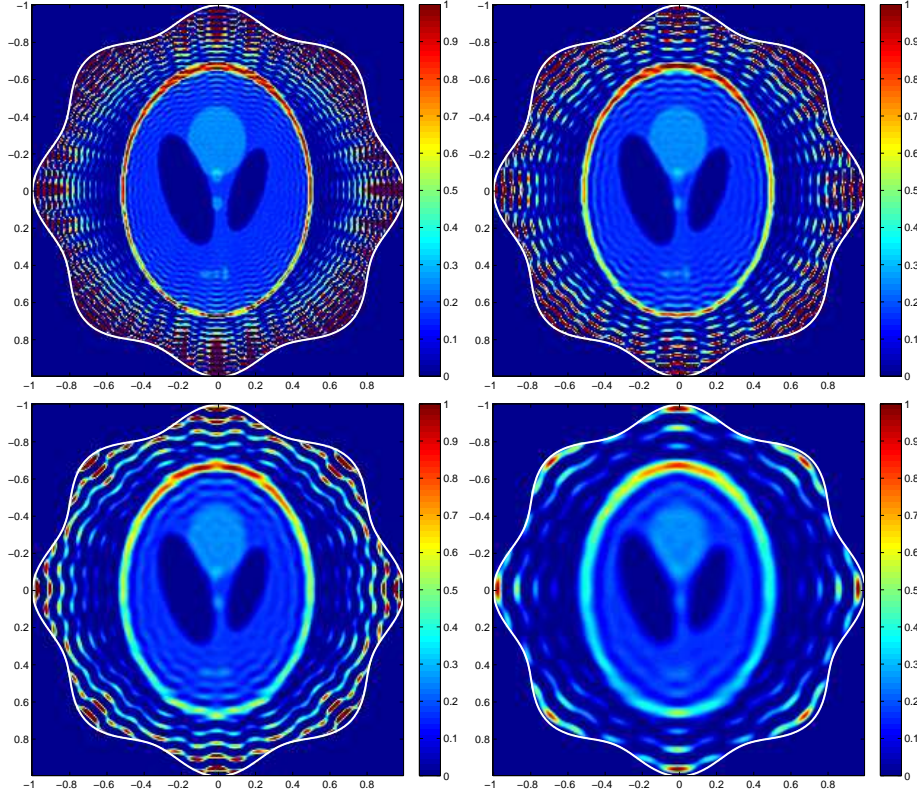


FIGURE 2.4. Cut-off frequency ρ for different values of a . First row: $a = 0.00025$, $\rho = 25\sqrt{2}$ (left), $a = 0.0005$, $\rho = 25$ (right). Second row: $a = 0.001$, $\rho = \frac{25}{\sqrt{2}}$ (left), $a = 0.002$, $\rho = \frac{25}{2}$ (right).

be done easily if the source f and the data g_a are known simultaneously. Indeed, in this situation, the ideal data g can be recovered from f and a can be estimated as the minimizer of energy J given by

$$J(a) = \left\{ \int_{\partial\Omega} \int_0^T \left| g_a(y, t) - \mathcal{L}_a[g](y, t) \right|^2 dt d\sigma(y) \right\}.$$

In fact, numerical tests using Newton algorithm to solve this optimization problem are quite successful. Figure 2.6 shows reconstructions of different values of the attenuation coefficient a when the source term f is respectively the Shepp-Logan phantom, a Gaussian, or a Dirac mass. It turns out that the smaller the attenuation coefficient, the better is the reconstruction. Moreover, the most reliable coefficient reconstruction corresponds to a Dirac mass.

A more involved scenario is when only the data g_a is known. We tried to recover the attenuation coefficient a and the source f simultaneously as the mini-

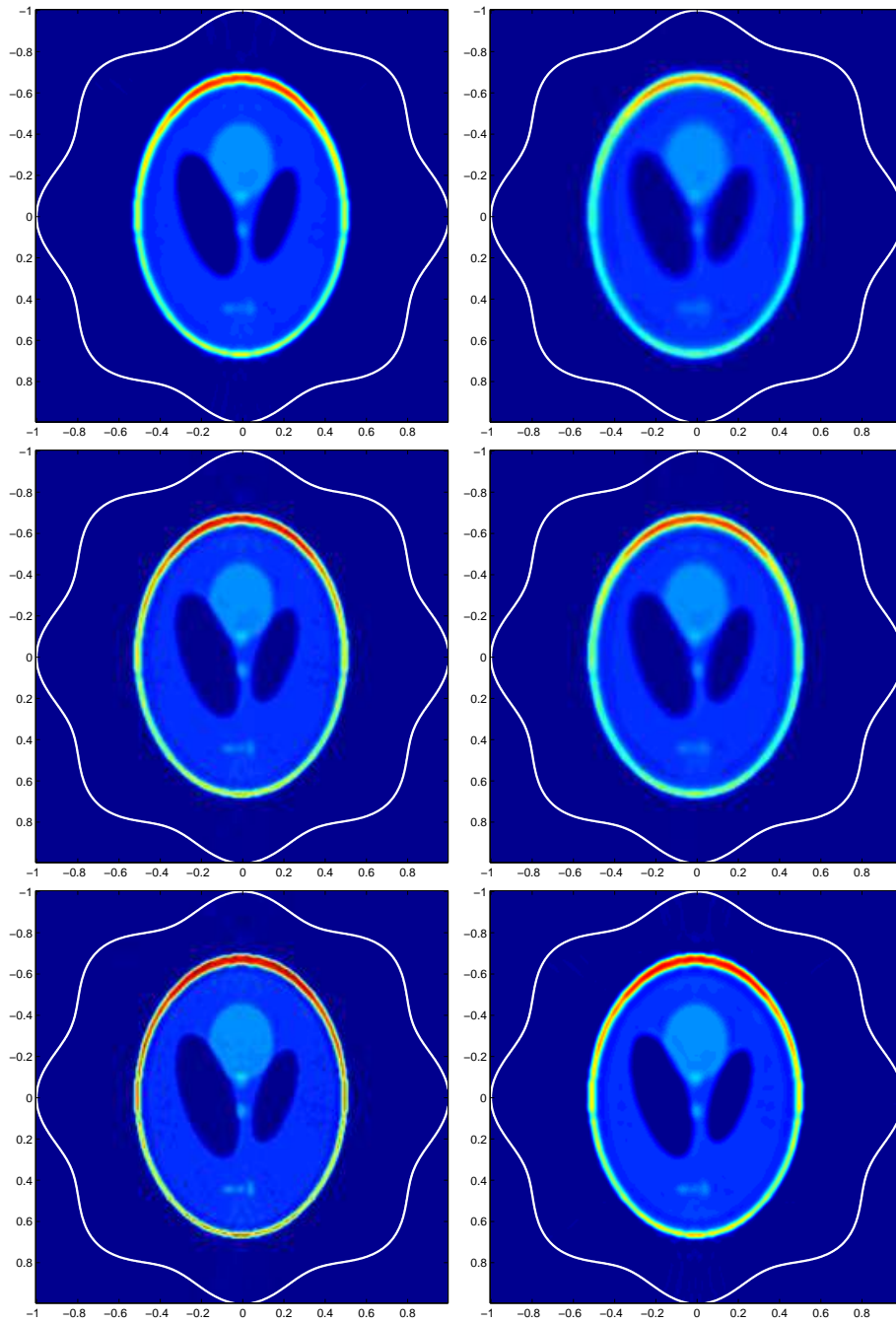


FIGURE 2.5. Reconstruction by preprocessing data with the filter $\mathcal{L}_{a,k}^{-1}$ followed by the functional \mathcal{F}_2 from attenuated data g_a . Left: $a = 0.0005$; Right: $a = 0.001$; Top to Bottom: $k = 1$, $k = 2$, $k = 4$

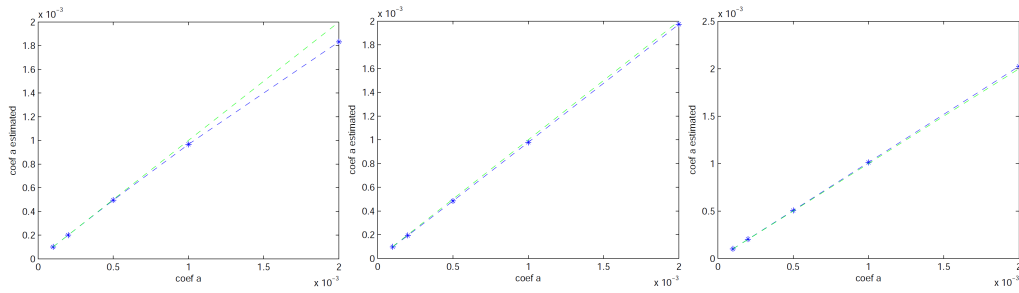


FIGURE 2.6. Reconstructions of the attenuation coefficient a . Left: the source term f is the Shepp-Logan phantom; Middle: f is a Gaussian; Right: f is a Dirac mass.

mizer (a^*, f^*) of the discrepancy functional

$$J(a, f) = \left\{ \int_{\partial\Omega} \int_0^T \left| g_a(y, t) - \mathcal{L}_a[\mathcal{T}f(y, t)] \right|^2 dt d\sigma(y) \right\},$$

where $\mathcal{T} : f \rightarrow g$. However, this optimization problem seems to have an inherent instability issue.

Another challenging problem is to extract the Green function for an attenuating medium by correlating waves exited by random sources and recorded at two locations [121]. It is expected that our results in this chapter would lead to an efficient approach for solving this problem.

To conclude, the time reversal technique using adjoint attenuated wave operator has clearly provided better resolution in image reconstruction than the classical one without attenuation consideration. We analyzed this approach and proved that it gives a reconstruction with a first order correction to the attenuation effect. Unfortunately, this technique is ill-posed and even if a regularization is used, it appears to be unstable and inefficient when the attenuation coefficient a becomes too large. We, therefore, proposed another approach which consists to apply a filter to the measured data followed by a classical time reversal method. This method seems to be more stable and accurate as illustrated in our numerical experiments. However, this approach cannot be adapted when a depends on spatial variable. In this situation, the attenuated time reversal technique the best option for attenuation compensation, known to us.

NOISE SOURCE LOCALIZATION IN ATTENUATING MEDIA

3.1 INTRODUCTION

The main objective of this chapter is to present an original approach for detecting the spatial support of noise sources in an attenuating electromagnetic or acoustic medium.

The main application envisaged by our work concerns robotic sound or microwave noise source localization and tracking; see, for instance, [79, 90, 91, 96, 135]. It is a quite challenging problem to build an autonomous robotic system for finding, investigating, and modeling ambient electromagnetic or sound noise sources in the environment. On the other hand, a robot can be a rather significant source of electromagnetic and/or acoustic noise. To mask the electromagnetic or acoustic signature of a robot in order to reduce the risk of being detected is another challenging problem. As will be seen in this chapter, at least two robots have to be used in order to locate noise sources by cross correlation.

Passive imaging from noisy signals has been a very active field. It has been shown that the Green function of the wave equation in inhomogeneous media can be estimated by cross correlating the signals emitted by ambient noise sources and recorded by a passive sensor array [51, 117, 122]. The idea has been used for travel time estimation and background velocity estimation in geophysical contexts, and also for passive sensor imaging of reflectors [67, 68], which consists of back-propagating or migrating the cross correlation matrix of the recorded signals. The relation between the cross correlation of ambient noise signals recorded at two observation points and the Green function between these two points can be proved using the Helmholtz-Kirchhoff identity when the ambient noise sources surround the observation region [32, 121].

In [69] the noise source imaging problem is analyzed in a high-frequency asymptotic regime and the support of the noise sources is identified with a special Radon transform. Here we shall consider a general context in both non-attenuating and attenuating media. In attenuating media, one can think to first

pre-process the data as originally done in Chapter 2 and then to back-propagate the cross correlation of the pre-processed data in a non-attenuating medium. However, this seems impossible because the recorded data are very long and usually contain a huge amount of additional measurement noise. Instead, we back-propagate the cross correlation of the recorded data with a regularized version of the adjoint operator. Our main tool is a generalization of the Helmholtz-Kirchhoff identity to attenuating media. Moreover, we address the problem of localizing spatially correlated noise sources. In particular, we consider two specific examples: an extended distribution of locally correlated sources and a collection of correlated point sources. We build functionals from the cross correlation that are capable of first locating the noise sources and then estimating the correlation structure between them.

The chapter is organized as follows. In Section 3.2, we introduce a model problem and recall the definition of cross correlation. In Section 3.3, we consider noise source localization in non-attenuating media. We propose and analyze a weighted imaging functional for locating noise sources which is based on back-propagating the cross correlation of the data and estimating the power spectral density of the noise sources. In Section 3.4, we consider the thermo-viscous wave model to incorporate the attenuation effect in wave propagation. Our strategy for localizing the noise sources is to back-propagate the cross correlation with a regularized version of the adjoint wave operator. We contrast this with the approach consisting of first preprocessing the data before back-propagating the cross correlation. In Section 3.5, we address the impact of spatial correlation on noise source localization. Some numerical illustrations to highlight the potential of proposed imaging functionals in the considered contexts are presented. Finally, the chapter ends with a short discussion and a conclusion.

3.2 MEDIA WITHOUT ATTENUATION

Let us consider the wave equation in a d -dimensional open medium

$$\left\{ \begin{array}{l} \frac{1}{c^2(\mathbf{x})} \frac{\partial^2 p}{\partial t^2}(t, \mathbf{x}) - \Delta p(t, \mathbf{x}) = n(t, \mathbf{x}), \quad (t, \mathbf{x}) \in \mathbb{R} \times \mathbb{R}^d, \\ p(t, \mathbf{x}) = 0, \quad t \ll 0, \\ \frac{\partial p(t, \mathbf{x})}{\partial t} = 0, \quad t \ll 0, \end{array} \right. \quad (3.1)$$

where $d = 2$ or 3 , $c(\mathbf{x})$ is a positive smooth function bounded from below and above, and the term $n(t, \mathbf{x})$ models a distribution of noise sources that is compactly supported in a smooth bounded domain Ω . The function $c(\mathbf{x})$ is supposed to be equal to one outside a large ball. Furthermore, we assume that $n(t, \mathbf{x})$ is a

stationary (in time) Gaussian process with mean zero and covariance function

$$\langle n(t, \mathbf{x})n(s, \mathbf{y}) \rangle = F(t-s)K(\mathbf{x})\delta(\mathbf{x}-\mathbf{y}), \quad (3.2)$$

where δ is the Dirac mass at the origin, the brackets stand for the statistical average, F is the time covariance of the noise signals (its Fourier transform is the power spectral density) and K characterizes the spatial support of the sources. The function K is the quantity we want to identify from the data set

$$\left\{ p(t, \mathbf{x}), \quad \forall t \in [0, T], \mathbf{x} \in \partial\Omega \right\}$$

recorded at the surface of the domain Ω .

In the sequel, we use $\hat{v}(\omega)$ to denote the Fourier transform of a function $v(t)$, that is,

$$\hat{v}(\omega) = \int_{\mathbb{R}} v(t) \exp(i\omega t) dt.$$

We also introduce

$$G(t, \mathbf{x}, \mathbf{y}) = \frac{1}{2\pi} \int_{\mathbb{R}} \hat{G}(\omega, \mathbf{x}, \mathbf{y}) \exp(-i\omega t) d\omega,$$

where \hat{G} is the outgoing fundamental solution to the Helmholtz equation $-(\Delta + \omega^2/c(\mathbf{x}))$ in \mathbb{R}^d i.e.

$$\left(\Delta_{\mathbf{x}} + \frac{\omega^2}{c^2(\mathbf{x})} \right) \hat{G}(\omega, \mathbf{x}, \mathbf{y}) = -\delta(\mathbf{x}-\mathbf{y}) \quad \text{in } \mathbb{R}^d.$$

The time-dependent Green function is causal in the sense that $G(t, \mathbf{x}, \mathbf{y}) = 0$ for all $t \leq 0$.

We observe the waves at the surface of the domain Ω and we compute the empirical cross correlation:

$$C_T(\tau, \mathbf{x}, \mathbf{y}) = \frac{1}{T} \int_0^T p(t, \mathbf{x}) p(t+\tau, \mathbf{y}) dt, \quad \mathbf{x}, \mathbf{y} \in \partial\Omega. \quad (3.3)$$

If the recording time window is long enough then the empirical cross correlation is equivalent to the statistical cross correlation [67]

$$\begin{aligned} C(\tau, \mathbf{x}, \mathbf{y}) &= \langle p(t, \mathbf{x}) p(t+\tau, \mathbf{y}) \rangle \\ &= \frac{1}{2\pi} \int_{\mathbb{R}} \left[\int_{\Omega} \overline{\hat{G}(\omega, \mathbf{x}, \mathbf{z})} \hat{G}(\omega, \mathbf{y}, \mathbf{z}) K(\mathbf{z}) d\mathbf{z} \right] \hat{F}(\omega) \exp(-i\omega\tau) d\omega. \end{aligned} \quad (3.4)$$

Note that the statistical cross correlation contains all the information about the data. Indeed the data set

$$\left\{ p(t, \mathbf{x}), \forall (t, \mathbf{x}) \in [0, T] \times \partial\Omega \right\}$$

has stationary Gaussian distribution with mean zero, so that its statistical distribution is fully characterized by the cross correlation.

3.3 SOURCE LOCALIZATION

We aim at identifying the source function K . The idea is to back-propagate the cross correlation of the data, which contains all the accessible information about the source distribution. The imaging functional for source localization is given by

$$\mathcal{I}(\mathbf{z}^S) = \int_{\mathbb{R}} \iint_{\partial\Omega \times \partial\Omega} \widehat{G}(\omega, \mathbf{x}, \mathbf{z}^S) \overline{\widehat{G}(\omega, \mathbf{y}, \mathbf{z}^S)} \widehat{C}(\omega, \mathbf{x}, \mathbf{y}) d\sigma(\mathbf{x}) d\sigma(\mathbf{y}) d\omega \quad (3.5)$$

for the search point $\mathbf{z}^S \in \Omega$. Here \widehat{C} is the Fourier transform of C defined by (3.4) and $d\sigma$ is the surface element on $\partial\Omega$. Definition (3.5) is equivalent to

$$\mathcal{I}(\mathbf{z}^S) = 2\pi \iint_{\partial\Omega \times \partial\Omega} \left[\int_0^\infty \int_0^\infty G(t, \mathbf{x}, \mathbf{z}^S) G(s, \mathbf{y}, \mathbf{z}^S) C(s-t, \mathbf{x}, \mathbf{y}) dt ds \right] d\sigma(\mathbf{x}) d\sigma(\mathbf{y}). \quad (3.6)$$

By Helmholtz-Kirchhoff identity [7]

$$\int_{\partial\Omega} \widehat{G}(\omega, \mathbf{x}, \mathbf{y}) \overline{\widehat{G}(\omega, \mathbf{z}, \mathbf{y})} d\sigma(\mathbf{y}) \simeq \frac{1}{\omega} \Im m \{ \widehat{G}(\omega, \mathbf{x}, \mathbf{z}) \}, \quad (3.7)$$

which holds as $|\mathbf{x} - \mathbf{y}|$ and $|\mathbf{z} - \mathbf{y}|$ are large enough compared to the wavelength $2\pi/\omega$, we find that

$$\mathcal{I}(\mathbf{z}^S) \simeq \int_{\mathbb{R}} \int_{\Omega} \frac{\widehat{F}(\omega)}{\omega^2} \Im m \{ \widehat{G}(\omega, \mathbf{z}^S, \mathbf{z}) \}^2 K(\mathbf{z}) d\mathbf{z} d\omega.$$

This gives the following proposition.

PROPOSITION 3.3.1. *The imaging functional (3.5) gives the source function K up to a smoothing operator, i.e.,*

$$\mathcal{I}(\mathbf{z}^S) \simeq \int_{\Omega} \mathcal{Q}(\mathbf{z}^S, \mathbf{z}) K(\mathbf{z}) d\mathbf{z} \quad (3.8)$$

with the smoothing kernel \mathcal{Q} defined by

$$\mathcal{Q}(\mathbf{z}^S, \mathbf{z}) = \int_{\mathbb{R}} \frac{\widehat{F}(\omega)}{\omega^2} \Im m \{ \widehat{G}(\omega, \mathbf{z}^S, \mathbf{z}) \}^2 d\omega. \quad (3.9)$$

In view of Proposition 3.3.1, the resolution of the imaging functional \mathcal{I} is determined by the kernel $\mathcal{Q}(\mathbf{z}^S, \mathbf{z})$. High-frequency components are penalized in this functional because of the factor ω^{-2} and therefore, the resolution is limited. In order to achieve a better resolution, we shall modify the imaging functional to make its smoothing kernel as close as possible to a Dirac distribution $\delta(\mathbf{z}^S - \mathbf{z})$. We should be aware that enhancing the high-frequency components may cause instability in the imaging procedure. In the next subsection we introduce a weighted imaging algorithm where the weight is chosen in terms of estimations of the power spectral density of the noise sources.

3.3.1 TWO- AND THREE-DIMENSIONAL HOMOGENEOUS MEDIA

In this subsection, we first show that the smoothing operator is a simple convolution operator in the case of a three-dimensional homogeneous background with $c(\mathbf{x}) \equiv 1$ in \mathbb{R}^3 . Indeed, the Green function is

$$G(t, \mathbf{x}, \mathbf{y}) = \frac{1}{4\pi|\mathbf{x}-\mathbf{y}|} \delta(t - |\mathbf{x}-\mathbf{y}|)$$

and hence the imaging functional takes the simple form

$$\mathcal{I}(\mathbf{z}^S) = \frac{1}{8\pi} \iint_{\partial\Omega \times \partial\Omega} \frac{1}{|\mathbf{x}-\mathbf{z}^S||\mathbf{y}-\mathbf{z}^S|} C(|\mathbf{y}-\mathbf{z}^S| - |\mathbf{x}-\mathbf{z}^S|, \mathbf{x}, \mathbf{y}) d\sigma(\mathbf{x}) d\sigma(\mathbf{y}).$$

We also have

$$\frac{1}{\omega} \Im m \{ \widehat{G}(\omega, \mathbf{z}^S, \mathbf{z}) \} = \frac{1}{4\pi} \text{sinc}(\omega|\mathbf{z}-\mathbf{z}^S|)$$

and therefore, the smoothing operator is a convolution

$$\mathcal{I}(\mathbf{z}^S) \simeq \int_{\Omega} Q(\mathbf{z}^S - \mathbf{z}) K(\mathbf{z}) d\mathbf{z}$$

with the convolution kernel

$$Q(\mathbf{z}) = \frac{1}{16\pi^2} \int_{\mathbb{R}} \widehat{F}(\omega) \text{sinc}^2(\omega|\mathbf{z}|) d\omega.$$

In a two-dimensional homogeneous medium, the convolution kernel has the form

$$Q(\mathbf{z}) = \frac{1}{16} \int_{\mathbb{R}} \frac{\widehat{F}(\omega)}{\omega^2} J_0^2(\omega|\mathbf{z}|) d\omega,$$

where J_0 is the Bessel function of the first kind and of order zero.

The presence of the factor ω^{-2} indicates that a frequency-dependent weight should be used (as explained below) in order to avoid this singularity that amplifies the low-frequency components, or that the back-propagation should be carried out with the time-derivative of the Green function, so that the factor ω^{-2} is cancelled.

The power spectral density of the noise sources plays a smoothing role in the kernel Q while we would like this kernel to be as close as possible to a Dirac distribution. The idea for an improved functional is based on the estimation of the power spectral density of the noise sources. Let us introduce

$$\mathcal{F}(\omega) = \int_{\partial\Omega} \widehat{C}(\omega, \mathbf{x}, \mathbf{x}) d\sigma(\mathbf{x}). \quad (3.10)$$

The power spectral density $\mathcal{F}(\omega)$ can be estimated from the data. However, one must pay attention to the fact that time-harmonic quantities are not statistically stable. It is a well-known problem that the variance of the periodogram remains

positive whatever the duration of the recorded signals may be. One must average the empirical estimations (3.10) over moving frequency windows, large enough to ensure statistical stability and small enough to capture the variations of the power spectral density $\hat{F}(\omega)$. This means that the width $\Delta\omega$ of the moving frequency window should be larger than $1/T$, where T is defined in (3.3), but smaller than the noise bandwidth:

$$\widetilde{\mathcal{F}}(\omega) = \frac{1}{\Delta\omega} \int_{\omega-\Delta\omega/2}^{\omega+\Delta\omega/2} \int_{\partial\Omega} \widehat{C}(\omega', \mathbf{x}, \mathbf{x}) d\sigma(\mathbf{x}) d\omega'.$$

Using once again Helmholtz-Kirchhoff identity, one can see that $\hat{F}(\omega)$ can be estimated by $\widetilde{\mathcal{F}}(\omega)$:

$$\widetilde{\mathcal{F}}(\omega) \simeq \hat{F}(\omega) \int_{\Omega} \frac{\Im m\{\widehat{G}(\omega, \mathbf{z}, \mathbf{z})\}}{\omega} K(\mathbf{z}) d\mathbf{z}.$$

In a three-dimensional homogeneous medium with $c(\mathbf{x}) \equiv 1$, we have

$$\frac{\Im m\{\widehat{G}(\omega, \mathbf{z}, \mathbf{z})\}}{\omega} = \frac{1}{4\pi}$$

and $\widetilde{\mathcal{F}}(\omega)$ is proportional to the power spectral density of the noise sources:

$$\widetilde{\mathcal{F}}(\omega) \simeq K_0 \hat{F}(\omega), \quad \text{with} \quad K_0 = \frac{1}{4\pi} \int_{\Omega} K(\mathbf{z}) d\mathbf{z}.$$

Let us introduce a weight function $W(\omega)$ and the weighted imaging functional \mathcal{I}_W as

$$\mathcal{I}_W(\mathbf{z}^S) = \int_{\mathbb{R}} \frac{W(\omega)}{\widetilde{\mathcal{F}}(\omega)} \iint_{\partial\Omega \times \partial\Omega} \widehat{G}(\omega, \mathbf{x}, \mathbf{z}^S) \overline{\widehat{G}(\omega, \mathbf{y}, \mathbf{z}^S)} \widehat{C}(\omega, \mathbf{x}, \mathbf{y}) d\sigma(\mathbf{x}) d\sigma(\mathbf{y}) d\omega. \quad (3.11)$$

PROPOSITION 3.3.2. *In a three-dimensional homogeneous background with $c(\mathbf{x}) \equiv 1$, we have*

$$\mathcal{I}_W(\mathbf{z}^S) \simeq \int_{\Omega} Q_W(\mathbf{z}^S - \mathbf{z}) \frac{K(\mathbf{z})}{K_0} d\mathbf{z} \quad (3.12)$$

with

$$Q_W(\mathbf{z}) = \frac{1}{16\pi^2} \int_{\mathbb{R}} W(\omega) \text{sinc}^2(\omega|\mathbf{z}|) d\omega. \quad (3.13)$$

In fact, the weight function $W(\omega)$ should be supported in the estimated band width $(-\omega_{\max}, \omega_{\max})$ of the recorded noise signals otherwise the ratio $W(\omega)/\widetilde{\mathcal{F}}(\omega)$ in (3.11) makes no sense. The idea is to choose $W(\omega)$ so that the convolution kernel (also called point spread function) Q_W is as close as possible to a Dirac distribution.

In a two-dimensional homogeneous medium, it is easy to check that (3.12) holds with

$$K_0 = \frac{1}{4} \int_{\Omega} K(\mathbf{z}) d\mathbf{z},$$

and

$$Q_W(\mathbf{z}) = \frac{1}{16} \int_{\mathbb{R}} \frac{W(\omega)}{\omega^2} J_0^2(\omega|\mathbf{z}|) d\omega. \quad (3.14)$$

The Fourier transform of the kernel Q_W is then

$$\widehat{Q}_W(\mathbf{k}) = \frac{1}{2|\mathbf{k}|^3} \int_{1/2}^{\infty} \frac{W(|\mathbf{k}|u)}{u^2(4u^2-1)^{1/2}} du. \quad (3.15)$$

To prove (3.15) we use [1, formula 6.522.11]

$$\int_0^{\infty} x J_0^2(ax) J_0(bx) dx = \frac{2}{\pi b(4a^2 - b^2)^{1/2}} \mathbf{1}_{0 < b < 2a},$$

where $\mathbf{1}$ denotes the characteristic function, to get

$$\int_{\mathbb{R}^2} J_0^2(\omega|\mathbf{z}|) \exp(i\mathbf{z} \cdot \mathbf{k}) d\mathbf{z} = \frac{4}{|\mathbf{k}|(4\omega^2 - |\mathbf{k}|^2)^{1/2}} \mathbf{1}_{|\mathbf{k}| < 2|\omega|.} \quad (3.16)$$

Substituting (3.16) into

$$\widehat{Q}_W(\mathbf{k}) = \frac{1}{16} \int_{\mathbb{R}} \int_{\mathbb{R}^2} \frac{W(\omega)}{\omega^2} J_0^2(\omega|\mathbf{z}|) \exp(i\mathbf{z} \cdot \mathbf{k}) d\mathbf{z} d\omega, \quad (3.17)$$

gives the desired formula (3.15).

With formulas (3.13) and (3.14) in hand, recalling the closure relations [100]

$$\int_0^{+\infty} \omega J_0^2(\omega|\mathbf{z}|) d\omega = \frac{1}{|\mathbf{z}|} \delta(\mathbf{z}), \quad (3.18)$$

and

$$\int_0^{+\infty} \omega^2 \text{sinc}^2(\omega|\mathbf{z}|) d\omega = \frac{1}{|\mathbf{z}|^2} \delta(\mathbf{z}), \quad (3.19)$$

which hold in the sense of distributions, a potential candidate for the filter $W(\omega)$ should be

$$W(\omega) = \begin{cases} |\omega|^3 \mathbf{1}_{|\omega| < \omega_{\max}} & \text{for } d = 2, \\ \omega^2 \mathbf{1}_{|\omega| < \omega_{\max}} & \text{for } d = 3, \end{cases}$$

where $(-\omega_{\max}, \omega_{\max})$ is the estimated support of $\widetilde{\mathcal{F}}(\omega)$. In particular, for $d = 2$, we have

$$\begin{cases} \widehat{Q}_W(\mathbf{k}) = \frac{\omega_{\max}}{4|\mathbf{k}|} \left(1 - \frac{|\mathbf{k}|^2}{4\omega_{\max}^2}\right)^{1/2} \mathbf{1}_{|\mathbf{k}| \leq 2\omega_{\max}}, \\ Q_W(\mathbf{z}) = \frac{\omega_{\max}^2}{4} \left[J_0^2(\omega_{\max}|\mathbf{z}|) + J_1^2(\omega_{\max}|\mathbf{z}|) \right]. \end{cases}$$

3.3.2 BACK-PROPAGATION IN A TWO-DIMENSIONAL MEDIUM

We show in this subsection how it is possible to implement a parallel version of the imaging functional. Here we do not assume that $c(\mathbf{x}) \equiv 1$. For the sake of simplicity, we consider only the two-dimensional case. Similar calculations can be carried out in three dimensions using spherical harmonics. We set Ω to be the unit disk centred at zero and denote by $C(\tau, \theta, \theta')$ the cross correlations measured between the points \mathbf{e}_θ and $\mathbf{e}_{\theta'}$, with $\mathbf{e}_\theta = (\cos \theta, \sin \theta)$. We can expand the cross correlation in the basis $\exp(in\theta)$:

$$C(\tau, \theta, \theta') = \sum_{n, m \in \mathbb{Z}} c_{n, m}(\tau) \exp(in\theta + im\theta'),$$

where

$$c_{n, m}(\tau) = \frac{1}{4\pi^2} \int_0^{2\pi} \int_0^{2\pi} C(\tau, \theta, \theta') \exp(-in\theta - im\theta') d\theta d\theta'.$$

Then the imaging functional takes the form

$$\mathcal{I}(\mathbf{z}^S) = 2\pi \sum_{n, m \in \mathbb{Z}} \int_0^\infty \int_0^\infty p_n(t, \mathbf{z}^S) p_m(s, \mathbf{z}^S) c_{n, m}(s-t) ds dt,$$

or

$$\mathcal{I}(\mathbf{z}^S) = \sum_{n, m \in \mathbb{Z}} \int_{\mathbb{R}} \hat{p}_n(\omega, \mathbf{z}^S) \overline{\hat{p}_m(\omega, \mathbf{z}^S)} \hat{c}_{n, m}(\omega) d\omega,$$

where

$$p_n(t, \mathbf{z}) = \int_0^{2\pi} G(t, \mathbf{e}_\theta, \mathbf{z}) \exp(in\theta) d\theta$$

is the solution to the problem

$$\begin{cases} \frac{1}{c^2(\mathbf{x})} \frac{\partial^2 p_n}{\partial t^2}(t, \mathbf{x}) - \Delta p_n(t, \mathbf{x}) = f_n(\mathbf{x}) \delta_{\partial\Omega}(\mathbf{x}) \delta_0(t), & (t, \mathbf{x}) \in \mathbb{R} \times \mathbb{R}^2, \\ p_n(t, \mathbf{x}) = 0, & t \ll 0, \\ \frac{\partial p_n(t, \mathbf{x})}{\partial t} = 0, & t \ll 0. \end{cases}$$

Here $\delta_{\partial\Omega}$ is the Dirac mass at $\partial\Omega$ and $f_n(\mathbf{x}) = (x_1 + ix_2)^n$ for $\mathbf{x} = (x_1, x_2)$ so that $\exp(in\theta) = f_n(\cos \theta, \sin \theta)$. Note that $f_{-n} = \overline{f_n}$ so that $p_{-n} = \overline{p_n}$. In practice the functional is truncated as follows

$$\mathcal{I}_N(\mathbf{z}^S) = 2\pi \sum_{n, m = -N}^N \int_0^\infty \int_0^\infty p_n(t, \mathbf{z}^S) p_m(s, \mathbf{z}^S) c_{n, m}(s-t) ds dt.$$

This version of the imaging functional can be implemented in a parallel way: on one hand, one needs to compute the functions $p_n(t, \mathbf{z})$ for $n = 0, \dots, N$, $t > 0$, $\mathbf{z} \in \Omega$ (we do not need to know the data), which requires to solve N wave equations; on the other hand one computes the coefficients $c_{n, m}(\tau)$, $n, m = 0, \dots, N$, $\tau \in \mathbb{R}$ from

the data set. However, the memory cost is huge, because one needs to store the full time-space solutions of the N wave equations (at least the solutions in the search region).

A numerical alternative consists of using a PDE description of the time reversal algorithm [7, 65]. Indeed, note that

$$\begin{aligned}
\mathcal{I}(\mathbf{z}^S) &= \int_{\mathbb{R}} \int_{\partial\Omega} \int_{\partial\Omega} \widehat{G}(\omega, \mathbf{x}, \mathbf{z}^S) \overline{\widehat{G}(\omega, \mathbf{y}, \mathbf{z}^S)} \widehat{C}(\omega, \mathbf{x}, \mathbf{y}) d\sigma(\mathbf{x}) d\sigma(\mathbf{y}) d\omega \\
&= \int_{\mathbb{R}} \int_{\partial\Omega} \int_{\partial\Omega} \widehat{G}(\omega, \mathbf{x}, \mathbf{z}^S) \overline{\widehat{G}(\omega, \mathbf{y}, \mathbf{z}^S)} \overline{\widehat{p}(\omega, \mathbf{x})} \widehat{p}(\omega, \mathbf{y}) d\sigma(\mathbf{x}) d\sigma(\mathbf{y}) d\omega \\
&= \int_{\mathbb{R}} \left| \int_{\partial\Omega} \widehat{G}(\omega, \mathbf{x}, \mathbf{z}^S) \overline{\widehat{p}(\omega, \mathbf{x})} d\sigma(\mathbf{x}) \right|^2 d\omega \\
&= 2\pi \int_0^T v(t, \mathbf{z}^S)^2 dt,
\end{aligned}$$

where the function v is expressed in the form

$$v(t, \mathbf{x}) = \int_0^T v_s(t, \mathbf{x}) ds,$$

and v_s is the solution of

$$\begin{cases} \frac{1}{c^2(\mathbf{x})} \frac{\partial^2 v_s(t, \mathbf{x})}{\partial t^2} - \Delta v_s(t, \mathbf{x}) = p(T-s) \delta_{\partial\Omega}(\mathbf{x}) \delta(t-s) & \forall (t, \mathbf{x}) \in \mathbb{R} \times \mathbb{R}^d, \\ v_s(t, \mathbf{x}) = 0, & \forall t \ll s, \\ \frac{\partial}{\partial t} v_s(t, \mathbf{x}) = 0, & \forall t \ll s. \end{cases}$$

More generally, the imaging functional $\mathcal{I}_W(\mathbf{z}^S)$ can be obtained by applying $\mathcal{I}(\mathbf{z}^S)$ on the filtered data $\widetilde{p}(t, \mathbf{x})$, obtained as

$$\widetilde{p}(\omega, \mathbf{x}) = \sqrt{\frac{W(\omega)}{\mathcal{F}(\omega)}} \widehat{p}(\omega, \mathbf{x}).$$

In this chapter, we use this method to perform some numerical experiments.

3.3.3 NUMERICAL SIMULATIONS

In this subsection, we first describe the discretization of the noise sources and recorded signals that will be used in numerical simulations. We introduce a regular grid of points $(\mathbf{x}_k)_{k=1, \dots, N_x}$ with grid step h_x covering the support of K and a regular grid of positive frequencies $(\omega_j)_{j=1, \dots, N_\omega}$ with grid step h_ω covering the support of \widehat{F} . The noise source term can be discretized in space as

$$n(t, \mathbf{x}) = \frac{1}{\pi^{d/2} h_x^{d/2}} \sum_{k=1}^{N_x} \exp\left(-\frac{|\mathbf{x}_k - \mathbf{x}|^2}{h_x^2}\right) K(\mathbf{x}_k)^{1/2} n_k(t), \quad (3.20)$$

where $n_k(t)$ are independent stationary Gaussian processes with mean zero and covariance function $F(t)$. They can be discretized in time/frequency as

$$n_k(t) = \frac{(2h_\omega)^{1/2}}{\pi^{1/2}} \Re e \left\{ \sum_{j=1}^{N_\omega} Z_{j,k} \hat{F}(\omega_j)^{1/2} \exp(-i\omega_j t) \right\},$$

where $Z_{k,j} = A_{k,j} + iB_{k,j}$ with $A_{k,j}$ and $B_{k,j}$ being independent Gaussian random variables with mean zero and variance $1/2$ (so that $\langle Z_{k,j}^2 \rangle = 0$ and $\langle |Z_{k,j}|^2 \rangle = 1$). We have indeed (remember that \hat{F} is even and non-negative real-valued)

$$\begin{aligned} \langle n_k(t) n_k(t+\tau) \rangle &= \frac{h_\omega}{2\pi} \left[\sum_{j=1}^{N_\omega} \hat{F}(\omega_j) \exp(-i\omega_j \tau) + \sum_{j=1}^{N_\omega} \hat{F}(-\omega_j) \exp(i\omega_j \tau) \right] \\ &\simeq \frac{1}{2\pi} \int_{\mathbb{R}} \hat{F}(\omega) \exp(-i\omega \tau) d\omega \\ &= F(\tau), \end{aligned}$$

provided h_ω is small enough, and

$$\begin{aligned} \langle n(t, \mathbf{x}) n(t+\tau, \mathbf{y}) \rangle &= \frac{1}{\pi^d h_x^d} \exp\left(-\frac{|\mathbf{x}-\mathbf{y}|^2}{2h_x^2}\right) \sum_{k=1}^{N_x} \exp\left(-2\frac{\left|\frac{\mathbf{x}+\mathbf{y}}{2}-\mathbf{x}_k\right|^2}{h_x^2}\right) K(\mathbf{x}_k) F(\tau) \\ &\simeq \frac{1}{\pi^d h_x^{2d}} \exp\left(-\frac{|\mathbf{x}-\mathbf{y}|^2}{2h_x^2}\right) \int_{\mathbb{R}^d} \exp\left(-2\frac{\left|\frac{\mathbf{x}+\mathbf{y}}{2}-\mathbf{z}\right|^2}{h_x^2}\right) K(\mathbf{z}) d\mathbf{z} F(\tau) \\ &= \frac{1}{\pi^d h_x^{2d}} \exp\left(-\frac{|\mathbf{x}-\mathbf{y}|^2}{2h_x^2}\right) \int_{\mathbb{R}^d} \exp\left(-2\frac{|\mathbf{z}|^2}{h_x^2}\right) K\left(\frac{\mathbf{x}+\mathbf{y}}{2}-\mathbf{z}\right) d\mathbf{z} F(\tau) \\ &\simeq \frac{1}{(2\pi)^{d/2} h_x^d} \exp\left(-\frac{|\mathbf{x}-\mathbf{y}|^2}{2h_x^2}\right) K\left(\frac{\mathbf{x}+\mathbf{y}}{2}\right) F(\tau) \\ &\simeq \delta(\mathbf{x}-\mathbf{y}) K(\mathbf{x}) F(\tau), \end{aligned}$$

provided h_x is small enough.

It is also possible to take

$$n(t, \mathbf{x}) = h_x^{d/2} \sum_{k=1}^{N_x} \delta(\mathbf{x}_k - \mathbf{x}) K(\mathbf{x}_k)^{1/2} n_k(t)$$

instead of (3.20), which is the simplest model for numerical simulations (a collection of uncorrelated point sources). In these conditions the recorded noise signal at \mathbf{x} is

$$p(t, \mathbf{x}) = \frac{(2h_\omega)^{1/2} h_x^{d/2}}{\pi^{1/2}} \Re e \left\{ \sum_{j=1}^{N_\omega} \sum_{k=1}^{N_x} \hat{G}(\omega_j, \mathbf{x}, \mathbf{x}_k) \hat{F}(\omega_j)^{1/2} K(\mathbf{x}_k)^{1/2} Z_{j,k} \exp(-i\omega_j t) \right\}$$

and the statistical cross correlation is (remember $\widehat{G}(-\omega, \mathbf{x}, \mathbf{y}) = \overline{\widehat{G}(\omega, \mathbf{x}, \mathbf{y})}$)

$$\begin{aligned} C(\tau, \mathbf{x}, \mathbf{y}) &= \frac{h_\omega h_x^d}{2\pi} \left[\sum_{j=1}^{N_\omega} \sum_{k=1}^{N_x} \overline{\widehat{G}(\omega_j, \mathbf{x}, \mathbf{x}_k)} \widehat{G}(\omega_j, \mathbf{y}, \mathbf{x}_k) \widehat{F}(\omega_j) K(\mathbf{x}_k) \exp(-i\omega_j \tau) \right. \\ &\quad \left. + \sum_{j=1}^{N_\omega} \sum_{k=1}^{N_x} \overline{\widehat{G}(-\omega_j, \mathbf{x}, \mathbf{x}_k)} \widehat{G}(-\omega_j, \mathbf{y}, \mathbf{x}_k) \widehat{F}(-\omega_j) K(\mathbf{x}_k) \exp(i\omega_j \tau) \right] \\ &\simeq \frac{1}{2\pi} \int_{\mathbb{R}} \int_{\Omega} \overline{\widehat{G}(\omega, \mathbf{x}, \mathbf{z})} \widehat{G}(\omega, \mathbf{y}, \mathbf{z}) \widehat{F}(\omega) K(\mathbf{z}) \exp(-i\omega \tau) d\mathbf{z} d\omega. \end{aligned}$$

For all numerical experiments presented in this chapter, Ω is assumed to be a unit disk centered at the origin. The function F is chosen as

$$\widehat{F}(\omega) = \exp\left(-\pi \frac{\omega^2}{\omega_{\max}^2}\right). \quad (3.21)$$

The solution v_s of the equation

$$\frac{1}{c^2(\mathbf{x})} \frac{\partial^2 v_s(t, \mathbf{x})}{\partial t^2} - \Delta v_s(t, \mathbf{x}) = p(T-s, \mathbf{x}) \delta_{\partial\Omega}(\mathbf{x}) \delta(t-s)$$

is computed over a larger box $\Omega \subset Q = [-L/2, L/2]^2$. We use a Fourier spectral approach coupled with a Perfectly Matched Layer (PML) technique to simulate a free outgoing interface on ∂Q . The boundary $\partial\Omega$ is discretized using steps of discretization given by $h_t = T/N_t$ and $h_x = L/N_x$.

Figure 3.1 contains the numerical reconstructions of the source location K using the imaging functionals \mathcal{I} and \mathcal{I}_W for $W(\omega) = |\omega|^3 \mathbf{1}_{|\omega| < \omega_{\max}}$. The first line corresponds to the case of well separated point sources. It turns out that both imaging functionals give an efficient reconstruction of the source K . The second line corresponds to the case of extended sources (five localized Gaussians). We observe in this case that the second imaging functional \mathcal{I}_W gives a better reconstruction of K . We expect that this observation is a consequence of the factor ω^{-2} which appears in the kernel associated to \mathcal{I} and penalizes the high-frequency components of the image.

Figure 3.2 presents estimations of the power spectral density. Averaging (3.10) over moving frequency windows yields a statistically stable estimation.

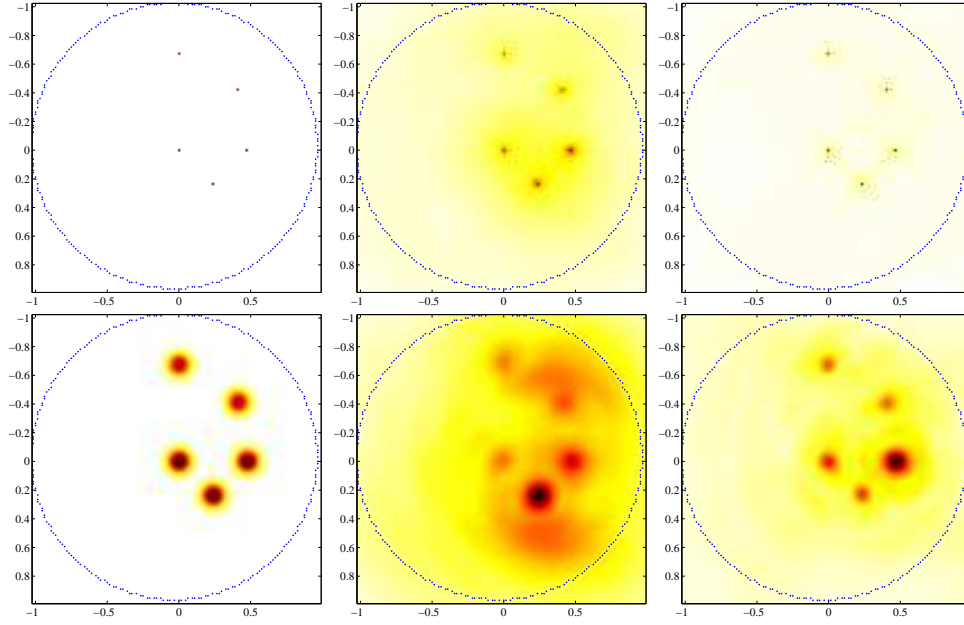


FIGURE 3.1. Non-attenuating medium with $T = 8$, $\omega_{\max} = 1000$, $N_x = 2^8$, and $N_t = 2^{11}$. Top line: five point sources; bottom line: five extended sources. Left: $K(\mathbf{x})$; middle: reconstruction of K using \mathcal{S} ; right: reconstruction of K using \mathcal{S}_W with $W(\omega) = |\omega|^3 \mathbf{1}_{|\omega| < \omega_{\max}}$.

3.4 LOCALIZATION OF SOURCES IN AN ATTENUATING MEDIUM

In this section, we consider the thermo-viscous wave model to incorporate the attenuation effect in wave propagation. Let p_a be the solution of the problem

$$\begin{cases} \frac{1}{c^2(\mathbf{x})} \frac{\partial^2 p_a}{\partial t^2}(t, \mathbf{x}) - \Delta p_a(t, \mathbf{x}) - a \frac{\partial}{\partial t} \Delta p_a(t, \mathbf{x}) = n(t, \mathbf{x}), & (t, \mathbf{x}) \in \mathbb{R} \times \mathbb{R}^d, \\ p_a(t, \mathbf{x}) = 0, & t \ll 0, \\ \frac{\partial p_a}{\partial t}(t, \mathbf{x}) = 0, & t \ll 0. \end{cases}$$

Again, the problem is to reconstruct the source function K from the data set

$$\{p_a(t, \mathbf{x}), t \in [0, T], \mathbf{x} \in \partial\Omega\}$$

recorded at the surface of the domain Ω .

We introduce the fundamental solution $\widehat{G}_a(\omega, \mathbf{x}, \mathbf{y})$ of the Helmholtz equation

$$\frac{\omega^2}{c^2(\mathbf{x})} \widehat{G}_a(\omega, \mathbf{x}, \mathbf{y}) + (1 - i a \omega) \Delta_{\mathbf{x}} \widehat{G}_a(\omega, \mathbf{x}, \mathbf{y}) = -\delta(\mathbf{y} - \mathbf{x}).$$

It is given by

$$\widehat{G}_a(\omega, \mathbf{x}, \mathbf{y}) = \frac{\kappa_a(\omega)^2}{\omega^2} \widehat{G}(\kappa_a(\omega), \mathbf{x}, \mathbf{y}) \quad (3.22)$$

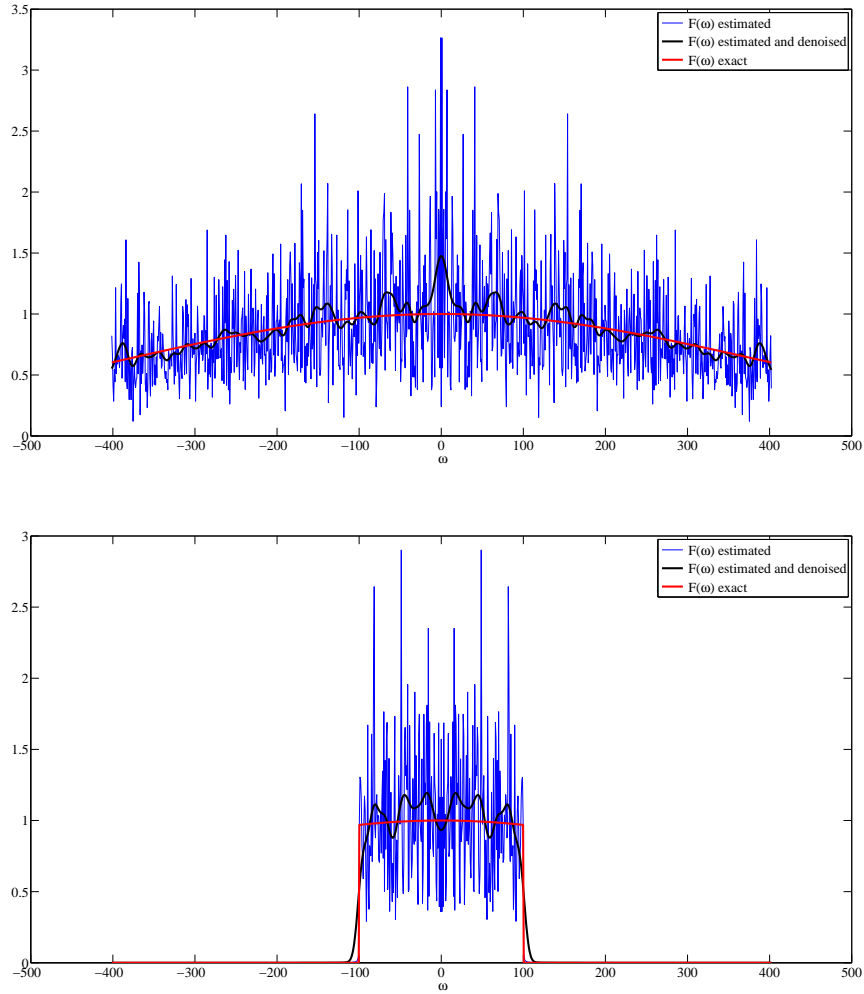


FIGURE 3.2. Estimations of the power spectral density with and without averaging over a moving frequency window. Top figure: $\hat{F}(\omega) = \exp\left(-\pi \frac{\omega^2}{\omega_{\max}^2}\right)$ (as in (3.21)) with $\omega_{\max} = 1000$. Bottom figure: $\hat{F}(\omega) = \mathbf{1}_{|\omega| \leq 100} \exp\left(-\pi \frac{\omega^2}{\omega_{\max}^2}\right)$.

in terms of the non-attenuating Green function $\widehat{G}(\omega, \mathbf{x}, \mathbf{y}) = \widehat{G}_0(\omega, \mathbf{x}, \mathbf{y})$, where

$$\kappa_a(\omega) = \frac{\omega}{\sqrt{1 - i a \omega}}.$$

The statistical cross correlation is

$$\begin{aligned} C_a(\tau, \mathbf{x}, \mathbf{y}) &= \langle p_a(t, \mathbf{x}) p_a(t + \tau, \mathbf{y}) \rangle \\ &= \frac{1}{2\pi} \int_{\mathbb{R}} \left[\int_{\Omega} \overline{\widehat{G}_a(\omega, \mathbf{x}, \mathbf{z})} \widehat{G}_a(\omega, \mathbf{y}, \mathbf{z}) K(\mathbf{z}) d\mathbf{z} \right] \widehat{F}(\omega) \exp(-i\omega\tau) d\omega. \end{aligned}$$

Our strategy to localize the sources is to back-propagate the cross correlation with a regularized version of the adjoint propagator.

3.4.1 HELMHOLTZ-KIRCHHOFF IDENTITY

Our main tool for studying noise source localization in attenuating media is the following result. It is a generalization to attenuating media of the Helmholtz-Kirchhoff identity (3.7).

LEMMA 3.4.1. *If Ω is a ball with large radius (compared to the wavelength $2\pi/\omega$) and $c(\mathbf{x})$ is equal to one outside the ball then*

$$\int_{\partial\Omega} \widehat{G}_{-a}(\omega, \mathbf{x}, \mathbf{z}^S) \overline{\widehat{G}_a(\omega, \mathbf{x}, \mathbf{z})} d\sigma(\mathbf{x}) \simeq \frac{1}{2i\overline{\kappa_a(\omega)}(1 + i a \omega)} (\widehat{G}_{-a}(\omega, \mathbf{z}, \mathbf{z}^S) - \overline{\widehat{G}_a(\omega, \mathbf{z}, \mathbf{z}^S)}). \quad (3.23)$$

We also have

$$\begin{aligned} (1 + a^2\omega^2)\kappa_{a,r}(\omega) \int_{\partial\Omega} \widehat{G}_a(\omega, \mathbf{x}, \mathbf{z}^S) \overline{\widehat{G}_a(\omega, \mathbf{x}, \mathbf{z})} d\sigma(\mathbf{x}) \\ + a\omega^3 \int_{\Omega} c^{-2}(\mathbf{z}) \widehat{G}_a(\omega, \mathbf{x}, \mathbf{z}^S) \overline{\widehat{G}_a(\omega, \mathbf{x}, \mathbf{z})} d\mathbf{x} \\ \simeq \Im m \left\{ \widehat{G}_a(\omega, \mathbf{z}^S, \mathbf{z}) \right\} - a\omega \Re e \left\{ \widehat{G}_a(\omega, \mathbf{z}^S, \mathbf{z}) \right\} \end{aligned} \quad (3.24)$$

with

$$\kappa_{a,r}(\omega) = \Re e \left\{ \kappa_a(\omega) \right\} = \frac{\omega}{\sqrt{2}\sqrt{1 + a^2\omega^2}} \sqrt{\sqrt{1 + a^2\omega^2} + 1}. \quad (3.25)$$

Proof. It is a consequence of Green's theorem and the fact that $\overline{\kappa_a(\omega)} = \kappa_{-a}(\omega)$. More precisely, we consider the equations

$$-\frac{\omega^2}{c^2(\mathbf{x})} \widehat{G}_{-a}(\omega, \mathbf{x}, \mathbf{z}^S) - (1 + i a \omega) \Delta_{\mathbf{x}} \widehat{G}_{-a}(\omega, \mathbf{x}, \mathbf{z}^S) = \delta(\mathbf{z}^S - \mathbf{x}) \quad (3.26)$$

and

$$-\frac{\omega^2}{c^2(\mathbf{x})} \overline{\widehat{G}_a(\omega, \mathbf{x}, \mathbf{z})} - (1 + i a \omega) \Delta_{\mathbf{x}} \overline{\widehat{G}_a(\omega, \mathbf{x}, \mathbf{z})} = \delta(\mathbf{z} - \mathbf{x}). \quad (3.27)$$

We then multiply (3.26) by $\overline{\widehat{G}_a(\omega, \mathbf{x}, \mathbf{z})}$ and (3.27) by $\widehat{G}_{-a}(\omega, \mathbf{x}, \mathbf{z}^S)$, subtract these two subsequent equations from each other, integrate over Ω and apply Green's divergence theorem. \square

Note the presence of the volume integral in (3.24) which shows that the adjoint Green function \widehat{G}_{-a} should be used for back-propagation and not the Green function \widehat{G}_a . The imaging functional for source localization should be

$$\mathcal{I}(\mathbf{z}^S) = \int_{\mathbb{R}} \iint_{\partial\Omega \times \partial\Omega} \widehat{G}_{-a}(\omega, \mathbf{x}, \mathbf{z}^S) \overline{\widehat{G}_{-a}(\omega, \mathbf{y}, \mathbf{z}^S)} \widehat{C}_a(\omega, \mathbf{x}, \mathbf{y}) d\sigma(\mathbf{x}) d\sigma(\mathbf{y}) d\omega \quad (3.28)$$

for the search point $\mathbf{z}^S \in \Omega$. However, the back-propagation uses the adjoint operator $\widehat{G}_{-a}(\omega, \mathbf{x}, \mathbf{z}^S)$ that has an exponentially growing part, since it can be seen from

$$\kappa_{a,i}(\omega) = \Im m\{\kappa_a(\omega)\} = \frac{|\omega| \operatorname{sgn}(a)}{\sqrt{2}\sqrt{1+a^2\omega^2}} \sqrt{\sqrt{1+a^2\omega^2}-1}, \quad (3.29)$$

where sgn denotes the sign function, that $\kappa_{-a,i}(\omega)$ is negative. Thus we should use a regularized version of the form

$$\mathcal{I}_\rho(\mathbf{z}^S) = \int_{|\omega| \leq \rho} \iint_{\partial\Omega \times \partial\Omega} \widehat{G}_{-a}(\omega, \mathbf{x}, \mathbf{z}^S) \overline{\widehat{G}_{-a}(\omega, \mathbf{y}, \mathbf{z}^S)} \widehat{C}_a(\omega, \mathbf{x}, \mathbf{y}) d\sigma(\mathbf{x}) d\sigma(\mathbf{y}) d\omega, \quad (3.30)$$

where ρ is a cut-off frequency. Using Lemma 3.4.1 we obtain the following result.

PROPOSITION 3.4.2. *The regularized imaging functional (3.30) satisfies*

$$\mathcal{I}_\rho(\mathbf{z}^S) \simeq \int_{\Omega} \mathcal{Q}_\rho(\mathbf{z}^S, \mathbf{z}) K(\mathbf{z}) d\mathbf{z} \quad (3.31)$$

with

$$\mathcal{Q}_\rho(\mathbf{z}^S, \mathbf{z}) = \int_{|\omega| \leq \rho} \frac{\widehat{F}(\omega)}{4\omega^2(1+a^2\omega^2)^{1/2}} \left| \widehat{G}_{-a}(\omega, \mathbf{z}, \mathbf{z}^S) - \overline{\widehat{G}_a(\omega, \mathbf{z}, \mathbf{z}^S)} \right|^2 d\omega. \quad (3.32)$$

The next subsection will show how to calibrate the cut-off parameter ρ in order to get a stable imaging functional.

3.4.2 THREE-DIMENSIONAL HOMOGENEOUS MEDIUM

Using the explicit expression of the homogeneous Green function we get the following lemma.

LEMMA 3.4.3. *The Green function $\widehat{G}_{-a}(\omega, \mathbf{x}, \mathbf{y})$ is given by*

$$\widehat{G}_{-a}(\omega, \mathbf{x}, \mathbf{y}) = \frac{\kappa_{-a}(\omega)^2}{\omega^2} \widehat{G}(\kappa_{-a}(\omega), \mathbf{x}, \mathbf{y}) \quad \text{with} \quad \widehat{G}(\omega, \mathbf{x}, \mathbf{y}) = \frac{\exp(i\omega|\mathbf{x}-\mathbf{y}|)}{4\pi|\mathbf{x}-\mathbf{y}|}.$$

If Ω is a ball with large radius (compared to the wavelength), then we have

$$\begin{aligned} & \int_{\partial\Omega} \widehat{G}_{-a}(\omega, \mathbf{x}, \mathbf{z}^S) \overline{\widehat{G}_a(\omega, \mathbf{x}, \mathbf{z})} d\sigma(\mathbf{x}) \\ & \simeq \frac{\kappa_{a,r}(\omega)}{4\pi\omega(1+i a\omega)^{3/2}} \operatorname{sinc}(\kappa_{a,r}(\omega)|\mathbf{z}^S - \mathbf{z}|) \cosh(\kappa_{a,i}(\omega)|\mathbf{z}^S - \mathbf{z}|) \\ & - i \frac{\kappa_{a,i}(\omega)}{4\pi\omega(1+i a\omega)^{3/2}} \cos(\kappa_{a,r}(\omega)|\mathbf{z}^S - \mathbf{z}|) \operatorname{sinhc}(\kappa_{a,i}(\omega)|\mathbf{z}^S - \mathbf{z}|), \end{aligned} \quad (3.33)$$

where $\text{sinc}(r) = \frac{\sin(r)}{r}$ and $\text{sinhc}(r) = \frac{\sinh(r)}{r}$.

The adjoint operator $\widehat{G}_{-a}(\omega, \mathbf{x}, \mathbf{z}^S)$ grows exponentially as $\exp(\kappa_{a,i}(\omega)|\mathbf{z}^S - \mathbf{x}|)$. This term should not be much larger than one, otherwise noise terms would be amplified in the back-propagation. Since $\kappa_{a,i}(\omega)$ grows like $a\omega^2/2$ for $a|\omega| < 1$, (and as $(|\omega|/(2a))^{1/2}$ for $a|\omega| > 1$), one should not back-propagate the high-frequency components, with frequencies larger than $(a \text{diam}(\Omega))^{-1/2}$, where diam denotes the diameter. This limitation also allows to neglect the exponential term in the right-hand side of (3.33) and to claim that identity (3.33) gives a localized kernel that has the form of a sinc with a width of the order of the wavelength.

The imaging functional for source localization is given by (3.30). The cut-off frequency ρ should be of the order of $(a \text{diam}(\Omega))^{-1/2}$. By (3.33) we arrive at the following proposition.

PROPOSITION 3.4.4. *In a three-dimensional homogeneous background with $c(\mathbf{x}) \equiv 1$ and $a > 0$, the regularized imaging functional (3.30) satisfies*

$$\mathcal{I}_\rho(\mathbf{z}^S) \simeq \int_{\Omega} Q_\rho(\mathbf{z}^S - \mathbf{z}) K(\mathbf{z}) d\mathbf{z} \quad (3.34)$$

with

$$\begin{aligned} Q_\rho(\mathbf{z}) &= \frac{1}{16\pi^2} \int_{|\omega| \leq \rho} \widehat{F}(\omega) \frac{\sqrt{1 + a^2\omega^2} + 1}{2(1 + a^2\omega^2)^{5/2}} \text{sinc}^2(\kappa_{a,r}(\omega)|\mathbf{z}|) d\omega \\ &\quad + \frac{1}{16\pi^2} \int_{|\omega| \leq \rho} \widehat{F}(\omega) \frac{\sqrt{1 + a^2\omega^2} - 1}{2(1 + a^2\omega^2)^{5/2}} \text{sinhc}^2(\kappa_{a,i}(\omega)|\mathbf{z}|) d\omega. \end{aligned} \quad (3.35)$$

The first term in (3.35) gives the peak centered at zero in the convolution kernel Q_ρ , with a width of the order of ρ^{-1} . The second term is responsible for the instability of the imaging functional (since it is exponentially growing). In order to make it small compared to the peak, we should cut the high frequencies and choose ρ smaller than $(a \text{diam}(\Omega))^{-1/2}$. This means that, at the expense of a loss in resolution, the imaging functional can be stable.

3.4.3 BACK-PROPAGATION IN A TWO-DIMENSIONAL MEDIUM

We consider that Ω is the unit disk centered at the origin. Here we do not assume that $c(\mathbf{x}) \equiv 1$. We expand the cross correlation as in Subsection 3.3.2:

$$C(\tau, \theta, \theta') = \sum_{n,m \in \mathbb{Z}} c_{n,m}(\tau) \exp(in\theta + im\theta'),$$

where

$$c_{n,m}(\tau) = \frac{1}{4\pi^2} \int_0^{2\pi} \int_0^{2\pi} C(\tau, \theta, \theta') \exp(-in\theta - im\theta') d\theta d\theta'.$$

Then the imaging functional takes the form

$$\mathcal{I}(\mathbf{z}^S) = 2\pi \sum_{n,m \in \mathbb{Z}} \int_0^\infty \int_0^\infty p_{-a,n}(t, \mathbf{z}^S) p_{-a,m}(s, \mathbf{z}^S) c_{n,m}(s-t) ds dt,$$

or

$$\mathcal{I}(\mathbf{z}^S) = \sum_{n,m \in \mathbb{Z}} \int_{\mathbb{R}} \hat{p}_{-a,n}(\omega, \mathbf{z}^S) \overline{\hat{p}_{-a,m}(\omega, \mathbf{z}^S)} \hat{c}_{n,m}(\omega) d\omega,$$

where

$$p_{-a,n}(t, \mathbf{z}) = \int_0^{2\pi} G_{-a}(t, \mathbf{e}_\theta, \mathbf{z}) \exp(in\theta) d\theta$$

is the solution to the problem

$$\begin{cases} \left[\frac{1}{c^2(\mathbf{x})} \frac{\partial^2}{\partial t^2} - \Delta + a \frac{\partial}{\partial t} \Delta \right] p_{-a,n}(t, \mathbf{x}) = f_n(\mathbf{x}) \delta_{\partial\Omega}(\mathbf{x}) \delta(t), & (t, \mathbf{x}) \in \mathbb{R} \times \mathbb{R}^2, \\ p_{-a,n}(t, \mathbf{x}) = \frac{\partial p_{-a,n}(t, \mathbf{x})}{\partial t} = 0, & t \ll 0. \end{cases}$$

As pointed out in Chapter 2, this adjoint problem is ill-posed. We need to regularize the high frequencies. The regularized imaging functional (3.30) can be expressed as

$$\mathcal{I}_\rho(\mathbf{z}^S) = 2\pi \sum_{n,m \in \mathbb{Z}} \int_0^\infty \int_0^\infty p_{-a,n,\rho}(t, \mathbf{z}^S) p_{-a,m,\rho}(s, \mathbf{z}^S) c_{n,m}(s-t) ds dt$$

or

$$\begin{aligned} \mathcal{I}_\rho(\mathbf{z}^S) &= \sum_{n,m \in \mathbb{Z}} \int_{\mathbb{R}} \hat{p}_{-a,n,\rho}(\omega, \mathbf{z}^S) \overline{\hat{p}_{-a,m,\rho}(\omega, \mathbf{z}^S)} \hat{c}_{n,m}(\omega) d\omega \\ &= \sum_{n,m \in \mathbb{Z}} \int_{|\omega| \leq \rho} \hat{p}_{-a,n}(\omega, \mathbf{z}^S) \overline{\hat{p}_{-a,m}(\omega, \mathbf{z}^S)} \hat{c}_{n,m}(\omega) d\omega, \end{aligned}$$

where

$$\hat{p}_{-a,n,\rho}(\omega, \mathbf{z}) = \hat{p}_{-a,n}(\omega, \mathbf{z}) \mathbf{1}_{|\omega| \leq \rho}.$$

REMARK 3.4.5. The function $p_{-a,n,\rho}(t, \mathbf{z})$ can be identified as the solution to the problem

$$\begin{cases} \left[\frac{1}{c^2(\mathbf{x})} \frac{\partial^2}{\partial t^2} - \Delta + a \frac{\partial}{\partial t} \Delta \right] p_{-a,n,\rho}(t, \mathbf{x}) = f_n(\mathbf{x}) \delta_{\partial\Omega}(\mathbf{x}) S_\rho[\delta](t), & (t, \mathbf{x}) \in \mathbb{R} \times \mathbb{R}^2, \\ p_{-a,n,\rho}(t, \mathbf{x}) = \frac{\partial p_{-a,n,\rho}(t, \mathbf{x})}{\partial t} = 0, & t \ll 0, \end{cases}$$

where S_ρ is the operator defined by

$$S_\rho[\phi](t) = \frac{1}{2\pi} \int_{|\omega| \leq \rho} \hat{\phi}(\omega) \exp(-i\omega t) d\omega.$$

Note also that the functional \mathcal{J}_ρ can be expressed in the form

$$\mathcal{J}_\rho(\mathbf{z}) = \int_0^T v_{-a,\rho}(t, \mathbf{z}) dt,$$

where

$$v_{-a,\rho}(t, \mathbf{z}) = \int_0^T v_{s,-a,\rho}(t, \mathbf{z}) ds,$$

and $v_{s,-a,\rho}$ being defined as the solution to the equation

$$\left[\frac{1}{c^2(\mathbf{x})} \frac{\partial^2}{\partial t^2} - \Delta + a \frac{\partial}{\partial t} \Delta \right] v_{s,-a,\rho}(t, \mathbf{x}) = p(T-s, \mathbf{x}) \delta_{\partial\Omega}(\mathbf{x}) S_\rho[\delta](t-s).$$

3.4.4 REMARK ON THE BACK-PROPAGATION OF PRE-PROCESSED DATA IN A NON-ATTENUATING MEDIUM

An idea that seems interesting is to try to build a regularized imaging functional as in the case of a source term that is a Dirac distribution in time. This can be done by first regularizing the data and then back-propagating it in the non-attenuating medium, as discussed in Chapter 2.

On the one hand, it is not possible to do this to the data themselves, since the recorded signals are very long and usually contain a huge amount of additional measurement noise (which disappears when one computes the cross correlation). Indeed, we have

$$\widehat{C}_a(\omega, \mathbf{x}, \mathbf{y}) = \widehat{F}(\omega) \int_{\Omega} \overline{\widehat{G}_a(\omega, \mathbf{x}, \mathbf{z})} \widehat{G}_a(\omega, \mathbf{y}, \mathbf{z}) K(\mathbf{z}) d\mathbf{z}, \quad (3.36)$$

and, although (3.22) holds, formula (3.36) is not in the form

$$\widehat{C}_a(\omega, \mathbf{x}, \mathbf{y}) = \widehat{F}(\omega) \frac{|\kappa_a(\omega)|^4}{\omega^4} \int_{\Omega} \widehat{H}(\kappa_a(\omega), \mathbf{x}, \mathbf{y}, \mathbf{z}) K(\mathbf{z}) d\mathbf{z}.$$

In fact, we have

$$\begin{aligned} \widehat{C}_a(\omega, \mathbf{x}, \mathbf{y}) = & \widehat{F}(\omega) \frac{|\kappa_a(\omega)|^4}{\omega^4} \int_0^\infty \left[\int_0^\infty \int_{\Omega} K(\mathbf{z}) G(s, \mathbf{x}, \mathbf{z}) G(s+v, \mathbf{y}, \mathbf{z}) d\mathbf{z} \right. \\ & \left. \times \exp(-2\kappa_{a,i}(\omega)s) ds \right] \exp(i\kappa_a(\omega)v) dv. \end{aligned}$$

The damping $\exp(-2\kappa_{a,i}(\omega)s)$ is quite problematic. It implies that the compensation of the attenuation can only be carried out -approximately- for a given target point \mathbf{z}^S , which means using the adjoint Green function or equivalently, back-propagating in an amplifying medium.

3.4.5 NUMERICAL EXPERIMENTS

Figure 3.3 presents some numerical source reconstructions in attenuating media. Each line respectively corresponds to the attenuation coefficient $a = 0.0005$, $a = 0.001$, and $a = 0.002$. In the first column, the sources are localized by applying the imaging functional \mathcal{I}_W . As expected, the attenuation affects the image quality. In the second and the third columns of Figure 3.3, we use the functional \mathcal{I}_ρ with $\rho = 7.5$ and $\rho = 15$, respectively. The reconstructions are improved, but as illustrated in the last figure of the third line, this technique is quite unstable for the case of a large attenuation coefficient a .

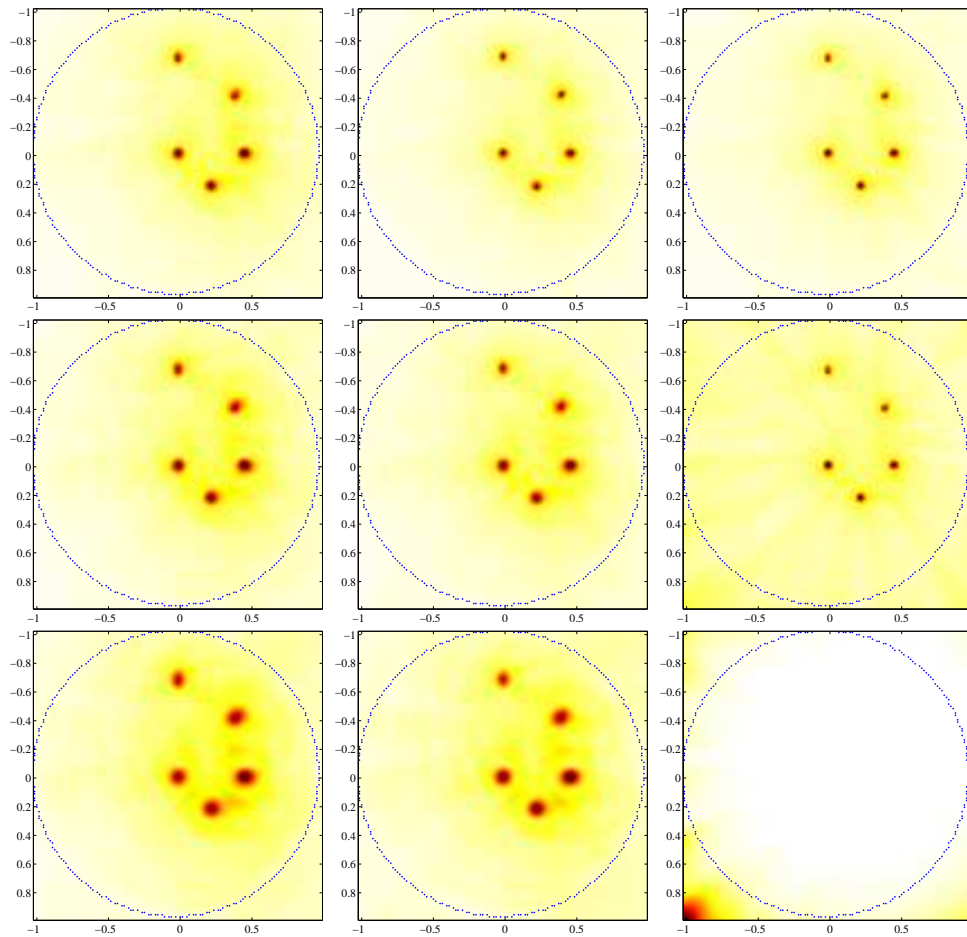


FIGURE 3.3. Five point sources in attenuating medium with $T = 8$, $\omega_{\max} = 1000$, $N_x = 2^8$, and $N_t = 2^{11}$. From top to bottom: $a = 0.0005$, $a = 0.001$, and $a = 0.002$. From left to right: \mathcal{I}_W , \mathcal{I}_ρ with $\rho = 7.5$, and \mathcal{I}_ρ with $\rho = 15$.

3.5 LOCALIZATION OF CORRELATED SOURCES

In the previous sections we have considered the case in which the noise sources are spatially uncorrelated, which translates in the fact that the covariance function (3.2) is delta-correlated in space. In this section we would like to address the impact of spatial correlation in the source localization. First we will address the general problem and then we will consider two specific examples: an extended distribution of locally correlated sources and a collection of correlated point sources.

3.5.1 SPATIALLY CORRELATED SOURCES

We assume in this section that the noise source term $n(t, \mathbf{x})$ is a stationary (in time) Gaussian process with mean zero and covariance function

$$\langle n(t, \mathbf{x})n(s, \mathbf{y}) \rangle = F(t - s)\Gamma(\mathbf{x}, \mathbf{y}), \quad (3.37)$$

where F is the time covariance of the noise signals and Γ characterizes the spatial support and covariance of the sources. The function Γ is the quantity we want to identify from the data set

$$\{p(t, \mathbf{x}), \quad \forall t \in [0, T], \mathbf{x} \in \partial\Omega\}$$

recorded at the surface of the domain Ω . We are primarily interested in identifying the support of Γ , but we would also like to extract information about the covariance structure of the noise sources.

The empirical cross correlation (3.3) is self-averaging as in the delta-correlated case and becomes equivalent to the statistical cross correlation C when the recording time $T \rightarrow \infty$, where

$$C(\tau, \mathbf{x}, \mathbf{y}) = \frac{1}{2\pi} \int_{\mathbb{R}} \left[\iint_{\Omega \times \Omega} \overline{\widehat{G}(\omega, \mathbf{x}, \mathbf{z})} \widehat{G}(\omega, \mathbf{y}, \mathbf{z}') \Gamma(\mathbf{z}, \mathbf{z}') d\mathbf{z} d\mathbf{z}' \right] \widehat{F}(\omega) \exp(-i\omega\tau) d\omega. \quad (3.38)$$

We can build two functionals from the cross correlation. The first one is \mathcal{J} defined by (3.5) and aims at estimating the support of the noise sources. The second one aims at estimating the covariance function Γ and is defined by

$$\mathcal{J}(\mathbf{z}^S, \mathbf{z}^{S'}) = \int_{\mathbb{R}} \iint_{\partial\Omega \times \partial\Omega} \widehat{G}(\omega, \mathbf{x}, \mathbf{z}^S) \overline{\widehat{G}(\omega, \mathbf{y}, \mathbf{z}^{S'})} \widehat{C}(\omega, \mathbf{x}, \mathbf{y}) d\sigma(\mathbf{x}) d\sigma(\mathbf{y}) d\omega. \quad (3.39)$$

Note that we have $\mathcal{J}(\mathbf{z}^S, \mathbf{z}^S) = \mathcal{J}(\mathbf{z}^S)$. Using Helmholtz-Kirchhoff formula, we obtain that

$$\mathcal{J}(\mathbf{z}^S, \mathbf{z}^{S'}) \simeq \iint_{\Omega \times \Omega} \Psi(\mathbf{z}^S, \mathbf{z}^{S'}, \mathbf{z}, \mathbf{z}') \Gamma(\mathbf{z}, \mathbf{z}') d\mathbf{z} d\mathbf{z}'$$

with

$$\Psi(\mathbf{z}^S, \mathbf{z}^{S'}, \mathbf{z}, \mathbf{z}') = \int_{\mathbb{R}} \frac{\widehat{F}(\omega)}{\omega^2} \Im m \{ \widehat{G}(\omega, \mathbf{z}, \mathbf{z}^S) \} \Im m \{ \widehat{G}(\omega, \mathbf{z}', \mathbf{z}^{S'}) \} d\omega.$$

In particular, in a three-dimensional homogeneous medium we have

$$\Psi(\mathbf{z}^S, \mathbf{z}^{S'}, \mathbf{z}, \mathbf{z}') = \psi(\mathbf{z}^S - \mathbf{z}, \mathbf{z}^{S'} - \mathbf{z}'), \quad (3.40)$$

with

$$\psi(\mathbf{z}, \mathbf{z}') = \frac{1}{16\pi^2} \int_{\mathbb{R}} \hat{F}(\omega) \text{sinc}(\omega|\mathbf{z}|) \text{sinc}(\omega|\mathbf{z}'|) d\omega, \quad (3.41)$$

which shows that the convolution kernel smooths, in both \mathbf{z} and \mathbf{z}' , the estimation of Γ by the functional \mathcal{J} .

3.5.2 EXTENDED DISTRIBUTIONS OF LOCALLY CORRELATED SOURCES

Let us assume that the covariance of the noise source term is of the form

$$\Gamma(\mathbf{z}, \mathbf{z}') = K\left(\frac{\mathbf{z} + \mathbf{z}'}{2}\right) \gamma(\mathbf{z} - \mathbf{z}').$$

Here, the function K characterizes the spatial support of the noise sources and γ characterizes the local covariance structure. This models an extended noise source distribution which has local correlation. Then, we find that

$$\mathcal{J}(\mathbf{z}^S) \simeq \int_{\Omega} \Phi(\mathbf{z}, \mathbf{z}^S) K(\mathbf{z}) d\mathbf{z}$$

with

$$\Phi(\mathbf{z}, \mathbf{z}^S) = \int_{\mathbb{R}} \frac{\hat{F}(\omega)}{\omega^2} \int \Im m\{\hat{G}(\omega, \mathbf{z} + \zeta/2, \mathbf{z}^S)\} \Im m\{\hat{G}(\omega, \mathbf{z} - \zeta/2, \mathbf{z}^S)\} \gamma(\zeta) d\zeta d\omega.$$

In particular, in a three-dimensional homogeneous medium we have

$$\Phi(\mathbf{z}, \mathbf{z}^S) = \phi(\mathbf{z} - \mathbf{z}^S), \quad (3.42)$$

with

$$\phi(\mathbf{z}) = \frac{1}{16\pi^2} \int_{\mathbb{R}} \hat{F}(\omega) \int \text{sinc}(\omega|\mathbf{z} + \zeta/2|) \text{sinc}(\omega|\mathbf{z} - \zeta/2|) \gamma(\zeta) d\zeta d\omega. \quad (3.43)$$

This shows that we recover the function K up to a smoothing which is large when γ is far from a Dirac distribution or a narrow peak. Spatial correlation in the noise sources blurs the source localization.

If the width of the function γ is smaller than ω_{\max}^{-1} where ω_{\max} is the maximal frequency of the power spectral density \hat{F} , then the spatial correlation of the sources plays no role and we recover the results obtained in the case of delta-correlated noise sources in which the convolution kernel (3.43) is given by

$$\phi(\mathbf{z}) = \frac{\hat{\gamma}(\mathbf{0})}{16\pi^2} \int_{\mathbb{R}} \hat{F}(\omega) \text{sinc}^2(\omega|\mathbf{z}|) d\omega. \quad (3.44)$$

If the width of the function γ is large and the function γ is isotropic so that $\tilde{\gamma}(\mathbf{k}) = \tilde{\gamma}(|\mathbf{k}|)$, then the convolution kernel (3.43) is given by

$$\phi(\mathbf{z}) = 2 \left[\int_0^\infty k \tilde{\gamma}(k) dk \right] \int_{\mathbb{R}} \frac{\hat{F}(\omega)}{\omega^2} \text{sinc}^2(\omega|\mathbf{z}|) d\omega. \quad (3.45)$$

The kernel is not nonnegative (which means that side lobes are likely to appear). Moreover, low-frequency components are amplified, so that it is necessary to use a frequency-dependent weight or to back-propagate with the time-derivative of the Green function in order to cancel out the factor ω^{-2} in (3.45). Note that formula (3.45) follows from the substitution of the representation formula

$$\text{sinc}(\omega|\mathbf{z}|) = \frac{1}{4\pi} \int_{\partial B(0,1)} \exp(i\omega\mathbf{z} \cdot \mathbf{k}) d\sigma(\mathbf{k})$$

in (3.43).

3.5.3 A COLLECTION OF CORRELATED POINT SOURCES

Let us assume that the covariance of the noise source term is of the form

$$\Gamma(\mathbf{z}, \mathbf{z}') = \sum_{i,j=1}^{N_s} \rho_{ij} \delta(\mathbf{z} - \mathbf{z}_i) \delta(\mathbf{z}' - \mathbf{z}_j),$$

where $(\rho_{ij})_{i,j=1,\dots,N_s}$ is a symmetric nonnegative matrix. This models a collection of N_s point sources located at \mathbf{z}_i , $i = 1, \dots, N_s$, which have respective power ρ_{ii} . The coefficients $\frac{\rho_{ij}}{\sqrt{\rho_{ii}\rho_{jj}}} \in [-1, 1]$ represent the correlation between the sources at \mathbf{z}_i and \mathbf{z}_j . Then we find that

$$\begin{aligned} \mathcal{J}(\mathbf{z}^S) &\simeq \sum_{i,j=1}^{N_s} \rho_{ij} \int_{\mathbb{R}} \frac{\hat{F}(\omega)}{\omega^2} \Im m \{ \hat{G}(\omega, \mathbf{z}_i, \mathbf{z}^S) \} \Im m \{ \hat{G}(\omega, \mathbf{z}_j, \mathbf{z}^S) \} d\omega \\ &\simeq \sum_{i=1}^{N_s} \rho_{ii} \mathcal{Q}(\mathbf{z}^S, \mathbf{z}_i), \end{aligned}$$

provided the sources are well separated, where \mathcal{Q} is defined as in (3.9) *i.e.*

$$\mathcal{Q}(\mathbf{z}^S, \mathbf{z}) = \int_{\mathbb{R}} \frac{\hat{F}(\omega)}{\omega^2} \Im m \{ \hat{G}(\omega, \mathbf{z}, \mathbf{z}^S) \}^2 d\omega.$$

In particular, in a three-dimensional homogeneous medium:

$$\mathcal{Q}(\mathbf{z}^S, \mathbf{z}) = \frac{1}{16\pi^2} \int_{\mathbb{R}} \hat{F}(\omega) \text{sinc}^2(\omega|\mathbf{z} - \mathbf{z}^S|) d\omega.$$

This shows that the functional \mathcal{Q} indeed exhibits peaks at the locations of the noise sources.

Once the local maxima $\hat{\mathbf{z}}_i$, $i = 1, \dots, N_s$, have been estimated, it is possible to estimate the correlation matrix between the noise sources by looking at the functional \mathcal{J} at these points. Indeed, we have

$$\mathcal{J}(\mathbf{z}^S, \mathbf{z}^{S'}) \simeq \sum_{i,j=1}^{N_s} \rho_{ij} \int_{\mathbb{R}} \frac{\hat{F}(\omega)}{\omega^2} \Im m \{ \hat{G}(\omega, \mathbf{z}_i, \mathbf{z}^S) \} \Im m \{ \hat{G}(\omega, \mathbf{z}_j, \mathbf{z}^{S'}) \} d\omega.$$

Therefore,

$$\mathcal{J}(\mathbf{z}_i, \mathbf{z}_j) \simeq \rho_{ij} \int_{\mathbb{R}} \frac{\hat{F}(\omega)}{\omega^2} \Im m \{ \hat{G}(\omega, \mathbf{z}_i, \mathbf{z}_i) \} \Im m \{ \hat{G}(\omega, \mathbf{z}_j, \mathbf{z}_j) \} d\omega.$$

In particular, in a three-dimensional homogeneous medium, it follows that

$$\mathcal{J}(\mathbf{z}_i, \mathbf{z}_j) \simeq \mathcal{J}_0 \rho_{ij}, \quad \mathcal{J}_0 = \frac{1}{16\pi^2} \int_{\mathbb{R}} \hat{F}(\omega) d\omega = \frac{1}{8\pi} F(0).$$

The estimation of correlation matrix can be important in robot sound or microwave source surveillance and tracking; see, for instance, [96].

3.5.4 NUMERICAL EXPERIMENTS FOR CORRELATED NOISE SOURCE LOCALIZATION

A numerical method to compute efficiently $\mathcal{J}(\mathbf{z}, \mathbf{z}')$ follows from

$$\begin{aligned} \mathcal{J}(\mathbf{z}, \mathbf{z}') &= \int_{\mathbb{R}} \iint_{\partial\Omega} \hat{G}(\omega, \mathbf{x}, \mathbf{z}) \overline{\hat{G}(\omega, \mathbf{y}, \mathbf{z}')} \hat{C}(\omega, \mathbf{x}, \mathbf{y}) d\sigma(\mathbf{x}) d\sigma(\mathbf{y}) d\omega \\ &= \int_{\mathbb{R}} \iint_{\partial\Omega} \hat{G}(\omega, \mathbf{x}, \mathbf{z}) \overline{\hat{G}(\omega, \mathbf{y}, \mathbf{z}')} \overline{\hat{p}(\omega, \mathbf{x})} \hat{p}(\omega, \mathbf{y}) d\sigma(\mathbf{x}) d\sigma(\mathbf{y}) d\omega \\ &= \int_{\mathbb{R}} \left(\int_{\partial\Omega} \hat{G}(\omega, \mathbf{x}, \mathbf{z}) \overline{\hat{p}(\omega, \mathbf{x})} d\sigma(\mathbf{x}) \right) \overline{\left(\int_{\partial\Omega} \hat{G}(\omega, \mathbf{y}, \mathbf{z}') \hat{p}(\omega, \mathbf{y}) d\sigma(\mathbf{y}) \right)} d\omega \\ &= 2\pi \int_0^T v(t, \mathbf{z}) v(t, \mathbf{z}') dt, \end{aligned}$$

where the function v can be expressed in the form

$$v(t, \mathbf{x}) = \int_0^T v_s(t, \mathbf{x}) ds,$$

and the function v_s being defined as the solution of

$$\begin{cases} \frac{1}{c^2(\mathbf{x})} \frac{\partial^2 v_s(t, \mathbf{x})}{\partial t^2} - \Delta v_s(t, \mathbf{x}) = p(T-s, \mathbf{x}) \delta_{\partial\Omega}(\mathbf{x}) \delta(t-s) & (t, \mathbf{x}) \in \mathbb{R} \times \Omega \\ v_s(t, \mathbf{x}) = 0, & t \ll s, \\ \frac{\partial}{\partial t} v_s(t, \mathbf{x}) = 0, & t \ll s. \end{cases}$$

More generally, the imaging functional $\mathcal{I}_W(\mathbf{z}, \mathbf{z}')$ can be defined by applying $\mathcal{I}(\mathbf{z}, \mathbf{z}')$ on the filtered data $\tilde{p}(t, \mathbf{x})$ given by

$$\hat{\tilde{p}}(\omega, \mathbf{x}) = \sqrt{\frac{W(\omega)}{\mathcal{F}(\omega)}} \hat{p}(\omega, \mathbf{x}).$$

In Figure 3.4, we consider four point noise sources with the power spectral density (3.21) and with the correlation matrix

$$\rho = \begin{pmatrix} 1 & \sqrt{2}/2 & \sqrt{2}/2 & 0 \\ \sqrt{2}/2 & 1 & 0 & 0 \\ \sqrt{2}/2 & 0 & 1 & 0 \\ 0 & 0 & 0 & 1 \end{pmatrix}.$$

The top-left figure presents the true distribution $K(\mathbf{x})$. The top-middle figure shows the reconstruction of K using the imaging functional \mathcal{I}_W . In particular, it appears that the source localization is not as efficient as in the case of uncorrelated data, but is sufficient for locating the noise sources. In the last four figures, we plot the imaging functional $\mathbf{z} \rightarrow \mathcal{I}_W(\mathbf{z}_i, \mathbf{z})$ for each source \mathbf{z}_i , which allows us to get the following estimate of the cross correlation matrix:

$$\hat{\rho} = \begin{pmatrix} 1.000 & 0.733 & 0.701 & 0.061 \\ 0.733 & 1.000 & 0.049 & 0.061 \\ 0.701 & 0.049 & 1.000 & 0.030 \\ 0.061 & 0.061 & 0.030 & 1.000 \end{pmatrix}$$

Note that each correlation is found quite well ($\sqrt{2}/2 \approx 0.707$). To conclude, some numerical results associated with the localization of Gaussian sources are also shown in Figure 3.5.

3.6 CONCLUSION

In this chapter, efficient weighted imaging algorithms for locating noise sources by cross correlation techniques have been introduced. We have provided a regularization approach to correct the effect of attenuation. We have successfully addressed the impact of spatial correlation in the noise source localization problem by designing appropriate imaging functionals.

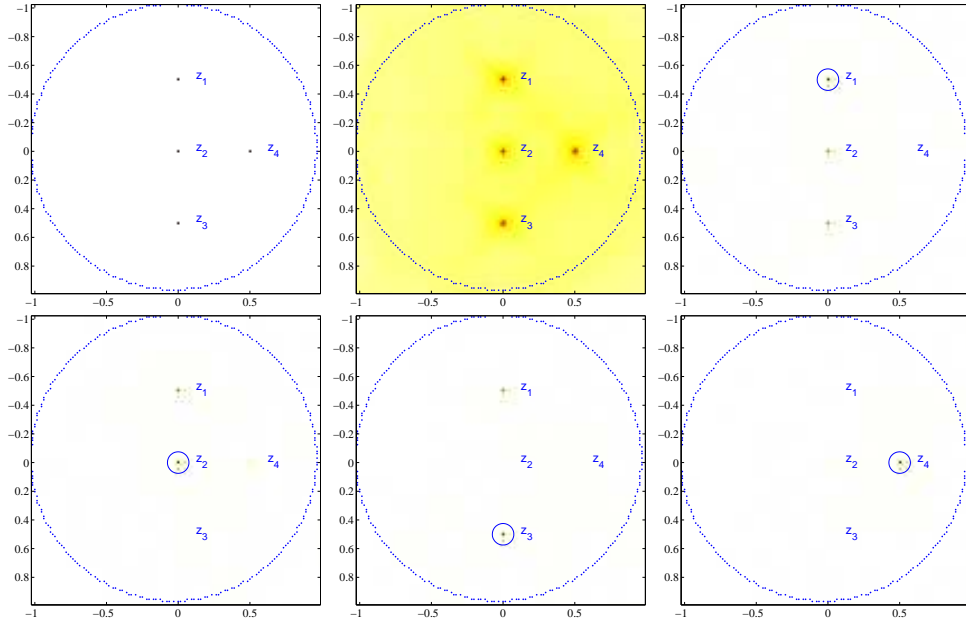


FIGURE 3.4. Four correlated source points $(\mathbf{z}_j)_{j=1,\dots,4}$ with $T = 8$, $\omega_{\max} = 1000$, $N_x = 2^8$, and $N_t = 2^{11}$. Top line: $K(\mathbf{z})$ (left), \mathcal{I}_W with $W(\omega) = |\omega|^3 \mathbf{1}_{|\omega| < \omega_{\max}}$ (middle), and $\mathbf{z} \rightarrow \mathcal{I}_W(\mathbf{z}_1, \mathbf{z})$ (right). Bottom line: $\mathbf{z} \rightarrow \mathcal{I}_W(\mathbf{z}_2, \mathbf{z})$ (left), $\mathbf{z} \rightarrow \mathcal{I}_W(\mathbf{z}_3, \mathbf{z})$ (middle), and $\mathbf{z} \rightarrow \mathcal{I}_W(\mathbf{z}_4, \mathbf{z})$ (right).

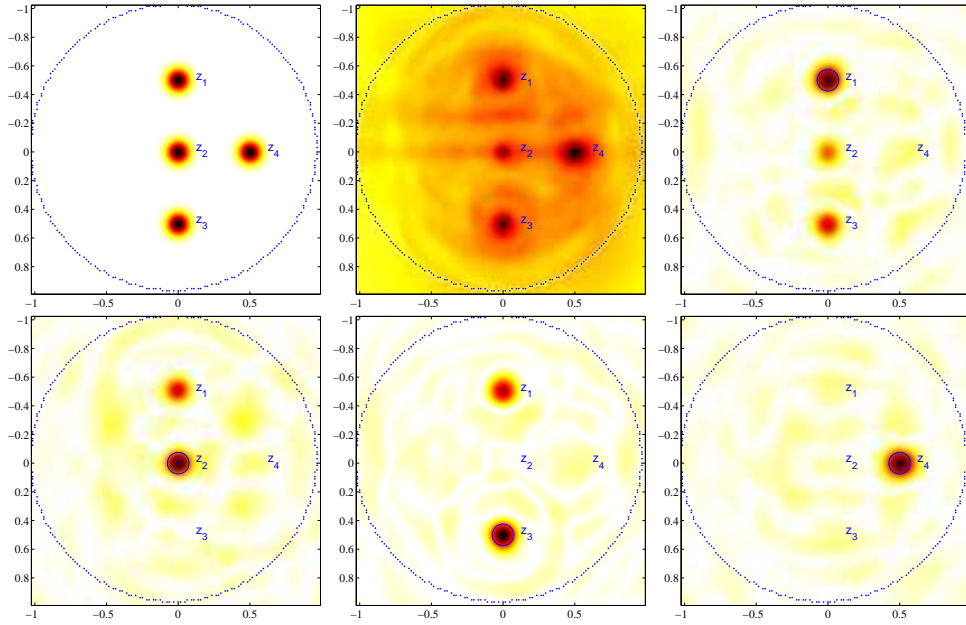


FIGURE 3.5. Four correlated extended sources centered at $(\mathbf{z}_j)_{j=1,\dots,4}$ with $T = 8$, $\omega_{\max} = 1000$, $N_x = 2^8$, and $N_t = 2^{11}$. Top line: $K(\mathbf{z})$ (left), \mathcal{I}_W with $W(\omega) = |\omega|^3 \mathbf{1}_{|\omega| < \omega_{\max}}$ (middle), $\mathbf{z} \rightarrow \mathcal{I}_W(\mathbf{z}_1, \mathbf{z})$ (right). Bottom line: $\mathbf{z} \rightarrow \mathcal{I}_W(\mathbf{z}_2, \mathbf{z})$ (left), $\mathbf{z} \rightarrow \mathcal{I}_W(\mathbf{z}_3, \mathbf{z})$ (middle), $\mathbf{z} \rightarrow \mathcal{I}_W(\mathbf{z}_4, \mathbf{z})$ (right).

Part II

Imaging in Viscoelastic Media

4.1 INTRODUCTION

The elastic properties of human soft tissues have been exploited extensively in various imaging modalities in recent past [71, 113]. They vary significantly in order of magnitude with different tissue types and are closely linked with the pathology of the tissues and their underlying structure. Consequently, these properties have inspired many investigations in biomedical imaging, leading to many interesting problems in mathematics, see for instance, [18, 23, 24, 25, 36] and references therein.

In elasticity imaging, most of the time underlying medium is considered to be inviscid (ideal). The fact that a wave loses some of its energy to the medium and its amplitude decreases with time due to viscosity, dissipation and other internal relaxation processes, is often neglected [110]. However, if not accounted for, this negligence can lead to serious blurring in image reconstruction. On the other hand, an estimation of the viscosity parameters can sometimes be very useful in the characterization and identification of an anomaly [36].

In order to address the problem of reconstructing small anomalies in viscoelastic media from wavefield measurements, it is important to first model the mechanical response of such media to excitations. The Voigt model is a common model to describe the viscoelastic properties of tissues. Catheline *et al.* [47] have shown that this model is well adapted to describe the viscoelastic response of tissues to low-frequency excitations. However, we choose a more general model derived by Szabo and Wu in [128] that describes observed power-law behavior of many viscoelastic materials including different soft tissues. This model is based on a time-domain statement of causality [83, 125] and reduces to the Voigt model for the specific case of quadratic frequency losses.

By expressing the purely elastic field (without any viscous effect) in terms of the measured field in a viscous medium, one can generalize the methods described in [7, 8, 19, 25, 26], namely the time reversal, back-propagation and

Kirchhoff imaging. Subsequently, one can recover the viscoelastic and geometric properties of an anomaly from wavefield measurements. In order to achieve this goal, we focus on the Green function in this chapter. We identify a relationship between the ideal Green function and the viscoelastic Green function in the limiting case when the compressional modulus $\lambda \rightarrow \infty$. We also provide an approximation of this relationship using the stationary phase theorem.

The rest of the chapter is organized as follows. In Section 4.2, we introduce a general viscoelastic wave equation based on the power-law model of Szabo and Wu. Section 4.3 is devoted to the derivation of the viscoelastic Green function. In Section 4.4, we approximate the ideal Green function for the media with quadratic frequency losses and sketch a procedure to use ideal image reconstruction algorithms for viscoelastic media. We highlight the potential of our approach with numerical illustrations, that are presented in Section 4.5.

4.2 GENERAL VISCOELASTIC WAVE EQUATION

When a wave travels through a biological medium, its amplitude decreases with time due to attenuation. The attenuation coefficient for soft tissues may be approximated by a power-law over a wide range of frequencies. The measured attenuation coefficients of soft tissues typically have linear or greater than linear dependence on frequency [58, 125, 128].

Let Ω be an open subset of \mathbb{R}^3 , filled with a homogeneous and isotropic viscoelastic material and

$$\mathbf{u}(\mathbf{x}, t) : \Omega \times \mathbb{R}^+ \rightarrow \mathbb{R}^3$$

be the displacement field at time t of the material particle at position $\mathbf{x} \in \Omega$ and $\nabla \mathbf{u}(\mathbf{x}, t)$ be its gradient. We define the order two strain tensor by

$$\underline{\underline{\varepsilon}} : (\mathbf{x}, t) \in \Omega \times \mathbb{R}^+ \mapsto \frac{1}{2} (\nabla \mathbf{u} + \nabla \mathbf{u}^T)(\mathbf{x}, t),$$

under the assumptions of linearity and small perturbations. Here the superscript T indicates a transpose operation.

Let $\underline{\underline{\mathbf{C}}} \in \mathcal{L}_s^2(\mathbb{R}^3)$ and $\underline{\underline{\mathbf{V}}} \in \mathcal{L}_s^2(\mathbb{R}^3)$ be the stiffness and viscosity tensors of the material respectively given by

$$\begin{aligned} \underline{\underline{\mathbf{C}}} &= [C_{ijkl}] = \left[\lambda \delta_{ij} \delta_{kl} + \mu (\delta_{ik} \delta_{jl} + \delta_{il} \delta_{jk}) \right], \\ \underline{\underline{\mathbf{V}}} &= [V_{ijkl}] = \left[\eta_s \delta_{ij} \delta_{kl} + \eta_p (\delta_{ik} \delta_{jl} + \delta_{il} \delta_{jk}) \right]. \end{aligned}$$

Here δ_{ab} is the Kronecker delta function, (λ, μ) are the Lamé parameters, (η_s, η_p) are the shear and the compressional viscosity moduli respectively, and $\mathcal{L}_s^2(\mathbb{R}^3)$ is the space of symmetric tensors of order four. These tensors are assumed to be positive definite, i.e. there exist constants $\beta_c, \beta_v > 0$ such that

$$(\underline{\underline{\mathbf{C}}} : \underline{\underline{\xi}}) : \underline{\underline{\xi}} \geq \beta_c |\underline{\underline{\xi}}|^2 \quad \text{and} \quad (\underline{\underline{\mathbf{V}}} : \underline{\underline{\xi}}) : \underline{\underline{\xi}} \geq \beta_v |\underline{\underline{\xi}}|^2, \quad \forall \underline{\underline{\xi}} \in \mathcal{L}_s(\mathbb{R}^3),$$

where $\mathcal{L}_s(\mathbb{R}^3)$ denotes the space of symmetric tensors of order two. Throughout this chapter, we suppose that

$$\eta_p, \eta_s \ll 1. \quad (4.1)$$

The generalized Hooke's Law [128] for power law media states that the stress distribution

$$\underline{\sigma} : \Omega \times \mathbb{R}^+ \rightarrow \mathcal{L}_s(\mathbb{R}^3)$$

produced by the deformation $\underline{\varepsilon}$, satisfies:

$$\underline{\sigma} = \underline{\underline{\mathbf{C}}} : \underline{\varepsilon} + \underline{\underline{\mathbf{V}}} : \mathcal{A}[\underline{\varepsilon}] \quad (4.2)$$

where \mathcal{A} is a convolution-type loss operator defined as

$$\mathcal{A}[\varphi] = \begin{cases} -(-1)^{\gamma/2} \frac{\partial^{\gamma-1} \varphi}{\partial t^{\gamma-1}}, & \gamma \text{ is an even integer,} \\ \frac{2}{\pi} (\gamma-1)! (-1)^{(\gamma+1)/2} \left[\frac{H(t)}{t^\gamma} \right] *_t \varphi, & \gamma \text{ is an odd integer,} \\ -\frac{2}{\pi} \Gamma(\gamma) \sin\left(\frac{\gamma\pi}{2}\right) \left[\frac{H(t)}{|t|^\gamma} \right] *_t \varphi, & \gamma \text{ is a non integer.} \end{cases} \quad (4.3)$$

Note that by convention,

$$\mathcal{A}[\mathbf{u}]_i = \mathcal{A}[u_i] \quad \text{and} \quad \mathcal{A}[\underline{\varepsilon}]_{ij} = \mathcal{A}[\varepsilon_{ij}] \quad 1 \leq i, j \leq 3.$$

Here $H(t)$ is the Heaviside function, Γ is the gamma function and $*_t$ represents convolution with respect to variable t . See [4, 44, 82, 127, 128, 131] for comprehensive details and discussion on fractional attenuation models, causality and the loss operator \mathcal{A} .

The general viscoelastic wave equation satisfied by the displacement field $\mathbf{u}(\mathbf{x}, t)$ reads now

$$\rho \frac{\partial^2 \mathbf{u}}{\partial t^2} - \mathbf{F} = \nabla \cdot \underline{\sigma} = \nabla \cdot \left(\underline{\underline{\mathbf{C}}} : \underline{\varepsilon} + \underline{\underline{\mathbf{V}}} : \mathcal{A}[\underline{\varepsilon}] \right),$$

or equivalently,

$$\rho \frac{\partial^2 \mathbf{u}}{\partial t^2} - \mathbf{F} = \left(\bar{\lambda} + \bar{\mu} \right) \nabla(\nabla \cdot \mathbf{u}) + \bar{\mu} \Delta \mathbf{u}. \quad (4.4)$$

where $\mathbf{F}(\mathbf{x}, t)$ is the applied force and ρ is the density (supposed to be constant) of the material and

$$\bar{\lambda} = \lambda + \eta_p \mathcal{A}[\cdot] \quad \text{and} \quad \bar{\mu} = \mu + \eta_s \mathcal{A}[\cdot].$$

REMARK 4.2.1. For quadratic frequency losses, i.e, when $\gamma = 2$, operator \mathcal{A} reduces to a first order time derivative. Therefore, power-law attenuation model (4.2) turns out to be the Voigt model in this case.

4.3 GREEN FUNCTION

In this section, we find the Green function for the viscoelastic wave equation (4.4). We first derive a Helmholtz decomposition result for the displacement field $\mathbf{u}(\mathbf{x}, t)$, which is essential for the subsequent analysis.

LEMMA 4.3.1. *Let the displacement field $\mathbf{u}(\mathbf{x}, t)$ satisfy (4.4) and the Helmholtz decomposition of $\frac{\partial \mathbf{u}}{\partial t}(\mathbf{x}, 0)$, $\mathbf{u}(\mathbf{x}, 0)$ and $\mathbf{F}(\mathbf{x}, t)$ be given by*

$$\begin{aligned} \frac{\partial \mathbf{u}}{\partial t}(\mathbf{x}, 0) &= \nabla A + \nabla \times \mathbf{B} && \text{with } \nabla \cdot \mathbf{B} = 0, \\ \mathbf{u}(\mathbf{x}, 0) &= \nabla C + \nabla \times \mathbf{D} && \text{with } \nabla \cdot \mathbf{D} = 0, \\ \mathbf{F}(\mathbf{x}, t) &= \nabla \varphi_f + \nabla \times \psi_f && \text{with } \nabla \cdot \psi_f = 0. \end{aligned}$$

Then there exist potentials φ_u and ψ_u such that

$$\mathbf{u} = \nabla \varphi_u + \nabla \times \psi_u \quad \text{with } \nabla \cdot \psi_u = 0.$$

Moreover, φ_u and ψ_u satisfy respectively

$$\begin{aligned} \frac{\partial^2 \varphi_u}{\partial t^2} &= \frac{1}{\rho} \varphi_f + c_p^2 \Delta \varphi_u + v_p \mathcal{A}[\Delta \varphi_u] \\ &\simeq \frac{1}{\rho} \varphi_f - \frac{v_p}{\rho c_p^2} \mathcal{A}[\varphi_f] + c_p^2 \Delta \varphi_u + \frac{v_p}{c_p^2} \mathcal{A}\left[\frac{\partial^2 \varphi_u}{\partial t^2}\right] \\ \frac{\partial^2 \psi_u}{\partial t^2} &= \frac{1}{\rho} \psi_f + c_s^2 \Delta \psi_u + v_s \mathcal{A}[\Delta \psi_u] \\ &\simeq \frac{1}{\rho} \psi_f - \frac{v_s}{\rho c_s^2} \mathcal{A}[\psi_f] + c_s^2 \Delta \psi_u + \frac{v_s}{c_s^2} \mathcal{A}\left[\frac{\partial^2 \psi_u}{\partial t^2}\right] \end{aligned}$$

where

$$c_p^2 = \frac{\lambda + 2\mu}{\rho}, \quad c_s^2 = \frac{\mu}{\rho}, \quad v_p = \frac{\eta_p + 2\eta_s}{\rho} \quad \text{and} \quad v_s = \frac{\eta_s}{\rho}.$$

Proof. For φ_u and ψ_u defined as:

$$\varphi_u(\mathbf{x}, t) := \int_0^t \int_0^\tau \left(\frac{1}{\rho} \varphi_f + (c_p^2 + v_p \mathcal{A})[\nabla \cdot \mathbf{u}] \right)(\mathbf{x}, s) ds d\tau + tA + C, \quad (4.5)$$

$$\psi_u(\mathbf{x}, t) := \int_0^t \int_0^\tau \left(\frac{1}{\rho} \psi_f - (c_s^2 + v_s \mathcal{A})[\nabla \times \mathbf{u}] \right)(\mathbf{x}, s) ds d\tau + t\mathbf{B} + \mathbf{D}, \quad (4.6)$$

we have the required expression for \mathbf{u} . Moreover, it is evident from (4.6) that $\nabla \cdot \psi_u = 0$

Now, on differentiating φ_u and ψ_u twice with respect to time variable t , we get

$$\frac{\partial^2 \varphi_u}{\partial t^2} = \frac{1}{\rho} \varphi_f + c_p^2 \Delta \varphi_u + v_p \mathcal{A}[\Delta \varphi_u]$$

$$\frac{\partial^2 \psi_u}{\partial t^2} = \frac{1}{\rho} \psi_f + c_s^2 \Delta \psi_u + v_s \mathcal{A} [\Delta \psi_u]$$

Finally, we apply \mathcal{A} on last two equations, inject back the expression for $\mathcal{A} [\Delta \varphi_u]$ and $\mathcal{A} [\Delta \psi_u]$ and neglect the higher order terms in v_s and v_p by invoking (4.1) to get the required differential equations for φ_u and ψ_u . \square

Let

$$\kappa_m(\omega) = \omega \sqrt{\left(1 - \frac{v_m}{c_m^2} \widehat{\mathcal{A}}(\omega)\right)}, \quad m = s, p, \quad (4.7)$$

where the multiplication operator $\widehat{\mathcal{A}}(\omega)$ is the Fourier transform of the kernel of the convolution operator \mathcal{A} and ω is the frequency.

REMARK 4.3.2. *If φ_u and ψ_u are causal, then it implies the causality of the inverse Fourier transform of $\kappa_m(\omega)$, $m = s, p$. Applying the Kramers-Krönig relations, it follows that*

$$-\Im\{\kappa_m(\omega)\} = \mathcal{H}[\Re\{\kappa_m(\omega)\}] \quad \text{and} \quad \Re\{\kappa_m(\omega)\} = \mathcal{H}[\Im\{\kappa_m(\omega)\}], \quad (4.8)$$

where \mathcal{H} is the Hilbert transform, \Im and \Re represent the imaginary and the real parts of a complex number respectively. Recall that $\mathcal{H}^2 = -I$. The convolution operator \mathcal{A} given by (4.3) is based on the constraint that causality imposes on (4.2). Under the smallness assumption (4.1), the expressions in (4.3) can be found from the Kramers-Krönig relations (4.8). One drawback of (4.8) is that the attenuation, $\Im\{\kappa_m(\omega)\}$, must be known at all frequencies to determine the dispersion, $\Re\{\kappa_m(\omega)\}$. However, bounds on the dispersion can be obtained from measurements of the attenuation over a finite frequency range [94].

4.3.1 SOLUTION OF (4.4) WITH A CONCENTRATED FORCE.

Let u_{ij} denote the i -th component of the solution \mathbf{u}_j of the viscoelastic wave equation (4.4) associated to a force \mathbf{F} concentrated in the x_j -direction. Let $j = 1$ for simplicity without loss of generality and suppose that

$$\mathbf{F} = -T(t)\delta(\mathbf{x} - \xi)\mathbf{e}_1 = -T(t)\delta(\mathbf{x} - \xi)(1, 0, 0), \quad (4.9)$$

where ξ is the source point and $(\mathbf{e}_1, \mathbf{e}_2, \mathbf{e}_3)$ is an orthonormal basis of \mathbb{R}^3 .

Let \mathbf{Z} be the solution of the Poisson equation

$$\nabla^2 \mathbf{Z} = \mathbf{F}$$

Then (see, for instance, [80])

$$\mathbf{Z}(\mathbf{x}, t; \xi) = \frac{T(t)}{4\pi r} \mathbf{e}_1.$$

Using the vector identity

$$\nabla^2 \mathbf{Z} = \nabla(\nabla \cdot \mathbf{Z}) - \nabla \times (\nabla \times \mathbf{Z}),$$

the force \mathbf{F} can be decomposed as [108]

$$\begin{aligned} \mathbf{F} &= (\nabla \varphi_f + \nabla \times \psi_f), \\ \varphi_f &= \nabla \cdot \mathbf{Z} = \frac{T(t)}{4\pi} \frac{\partial}{\partial x_1} \left(\frac{1}{r} \right), \\ \psi_f &= -\nabla \times \mathbf{Z} = -\frac{T(t)}{4\pi} \left(0, \frac{\partial}{\partial x_3} \left(\frac{1}{r} \right), -\frac{\partial}{\partial x_2} \left(\frac{1}{r} \right) \right), \end{aligned} \quad (4.10)$$

where $r = |\mathbf{x} - \xi|$.

Consider the Helmholtz decomposition for \mathbf{u}_1 as

$$\mathbf{u}_1 = \nabla \varphi_1 + \nabla \times \psi_1. \quad (4.11)$$

Then, by Lemma 4.3.1, φ_1 and ψ_1 are respectively the solutions to the equations

$$\Delta \varphi_1 - \frac{1}{c_p^2} \frac{\partial^2 \varphi_1}{\partial t^2} + \frac{\nu_p}{c_p^4} \mathcal{A} \left[\frac{\partial^2 \varphi_1}{\partial t^2} \right] = \frac{\nu_p}{\rho c_p^4} \mathcal{A}[\varphi_f] - \frac{1}{c_p^2 \rho} \varphi_f, \quad (4.12)$$

$$\Delta \psi_1 - \frac{1}{c_s^2} \frac{\partial^2 \psi_1}{\partial t^2} + \frac{\nu_s}{c_s^4} \mathcal{A} \left[\frac{\partial^2 \psi_1}{\partial t^2} \right] = \frac{\nu_s}{\rho c_s^4} \mathcal{A}[\psi_f] - \frac{1}{c_s^2 \rho} \psi_f. \quad (4.13)$$

Equivalently, their Fourier transforms $\hat{\mathbf{u}}_1$, $\hat{\varphi}_1$ and $\hat{\psi}_1$ satisfy:

$$\hat{\mathbf{u}}_1 = \nabla \hat{\varphi}_1 + \nabla \times \hat{\psi}_1, \quad (4.14)$$

$$\Delta \hat{\varphi}_1 + \frac{1}{c_p^2} \kappa_p^2(\omega) \hat{\varphi}_1 = \frac{\nu_p}{\rho c_p^4} \widehat{\mathcal{A}}(\omega) \hat{\varphi}_f - \frac{1}{\rho c_p^2} \hat{\varphi}_f, \quad (4.15)$$

$$\Delta \hat{\psi}_1 + \frac{1}{c_s^2} \kappa_s^2(\omega) \hat{\psi}_1 = \frac{\nu_s}{\rho c_s^4} \widehat{\mathcal{A}}(\omega) \hat{\psi}_f - \frac{1}{\rho c_s^2} \hat{\psi}_f, \quad (4.16)$$

where $\kappa_m(\omega)$ is defined in (4.7) for $m = p, s$.

We recall that the Green function of the Helmholtz equations (4.15) and (4.16) can be given by (see, for instance, [98]):

$$\hat{g}^m(\mathbf{x}, \omega) = \frac{\exp \left\{ \sqrt{-1} \frac{\kappa_m(\omega)}{c_m} |\mathbf{x}| \right\}}{4\pi |\mathbf{x}|}, \quad m = s, p.$$

We closely follow the arguments in [108], and write $\hat{\varphi}_1$ as

$$\begin{aligned} \hat{\varphi}_1(\mathbf{x}, \omega; \xi) &= \hat{g}^m(\mathbf{x}, \omega) *_x \left(\frac{\nu_p}{\rho c_p^4} \widehat{\mathcal{A}}(\omega) \hat{\varphi}_f - \frac{1}{c_p^2 \rho} \hat{\varphi}_f \right) \\ &= - \left(1 - \frac{\nu_p}{c_p^2} \widehat{\mathcal{A}}(\omega) \right) \frac{\hat{T}(\omega)}{\rho (4\pi c_p)^2} \int_{\mathbb{R}^3} \hat{g}^p(\mathbf{x} - \mathbf{z}, \omega) \frac{\partial}{\partial z_1} \frac{1}{|\mathbf{z} - \xi|} dz. \end{aligned}$$

Remark that $\mathbf{z} \rightarrow \widehat{g}^p(\mathbf{x} - \zeta, \omega)$ is constant on each sphere $\partial B(\mathbf{x}, h)$, centered at \mathbf{x} with radius h . Therefore, the use of spherical coordinates leads to

$$\widehat{\varphi}_1(\mathbf{x}, \omega; \xi) = - \left(1 - \frac{v_p}{c_p^2} \widehat{\mathcal{A}}(\omega) \right) \frac{1}{\rho(4\pi c_p)^2} \widehat{T}(\omega) \int_0^\infty \widehat{g}^p(h, \omega) \int_{\partial B(\mathbf{x}, h)} \frac{\partial}{\partial z_1} \left(\frac{1}{|\mathbf{z} - \xi|} \right) d\sigma(\mathbf{z}) dh$$

where $d\sigma(\mathbf{z})$ is the surface element on $\partial B(\mathbf{x}, h)$.

From [3, Sec. 4.2], it follows that

$$\int_{\partial B(\mathbf{x}, h)} \frac{\partial}{\partial z_1} \left(\frac{1}{|\mathbf{z} - \xi|} \right) d\sigma(\mathbf{z}) = \begin{cases} 0 & \text{if } h > r \\ 4\pi h^2 \frac{\partial}{\partial x_1} \left(\frac{1}{r} \right) & \text{if } h < r. \end{cases}$$

Therefore, we have following expression for $\widehat{\varphi}_1$:

$$\begin{aligned} \widehat{\varphi}_1(\mathbf{x}, \omega; \xi) &= - \left(1 - \frac{v_p}{c_p^2} \widehat{\mathcal{A}}(\omega) \right) \frac{1}{4\pi\rho c_p^2} \widehat{T}(\omega) \frac{\partial}{\partial x_1} \left(\frac{1}{r} \right) \int_0^r h \exp \left[\sqrt{-1} \frac{\kappa_p(\omega)}{c_p} h \right] dh, \\ &= - \left(1 - \frac{v_p}{c_p^2} \widehat{\mathcal{A}}(\omega) \right) \frac{1}{4\pi\rho} \widehat{T}(\omega) \frac{\partial}{\partial x_1} \left(\frac{1}{r} \right) \int_0^{r/c_p} \zeta e^{\sqrt{-1} \kappa_p(\omega) \zeta} d\zeta. \end{aligned}$$

Similarly, $\widehat{\psi}_1$ is given by

$$\widehat{\psi}_1(\mathbf{x}, \omega; \xi) = \left(1 - \frac{v_s}{c_s^2} \widehat{\mathcal{A}}(\omega) \right) \frac{1}{4\pi\rho} \widehat{T}(\omega) \left(0, \frac{\partial}{\partial x_3} \left(\frac{1}{r} \right), -\frac{\partial}{\partial x_2} \left(\frac{1}{r} \right) \right) \int_0^{r/c_s} \zeta e^{\sqrt{-1} \kappa_s(\omega) \zeta} d\zeta.$$

In the sequel, we use following notations for brevity:

$$I_m(r, \omega) = A_m \int_0^{r/c_m} \zeta e^{\sqrt{-1} \kappa_m(\omega) \zeta} d\zeta, \quad (4.17)$$

$$E_m(r, \omega) = A_m \exp \left\{ \sqrt{-1} \kappa_m(\omega) \frac{r}{c_m} \right\}, \quad (4.18)$$

$$A_m(\omega) = \left(1 - \frac{v_m}{c_m^2} \widehat{\mathcal{A}}(\omega) \right), \quad m = p, s. \quad (4.19)$$

We have for all $i = 1, 2, 3$:

$$\begin{aligned} (\nabla \widehat{\varphi}_1)_i &= - \frac{\partial}{\partial x_i} \left[\left(1 - \frac{v_p}{c_p^2} \widehat{\mathcal{A}}(\omega) \right) \frac{1}{4\pi\rho} \widehat{T}(\omega) \frac{\partial}{\partial x_1} \left(\frac{1}{r} \right) \int_0^{r/c_p} \zeta e^{\sqrt{-1} \kappa_p(\omega) \zeta} d\zeta \right], \\ &= - \left(1 - \frac{v_p}{c_p^2} \widehat{\mathcal{A}}(\omega) \right) \frac{1}{4\pi\rho} \widehat{T}(\omega) \frac{\partial^2}{\partial x_1 x_i} \left(\frac{1}{r} \right) \int_0^{r/c_p} \zeta e^{\sqrt{-1} \kappa_p(\omega) \zeta} d\zeta \\ &\quad - \left(1 - \frac{v_p}{c_p^2} \widehat{\mathcal{A}}(\omega) \right) \frac{1}{4\pi\rho} \widehat{T}(\omega) \frac{\partial}{\partial x_1} \left(\frac{1}{r} \right) \frac{\partial r}{\partial x_i} \left(\frac{r}{c_p} \exp \left\{ \sqrt{-1} \kappa_p(\omega) \frac{r}{c_p} \right\} \right), \\ &= - \frac{1}{4\pi\rho} \widehat{T}(\omega) \frac{\partial^2}{\partial x_i \partial x_1} \left(\frac{1}{r} \right) I_p(r, \omega) + \frac{1}{4\pi\rho c_p^2 r} \widehat{T}(\omega) \frac{\partial r}{\partial x_1} \frac{\partial r}{\partial x_i} E_p(r, \omega), \end{aligned}$$

where we have used the identity $\frac{\partial}{\partial x_1} \left(\frac{1}{r} \right) = -\frac{1}{r^2} \frac{\partial r}{\partial x_1}$.

Similarly,

$$(\nabla \times \hat{\psi}_1)_i = \frac{1}{4\pi\rho} \hat{T}(\omega) \frac{\partial^2}{\partial x_i \partial x_1} \left(\frac{1}{r} \right) I_s(r, \omega) + \frac{1}{4\pi\rho c_s^2 r} \hat{T}(\omega) \left(\delta_{i1} - \frac{\partial r}{\partial x_i} \frac{\partial r}{\partial x_1} \right) E_s(r, \omega).$$

Therefore

$$\begin{aligned} \hat{u}_{i1} &= \frac{1}{4\pi\rho} \hat{T}(\omega) \frac{\partial^2}{\partial x_i \partial x_1} \left(\frac{1}{r} \right) [I_s(r, \omega) - I_p(r, \omega)] + \frac{1}{4\pi\rho c_p^2 r} \hat{T}(\omega) \frac{\partial r}{\partial x_i} \frac{\partial r}{\partial x_1} E_p(r, \omega) \\ &\quad + \frac{1}{4\pi\rho c_s^2 r} \hat{T}(\omega) \left(\delta_{i1} - \frac{\partial r}{\partial x_i} \frac{\partial r}{\partial x_1} \right) E_s(r, \omega). \end{aligned}$$

In general, \hat{u}_{ij} , the i -th component of the solution $\hat{\mathbf{u}}_j$ for an arbitrary j , is

$$\begin{aligned} \hat{u}_{ij} &= \frac{1}{4\pi\rho} \hat{T}(\omega) (3\hat{\mathbf{r}}_i \hat{\mathbf{r}}_j - \delta_{ij}) \frac{1}{r^3} [I_s(r, \omega) - I_p(r, \omega)] + \frac{1}{4\pi\rho c_p^2} \hat{T}(\omega) \hat{\mathbf{r}}_i \hat{\mathbf{r}}_j \frac{1}{r} E_p(r, \omega) \\ &\quad + \frac{1}{4\pi\rho c_s^2} \hat{T}(\omega) (\delta_{ij} - \hat{\mathbf{r}}_i \hat{\mathbf{r}}_j) \frac{1}{r} E_s(r, \omega), \end{aligned}$$

where $\hat{\mathbf{r}}_i = \frac{\partial r}{\partial x_i} = \frac{(x_i - \xi_i)}{r}$. I_m and E_m are given by equations (4.17) and (4.18).

4.3.2 VISCOELASTIC GREEN FUNCTION

Let $T(t)$ be a Dirac mass, that is, $T(t) = \delta(t)$. Let G_{ij} be the i -th component of the Green function related to the force concentrated in the x_j -direction and \hat{G}_{ij} be the Fourier transform of G_{ij} . Then,

$$\begin{aligned} \hat{G}_{ij}(\mathbf{x}, \omega; \xi) &= \frac{1}{4\pi\rho} (3\hat{\mathbf{r}}_i \hat{\mathbf{r}}_j - \delta_{ij}) \frac{1}{r^3} [I_s(r, \omega) - I_p(r, \omega)] + \frac{1}{4\pi\rho c_p^2} \hat{\mathbf{r}}_i \hat{\mathbf{r}}_j \frac{1}{r} E_p(r, \omega) \\ &\quad + \frac{1}{4\pi\rho c_s^2} (\delta_{ij} - \hat{\mathbf{r}}_i \hat{\mathbf{r}}_j) \frac{1}{r} E_s(r, \omega), \end{aligned}$$

or equivalently,

$$\hat{G}_{ij}(\mathbf{x}, \omega; \xi) = \hat{g}_{ij}^p(\mathbf{x}, \omega; \xi) + \hat{g}_{ij}^s(\mathbf{x}, \omega; \xi) + \hat{g}_{ij}^{ps}(\mathbf{x}, \omega; \xi), \quad (4.20)$$

where

$$\hat{g}_{ij}^{ps}(\mathbf{x}, \omega; \xi) = \frac{1}{4\pi\rho} (3\hat{\mathbf{r}}_i \hat{\mathbf{r}}_j - \delta_{ij}) \frac{1}{r^3} [I_s(r, \omega) - I_p(r, \omega)], \quad (4.21)$$

$$\hat{g}_{ij}^p(\mathbf{x}, \omega; \xi) = \frac{1}{\rho c_p^2} A_p(\omega) \hat{\mathbf{r}}_i \hat{\mathbf{r}}_j \hat{g}^p(r, \omega), \quad (4.22)$$

and

$$\hat{g}_{ij}^s(\mathbf{x}, \omega; \xi) = \frac{1}{\rho c_s^2} A_s(\omega) (\delta_{ij} - \hat{\mathbf{r}}_i \hat{\mathbf{r}}_j) \hat{g}^s(r, \omega). \quad (4.23)$$

Let $\underline{\mathbf{G}}(\mathbf{x}, t; \xi) = (G_{ij}(\mathbf{x}, t; \xi))_{i,j=1}^3$ denote the transient Green function of (4.4) associated with the source point ξ . Let $G^m(r, t)$ and $W_m(\mathbf{x}, t)$ be the inverse

Fourier transforms of $A_m(\omega)\widehat{g}^m(r, \omega)$ and $I_m(r, \omega)$, $m = p, s$, respectively. Then, from Equations (4.20) to (4.23) yield:

$$\begin{aligned} G_{ij}(\mathbf{x}, t; \xi) &= \frac{1}{\rho c_p^2} \widehat{\mathbf{r}}_i \widehat{\mathbf{r}}_j G^p(r, t) + \frac{1}{\rho c_s^2} (\delta_{ij} - \widehat{\mathbf{r}}_i \widehat{\mathbf{r}}_j) G^s(r, t) \\ &+ \frac{1}{4\pi\rho} (3\widehat{\mathbf{r}}_i \widehat{\mathbf{r}}_j - \delta_{ij}) \frac{1}{r^3} [W_s(r, t) - W_p(r, t)], \end{aligned} \quad (4.24)$$

where by a change of variables,

$$W_m(r, t) = \frac{4\pi}{c_m^2} \int_0^r \zeta^2 G^m(\zeta, t; \xi) d\zeta.$$

4.4 IDEAL GREEN FUNCTION RETRIEVAL AND IMAGING PROCEDURE

Consider the limiting case when the compressional modulus $\lambda \rightarrow +\infty$. The Green function for this quasi-incompressible viscoelastic medium is given by

$$G_{ij}(\mathbf{x}, t; \xi) = \frac{1}{\rho c_s^2} (\delta_{ij} - \widehat{\mathbf{r}}_i \widehat{\mathbf{r}}_j) G^s(r, t) + \frac{1}{\rho c_s^2} (3\widehat{\mathbf{r}}_i \widehat{\mathbf{r}}_j - \delta_{ij}) \frac{1}{r^3} \int_0^r \zeta^2 G^s(\zeta, t) d\zeta.$$

In order to generalize the detection algorithms presented in [7, 8, 19, 25] to this viscoelastic case we shall express the ideal Green function in terms of the viscoelastic Green function.

From

$$G^s(r, t) = \frac{1}{\sqrt{2\pi}} \int_{\mathbb{R}} \exp\{-\sqrt{-1}\omega t\} A_s(\omega) g^s(r, \omega) d\omega,$$

it follows that

$$G^s(r, t) = \frac{1}{\sqrt{2\pi}} \int_{\mathbb{R}} A_s(\omega) \frac{\exp\left\{\sqrt{-1}\left(-\omega t + \frac{\kappa_s(\omega)}{c_s} r\right)\right\}}{4\pi r} d\omega.$$

Let us introduce the operator

$$\mathcal{L}[\phi](t) = \frac{1}{2\pi} \int_{\mathbb{R}} \int_0^{+\infty} A_s(\omega) \phi(\tau) \exp\{\sqrt{-1}\kappa_s(\omega)\tau\} \exp\{-\sqrt{-1}\omega t\} d\tau d\omega,$$

for a causal function ϕ . Then we have

$$G^s(r, t; \xi) = \mathcal{L} \left[\frac{\delta(\tau - r/c_s)}{4\pi r} \right], \quad (4.25)$$

and therefore,

$$\mathcal{L}^* [G^s](r, t) = \mathcal{L}^* \mathcal{L} \left[\frac{\delta(\tau - r/c_s)}{4\pi r} \right], \quad (4.26)$$

where \mathcal{L}^* is the $L^2(0, +\infty)$ -adjoint of \mathcal{L} .

4.4.1 ASYMPTOTICS OF ATTENUATION OPERATOR FOR VOIGT MODEL

Consider for simplicity the Voigt model. Then, $\widehat{\mathcal{A}}(\omega) = -\sqrt{-1}\omega$ and hence,

$$\kappa_s(\omega) = \omega \sqrt{1 + \frac{\sqrt{-1}v_s}{c_s^2}\omega} \simeq \omega + \frac{\sqrt{-1}v_s}{2c_s^2}\omega^2,$$

under the smallness condition (4.1). The operator \mathcal{L} can then be approximated by

$$\widetilde{\mathcal{L}}[\phi](t) = \frac{1}{2\pi} \int_{\mathbb{R}} \int_0^{+\infty} A_s(\omega) \phi(\tau) \exp\left\{-\frac{v_s}{2c_s^2}\omega^2\tau\right\} \exp\left\{\sqrt{-1}\omega(\tau-t)\right\} d\tau d\omega.$$

Since

$$\int_{\mathbb{R}} \exp\left\{-\frac{v_s}{2c_s^2}\omega^2\tau\right\} \exp\left\{\sqrt{-1}\omega(\tau-t)\right\} d\omega = \frac{\sqrt{2\pi}c_s}{\sqrt{v_s\tau}} \exp\left\{-\frac{c_s^2(\tau-t)^2}{2v_s\tau}\right\},$$

and

$$\sqrt{-1} \int_{\mathbb{R}} \omega \exp\left\{-\frac{v_s}{2c_s^2}\omega^2\tau\right\} \exp\left\{\sqrt{-1}\omega(\tau-t)\right\} d\omega = -\frac{\sqrt{2\pi}c_s}{\sqrt{v_s\tau}} \frac{\partial}{\partial t} \left[\exp\left\{-\frac{c_s^2(\tau-t)^2}{2v_s\tau}\right\} \right],$$

it follows that

$$\widetilde{\mathcal{L}}[\phi](t) = \int_0^{+\infty} \frac{t}{\tau} \phi(\tau) \frac{c_s}{\sqrt{2\pi v_s \tau}} \exp\left\{-\frac{c_s^2(\tau-t)^2}{2v_s\tau}\right\} d\tau. \quad (4.27)$$

Analogously,

$$\widetilde{\mathcal{L}}^*[\phi](t) = \int_0^{+\infty} \frac{\tau}{t} \phi(\tau) \frac{c_s}{\sqrt{2\pi v_s t}} \exp\left\{-\frac{c_s^2(\tau-t)^2}{2v_s t}\right\} d\tau. \quad (4.28)$$

Since the phase in (4.27) and (4.28) is quadratic and v_s is very small then by consequence of the stationary phase theorem (cf. Appendix 4.A), we have following main result of this chapter:

THEOREM 4.4.1. *Let $\phi(t) \in \mathcal{D}([0, \infty[)$, where $\mathcal{D}([0, \infty[)$ is the space of C^∞ -functions of compact support in $[0, \infty[$. Then*

$$\begin{cases} \widetilde{\mathcal{L}}^*[\phi](t) = \phi + \frac{v_s}{2c_s^2} \frac{d^2}{dt^2}(t\phi) + o\left(\frac{v_s}{c_s^2}\right), \\ \widetilde{\mathcal{L}}[\phi](t) = \phi + \frac{v_s}{2c_s^2} t \frac{d^2}{dt^2}(\phi) + o\left(\frac{v_s}{c_s^2}\right), \end{cases} \quad (4.29)$$

and therefore

$$\widetilde{\mathcal{L}}^* \widetilde{\mathcal{L}}[\phi](t) = \phi + \frac{v_s}{c_s^2} \frac{d}{dt} \left(t \frac{d}{dt} \phi \right) + o\left(\frac{v_s}{c_s^2}\right), \quad (4.30)$$

and,

$$(\mathcal{L}^* \widetilde{\mathcal{L}})^{-1}[\phi](t) = \phi - \frac{v_s}{c_s^2} \frac{d}{dt} \left(t \frac{d}{dt} \phi \right) + o\left(\frac{v_s}{c_s^2}\right). \quad (4.31)$$

Proof. 1. *Proof of approximation (4.29):*

Let us first consider the case of operator \mathcal{L}^* . We have

$$\begin{aligned}\widetilde{\mathcal{L}}^*[\phi](t) &= \int_0^{+\infty} \frac{\tau}{t} \phi(\tau) \frac{c_s}{\sqrt{2\pi v_s t}} \exp\left\{-\frac{c_s^2(\tau-t)^2}{2v_s t}\right\} d\tau \\ &= \frac{1}{t\sqrt{\epsilon}} \int_0^{+\infty} \psi(\tau) \exp\left\{\frac{\sqrt{-1}f(\tau)}{\epsilon}\right\} d\tau,\end{aligned}$$

with,

$$f(\tau) = \sqrt{-1}\pi(\tau-t)^2, \quad \epsilon = \left(\frac{2\pi v_s t}{c_s^2}\right), \quad \text{and} \quad \psi(\tau) = \tau\phi(\tau).$$

Remark that the phase f satisfies at $\tau = t$,

$$f(t) = 0, \quad f'(t) = 0, \quad f''(t) = 2\sqrt{-1}\pi \neq 0.$$

Moreover, in order to apply stationary phase theorem, we have

$$\begin{cases} \exp\left\{\frac{\sqrt{-1}f(t)}{\epsilon}\right\} \left(\epsilon^{-1} \frac{f''(t)}{2\sqrt{-1}\pi}\right)^{-1/2} = \sqrt{\epsilon} \\ g_t(\tau) = f(\tau) - f(t) - \frac{1}{2}f''(t)(\tau-t)^2 = 0 \\ L_1[\psi](t) = L_1^{(1)}[\psi](t) = \frac{-1}{2\sqrt{-1}}f''(t)^{-1}\psi''(t) = \frac{1}{4\pi}(t\phi)''.\end{cases}$$

Thus, Theorem 4.A.1 implies that

$$\left|\widetilde{\mathcal{L}}^*[\phi](t) - \left(\phi(t) + \frac{v_s}{2c_s^2}(t\phi)''\right)\right| \leq \frac{C}{t}\epsilon^{3/2} \sum_{\alpha \leq 4} \sup_s |(s\phi(s))^{(\alpha)}|.$$

The case of the operator $\widetilde{\mathcal{L}}$ is very similar. Note that

$$\begin{aligned}\widetilde{\mathcal{L}}[\phi](t) &= \int_0^{+\infty} \frac{t}{\tau} \phi(\tau) \frac{c_s}{\sqrt{2\pi v_s \tau}} \exp\left\{-\frac{c_s^2(\tau-t)^2}{2v_s \tau}\right\} d\tau \\ &= \frac{t}{\sqrt{\epsilon}} \int_0^{+\infty} \psi(\tau) \exp\left\{\frac{\sqrt{-1}f(\tau)}{\epsilon}\right\},\end{aligned}$$

with

$$f(\tau) = \sqrt{-1}\pi \frac{(\tau-t)^2}{\tau}, \quad \epsilon = \frac{v_s}{2\pi c_s^2} \quad \text{and} \quad \psi(\tau) = \frac{\phi(\tau)}{\tau^{3/2}}.$$

It follows that

$$f'(\tau) = \sqrt{-1}\pi \left(1 - \frac{t^2}{\tau^2}\right), \quad f''(\tau) = 2\sqrt{-1}\pi \frac{t^2}{\tau^3}, \quad f'''(\tau) = 2\sqrt{-1}\pi \frac{1}{\tau^4},$$

and the function $g_t(\tau)$ is equal to

$$g_t(\tau) = \sqrt{-1}\pi \frac{(\tau-t)^2}{\tau} - \sqrt{-1}\pi \frac{(\tau-t)^2}{t} = \sqrt{-1}\pi \frac{(t-\tau)^3}{\tau t}.$$

We deduce that

$$\left\{ \begin{array}{l} (g_t \psi)^{(4)}(t) = (g_t^{(4)}(t)\psi(t) + 4g_t^{(3)}(t)\psi'(t)) \\ \quad = \sqrt{-1}\pi \left(\frac{24}{t^3}\psi(t) - \frac{24}{t^2}\psi'(t) \right) \\ (g_t^2 \psi)^{(6)}(t) = (g_t^2)^{(6)}(t)\psi(t) \\ \quad = -\pi^2 \frac{6!}{t^4}\psi(t), \end{array} \right.$$

and then,

$$\left\{ \begin{array}{l} L_1^{(1)}[\psi](t) = \frac{-1}{\sqrt{-1}} \left(\frac{1}{2} (f''(t))^{-1} \psi''(t) \right) \\ \quad = \frac{1}{4\pi} t \left(\frac{\tilde{\phi}(t)}{\sqrt{t}} \right)'' \\ \quad = \frac{1}{4\pi} \left(\sqrt{t} \tilde{\phi}''(t) - \frac{\tilde{\phi}'(t)}{\sqrt{t}} + \frac{3}{4} \frac{\tilde{\phi}(t)}{t^{3/2}} \right) \\ L_1^{(2)}[\psi](t) = \frac{1}{8\sqrt{-1}} f''(t)^{-2} \left(g_t^{(4)}(s)\psi(s) + 4g_t^{(3)}(t)\psi'(t) \right) \\ \quad = \frac{1}{4\pi} \left(3 \left(\frac{\tilde{\phi}(t)}{\sqrt{t}} \right)' - 3 \frac{\tilde{\phi}(t)}{t^{3/2}} \right) \\ \quad = \frac{1}{4\pi} \left(3 \frac{\tilde{\phi}'(t)}{\sqrt{t}} - \frac{9}{2} \frac{\tilde{\phi}(t)}{t^{3/2}} \right) \\ L_1^{(3)}[\psi](t) = \frac{-1}{2^3 2! 3! \sqrt{-1}} f''(t)^{-3} (g_t^2)^{(6)}(t)\psi(s) \\ \quad = \frac{1}{4\pi} \left(\frac{15}{4} \frac{\tilde{\phi}(t)}{t^{3/2}} \right), \end{array} \right.$$

where $\tilde{\phi}(\tau) = \frac{\phi(\tau)}{\tau}$. Therefore, we have

$$\begin{aligned} L_1[\psi](t) &= L_1^{(1)}[\psi](t) + L_1^{(2)}[\psi](t) + L_1^{(3)}[\psi](t) \\ &= \frac{1}{4\pi} \left(\sqrt{t} \tilde{\phi}''(t) + (3-1) \frac{\tilde{\phi}'(t)}{\sqrt{t}} + \left(\frac{3}{4} - \frac{9}{2} + \frac{15}{4} \right) \frac{\tilde{\phi}(t)}{t^{3/2}} \right) \\ &= \frac{1}{4\pi\sqrt{t}} (t\tilde{\phi}(t))'' \\ &= \frac{1}{4\pi\sqrt{t}} \phi''(t), \end{aligned}$$

and again we invoke Theorem 4.A.1 to conclude that

$$\left| \widetilde{\mathcal{L}}[\phi](t) - \left(\phi(t) + \frac{v_s}{2c_s^2} t \phi''(t) \right) \right| \leq C t \epsilon^{3/2} \sum_{\alpha \leq 4} \sup_s |\psi^{(\alpha)}(s)|.$$

2. *Proof of approximation (4.30):*

Approximation (4.30) is evident and a direct consequence of (4.29).

3. *Proof of approximation (4.31):*

Note that $\psi = (\mathcal{L}^* \widetilde{\mathcal{L}})^{-1}[\phi]$ implies $(\mathcal{L}^* \widetilde{\mathcal{L}})[\psi] = \phi$. As, by assumption 4.1, we have $\frac{v_s}{c_s^2} \ll 1$, let us introduce the asymptotic development of ψ as

$$\psi = \sum_{i=0}^{\infty} \left(\frac{v_s}{c_s^2} \right)^i \psi_i.$$

From (4.30), it holds

$$\psi_0 + \left(\frac{v_s}{c_s^2} \right) \left((t\psi_0)' + \psi_1 \right) + o\left(\frac{v_s}{c_s^2} \right) = \phi,$$

$$\psi_0 = \phi, \quad \text{and} \quad \psi_1 = -(t(\psi_0))' = -(t(\phi))'.$$

Therefore,

$$(\mathcal{L}^* \widetilde{\mathcal{L}})^{-1}[\phi](t) = \phi - \frac{v_s}{c_s^2} (t\phi)' + o\left(\frac{v_s}{c_s^2} \right).$$

□

REMARK 4.4.2. For more general media with a fractional power-law exponent γ , one can recover the ideal Green function from the viscous one in a very similar fashion by inverting a fractional differential operator. Such an approximation has been reported in Chapter 1, Section 1.2.6.2, in the context of Photoacoustic imaging.

4.4.2 IMAGING PROCEDURE

An important consequence of Theorem 4.4.1 is that the ideal Green function, $\frac{\delta(\tau - r/c_s)}{4\pi r}$, can be approximately reconstructed from the viscous Green function, $G^s(r, t; \xi)$, by either solving the ordinary differential equation

$$\phi + \frac{v_s}{c_s^2} \frac{\partial}{\partial t} \left(t \frac{\partial}{\partial t} \phi \right) = \mathcal{L}^* [G^s](r, t; \xi),$$

with $\phi = 0, t \ll 0$, which results from (4.25) and (4.29) or making the approximation

$$\frac{1}{(4\pi r)} \delta\left(\tau - \frac{r}{c_s}\right) \simeq \mathcal{L}^* [G^s](r, t; \xi) - \frac{v_s}{c_s^2} \frac{d}{dt} \left(t \frac{d}{dt} [\mathcal{L}^* [G^s](r, t; \xi)] \right).$$

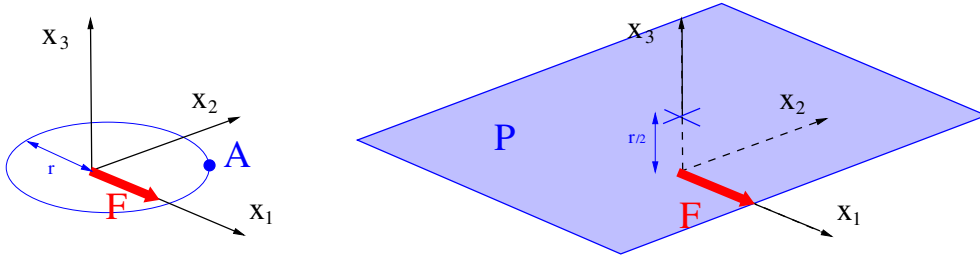


FIGURE 4.1. Left: $A = \left(\frac{1}{\sqrt{2}}r, \frac{1}{\sqrt{2}}r, 0\right)$. Right: Plane $P = \{\mathbf{x} \in \mathbb{R}^3, x_3 = \frac{r}{2}\}$

using (4.26) together with (4.31).

Once the ideal Green function $\frac{\delta(\tau - r/c_s)}{4\pi r}$ is reconstructed, one can find its source ξ using a time-reversal, a Kirchhoff or a back propagation algorithm; see [7, 8, 19, 25]. One can also find the shear modulus of the anomaly from the ideal near-field measurements using the asymptotic formalism developed in [25, 27, 28]. These ideal near field measurements can be reconstructed, in turn, from the near-field measurements in the viscous medium using Theorem 4.4.1. The asymptotic formalism reduces the anomaly imaging problem to the detection of the location and the reconstruction of a certain polarization tensor in the far-field and separates the scales in the near-field.

4.5 NUMERICAL ILLUSTRATIONS

In order to substantiate the potential of our approach, we present some numerical experiments in this section.

4.5.1 PROFILE OF THE GREEN FUNCTION

In this section, we illustrate the profile of the Green function for different values of the power law exponent γ , shear viscosity η_s and time parameter t . We opt for the same parameters of simulation as taken in the work of Bercoff *et al.* [36], that is, we take $\rho = 1000$, $c_s = 1$, $c_p = 40$, $\eta_p = 0$.

In Figure 4.2, we plot the first component, G_{11} , of the Green function observed at the point $A = \left(\frac{1}{\sqrt{2}}r, \frac{1}{\sqrt{2}}r, 0\right)$ (see image on the left in Figure 4.1) with $r = 0.015$ for three different values of γ and two different values of η_s . We can clearly remark that the attenuation behavior varies significantly for different choices of power law exponent γ and the viscosity parameter η_s .

In Figure 4.3, we plot G_{11} , evaluated at the plane $P = \{\mathbf{x} \in \mathbb{R}^3; x_3 = \frac{r}{2}\}$ (see second image in Figure 4.1), at three different times. As expected, we get a

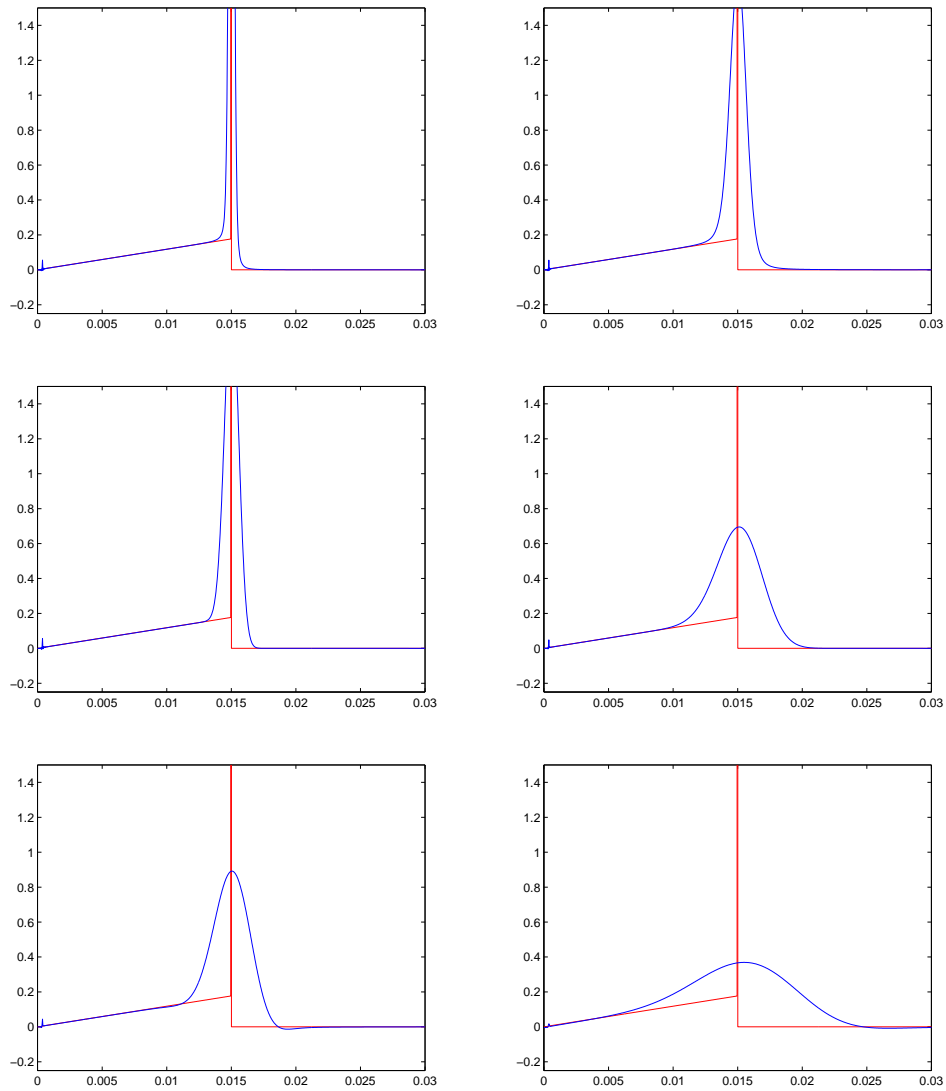


FIGURE 4.2. Temporal response $t \rightarrow G_{11}(A, t, 0)$ using a purely elastic Green function (red line) and a viscous Green function (blue line). First line: $\gamma = 1.75$, second line: $\gamma = 2$ and third line: $\gamma = 2.25$. Left: $\eta_s = 0.02$, right: $\eta_s = 0.2$.

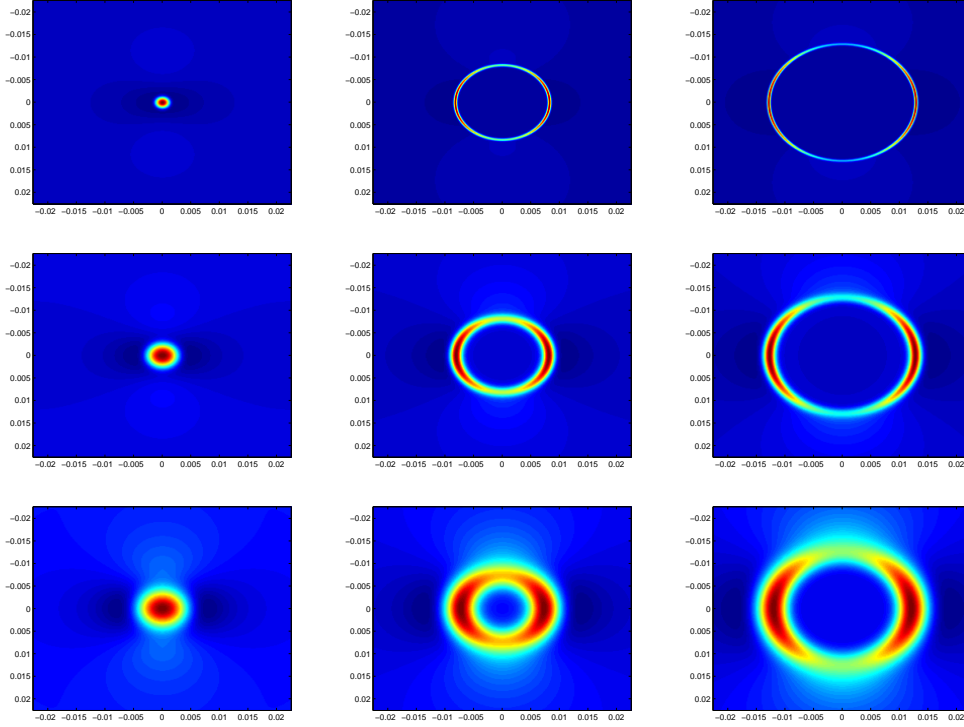


FIGURE 4.3. 2D spatial response $\mathbf{x} \rightarrow G_{11}(\mathbf{x}, t, 0)$ at the plane P to a spatiotemporal delta function with (top to bottom): a purely elastic Green function, a viscous Green function with $(\gamma = 1.75, \eta_s = 0.2)$ and $(\gamma = 2, \eta_s = 0.2)$. Left to right: $t = 0.0075$, $t = 0.0112$ and $t = 0.015$

diffusion of the wavefront with the increasing values of the power law exponent γ and depending on the choice of η_s .

4.5.2 APPROXIMATION OF ATTENUATION OPERATOR \mathcal{L}

Consider the limiting case when compressional modulus $\lambda \rightarrow +\infty$ with $\gamma = 2$. We take $\rho = 1000$, $c_s = 1$ and a concentrated force \mathbf{F} of the form $\mathbf{F} = -T(t)\delta(\mathbf{x})\mathbf{e}_1$ where the time profile of the pulse, $T(t)$, is a Gaussian with central frequency ω_0 and bandwidth ρ . Denote by $\mathbf{u}_{ideal}(\mathbf{x}, t)$ the ideal response without attenuation and by $\mathbf{u}_{v_s}(\mathbf{x}, t)$ the response associated to the attenuation coefficient v_s . Following Section 4.4, we have

$$\mathbf{u}_{v_s} \simeq \mathcal{L}[\mathbf{u}_{ideal}].$$

In Figure 4.4, we plot the first components of $t \rightarrow \mathbf{u}_{ideal}(A, t)$, $t \rightarrow \mathbf{u}_{v_s}(A, t)$ and $t \rightarrow \mathcal{L}[\mathbf{u}_{ideal}](A, t)$ for different values of ω_0 and $\eta_s = 0.02$. As expected, the function $t \rightarrow \mathbf{u}_{v_s}(A, t)$ and $t \rightarrow \mathcal{L}[\mathbf{u}_{ideal}](A, t)$ are very close and almost overlapping. It substantiates that the attenuation operator, \mathcal{L} , effectively describes the viscos effects and the approximations presented in Section 4.4 are quite adequate.

Finally, in Figure 4.5, we plot in logarithmic scale the error of approximation

$$\frac{v_s}{c_s^2} \rightarrow \left\| \mathcal{L}[\phi] - \left(\phi + \frac{v_s}{2c_s^2} t \phi'' \right) \right\|_{\infty},$$

where $\phi(t)$ is the first component of $\mathbf{u}_{ideal}(\mathbf{x}, t)$, computed at the point $\mathbf{x} = A$ with $\omega_0 = \rho$. It clearly appears to be an approximation of order greater than one.

4.6 CONCLUSION

In this chapter, we have computed the Green function in a viscoelastic medium obeying a frequency power-law. For the Voigt model, which corresponds to quadratic frequency losses, we have used the stationary phase theorem 4.A.1 to reconstruct the ideal Green function from the viscous one by solving an ordinary differential equation. Once the ideal Green function is reconstructed, one can find its source point ξ using the algorithms such as time reversal, back-propagation, and Kirchhoff imaging [7, 8, 25]. One can also estimate the shear modulus of the medium using asymptotic formalism and reconstructing a certain polarization tensor in the far field [23, 26, 27]. For more general power-law media, one can recover the ideal Green function from the viscous one by inverting a fractional differential operator (cf. Chapter 1, Section 1.2.6.2).

4.A STATIONARY PHASE METHOD

The proof of the following theorem is established in [78, Theorem 7.7.1].

THEOREM 4.A.1. (*Stationary phase*) Let $K \subset [0, \infty)$ be a compact set, X an open neighborhood of K and k a positive integer. If $\psi \in C_0^{2k}(K)$, $f \in C^{3k+1}(X)$ such that

$$\Im m\{f\} \geq 0 \text{ in } X, \quad \Im m\{f(t_0)\} = 0, \quad f'(t_0) = 0, \quad f''(t_0) \neq 0, \quad f' \neq 0 \text{ in } K \setminus \{t_0\}$$

then for $\epsilon > 0$

$$\left| \int_K \psi(t) e^{if(t)/\epsilon} dt - e^{if(t_0)/\epsilon} \left(\lambda \frac{f''(t_0)}{2\pi i} \right)^{-1/2} \sum_{j < k} \epsilon^j L_j[\psi] \right| \leq C \epsilon^k \sum_{\alpha \leq 2k} \sup_s |\psi^{(\alpha)}(s)|.$$

Here C is bounded when f stays in a bounded set in $C^{3k+1}(X)$ and $\frac{|t-t_0|}{|f'(t)|}$ has a uniform bound. With,

$$g_{t_0}(t) = f(t) - f(t_0) - \frac{1}{2} f''(t_0)(t-t_0)^2,$$

which vanishes up to third order at t_0 , we have

$$L_j[\psi] = \sum_{\nu-\mu=j} \sum_{2\nu \geq 3\mu} i^{-j} \frac{2^{-\nu}}{\nu! \mu!} (-1)^\nu f''(t_0)^{-\nu} \left(g_{t_0}^\mu \psi \right)^{(2\nu)}(t_0).$$

□

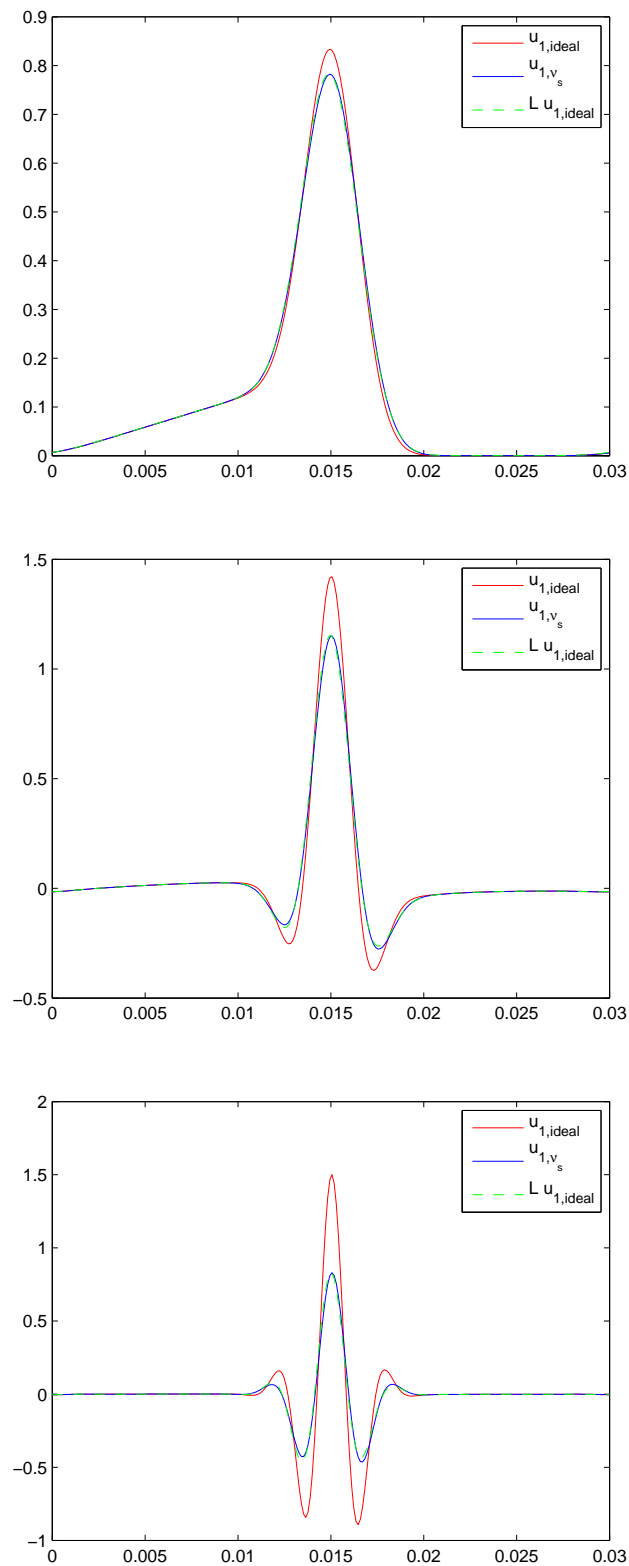


FIGURE 4.4. Comparison between $u_{1,v_s}(x, t)$ and $\mathcal{L}[u_{1,ideal}](x, t)$ observed at $x = A$ with $\gamma = 2$ and $\eta_s = 0.02$; Top: $\omega_0 = 0$; Center: $\omega_0 = \rho$; Bottom: $\omega_0 = 2\rho$.

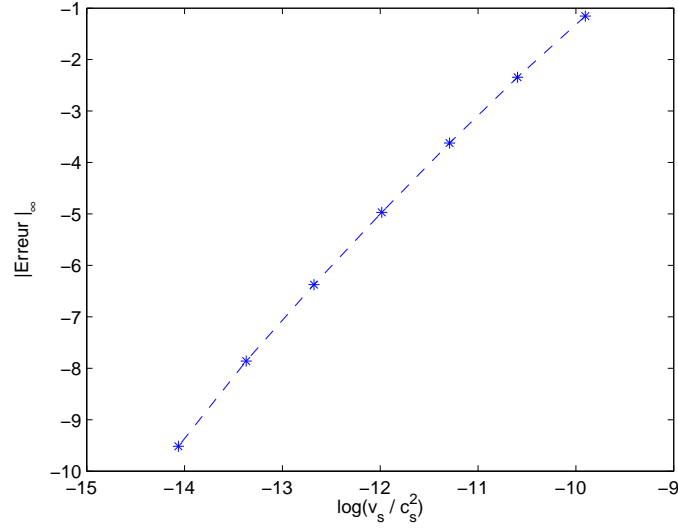


FIGURE 4.5. Approximation of operator \mathcal{L} : Error $\frac{v_s}{c_s^2} \rightarrow \left\| \mathcal{L}[\phi] - \left(\phi + \frac{v_s}{2c_s^2} t\phi'' \right) \right\|_\infty$ in logarithmic scale in the case when $\phi(t) = u_{1,ideal}(A, t)$ with $\omega_0 = \rho$.

Note that L_1 can be expressed as the sum

$$L_1[\psi] = L_1^{(1)}[\psi] + L_1^{(2)}[\psi] + L_1^{(3)}[\psi],$$

where L_1^j , for $j = 1, 2, 3$ are respectively associate to the pair $(\nu_j, \mu_j) = (1, 0), (2, 1), (3, 2)$ and are identified as:

$$\left\{ \begin{array}{l} L_1^{(1)}[\psi] = \frac{-1}{2i} f''(t_0)^{-1} \psi^{(2)}(t_0), \\ L_1^{(2)}[\psi] = \frac{1}{2^2 2! i} f''(t_0)^{-2} (g_{t_0} u)^{(4)}(t_0) \\ \quad = \frac{1}{8i} f''(t_0)^{-2} \left(g_{t_0}^{(4)}(t_0) \psi(t_0) + 4g_{t_0}^{(3)}(t_0) \psi'(t_0) \right), \\ L_1^{(3)}[\psi] = \frac{-1}{2^3 2! 3! i} f''(t_0)^{-3} (g_{t_0}^2 \psi)^{(6)}(t_0) \\ \quad = \frac{-1}{2^3 2! 3! i} f''(t_0)^{-3} (g_{t_0}^2)^{(6)}(t_0) \psi(t_0). \end{array} \right.$$

5.1 INTRODUCTION

Waves in *loss-less* media are invariant under time transformation $t \rightarrow -t$. This simple observation has provided very promising techniques in a variety of domains including biomedical imaging [63], seismology [87], material analysis [107], land-mine detection [101], telecommunication [89] and underwater acoustics [62].

The robustness and simplicity of time-reversal techniques make them an ideal choice to resolve *source localization problems*. These inverse problems have been of significant interest in recent years and find numerous applications in different fields, particularly in biomedical imaging [11, 19, 20, 106, 130]. In this chapter, we consider the problem of reconstructing sources in a viscoelastic medium from wavefield measurements using time-reversal methods. Our motivation is the recent advances on hybrid methods in biomedical imaging exploiting elastic properties of the soft tissues [71]. Examples of these hybrid methods include magnetic resonance elastography [23, 46, 47], transient elasticity imaging [25], shear wave imaging [113] and acoustic radiation force imaging [20, 36]. The envisaged problem is quite challenging, indeed, because the time reversibility of the wave equations breaks down in lossy media. Further, if not accounted for, these losses produce serious blurring in source reconstruction using classical time-reversal methods. In this chapter, we use a thermo-viscous approximation to frequency power-law model for the attenuation losses. We refer, for instance, to [82, 83, 128] for detailed discussions on the attenuation models in wave propagation and their causality properties.

The main contributions of this chapter are twofold. We first provide a modified time-reversal imaging algorithm in inviscid media based on a weighted Helmholtz decomposition in Section 5.2. We justify both analytically and numerically that it provides a better approximation than by simply time reversing the displacement field. Then, we give a regularized time-reversal imaging al-

gorithm for source reconstruction in attenuated media in Section 5.3. We show that it leads to an approximation of the source term with attenuation correction of first order in terms of the viscosity parameters. We present a variety of numerical illustrations to compare different time-reversal algorithms and to highlight the potential of our original approach.

5.2 TIME REVERSAL IN HOMOGENEOUS ELASTIC MEDIA WITHOUT VISCOSITY

Let us consider the homogeneous isotropic elastic wave equation in an open d -dimensional medium:

$$\begin{cases} \frac{\partial^2 \mathbf{u}}{\partial t^2}(\mathbf{x}, t) - \mathcal{L}_{\lambda, \mu} \mathbf{u}(\mathbf{x}, t) = \frac{d\delta_0(t)}{dt} \mathbf{F}(\mathbf{x}), & (\mathbf{x}, t) \in \mathbb{R}^d \times \mathbb{R}, \\ \mathbf{u}(\mathbf{x}, t) = \frac{\partial \mathbf{u}}{\partial t}(\mathbf{x}, t) = \mathbf{0}, & \mathbf{x} \in \mathbb{R}^d, t < 0, \end{cases} \quad (5.1)$$

where

$$\mathcal{L}_{\lambda, \mu} \mathbf{u} = \mu \Delta \mathbf{u} + (\lambda + \mu) \nabla (\nabla \cdot \mathbf{u}). \quad (5.2)$$

Here (λ, μ) are the Lamé coefficients of the medium and its density is assumed to be equal to one. The aim in this section is to design an efficient algorithm for reconstructing the compactly supported source function \mathbf{F} from the recorded data

$$\left\{ \mathbf{g}(\mathbf{y}, t) = \mathbf{u}(\mathbf{y}, t), t \in [0, T], \mathbf{y} \in \partial\Omega \right\}, \quad (5.3)$$

where Ω is supposed to strictly contain the support of \mathbf{F} . We are interested in the following time-reversal functional:

$$\mathcal{I}(\mathbf{x}) = \int_0^T \mathbf{v}_s(\mathbf{x}, T) ds, \quad \mathbf{x} \in \Omega, \quad (5.4)$$

where the vector field \mathbf{v}_s is defined as the solution of

$$\begin{cases} \frac{\partial^2 \mathbf{v}_s}{\partial t^2}(\mathbf{x}, t) - \mathcal{L}_{\lambda, \mu} \mathbf{v}_s(\mathbf{x}, t) = \frac{d\delta_s(t)}{dt} \mathbf{g}(\mathbf{x}, T - s) \delta_{\partial\Omega}(\mathbf{x}), & (\mathbf{x}, t) \in \mathbb{R}^d \times \mathbb{R}, \\ \mathbf{v}_s(\mathbf{x}, t) = \frac{\partial \mathbf{v}_s}{\partial t}(\mathbf{x}, t) = \mathbf{0}, & \mathbf{x} \in \mathbb{R}^d, t < s. \end{cases} \quad (5.5)$$

Here, $\delta_{\partial\Omega}$ is the surface Dirac mass on $\partial\Omega$ and $\mathbf{g} := \mathbf{u}$ on $\partial\Omega \times \mathbb{R}$ is the measured displacement field.

The time-reversal imaging functional \mathcal{I} is usually implemented to reconstruct the source distribution in an elastic medium [46, 101, 106]. It is motivated by the time reversibility property of the elastic waves. In a general setting, however, it is not sure that it provides a good reconstruction of the source distribution \mathbf{F} . Indeed the problem is that the recorded displacement field at the surface

of the domain is a mixture of pressure and shear wave components. By time reversing and back-propagating these signals as in (5.4) a blurred image is obtained due to the fact that the pressure and shear wave speeds are different.

In this work, we first present a modified time-reversal imaging functional $\tilde{\mathcal{I}}$, and justify mathematically that it provides a better approximation than \mathcal{I} of the source \mathbf{F} . This new functional $\tilde{\mathcal{I}}$ can be seen as a correction based on a *weighted Helmholtz decomposition* to \mathcal{I} (which is considered as an *initial guess*). In fact, we find the compressional and the shear components of \mathcal{I} such that

$$\mathcal{I} = \nabla \times \psi_{\mathcal{I}} + \nabla \phi_{\mathcal{I}}. \quad (5.6)$$

Then we multiply these components with $c_p = \sqrt{\lambda + 2\mu}$ and $c_s = \sqrt{\mu}$, the pressure and the shear wave speeds respectively. Finally, we define $\tilde{\mathcal{I}}$ by

$$\tilde{\mathcal{I}} = c_s \nabla \times \psi_{\mathcal{I}} + c_p \nabla \phi_{\mathcal{I}}. \quad (5.7)$$

We rigorously explain why should this new functional be better than the original one. We substantiate this argument with numerical illustrations.

In the sequel, we define respectively the Helmholtz decomposition operators \mathcal{H}^p and \mathcal{H}^s by

$$\mathcal{H}^p[\mathcal{I}] := \nabla \phi_{\mathcal{I}} \quad \text{and} \quad \mathcal{H}^s[\mathcal{I}] := \nabla \times \psi_{\mathcal{I}}. \quad (5.8)$$

5.2.1 TIME-REVERSAL IMAGING ANALYSIS

In order to establish some results about time reversal using \mathcal{I} and $\tilde{\mathcal{I}}$, we use the following integral formulation based on the elastic Green tensor.

5.2.1.1 INTEGRAL FORMULATION

Let us introduce the outgoing Green tensor $\mathbb{G}_{\omega,0}$ associated to the elastic wave equation

$$(\mathcal{L}_{\lambda,\mu} + \omega^2) \mathbb{G}_{\omega,0}(\mathbf{x}) = -\delta_0 \mathbb{I}, \quad \mathbf{x} \in \mathbb{R}^d. \quad (5.9)$$

It can be expressed in the form [3, 27]

$$\mathbb{G}_{\omega,0}(\mathbf{x}) = \frac{1}{\mu \kappa_s^2} \left(\kappa_s^2 G_{\omega,0}^s(\mathbf{x}) \mathbb{I} + \mathbb{D} \left(G_{\omega,0}^s - G_{\omega,0}^p \right) (\mathbf{x}) \right), \quad \mathbf{x} \in \mathbb{R}^d, \quad (5.10)$$

where $\mathbb{I} = (\delta_{ij})_{i,j=1}^d$, $\mathbb{D} = \left(\frac{\partial^2}{\partial x_i \partial x_j} \right)_{i,j=1}^d$ and $\kappa_s^2 = \frac{\omega^2}{\mu}$ and $\kappa_p^2 = \frac{\omega^2}{\lambda + 2\mu}$ are the shear and the pressure wavenumbers respectively. Here, $G_{\omega,0}^\alpha(\mathbf{x})$ is the fundamental solution of the Helmholtz operator $\Delta + \kappa_\alpha^2$ in \mathbb{R}^d subject to outgoing radiation conditions, with $\alpha = p, s$. For example, when $d = 3$, we have

$$G_{\omega,0}^\alpha(\mathbf{x}) = \frac{\exp\{i\kappa_\alpha|\mathbf{x}|\}}{4\pi|\mathbf{x}|}, \quad \alpha = p, s. \quad (5.11)$$

The functional $\mathcal{I}(\mathbf{x})$ defined by (5.4) can be expressed in the form (see, for instance, Chapter 2)

$$\begin{aligned}\mathcal{I}(\mathbf{x}) &= \Re e \left[\frac{1}{2\pi} \int_{\mathbb{R}^d} \int_{\mathbb{R}} \omega^2 \left[\int_{\partial\Omega} \mathbb{G}_\omega(\mathbf{x}, \mathbf{y}) \bar{\mathbb{G}}_\omega(\mathbf{y}, \mathbf{z}) d\sigma(\mathbf{y}) \right] d\omega \mathbf{F}(\mathbf{z}) d\mathbf{z} \right] \\ &= \frac{1}{4\pi} \int_{\mathbb{R}^d} \int_{\mathbb{R}} \omega^2 \left[\int_{\partial\Omega} \left[\mathbb{G}_\omega(\mathbf{x}, \mathbf{y}) \bar{\mathbb{G}}_\omega(\mathbf{y}, \mathbf{z}) + \bar{\mathbb{G}}_\omega(\mathbf{x}, \mathbf{y}) \mathbb{G}_\omega(\mathbf{y}, \mathbf{z}) \right] d\sigma(\mathbf{y}) \right] d\omega \mathbf{F}(\mathbf{z}) d\mathbf{z},\end{aligned}\quad (5.12)$$

where $d\sigma$ is the surface element and we have introduced the outgoing Green tensor for a point source at \mathbf{y} :

$$\mathbb{G}_\omega(\mathbf{x}, \mathbf{y}) = \mathbb{G}_{\omega,0}(\mathbf{x} - \mathbf{y}). \quad (5.13)$$

We also introduce the decomposition of $\mathbb{G}_{\omega,0}$ into shear and compressional components as

$$\mathbb{G}_{\omega,0}(\mathbf{x}) = \mathbb{G}_{\omega,0}^p(\mathbf{x}) + \mathbb{G}_{\omega,0}^s(\mathbf{x}), \quad (5.14)$$

with

$$\mathbb{G}_{\omega,0}^p = -\frac{1}{\omega^2} \mathbb{D} G_{\omega,0}^p \quad \text{and} \quad \mathbb{G}_{\omega,0}^s = \frac{1}{\omega^2} (\kappa_s^2 \mathbb{I} + \mathbb{D}) G_{\omega,0}^s. \quad (5.15)$$

We can extend Helmholtz operator \mathcal{H}^p and \mathcal{H}^s to tensors \mathbb{G} as follows:

$$\mathcal{H}^p[\mathbb{G}]\mathbf{p} = \mathcal{H}^p[\mathbb{G}\mathbf{p}] \quad \text{and} \quad \mathcal{H}^s[\mathbb{G}]\mathbf{p} = \mathcal{H}^s[\mathbb{G}\mathbf{p}] \quad \text{for all vectors } \mathbf{p}.$$

Note that $\mathbb{G}_{\omega,0}^p$ and $\mathbb{G}_{\omega,0}^s$ satisfy, respectively

$$(\mathcal{L}_{\lambda,\mu} + \omega^2) \mathbb{G}_{\omega,0}^p = \mathcal{H}^p[-\delta_0 \mathbb{I}] \quad \text{and} \quad (\mathcal{L}_{\lambda,\mu} + \omega^2) \mathbb{G}_{\omega,0}^s = \mathcal{H}^s[-\delta_0 \mathbb{I}]. \quad (5.16)$$

Consequently, the Helmholtz decomposition of \mathcal{I} can be derived explicitly

$$\mathcal{I}(\mathbf{x}) = \mathcal{H}^p[\mathcal{I}](\mathbf{x}) + \mathcal{H}^s[\mathcal{I}](\mathbf{x}), \quad (5.17)$$

with

$$\mathcal{H}^p[\mathcal{I}](\mathbf{x}) = \frac{1}{4\pi} \int_{\mathbb{R}^d} \int_{\mathbb{R}} \omega^2 \left[\int_{\partial\Omega} \left[\mathbb{G}_\omega^p(\mathbf{x}, \mathbf{y}) \bar{\mathbb{G}}_\omega(\mathbf{y}, \mathbf{z}) + \bar{\mathbb{G}}_\omega^p(\mathbf{x}, \mathbf{y}) \mathbb{G}_\omega(\mathbf{y}, \mathbf{z}) \right] d\sigma(\mathbf{y}) \right] d\omega \mathbf{F}(\mathbf{z}) d\mathbf{z},$$

and

$$\mathcal{H}^s[\mathcal{I}](\mathbf{x}) = \frac{1}{4\pi} \int_{\mathbb{R}^d} \int_{\mathbb{R}} \omega^2 \left[\int_{\partial\Omega} \left[\mathbb{G}_\omega^s(\mathbf{x}, \mathbf{y}) \bar{\mathbb{G}}_\omega(\mathbf{y}, \mathbf{z}) + \bar{\mathbb{G}}_\omega^s(\mathbf{x}, \mathbf{y}) \mathbb{G}_\omega(\mathbf{y}, \mathbf{z}) \right] d\sigma(\mathbf{y}) \right] d\omega \mathbf{F}(\mathbf{z}) d\mathbf{z}.$$

Finally, the integral formulation of the modified imaging functional $\tilde{\mathcal{I}}$ defined by (5.7) reads

$$\tilde{\mathcal{I}}(\mathbf{x}) = \Re e \left[\frac{1}{2\pi} \int_{\mathbb{R}^d} \int_{\mathbb{R}} \omega^2 \left[\int_{\partial\Omega} \left[c_s \mathbb{G}_\omega^s(\mathbf{x}, \mathbf{y}) + c_p \mathbb{G}_\omega^p(\mathbf{x}, \mathbf{y}) \right] \bar{\mathbb{G}}_\omega(\mathbf{y}, \mathbf{z}) d\sigma(\mathbf{y}) \right] d\omega \mathbf{F}(\mathbf{z}) d\mathbf{z} \right]. \quad (5.18)$$

5.2.1.2 HELMHOLTZ-KIRCHHOFF IDENTITY

In order to approximate the integral formulation (5.18) we use a Helmholtz-Kirchhoff identity for elastic media. Some of the results presented in this subsection can be found in [141, 142] in the context of elastodynamic seismic interferometry. Indeed, the elastodynamic reciprocity theorems (Propositions 5.2.1 and 5.2.5) are the key ingredient to understand the relation between the cross correlations of signals emitted by uncorrelated noise sources and the Green function between the observation points.

Let us introduce the conormal derivative $\frac{\partial \mathbf{u}}{\partial \nu}(\mathbf{y})$ for $\mathbf{y} \in \partial\Omega$, of the displacement field \mathbf{u} at the surface $\partial\Omega$ in the outward unit normal direction \mathbf{n} by

$$\frac{\partial \mathbf{u}}{\partial \nu} := \lambda(\nabla \cdot \mathbf{u})\mathbf{n} + \mu(\nabla \mathbf{u}^T + (\nabla \mathbf{u}^T)^T)\mathbf{n}, \quad (5.19)$$

where T denotes the transpose.

Note also that the conormal derivative tensor $\frac{\partial \mathbb{G}}{\partial \nu}$ means that for all constant vectors \mathbf{p} ,

$$\left[\frac{\partial \mathbb{G}_\omega}{\partial \nu} \right] \mathbf{p} := \frac{\partial [\mathbb{G}_\omega \mathbf{p}]}{\partial \nu}.$$

The following proposition is equivalent to [142, Eq. (73)]. Since our formulation is slightly different and this is the first building block of our theory, we give its proof for consistency. Moreover, elements of the proof are used in Proposition 5.2.2.

PROPOSITION 5.2.1. *For all $\mathbf{x}, \mathbf{z} \in \Omega$, we have*

$$\int_{\partial\Omega} \left[\frac{\partial \mathbb{G}_\omega(\mathbf{x}, \mathbf{y})}{\partial \nu} \overline{\mathbb{G}_\omega(\mathbf{y}, \mathbf{z})} - \mathbb{G}_\omega(\mathbf{x}, \mathbf{y}) \frac{\partial \overline{\mathbb{G}_\omega(\mathbf{y}, \mathbf{z})}}{\partial \nu} \right] d\sigma(\mathbf{y}) = 2i \Im m \{ \mathbb{G}_\omega(\mathbf{x}, \mathbf{z}) \}. \quad (5.20)$$

Proof. By reciprocity we have

$$\mathbb{G}_\omega(\mathbf{y}, \mathbf{x}) = [\mathbb{G}_\omega(\mathbf{x}, \mathbf{y})]^T. \quad (5.21)$$

Additionally, in the homogeneous case we have $\mathbb{G}_\omega(\mathbf{y}, \mathbf{x}) = \mathbb{G}_\omega(\mathbf{x}, \mathbf{y})$, but we will not use this property here. Our goal is to show that for all constant vectors \mathbf{p} and \mathbf{q} , we have

$$\int_{\partial\Omega} \left[\mathbf{q} \cdot \frac{\partial \mathbb{G}_\omega(\mathbf{x}, \mathbf{y})}{\partial \nu} \overline{\mathbb{G}_\omega(\mathbf{y}, \mathbf{z})} \mathbf{p} - \mathbf{q} \cdot \mathbb{G}_\omega(\mathbf{x}, \mathbf{y}) \frac{\partial \overline{\mathbb{G}_\omega(\mathbf{y}, \mathbf{z})}}{\partial \nu} \mathbf{p} \right] d\sigma(\mathbf{y}) = 2i \mathbf{q} \cdot \Im m \{ \mathbb{G}_\omega(\mathbf{x}, \mathbf{z}) \} \mathbf{p}.$$

Taking scalar product of equations

$$(\mathcal{L}_{\lambda, \mu} + \omega^2) \mathbb{G}_\omega(\mathbf{y}, \mathbf{x}) \mathbf{q} = -\delta_{\mathbf{x}} \mathbf{q} \quad \text{and} \quad (\mathcal{L}_{\lambda, \mu} + \omega^2) \overline{\mathbb{G}_\omega(\mathbf{y}, \mathbf{z})} \mathbf{p} = -\delta_{\mathbf{z}} \mathbf{p}$$

with $\overline{\mathbb{G}}_\omega(\mathbf{y}, \mathbf{z})\mathbf{p}$ and $\mathbb{G}_\omega(\mathbf{y}, \mathbf{x})\mathbf{q}$ respectively, subtracting the second result from the first, and integrating in \mathbf{y} over Ω , we obtain

$$\begin{aligned} & \int_{\Omega} \left[(\overline{\mathbb{G}}_\omega(\mathbf{y}, \mathbf{z})\mathbf{p}) \cdot \mathcal{L}_{\lambda, \mu}(\mathbb{G}_\omega(\mathbf{y}, \mathbf{x})\mathbf{q}) - \mathcal{L}_{\lambda, \mu}(\overline{\mathbb{G}}_\omega(\mathbf{y}, \mathbf{z})\mathbf{p}) \cdot (\mathbb{G}_\omega(\mathbf{y}, \mathbf{x})\mathbf{q}) \right] d\mathbf{y} \\ & = \mathbf{p} \cdot (\mathbb{G}_\omega(\mathbf{z}, \mathbf{x})\mathbf{q}) - \mathbf{q} \cdot (\overline{\mathbb{G}}_\omega(\mathbf{x}, \mathbf{z})\mathbf{p}) = 2i\mathbf{q} \cdot \Im m\{\mathbb{G}_\omega(\mathbf{x}, \mathbf{z})\}\mathbf{p}. \end{aligned}$$

Using the form of the operator $\mathcal{L}_{\lambda, \mu}$, this gives

$$\begin{aligned} & 2i\mathbf{q} \cdot \Im m\{\mathbb{G}_\omega(\mathbf{x}, \mathbf{z})\}\mathbf{p} \\ & = \lambda \int_{\Omega} \left[(\overline{\mathbb{G}}_\omega(\mathbf{y}, \mathbf{z})\mathbf{p}) \cdot \left\{ \nabla \nabla \cdot (\mathbb{G}_\omega(\mathbf{y}, \mathbf{x})\mathbf{q}) \right\} - (\mathbb{G}_\omega(\mathbf{y}, \mathbf{x})\mathbf{q}) \cdot \left\{ \nabla \nabla \cdot (\overline{\mathbb{G}}_\omega(\mathbf{y}, \mathbf{z})\mathbf{p}) \right\} \right] d\mathbf{y} \\ & \quad + \mu \int_{\Omega} \left[(\overline{\mathbb{G}}_\omega(\mathbf{y}, \mathbf{z})\mathbf{p}) \cdot \left\{ (\Delta + \nabla \nabla \cdot)(\mathbb{G}_\omega(\mathbf{y}, \mathbf{x})\mathbf{q}) \right\} - (\mathbb{G}_\omega(\mathbf{y}, \mathbf{x})\mathbf{q}) \cdot \left\{ (\Delta + \nabla \nabla \cdot)(\overline{\mathbb{G}}_\omega(\mathbf{y}, \mathbf{z})\mathbf{p}) \right\} \right] d\mathbf{y}. \end{aligned}$$

We recall that, for two functions $\mathbf{u}, \mathbf{v}: \mathbb{R}^d \rightarrow \mathbb{R}^d$, we have

$$\begin{aligned} (\Delta \mathbf{u} + \nabla(\nabla \cdot \mathbf{u})) \cdot \mathbf{v} &= \nabla \cdot [(\nabla \mathbf{u}^T + (\nabla \mathbf{u}^T)^T)\mathbf{v}] - \frac{1}{2}(\nabla \mathbf{u}^T + (\nabla \mathbf{u}^T)^T) \cdot (\nabla \mathbf{v}^T + (\nabla \mathbf{v}^T)^T), \\ \nabla(\nabla \cdot \mathbf{u}) \cdot \mathbf{v} &= \nabla \cdot [(\nabla \cdot \mathbf{u})\mathbf{v}] - (\nabla \cdot \mathbf{u})(\nabla \cdot \mathbf{v}). \end{aligned}$$

Therefore, we find

$$\begin{aligned} & 2i\mathbf{q} \cdot \Im m\{\mathbb{G}_\omega(\mathbf{x}, \mathbf{z})\}\mathbf{p} \\ & = \lambda \int_{\Omega} \left[\nabla \cdot \left\{ [\nabla \cdot (\mathbb{G}_\omega(\mathbf{y}, \mathbf{x})\mathbf{q})](\overline{\mathbb{G}}_\omega(\mathbf{y}, \mathbf{z})\mathbf{p}) \right\} - \nabla \cdot \left\{ [\nabla \cdot (\overline{\mathbb{G}}_\omega(\mathbf{y}, \mathbf{z})\mathbf{p})](\mathbb{G}_\omega(\mathbf{y}, \mathbf{x})\mathbf{q}) \right\} \right] d\mathbf{y} \\ & \quad + \mu \int_{\Omega} \left[\nabla \cdot \left\{ (\nabla(\mathbb{G}_\omega(\mathbf{y}, \mathbf{x})\mathbf{q})^T + [\nabla(\mathbb{G}_\omega(\mathbf{y}, \mathbf{x})\mathbf{q})^T]^T)\overline{\mathbb{G}}_\omega(\mathbf{y}, \mathbf{z})\mathbf{p} \right\} \right. \\ & \quad \quad \left. - \nabla \cdot \left\{ (\nabla(\overline{\mathbb{G}}_\omega(\mathbf{y}, \mathbf{z})\mathbf{p})^T + [\nabla(\overline{\mathbb{G}}_\omega(\mathbf{y}, \mathbf{z})\mathbf{p})^T]^T)\mathbb{G}_\omega(\mathbf{y}, \mathbf{x})\mathbf{q} \right\} \right] d\mathbf{y} \\ & = \lambda \int_{\partial\Omega} \left[\mathbf{n} \cdot \left\{ [\nabla \cdot (\mathbb{G}_\omega(\mathbf{y}, \mathbf{x})\mathbf{q})](\overline{\mathbb{G}}_\omega(\mathbf{y}, \mathbf{z})\mathbf{p}) \right\} - \mathbf{n} \cdot \left\{ [\nabla \cdot (\overline{\mathbb{G}}_\omega(\mathbf{y}, \mathbf{z})\mathbf{p})](\mathbb{G}_\omega(\mathbf{y}, \mathbf{x})\mathbf{q}) \right\} \right] d\sigma(\mathbf{y}) \\ & \quad + \int_{\Omega} \left[\mathbf{n} \cdot \left\{ (\nabla(\mathbb{G}_\omega(\mathbf{y}, \mathbf{x})\mathbf{q})^T + [\nabla(\mathbb{G}_\omega(\mathbf{y}, \mathbf{x})\mathbf{q})^T]^T)\overline{\mathbb{G}}_\omega(\mathbf{y}, \mathbf{z})\mathbf{p} \right\} \right. \\ & \quad \quad \left. - \mathbf{n} \cdot \left\{ (\nabla(\overline{\mathbb{G}}_\omega(\mathbf{y}, \mathbf{z})\mathbf{p})^T + [\nabla(\overline{\mathbb{G}}_\omega(\mathbf{y}, \mathbf{z})\mathbf{p})^T]^T)\mathbb{G}_\omega(\mathbf{y}, \mathbf{x})\mathbf{q} \right\} \right] d\sigma(\mathbf{y}) \\ & = \lambda \int_{\partial\Omega} \left[(\overline{\mathbb{G}}_\omega(\mathbf{y}, \mathbf{z})\mathbf{p}) \cdot \left\{ \nabla \cdot (\mathbb{G}_\omega(\mathbf{y}, \mathbf{x})\mathbf{q})\mathbf{n} \right\} - (\mathbb{G}_\omega(\mathbf{y}, \mathbf{x})\mathbf{q}) \cdot \left\{ \nabla \cdot (\overline{\mathbb{G}}_\omega(\mathbf{y}, \mathbf{z})\mathbf{p})\mathbf{n} \right\} \right] d\sigma(\mathbf{y}) \\ & \quad + \mu \int_{\partial\Omega} \left[(\overline{\mathbb{G}}_\omega(\mathbf{y}, \mathbf{z})\mathbf{p}) \cdot \left\{ (\nabla(\mathbb{G}_\omega(\mathbf{y}, \mathbf{x})\mathbf{q})^T + [\nabla(\mathbb{G}_\omega(\mathbf{y}, \mathbf{x})\mathbf{q})^T]^T)\mathbf{n} \right\} \right. \\ & \quad \quad \left. - (\mathbb{G}_\omega(\mathbf{y}, \mathbf{x})\mathbf{q}) \cdot \left\{ (\nabla(\overline{\mathbb{G}}_\omega(\mathbf{y}, \mathbf{z})\mathbf{p})^T + [\nabla(\overline{\mathbb{G}}_\omega(\mathbf{y}, \mathbf{z})\mathbf{p})^T]^T)\mathbf{n} \right\} \right] d\sigma(\mathbf{y}) \\ & = \lambda \int_{\partial\Omega} \left[(\overline{\mathbb{G}}_\omega(\mathbf{y}, \mathbf{z})\mathbf{p}) \cdot \left\{ \nabla \cdot (\mathbb{G}_\omega(\mathbf{y}, \mathbf{x})\mathbf{q})\mathbf{n} \right\} - (\mathbb{G}_\omega(\mathbf{y}, \mathbf{x})\mathbf{q}) \cdot \left\{ \nabla \cdot (\overline{\mathbb{G}}_\omega(\mathbf{y}, \mathbf{z})\mathbf{p})\mathbf{n} \right\} \right] d\sigma(\mathbf{y}) \\ & \quad + \mu \int_{\partial\Omega} \left[(\overline{\mathbb{G}}_\omega(\mathbf{y}, \mathbf{z})\mathbf{p}) \cdot \left\{ (\nabla(\mathbb{G}_\omega(\mathbf{y}, \mathbf{x})\mathbf{q})^T + [\nabla(\mathbb{G}_\omega(\mathbf{y}, \mathbf{x})\mathbf{q})^T]^T)\mathbf{n} \right\} \right. \\ & \quad \quad \left. - (\mathbb{G}_\omega(\mathbf{y}, \mathbf{x})\mathbf{q}) \cdot \left\{ (\nabla(\overline{\mathbb{G}}_\omega(\mathbf{y}, \mathbf{z})\mathbf{p})^T + [\nabla(\overline{\mathbb{G}}_\omega(\mathbf{y}, \mathbf{z})\mathbf{p})^T]^T)\mathbf{n} \right\} \right] d\sigma(\mathbf{y}), \end{aligned}$$

where we have made use of the divergence theorem. Finally, we use the definition of the co-normal derivative to get

$$\begin{aligned} 2i\mathbf{q} \cdot \Im m\{\mathbb{G}_\omega(\mathbf{x}, \mathbf{z})\} \mathbf{p} &= \int_{\partial\Omega} \left[(\overline{\mathbb{G}_\omega(\mathbf{y}, \mathbf{z})} \mathbf{p}) \cdot \frac{\partial \mathbb{G}_\omega(\mathbf{y}, \mathbf{x}) \mathbf{q}}{\partial \nu} - (\mathbb{G}_\omega(\mathbf{y}, \mathbf{x}) \mathbf{q}) \cdot \frac{\partial \overline{\mathbb{G}_\omega(\mathbf{y}, \mathbf{z})} \mathbf{p}}{\partial \nu} \right] d\sigma(\mathbf{y}) \\ &= \int_{\partial\Omega} \left[\mathbf{q} \cdot \frac{\partial \mathbb{G}_\omega(\mathbf{x}, \mathbf{y})}{\partial \nu} \overline{\mathbb{G}_\omega(\mathbf{y}, \mathbf{z})} \mathbf{p} - \mathbf{q} \cdot \mathbb{G}_\omega(\mathbf{x}, \mathbf{y}) \frac{\partial \overline{\mathbb{G}_\omega(\mathbf{y}, \mathbf{z})} \mathbf{p}}{\partial \nu} \right] d\sigma(\mathbf{y}), \end{aligned}$$

which is the desired result. Note that for establishing the last equality we have used the reciprocity relation (5.21). \square

The proof of Proposition 5.2.1 uses only the reciprocity relation and the divergence theorem. Consequently, Proposition 5.2.1 also holds in a heterogeneous medium, as shown in [142]. The following proposition cannot be found in the literature, probably because its application in the context of seismic interferometry has not been identified. It is an important ingredient in the analysis of our improved imaging functional. Note that the proofs of Propositions 5.2.2 and 5.2.3 require the medium to be homogeneous (so that \mathcal{H}^s and \mathcal{H}^p commute with $\mathcal{L}_{\lambda, \mu}$), and we cannot expect them to be true in a heterogeneous medium because of mode conversion between pressure and shear waves.

PROPOSITION 5.2.2. *For all $\mathbf{x}, \mathbf{z} \in \Omega$, we have*

$$\int_{\partial\Omega} \left[\frac{\partial \mathbb{G}_\omega^s(\mathbf{x}, \mathbf{y})}{\partial \nu} \overline{\mathbb{G}_\omega^p(\mathbf{y}, \mathbf{z})} - \mathbb{G}_\omega^s(\mathbf{x}, \mathbf{y}) \frac{\partial \overline{\mathbb{G}_\omega^p(\mathbf{y}, \mathbf{z})}}{\partial \nu} \right] d\sigma(\mathbf{y}) = 0. \quad (5.22)$$

Proof. First, we recall that $\mathbb{G}_\omega^p(\mathbf{y}, \mathbf{x})$ and $\mathbb{G}_\omega^s(\mathbf{y}, \mathbf{x})$ are solutions of (5.16). We proceed as in the proof of the previous proposition to find:

$$\begin{aligned} &\int_{\partial\Omega} \left[\frac{\partial \mathbb{G}_\omega^s(\mathbf{x}, \mathbf{y})}{\partial \nu} \overline{\mathbb{G}_\omega^p(\mathbf{y}, \mathbf{z})} - \mathbb{G}_\omega^s(\mathbf{x}, \mathbf{y}) \frac{\partial \overline{\mathbb{G}_\omega^p(\mathbf{y}, \mathbf{z})}}{\partial \nu} \right] d\sigma(\mathbf{y}) \\ &= \int_{\Omega} \left[\mathcal{H}^s[-\delta_{\mathbf{x}\parallel}](\mathbf{y}) \overline{\mathbb{G}_\omega^p(\mathbf{y}, \mathbf{z})} - \mathbb{G}_\omega^s(\mathbf{x}, \mathbf{y}) \mathcal{H}^p[-\delta_{\mathbf{z}\parallel}](\mathbf{y}) \right] d\mathbf{y} \\ &= \left[\mathcal{H}^s[-\delta_{\mathbf{0}\parallel}] * \overline{\mathbb{G}_\omega^p(\cdot, \mathbf{z})} \right](\mathbf{x}) - \left[\mathbb{G}_\omega^s(\mathbf{x}, \cdot) * \mathcal{H}^p[-\delta_{\mathbf{0}\parallel}] \right](\mathbf{z}). \end{aligned}$$

Using the fact that $\mathbb{G}_\omega^p = \mathcal{H}^p[\mathbb{G}_\omega]$ and $\mathcal{H}^s \mathcal{H}^p = \mathcal{H}^p \mathcal{H}^s = 0$ we get

$$\mathcal{H}^s \left[\mathcal{H}^s[-\delta_{\mathbf{0}\parallel}] * \overline{\mathbb{G}_\omega^p(\cdot, \mathbf{z})} \right] = 0 \quad \text{and} \quad \mathcal{H}^p \left[\mathcal{H}^s[-\delta_{\mathbf{0}\parallel}] * \overline{\mathbb{G}_\omega^p(\cdot, \mathbf{z})} \right] = 0.$$

Therefore, we conclude

$$\left[\mathcal{H}^s[-\delta_{\mathbf{0}\parallel}] * \overline{\mathbb{G}_\omega^p(\cdot, \mathbf{z})} \right](\mathbf{x}) = 0.$$

Similarly, we have

$$\left[\mathbb{G}_\omega^s(\mathbf{x}, \cdot) * \mathcal{H}^p[-\delta_{\mathbf{0}\parallel}] \right](\mathbf{z}) = 0,$$

which gives the desired result. \square

Finally the following proposition shows that the elastodynamic reciprocity theorem (Proposition 5.2.1) holds for each wave component in a homogeneous medium.

PROPOSITION 5.2.3. *For all $\mathbf{x}, \mathbf{z} \in \mathbb{R}^d$ and $\alpha = p, s$,*

$$\int_{\partial\Omega} \left[\frac{\partial \mathbb{G}_\omega^\alpha(\mathbf{x}, \mathbf{y})}{\partial \nu} \overline{\mathbb{G}_\omega^\alpha(\mathbf{y}, \mathbf{z})} - \mathbb{G}_\omega^\alpha(\mathbf{x}, \mathbf{y}) \frac{\partial \overline{\mathbb{G}_\omega^\alpha(\mathbf{y}, \mathbf{z})}}{\partial \nu} \right] d\sigma(\mathbf{y}) = 2i \Im m \{ \mathbb{G}_\omega^\alpha(\mathbf{x}, \mathbf{z}) \}. \quad (5.23)$$

Proof. As both choices of α are similar, we only provide a proof for $\alpha = p$. For $\alpha = p$, indeed, we have

$$\begin{aligned} \int_{\partial\Omega} \left[\frac{\partial \mathbb{G}_\omega^p(\mathbf{x}, \mathbf{y})}{\partial \nu} \overline{\mathbb{G}_\omega^p(\mathbf{y}, \mathbf{z})} - \mathbb{G}_\omega^p(\mathbf{x}, \mathbf{y}) \frac{\partial \overline{\mathbb{G}_\omega^p(\mathbf{y}, \mathbf{z})}}{\partial \nu} \right] d\sigma(\mathbf{y}) \\ = \left[\mathcal{H}^p[-\delta_0] * \overline{\mathbb{G}_\omega^p(\cdot, \mathbf{z})} \right](\mathbf{x}) - \left[\mathbb{G}_\omega^p(\mathbf{x}, \cdot) * \mathcal{H}^p[-\delta_0] \right](\mathbf{z}). \end{aligned}$$

Using the fact that $\mathbb{G}_\omega^p(\mathbf{y}, \mathbf{z}) = \mathbb{G}_{\omega,0}^p(\mathbf{y} - \mathbf{z}) = \mathbb{G}_{\omega,0}^p(\mathbf{z} - \mathbf{y})$, we can write

$$\left[\mathcal{H}^p[-\delta_0] * \overline{\mathbb{G}_\omega^p(\cdot, \mathbf{z})} \right](\mathbf{x}) = \left[\mathcal{H}^p[-\delta_0] * \overline{\mathbb{G}_{\omega,0}^p(\cdot)} \right](\mathbf{x} - \mathbf{z})$$

and

$$\left[\mathbb{G}_\omega^p(\mathbf{x}, \cdot) * \mathcal{H}^p[-\delta_0] \right](\mathbf{z}) = \left[\mathbb{G}_{\omega,0}^p(\cdot) * \mathcal{H}^p[-\delta_0] \right](\mathbf{z} - \mathbf{x}) = \left[\mathcal{H}^p[-\delta_0] * \mathbb{G}_{\omega,0}^p(\cdot) \right](\mathbf{x} - \mathbf{z}).$$

Therefore,

$$\begin{aligned} \int_{\partial\Omega} \left[\frac{\partial \mathbb{G}_\omega^p(\mathbf{x}, \mathbf{y})}{\partial \nu} \overline{\mathbb{G}_\omega^p(\mathbf{y}, \mathbf{z})} - \mathbb{G}_\omega^p(\mathbf{x}, \mathbf{y}) \frac{\partial \overline{\mathbb{G}_\omega^p(\mathbf{y}, \mathbf{z})}}{\partial \nu} \right] d\sigma(\mathbf{y}) &= \mathcal{H}^p \left[2i \Im m \{ \mathbb{G}_\omega^p(\mathbf{x}, \mathbf{z}) \} \right] \\ &= 2i \Im m \{ \mathbb{G}_\omega^p(\mathbf{x}, \mathbf{z}) \}, \end{aligned}$$

where the last equality results from the fact that $\mathcal{H}^s \mathcal{H}^p = 0$. \square

5.2.1.3 APPROXIMATION OF THE CO-NORMAL DERIVATIVE

In this subsection, we derive an approximation of the conormal derivative $\frac{\partial \mathbb{G}_\omega(\mathbf{x}, \mathbf{y})}{\partial \nu}$, $\mathbf{y} \in \partial\Omega$, $\mathbf{x} \in \Omega$. In general, this approximation involves the angles between the pressure and shear rays and the normal on $\partial\Omega$. The approximation becomes simple when Ω is a ball with very large radius, since in this case all rays are normal to $\partial\Omega$ (Proposition 5.2.4). It allows us to use a simplified version of the Helmholtz-Kirchhoff identity in order to analyze the imaging functional $\tilde{\mathcal{I}}$ when Ω is a ball with a large radius (Proposition 5.2.5).

PROPOSITION 5.2.4. *If $\mathbf{n} = \widehat{\mathbf{y} - \mathbf{x}}$ and $|\mathbf{x} - \mathbf{y}| \gg 1$, then, for $\alpha = p, s$,*

$$\frac{\partial \mathbb{G}_\omega^\alpha(\mathbf{x}, \mathbf{y})}{\partial \nu} = i\omega c_\alpha \mathbb{G}_\omega^\alpha(\mathbf{x}, \mathbf{y}) + o\left(\frac{1}{|\mathbf{x} - \mathbf{y}|^{d-1/2}}\right). \quad (5.24)$$

Proof. For simplicity, let us take $d = 3$. We emphasize that similar arguments hold for $d = 2$. It is enough to show that for all constant vectors \mathbf{q} ,

$$\frac{\partial \mathbb{G}_\omega^p(\mathbf{x}, \mathbf{y}) \mathbf{q}}{\partial \nu} = i\omega c_p \mathbb{G}_\omega^p(\mathbf{x}, \mathbf{y}) \mathbf{q} + o\left(\frac{1}{|\mathbf{x} - \mathbf{y}|}\right)$$

and

$$\frac{\partial \mathbb{G}_\omega^s(\mathbf{x}, \mathbf{y}) \mathbf{q}}{\partial \nu} = i\omega c_s \mathbb{G}_\omega^s(\mathbf{x}, \mathbf{y}) \mathbf{q} + o\left(\frac{1}{|\mathbf{x} - \mathbf{y}|}\right).$$

Pressure component: Recall that

$$\mathbb{G}_\omega^p(\mathbf{x}, \mathbf{y}) = -\frac{1}{\omega^2} \mathbb{D} G_\omega^p(\mathbf{x}, \mathbf{y}) = \frac{1}{c_p^2} G_\omega^p(\mathbf{x}, \mathbf{y}) \widehat{\mathbf{y} - \mathbf{x}} \otimes \widehat{\mathbf{y} - \mathbf{x}} + o\left(\frac{1}{|\mathbf{x} - \mathbf{y}|}\right),$$

so that we have

$$\mathbb{G}_\omega^p(\mathbf{x}, \mathbf{y}) \mathbf{q} = \frac{1}{c_p^2} G_\omega^p(\mathbf{x}, \mathbf{y}) (\widehat{\mathbf{y} - \mathbf{x}} \cdot \mathbf{q}) \widehat{\mathbf{y} - \mathbf{x}} + o\left(\frac{1}{|\mathbf{x} - \mathbf{y}|}\right).$$

Therefore,

$$\begin{aligned} \frac{\partial \mathbb{G}_\omega^p(\mathbf{x}, \mathbf{y}) \mathbf{q}}{\partial \nu} &= \lambda \nabla_{\mathbf{y}} \cdot (\mathbb{G}_\omega^p(\mathbf{x}, \mathbf{y}) \mathbf{q}) \mathbf{n}(\mathbf{y}) + \mu \left\{ \nabla_{\mathbf{y}} (\mathbb{G}_\omega^p(\mathbf{x}, \mathbf{y}) \mathbf{q})^T + [\nabla_{\mathbf{y}} (\mathbb{G}_\omega^p(\mathbf{x}, \mathbf{y}) \mathbf{q})^T]^T \right\} \mathbf{n}(\mathbf{y}) \\ &= \frac{\widehat{\mathbf{y} - \mathbf{x}} \cdot \mathbf{q}}{c_p^3} i\omega G_\omega^p(\mathbf{x}, \mathbf{y}) \left[\lambda \widehat{\mathbf{y} - \mathbf{x}} \cdot \widehat{\mathbf{y} - \mathbf{x}} \mathbf{n} + 2\mu (\widehat{\mathbf{y} - \mathbf{x}} \otimes \widehat{\mathbf{y} - \mathbf{x}}) \mathbf{n} \right] + o\left(\frac{1}{|\mathbf{y} - \mathbf{x}|}\right) \\ &= \frac{\widehat{\mathbf{y} - \mathbf{x}} \cdot \mathbf{q}}{c_p^3} i\omega G_\omega^p(\mathbf{x}, \mathbf{y}) \left[\lambda \mathbf{n} + 2\mu (\widehat{\mathbf{y} - \mathbf{x}} \cdot \mathbf{n}) \widehat{\mathbf{y} - \mathbf{x}} \right] + o\left(\frac{1}{|\mathbf{y} - \mathbf{x}|}\right) \\ &= \frac{\widehat{\mathbf{y} - \mathbf{x}} \cdot \mathbf{q}}{c_p^3} i\omega G_\omega^p(\mathbf{x}, \mathbf{y}) \left[\lambda (\mathbf{n} - \widehat{\mathbf{y} - \mathbf{x}}) + 2\mu (\widehat{\mathbf{y} - \mathbf{x}} \cdot \mathbf{n} - 1) \widehat{\mathbf{y} - \mathbf{x}} \right] \\ &\quad + i\omega c_p \mathbb{G}_\omega^p(\mathbf{x}, \mathbf{y}) \mathbf{q} + o\left(\frac{1}{|\mathbf{y} - \mathbf{x}|}\right). \end{aligned}$$

In particular, when $\mathbf{n} = \widehat{\mathbf{y} - \mathbf{x}}$, we have

$$\frac{\partial \mathbb{G}_\omega^p(\mathbf{x}, \mathbf{y}) \mathbf{q}}{\partial \nu} = i\omega c_p \mathbb{G}_\omega^p(\mathbf{x}, \mathbf{y}) \mathbf{q} + o\left(\frac{1}{|\mathbf{y} - \mathbf{x}|}\right).$$

Shear components: As

$$\mathbb{G}_\omega^s(\mathbf{x}, \mathbf{y}) = \frac{1}{\omega^2} (\kappa_s^2 \mathbb{I} + \mathbb{D}) G_\omega^s(\mathbf{x}, \mathbf{y}) = \frac{1}{c_s^2} G_\omega^s(\mathbf{x}, \mathbf{y}) (\mathbb{I} - \widehat{\mathbf{y} - \mathbf{x}} \otimes \widehat{\mathbf{y} - \mathbf{x}}) + o\left(\frac{1}{|\mathbf{x} - \mathbf{y}|}\right),$$

we have

$$\mathbb{G}_\omega^s(\mathbf{x}, \mathbf{y}) \mathbf{q} = \frac{1}{c_s^2} G_\omega^s(\mathbf{x}, \mathbf{y}) \left(\mathbf{q} - (\widehat{\mathbf{y} - \mathbf{x}} \cdot \mathbf{q}) \widehat{\mathbf{y} - \mathbf{x}} \right) + o\left(\frac{1}{|\mathbf{x} - \mathbf{y}|}\right).$$

Therefore,

$$\frac{\partial \mathbb{G}_\omega^s(\mathbf{x}, \mathbf{y}) \mathbf{q}}{\partial \nu} = \lambda \nabla_{\mathbf{y}} \cdot (\mathbb{G}_\omega^s(\mathbf{x}, \mathbf{y}) \mathbf{q}) \mathbf{n}(\mathbf{y}) + \mu \left\{ \nabla_{\mathbf{y}} (\mathbb{G}_\omega^s(\mathbf{x}, \mathbf{y}) \mathbf{q})^T + [\nabla_{\mathbf{y}} (\mathbb{G}_\omega^s(\mathbf{x}, \mathbf{y}) \mathbf{q})^T]^T \right\} \mathbf{n}(\mathbf{y}).$$

Now, remark that

$$\begin{aligned}\lambda \nabla \cdot (\mathbb{G}_\omega^s(\mathbf{x}, \mathbf{y}) \mathbf{q}) \mathbf{n} &= \lambda \frac{i\omega}{c_s^3} G_\omega^s(\mathbf{x}, \mathbf{y}) \left\{ \left[\mathbf{q} - (\widehat{\mathbf{y}-\mathbf{x}} \cdot \mathbf{q}) \widehat{\mathbf{y}-\mathbf{x}} \right] \cdot \widehat{\mathbf{y}-\mathbf{x}} \right\} \mathbf{n} + o\left(\frac{1}{|\mathbf{x}-\mathbf{y}|}\right) \\ &= o\left(\frac{1}{|\mathbf{x}-\mathbf{y}|}\right),\end{aligned}$$

and

$$\begin{aligned}\mu \left[\nabla \mathbb{G}_\omega^s(\mathbf{x}, \mathbf{y}) \mathbf{q} + \nabla \mathbb{G}_\omega^s(\mathbf{x}, \mathbf{y}) \mathbf{q}^T \right] \mathbf{n} \\ &= \mu \frac{i\omega}{c_s^3} G_\omega^s(\mathbf{x}, \mathbf{y}) \left[\mathbf{q} \otimes \widehat{\mathbf{y}-\mathbf{x}} + \widehat{\mathbf{y}-\mathbf{x}} \otimes \mathbf{q} - 2(\widehat{\mathbf{y}-\mathbf{x}} \cdot \mathbf{q}) \widehat{\mathbf{y}-\mathbf{x}} \otimes \widehat{\mathbf{y}-\mathbf{x}} \right] \mathbf{n} + o\left(\frac{1}{|\mathbf{x}-\mathbf{y}|}\right) \\ &= \mu \frac{i\omega}{c_s^3} G_\omega^s(\mathbf{x}, \mathbf{y}) \left[(\widehat{\mathbf{y}-\mathbf{x}} \cdot \mathbf{n}) \mathbf{q} + (\mathbf{q} \cdot \mathbf{n}) \widehat{\mathbf{y}-\mathbf{x}} - 2(\widehat{\mathbf{y}-\mathbf{x}} \cdot \mathbf{q}) (\widehat{\mathbf{y}-\mathbf{x}} \cdot \mathbf{n}) \widehat{\mathbf{y}-\mathbf{x}} \right] + o\left(\frac{1}{|\mathbf{x}-\mathbf{y}|}\right) \\ &= \mu \frac{i\omega}{c_s^3} G_\omega^s(\mathbf{x}, \mathbf{y}) \left[(\widehat{\mathbf{y}-\mathbf{x}} \cdot \mathbf{n}) - 1 \right] \left[\mathbf{q} - (\widehat{\mathbf{y}-\mathbf{x}} \cdot \mathbf{q}) \widehat{\mathbf{y}-\mathbf{x}} \right] \\ &\quad + \mu \frac{i\omega}{c_s^3} G_\omega^s(\mathbf{x}, \mathbf{y}) \left[\mathbf{q} \cdot \mathbf{n} - (\widehat{\mathbf{y}-\mathbf{x}} \cdot \mathbf{q}) (\widehat{\mathbf{y}-\mathbf{x}} \cdot \mathbf{n}) \right] \widehat{\mathbf{y}-\mathbf{x}} + o\left(\frac{1}{|\mathbf{x}-\mathbf{y}|}\right).\end{aligned}$$

In particular, when $\mathbf{n} = \widehat{\mathbf{y}-\mathbf{x}}$, we have

$$\frac{\partial \mathbb{G}_\omega^s(\mathbf{x}, \mathbf{y}) \mathbf{q}}{\partial \mathbf{v}} = i\omega c_s \mathbb{G}_\omega^s(\mathbf{x}, \mathbf{y}) \mathbf{q} + o\left(\frac{1}{|\mathbf{y}-\mathbf{x}|}\right).$$

□

The following is a direct consequence of Propositions 5.2.2, 5.2.3, and 5.2.4.

PROPOSITION 5.2.5. *Let $\Omega \subset \mathbb{R}^d$ be a ball with radius R . Then, for all $\mathbf{x}, \mathbf{z} \in \Omega$ sufficiently far from the boundary $\partial\Omega$, we have*

$$\Re e \left\{ \int_{\partial\Omega} \mathbb{G}_\omega^\alpha(\mathbf{x}, \mathbf{y}) \overline{\mathbb{G}_\omega^\alpha(\mathbf{y}, \mathbf{z})} d\sigma(\mathbf{y}) \right\} \simeq \frac{1}{\omega c_\alpha} \Im m \{ \mathbb{G}_\omega^\alpha(\mathbf{x}, \mathbf{z}) \}, \quad \alpha = p, s, \quad (5.25)$$

$$\Re e \left\{ \int_{\partial\Omega} \mathbb{G}_\omega^s(\mathbf{x}, \mathbf{y}) \overline{\mathbb{G}_\omega^p(\mathbf{y}, \mathbf{z})} d\sigma(\mathbf{y}) \right\} \simeq 0. \quad (5.26)$$

5.2.1.4 ANALYSIS OF THE IMAGING FUNCTIONAL $\tilde{\mathcal{F}}$

In this subsection, we assume that Ω is a ball of radius R in \mathbb{R}^d and that the support, $\text{supp}\{\mathbf{F}\}$, of \mathbf{F} is sufficiently localized at the center of Ω so that for all $\mathbf{x} \in \text{supp}\{\mathbf{F}\}$ and for all $\mathbf{y} \in \partial\Omega$

$$\widehat{\mathbf{y}-\mathbf{x}} = \mathbf{n}(\mathbf{y}) + o\left(\frac{1}{|\mathbf{y}-\mathbf{x}|}\right).$$

Then, we have the following theorem.

THEOREM 5.2.6. *Let $\mathbf{x} \in \Omega$ be sufficiently far from the boundary $\partial\Omega$ and $\tilde{\mathcal{F}}$ be defined by (5.7). Then,*

$$\tilde{\mathcal{F}}(\mathbf{x}) \simeq \mathbf{F}(\mathbf{x}). \quad (5.27)$$

Proof. From (5.18) we have

$$\tilde{\mathcal{F}}(\mathbf{x}) = \frac{1}{4\pi} \int_{\mathbb{R}^d} \int_{\mathbb{R}} \omega^2 \left[\int_{\partial\Omega} \tilde{\mathbb{G}}_\omega(\mathbf{x}, \mathbf{y}) \bar{\mathbb{G}}_\omega(\mathbf{y}, \mathbf{z}) + \bar{\tilde{\mathbb{G}}}_\omega(\mathbf{x}, \mathbf{y}) \mathbb{G}_\omega(\mathbf{y}, \mathbf{z}) d\sigma(\mathbf{y}) \right] d\omega \mathbf{F}(\mathbf{z}) d\mathbf{z},$$

where

$$\tilde{\mathbb{G}}_\omega(\mathbf{x}, \mathbf{y}) = c_s \mathbb{G}_\omega^s(\mathbf{x}, \mathbf{y}) + c_p \mathbb{G}_\omega^p(\mathbf{x}, \mathbf{y}).$$

Proposition 5.2.5 allows us to write

$$\begin{aligned} \tilde{\mathcal{F}}(\mathbf{x}) &\simeq \frac{1}{4\pi} \int_{\mathbb{R}^d} \int_{\mathbb{R}} \omega^2 \left[\int_{\partial\Omega} \tilde{\mathbb{G}}_\omega(\mathbf{x}, \mathbf{y}) \bar{\mathbb{G}}_\omega(\mathbf{y}, \mathbf{z}) + \bar{\tilde{\mathbb{G}}}_\omega(\mathbf{x}, \mathbf{y}) \tilde{\mathbb{G}}_\omega(\mathbf{y}, \mathbf{z}) d\sigma(\mathbf{y}) \right] d\omega \mathbf{F}(\mathbf{z}) d\mathbf{z} \\ &\simeq \frac{1}{4\pi} \int_{\mathbb{R}^d} \int_{\mathbb{R}} \omega^2 \left[\int_{\partial\Omega} \tilde{\mathbb{G}}_\omega(\mathbf{x}, \mathbf{y}) \bar{\mathbb{G}}_\omega(\mathbf{y}, \mathbf{z}) + \mathbb{G}_\omega(\mathbf{x}, \mathbf{y}) \bar{\tilde{\mathbb{G}}}_\omega(\mathbf{y}, \mathbf{z}) d\sigma(\mathbf{y}) \right] d\omega \mathbf{F}(\mathbf{z}) d\mathbf{z}. \end{aligned}$$

Proposition 5.2.4 then gives

$$\begin{aligned} \tilde{\mathcal{F}}(\mathbf{x}) &\simeq \frac{1}{4\pi} \int_{\mathbb{R}^d} \int_{\mathbb{R}} -i\omega \left[\frac{\partial \mathbb{G}_\omega(\mathbf{x}, \mathbf{y})}{\partial \nu} \bar{\mathbb{G}}_\omega(\mathbf{y}, \mathbf{z}) - \mathbb{G}_\omega(\mathbf{x}, \mathbf{y}) \frac{\partial \bar{\tilde{\mathbb{G}}}_\omega(\mathbf{y}, \mathbf{z})}{\partial \nu} \right] d\omega \mathbf{F}(\mathbf{z}) d\mathbf{z} \\ &\simeq \frac{1}{2\pi} \int_{\mathbb{R}^d} \int_{\mathbb{R}} \omega \Im m \{ \mathbb{G}_\omega(\mathbf{x}, \mathbf{z}) \} d\omega \mathbf{F}(\mathbf{z}) d\mathbf{z} \\ &\simeq \mathbf{F}(\mathbf{x}). \end{aligned}$$

The last approximation results from the identity

$$\frac{1}{2\pi} \int_{\mathbb{R}} -i\omega \mathbb{G}_\omega(\mathbf{x}, \mathbf{z}) d\omega = \delta_{\mathbf{x}}(\mathbf{z}) \mathbb{1},$$

which comes from the integration of the time-dependent version of (5.9) between $t = 0^-$ and $t = 0^+$. \square

If the unweighted time-reversal imaging function \mathcal{I} is used instead of $\tilde{\mathcal{F}}$, then crossed terms remain. Indeed, by using the same arguments as above, we find

$$\begin{aligned} \mathcal{I}(\mathbf{x}) &\simeq \frac{c_s + c_p}{c_s c_p} \frac{1}{4\pi} \int_{\mathbb{R}^d} \int_{\mathbb{R}} \omega \Im m \{ (\mathbb{G}_\omega^p + \mathbb{G}_\omega^s)(\mathbf{x}, \mathbf{z}) \} d\omega \mathbf{F}(\mathbf{z}) d\mathbf{z} \\ &\quad + \frac{c_s - c_p}{c_s c_p} \frac{1}{4\pi} \int_{\mathbb{R}^d} \int_{\mathbb{R}} \omega \Im m \{ (\mathbb{G}_\omega^p - \mathbb{G}_\omega^s)(\mathbf{x}, \mathbf{z}) \} d\omega \mathbf{F}(\mathbf{z}) d\mathbf{z} \\ &\simeq \frac{c_s + c_p}{2c_s c_p} \mathbf{F}(\mathbf{x}) + \frac{c_s - c_p}{2c_s c_p} \int_{\mathbb{R}^d} \mathbb{B}(\mathbf{x}, \mathbf{z}) \mathbf{F}(\mathbf{z}) d\mathbf{z}. \end{aligned} \quad (5.28)$$

Here

$$\mathbb{B}(\mathbf{x}, \mathbf{z}) = \frac{1}{2\pi} \int_{\mathbb{R}} \omega \Im m \left\{ (\mathbb{G}_{\omega}^p - \mathbb{G}_{\omega}^s)(\mathbf{x}, \mathbf{z}) \right\} d\omega \quad (5.29)$$

is the operator that describes the error in the reconstruction of the source \mathbf{F} obtained with \mathcal{S} when $c_s \neq c_p$. In particular the operator \mathbb{B} is not diagonal, which means that the reconstruction mixes the components of \mathbf{F} .

5.2.2 NUMERICAL SIMULATIONS

In this subsection, we present numerical illustrations and describe our algorithms for numerical resolution of the source problem to show that $\tilde{\mathcal{S}}$ provides a better reconstruction than \mathcal{S} .

5.2.2.1 DESCRIPTION OF THE ALGORITHM

This subsection is devoted to the algorithm we used for the numerical resolution of the elastic wave equation in 2D:

$$\begin{cases} \frac{\partial^2 \mathbf{u}}{\partial t^2}(\mathbf{x}, t) = [\mu \Delta \mathbf{u} + (\lambda + \mu) \nabla(\nabla \cdot \mathbf{u})](\mathbf{x}, t), & (\mathbf{x}, t) \in \mathbb{R}^2 \times \mathbb{R}, \\ \mathbf{u}(\mathbf{x}, 0) = \mathbf{F}(\mathbf{x}) \quad \text{and} \quad \frac{\partial \mathbf{u}}{\partial t}(\mathbf{x}, 0) = \mathbf{0}. \end{cases} \quad (5.30)$$

This equation is computed on the box $Q = [-L/2, L/2]^2$ such that $\Omega \subset Q$ with periodic boundary conditions. We use a *splitting spectral Fourier* approach [43] coupled with a perfectly matched layer (PML) technique [75] to simulate a free outgoing interface on ∂Q .

With the notation $\mathbf{u} = (u_1, u_2)$ and $\mathbf{x} = (x_1, x_2)$, the elastic wave equation can be rewritten as a first order partial differential equation:

$$\partial_t P = AP + BP,$$

where

$$P = \begin{pmatrix} u_1 \\ \partial_t u_1 \\ u_2 \\ \partial_t u_2 \end{pmatrix}, \quad A = \begin{pmatrix} 0 & 1 & 0 & 0 \\ (\lambda + 2\mu)\partial_{x_1}^2 + \mu\partial_{x_2}^2 & 0 & 0 & 0 \\ 0 & 0 & 0 & 1 \\ 0 & 0 & (\lambda + 2\mu)\partial_{x_2}^2 + \mu\partial_{x_1}^2 & 0 \end{pmatrix},$$

and

$$B = \begin{pmatrix} 0 & 0 & 0 & 0 \\ 0 & 0 & (\lambda + \mu)\partial_{x_1}\partial_{x_2} & 0 \\ 0 & 0 & 0 & 0 \\ (\lambda + \mu)\partial_{x_1}\partial_{x_2} & 0 & 0 & 0 \end{pmatrix}.$$

This equation is integrated via *Strang's splitting method* [123]. This splitting approach is known to be of order 2 and reads

$$\exp\{-t(A+B)\} = \exp\left\{-\frac{t}{2}B\right\} \exp\{-tA\} \exp\left\{-\frac{t}{2}B\right\} + o(t^2).$$

The first operator A is then computed exactly in the spatial Fourier space. Indeed, the Fourier transform of $P_A(\mathbf{x}, t) = \exp\{-At\}P(\mathbf{x})$ satisfies

$$\begin{cases} \widehat{u_{A,1}}(\boldsymbol{\xi}, t) &= \cos\left(\sqrt{\xi_{\lambda,\mu,1}^2} t\right) \widehat{u_1}(\boldsymbol{\xi}) + t \operatorname{sinc}\left(\sqrt{\xi_{\lambda,\mu,1}^2} t\right) \widehat{\partial_t u_1}(\boldsymbol{\xi}), \\ \widehat{\partial_t u_{A,1}}(\boldsymbol{\xi}, t) &= \cos\left(\sqrt{\xi_{\lambda,\mu,1}^2} t\right) \widehat{\partial_t u_1}(\boldsymbol{\xi}) - \sqrt{\xi_{\lambda,\mu,1}^2} \sin\left(\sqrt{\xi_{\lambda,\mu,1}^2} t\right) \widehat{u_1}(\boldsymbol{\xi}), \\ \widehat{u_{A,2}}(\boldsymbol{\xi}, t) &= \cos\left(\sqrt{\xi_{\lambda,\mu,2}^2} t\right) \widehat{u_2}(\boldsymbol{\xi}) + t \operatorname{sinc}\left(\sqrt{\xi_{\lambda,\mu,2}^2} t\right) \widehat{\partial_t u_2}(\boldsymbol{\xi}), \\ \widehat{\partial_t u_{A,2}}(\boldsymbol{\xi}, t) &= \cos\left(\sqrt{\xi_{\lambda,\mu,2}^2} t\right) \widehat{\partial_t u_2}(\boldsymbol{\xi}) - \sqrt{\xi_{\lambda,\mu,2}^2} \sin\left(\sqrt{\xi_{\lambda,\mu,2}^2} t\right) \widehat{u_2}(\boldsymbol{\xi}), \end{cases}$$

with

$$\xi_{\lambda,\mu,1}^2 = 4\pi^2(\lambda + 2\mu)\xi_1^2 + \mu\xi_2^2, \quad \xi_{\lambda,\mu,2}^2 = 4\pi^2(\lambda + 2\mu)\xi_2^2 + \mu\xi_1^2, \quad \text{and} \quad \operatorname{sinc}(t) = \frac{\sin(t)}{t}.$$

The second operator B is also integrated exactly. We have

$$P_B(\mathbf{x}, t) = \exp(-Bt)P(\mathbf{x}) = \begin{pmatrix} u_1(\mathbf{x}) \\ \partial_t u_1(\mathbf{x}) - t(\lambda + \mu)\partial_{x_1}\partial_{x_2}u_2(\mathbf{x}) \\ u_2(\mathbf{x}) \\ \partial_t u_2(\mathbf{x}) - t(\lambda + \mu)\partial_{x_1}\partial_{x_2}u_1(\mathbf{x}) \end{pmatrix}.$$

This global algorithm appears to be stable under a classical condition of the form

$$\delta_t \leq c(\lambda, \mu)\delta_x^2,$$

where δ_t and δ_x denote respectively the time and the spatial step of discretization. Here $c(\lambda, \mu)$ is a constant which depends only on Lamé coefficients λ and μ .

The functional $\tilde{\mathcal{F}}(\mathbf{x})$ requires also a Helmholtz decomposition algorithm. As the support of the function $\tilde{\mathcal{F}}(\mathbf{x})$ is included in $\Omega \subset Q$, we apply a Dirichlet boundary condition on ∂Q . This decomposition is numerically obtained with a fast algorithm (see [144]) based on a symmetry principle and a Fourier Helmholtz decomposition algorithm.

5.2.2.2 EXPERIMENTS

In the sequel, for numerical illustrations, Ω is taken as a unit disk centred at origin. Its boundary is discretized by 1024 sensors. Each solution of elastic wave equation is computed over $(\mathbf{x}, t) \in [-L/2, L/2]^2 \times [0, T]$ with $L = 4$ and $T = 2$. We use a step of discretization given by $dt = T/2^{13}$ and $dx = L/2^9$.

Figure 5.1 presents an experiment with Lamé parameters $(\lambda, \mu) = (1, 1)$. The first line corresponds to the 2 components of initial source \mathbf{F} . The second line corresponds to the data $\mathbf{g}(\mathbf{y}, t) = \mathbf{u}(\mathbf{y}, t)$ recorded over $(\mathbf{y}, t) \in \partial\Omega \times [0, T]$. Note that the shear and pressure waves are coupled in the recorded signal and it seems difficult to separate them. The third line corresponds to the imaging functional $\mathcal{I}(\mathbf{x})$. This example clearly shows that the reconstruction of the source \mathbf{F} is not so accurate with classical time-reversal imaging. However, illustrations presented in the last row, which correspond to the modified imaging functional $\tilde{\mathcal{I}}(\mathbf{x})$, present a much better (nearly optimal) reconstruction.

Figure 5.2 shows another example with different Lamé parameters $(\lambda, \mu) = (10, 1)$. The same conclusion holds.

In Figure 5.3, we use a *less localized* (large) source distribution. We observe some artefacts in the reconstruction of the imaging functional $\tilde{\mathcal{I}}$. We can also observe, from the recorded data, that the pressure and shear waves are very much *mixed* with each other. We expect that the artefacts in the reconstruction are the consequence of such coupling. In this situation, we do not have a real orthogonality between the two waves on $\partial\Omega$!

To conclude, $\tilde{\mathcal{I}}$ provides a better reconstruction of the sources than \mathcal{I} . However, in certain cases, the reconstructions by $\tilde{\mathcal{I}}$ are not optimal and need further improvements.

5.3 TIME-REVERSAL ALGORITHM FOR A VISCOELASTIC MEDIUM

In this section, we investigate the inverse source problem in viscoelastic media. We provide an efficient regularized time-reversal imaging algorithm which corrects the attenuation effect.

Consider the viscoelastic wave equation in an open medium $\Omega \in \mathbb{R}^d$ with $d = 2, 3$, that is,

$$\begin{cases} \left(\frac{\partial^2}{\partial t^2} - \mathcal{L}_{\lambda, \mu} - \frac{\partial}{\partial t} \mathcal{L}_{\eta_\lambda, \eta_\mu} \right) \mathbf{u}_a(\mathbf{x}, t) = \frac{d\delta_0(t)}{dt} \mathbf{F}(\mathbf{x}), & \mathbf{x} \in \mathbb{R}^d, t \in \mathbb{R}, \\ \mathbf{u}_a(\mathbf{x}, t) = \frac{\partial \mathbf{u}_a}{\partial t}(\mathbf{x}, t) = \mathbf{0}, & \mathbf{x} \in \mathbb{R}^d, t < 0, \end{cases} \quad (5.31)$$

where the viscosity parameters η_μ and η_λ are positive constants and account for losses in the medium.

Analogous to the acoustic case studied in Chapter 2, the strategy of time reversal is to consider the functional

$$\mathcal{I}_a(\mathbf{x}) = \int_0^T \mathbf{v}_{s,a}(\mathbf{x}, T) ds, \quad (5.32)$$

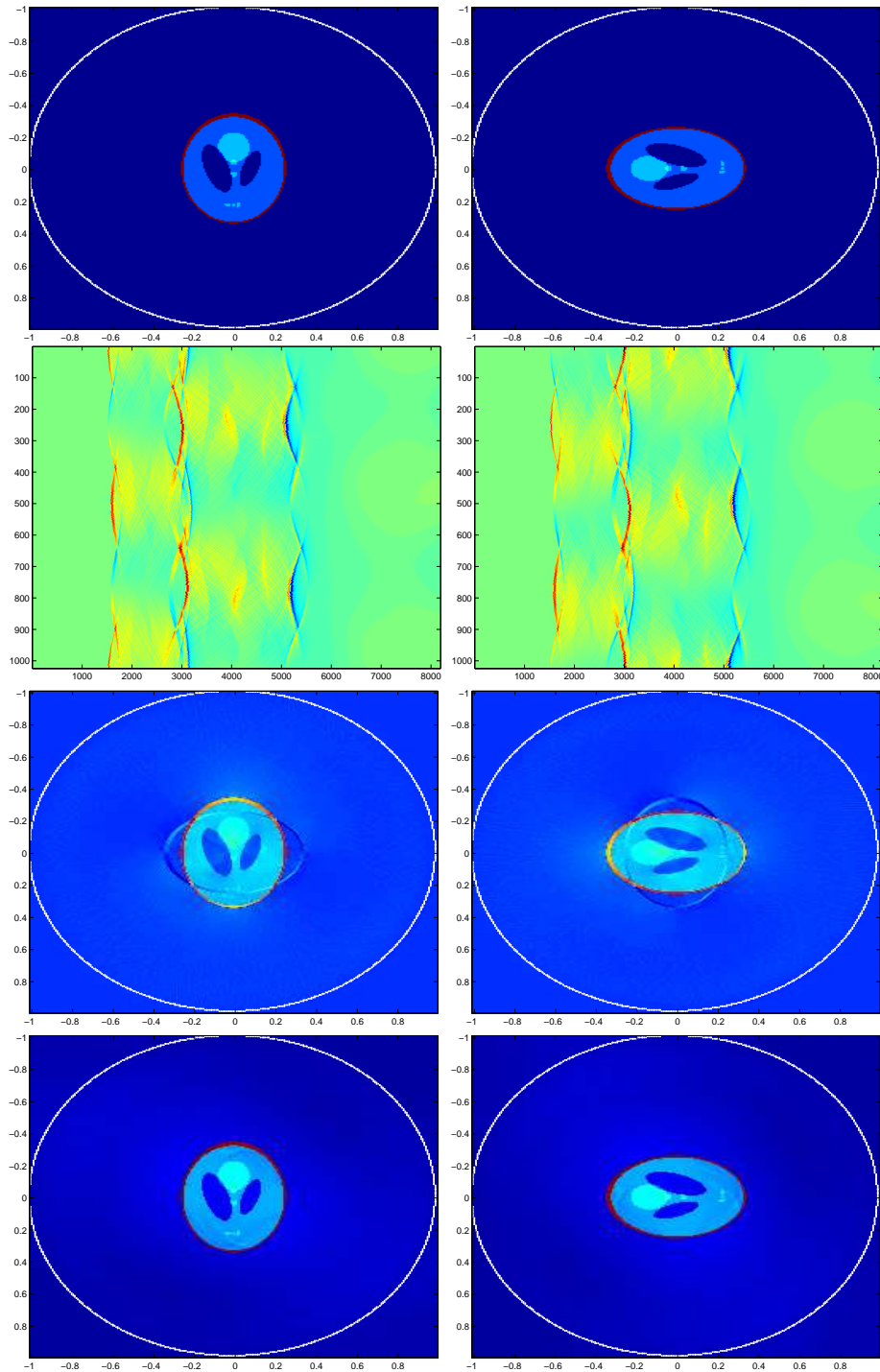


FIGURE 5.1. Source reconstruction; Comparison between the imaging functionals \mathcal{I} and $\tilde{\mathcal{I}}$ with Lamé coefficients $(\lambda, \mu) = (1, 1)$. First line: the source \mathbf{F} ; Second line: recorded data $\mathbf{g}(\mathbf{y}, t)$; Third line: imaging functional \mathcal{I} ; Last line: imaging functional $\tilde{\mathcal{I}}$.

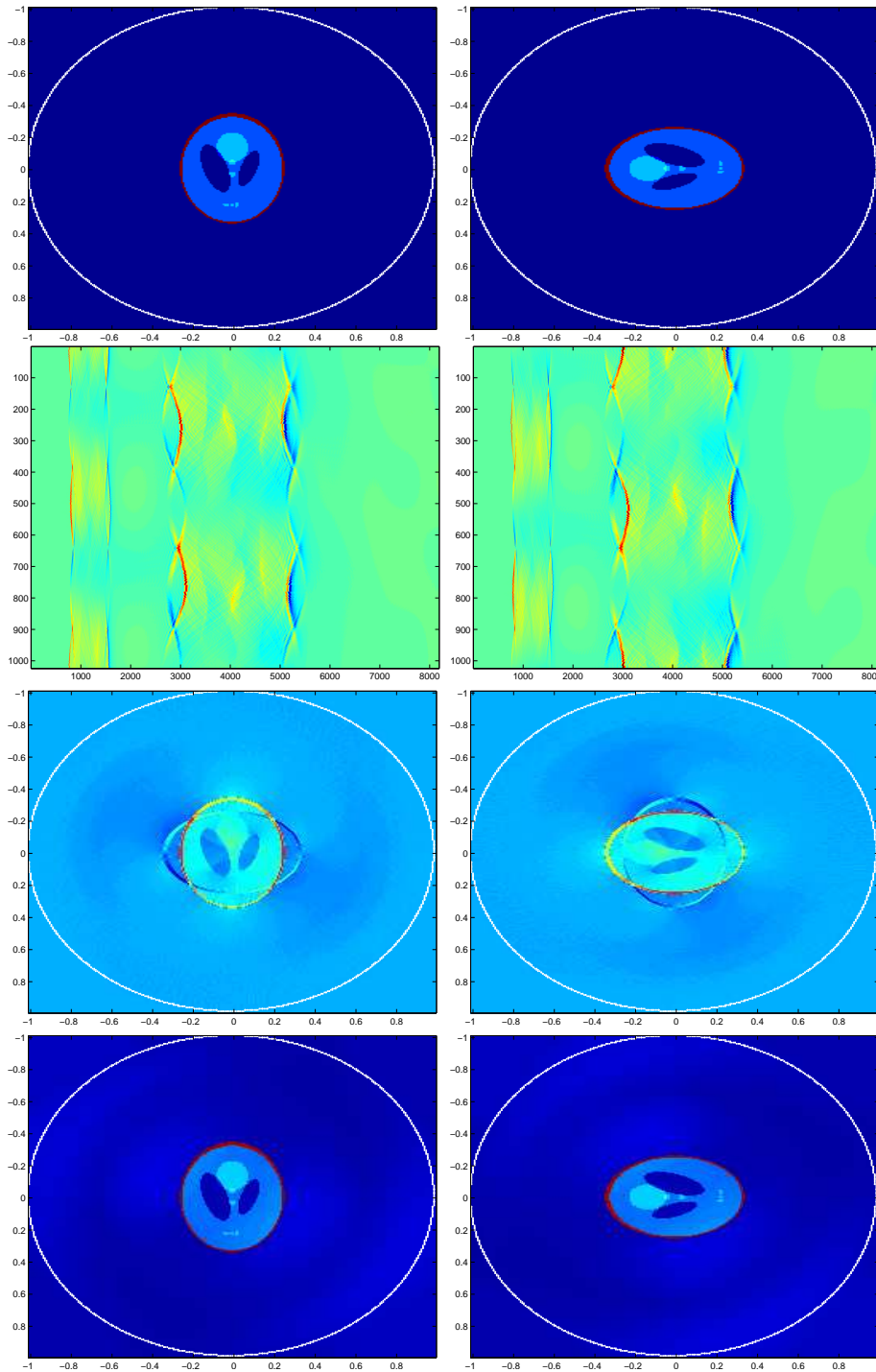


FIGURE 5.2. Source reconstruction; Comparison between the imaging functionals \mathcal{I} and $\tilde{\mathcal{I}}$ with Lamé constants $(\lambda, \mu) = (10, 1)$; First line: the source \mathbf{F} ; Second line: recorded data $\mathbf{g}(\mathbf{y}, t)$; Third line: imaging functional \mathcal{I} ; Last line: imaging functional $\tilde{\mathcal{I}}$.

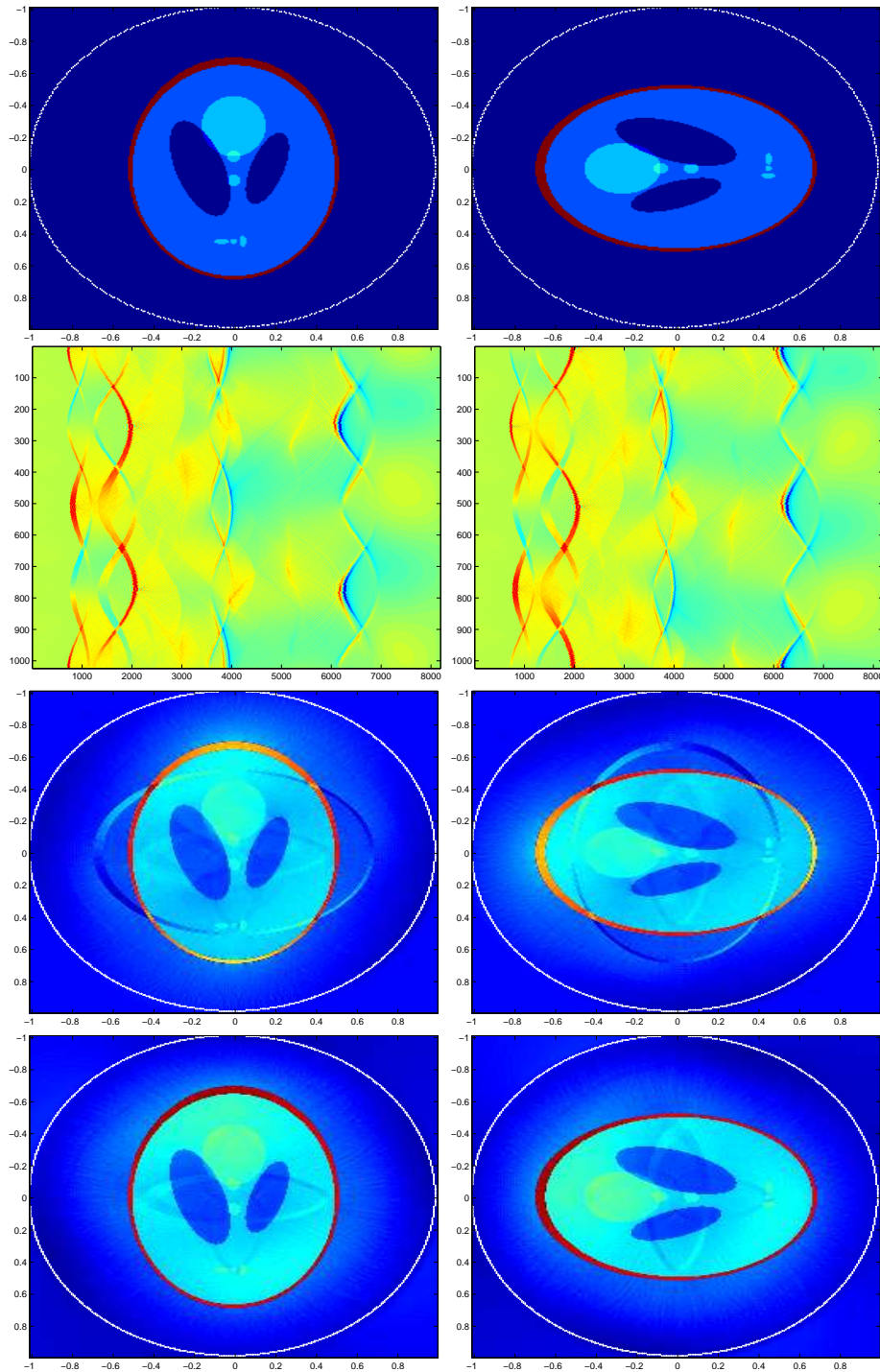


FIGURE 5.3. Source reconstruction; Comparison between the imaging functionals \mathcal{I} and $\tilde{\mathcal{I}}$ with Lamé coefficients $(\lambda, \mu) = (1, 1)$ and a less localized source than that in Figure 5.1; First line: the source \mathbf{F} ; Second line: imaging functional \mathcal{I} ; Last line: imaging functional $\tilde{\mathcal{I}}$.

where $\mathbf{v}_{s,a}$ should be the *solution* of the adjoint (time-reverted) viscoelastic wave equation, that is,

$$\begin{cases} \left(\frac{\partial^2}{\partial t^2} - \mathcal{L}_{\lambda,\mu} + \frac{\partial}{\partial t} \mathcal{L}_{\eta_\lambda,\eta_\mu} \right) \mathbf{v}_{s,a}(\mathbf{x}, t) = \frac{d\delta_s(t)}{dt} \mathbf{g}_a(\mathbf{x}, T-s) \delta_{\partial\Omega}(\mathbf{x}), & \mathbf{x} \in \mathbb{R}^d, t \in \mathbb{R}, \\ \mathbf{v}_s(\mathbf{x}, t) = \frac{\partial \mathbf{v}_s}{\partial t}(\mathbf{x}, t) = \mathbf{0}, & \mathbf{x} \in \mathbb{R}^d, t < s. \end{cases} \quad (5.33)$$

Further, the idea is to enhance image resolution using $\tilde{\mathcal{I}}_a$, as in purely elastic media, where

$$\tilde{\mathcal{I}}_a = c_s \mathcal{H}^s[\mathcal{I}_a] + c_p \mathcal{H}^p[\mathcal{I}_a].$$

Unfortunately, the adjoint viscoelastic problem (5.33) is severely ill-posed. Indeed, the frequency component is exponentially increasing due to the presence of the *anti-damping* term ($+\partial_t \mathcal{L}_{\eta_\lambda,\eta_\mu} \mathbf{v}_{s,a}$), which induces instability. Therefore, we need to regularize the adjoint problem by suppressing high-frequency components either in time or in space.

Let us introduce the outgoing Green tensor $\mathbb{G}_{a,\omega}$ associated to the viscoelastic wave equation

$$(\mathcal{L}_{\lambda,\mu} - i\omega \mathcal{L}_{\eta_\lambda,\eta_\mu} + \omega^2) \mathbb{G}_{a,\omega}(\mathbf{x}, \mathbf{y}) = -\delta_{\mathbf{y}}(\mathbf{x}), \quad \mathbf{x}, \mathbf{y} \in \mathbb{R}^d, \quad (5.34)$$

and let $\mathbb{G}_{-a,\omega}$ be the *adjoint* viscoelastic Green tensor, that is, the solution to

$$(\mathcal{L}_{\lambda,\mu} + i\omega \mathcal{L}_{\eta_\lambda,\eta_\mu} + \omega^2) \mathbb{G}_{-a,\omega}(\mathbf{x}, \mathbf{y}) = -\delta_{\mathbf{y}}(\mathbf{x}), \quad \mathbf{x}, \mathbf{y} \in \mathbb{R}^d. \quad (5.35)$$

We introduce an approximation $\mathbf{v}_{s,a,\rho}$ of the adjoint wave $\mathbf{v}_{s,a}$ by

$$\mathbf{v}_{s,a,\rho}(\mathbf{x}, t) = -\frac{1}{2\pi} \int_{|\omega| \leq \rho} \left\{ \int_{\partial\Omega} i\omega \mathbb{G}_{-a,\omega}(\mathbf{x}, \mathbf{y}) \mathbf{g}_a(\mathbf{y}, T-s) d\sigma(\mathbf{y}) \right\} \exp\{-i\omega(t-s)\} d\omega, \quad (5.36)$$

where $\rho \in \mathbb{R}^+$ is the cut-off parameter. The regularized time-reversal imaging functional defined by

$$\mathcal{I}_{a,\rho}(\mathbf{x}) = \int_0^T \mathbf{v}_{s,a,\rho}(\mathbf{x}, T) ds, \quad (5.37)$$

can be written as

$$\mathcal{I}_{a,\rho}(\mathbf{x}) = \int_{\partial\Omega} \int_0^T \frac{\partial}{\partial t} \mathbb{G}_{-a,\rho}(\mathbf{x}, \mathbf{y}, T-s) \mathbf{g}_a(\mathbf{y}, T-s) ds d\sigma(\mathbf{y}), \quad (5.38)$$

where

$$\mathbb{G}_{-a,\rho}(\mathbf{x}, \mathbf{y}, t) = \frac{1}{2\pi} \int_{|\omega| \leq \rho} \mathbb{G}_{-a,\omega}(\mathbf{x}, \mathbf{y}) \exp\{-i\omega t\} d\omega. \quad (5.39)$$

REMARK 5.3.1. Let \mathcal{S}' be the space of tempered distributions, i.e., the dual of the Schwartz space \mathcal{S} of rapidly decreasing functions [78]. The function $\mathbf{v}_{s,a,\rho}(\mathbf{x}, t)$ can be identified as the solution of the following wave equation:

$$\left(\frac{\partial^2}{\partial t^2} - \mathcal{L}_{\lambda,\mu} + \frac{\partial}{\partial t} \mathcal{L}_{\eta_\lambda,\eta_\mu} \right) \mathbf{v}_{s,a,\rho}(\mathbf{x}, t) = S_\rho \left[\frac{d\delta_s(t)}{dt} \right] \mathbf{g}_a(\mathbf{x}, T-s) \delta_{\partial\Omega}(\mathbf{x}), \quad (5.40)$$

where the operator S_ρ is defined on the space \mathcal{S}' by

$$S_\rho [\psi] (t) = \frac{1}{2\pi} \int_{|\omega| \leq \rho} \exp \{ -i\omega t \} \widehat{\psi}(\omega) d\omega, \quad (5.41)$$

with

$$\widehat{\psi}(\omega) = \int_{\mathbb{R}} \psi(t) \exp \{ i\omega t \} dt. \quad (5.42)$$

5.3.1 GREEN TENSOR IN VISCOELASTIC MEDIA

As in Section 5.2, we decompose $\mathbb{G}_{\pm a, \omega}$ in the form

$$\mathbb{G}_{\pm a, \omega} = \mathbb{G}_{\pm a, \omega}^s + \mathbb{G}_{\pm a, \omega}^p, \quad (5.43)$$

where $\mathbb{G}_{\pm a, \omega}^s$ and $\mathbb{G}_{\pm a, \omega}^p$ are respectively the fundamental solutions of

$$(\mathcal{L}_{\lambda, \mu} \mp i\omega \mathcal{L}_{\eta_\lambda, \eta_\mu} + \omega^2) \mathbb{G}_{\pm a, \omega}^\alpha (\mathbf{x}, \mathbf{y}) = \mathcal{H}^\alpha [-\delta_{\mathbf{y}\mathbb{I}}], \quad \alpha = p, s. \quad (5.44)$$

Let us also introduce the decomposition of the operator $\mathcal{L}_{\lambda, \mu}$ into shear and pressure components as

$$\mathcal{L}_{\lambda, \mu} = \mathcal{L}_{\lambda, \mu}^s + \mathcal{L}_{\lambda, \mu}^p, \quad \text{and} \quad \mathcal{L}_{\eta_\lambda, \eta_\mu} = \mathcal{L}_{\eta_\lambda, \eta_\mu}^s + \mathcal{L}_{\eta_\lambda, \eta_\mu}^p, \quad (5.45)$$

where

$$\mathcal{L}_{\lambda, \mu}^s \mathbf{u} = c_s^2 [\Delta \mathbf{u} - \nabla (\nabla \cdot \mathbf{u})] \quad \text{and} \quad \mathcal{L}_{\lambda, \mu}^p \mathbf{u} = c_p^2 \nabla (\nabla \cdot \mathbf{u}), \quad (5.46)$$

and

$$\mathcal{L}_{\eta_\lambda, \eta_\mu}^s \mathbf{u} = v_s^2 [\Delta \mathbf{u} - \nabla (\nabla \cdot \mathbf{u})] \quad \text{and} \quad \mathcal{L}_{\eta_\lambda, \eta_\mu}^p \mathbf{u} = v_p^2 \nabla (\nabla \cdot \mathbf{u}). \quad (5.47)$$

Here, $v_s^2 = \eta_\mu$ and $v_p^2 = \eta_\lambda + 2\eta_\mu$. Therefore, the tensors $\mathbb{G}_{\pm a, \omega}^s$ and $\mathbb{G}_{\pm a, \omega}^p$ can also be seen as the solutions of

$$(\mathcal{L}_{\lambda, \mu}^\alpha \mp i\omega \mathcal{L}_{\eta_\lambda, \eta_\mu}^\alpha + \omega^2) \mathbb{G}_{\pm a, \omega}^\alpha (\mathbf{x}, \mathbf{y}) = \mathcal{H}^\alpha [-\delta_{\mathbf{y}\mathbb{I}}] (\mathbf{x}), \quad \alpha = p, s. \quad (5.48)$$

The corrected regularized time-reversal imaging functional defined by

$$\tilde{\mathcal{I}}_{a, \rho} = c_s \mathcal{H}^s [\mathcal{I}_{a, \rho}] + c_p \mathcal{H}^p [\mathcal{I}_{a, \rho}], \quad (5.49)$$

is then given by

$$\tilde{\mathcal{I}}_{a, \rho} (\mathbf{x}) = \int_{\partial\Omega} \int_0^T \frac{\partial}{\partial t} \left[c_p \mathbb{G}_{-a, \rho}^p (\mathbf{x}, \mathbf{y}, T-s) + c_s \mathbb{G}_{-a, \rho}^s (\mathbf{x}, \mathbf{y}, T-s) \right] \mathbf{g}_a (\mathbf{y}, T-s) ds d\sigma (\mathbf{y}), \quad (5.50)$$

where

$$\mathbb{G}_{-a, \rho}^\alpha (\mathbf{x}, \mathbf{y}, t) = \frac{1}{2\pi} \int_{|\omega| \leq \rho} \mathbb{G}_{-a, \omega}^\alpha (\mathbf{x}, \mathbf{y}) \exp \{ -i\omega t \} d\omega, \quad \alpha = p, s. \quad (5.51)$$

In the next subsection we express the relationship between the data \mathbf{g}_a and the ideal measurements \mathbf{g} obtained in the non-attenuated case. By doing so, we prove with the help of a new Helmholtz-Kirchhoff identity that a regularized image of the source \mathbf{F} can be obtained.

5.3.2 ATTENUATION OPERATOR AND ITS ASYMPTOTICS

Recall that \mathbf{u} and \mathbf{u}_a are respectively the solutions of the wave equations

$$\frac{\partial^2 \mathbf{u}}{\partial t^2}(\mathbf{x}, t) - \mathcal{L}_{\lambda, \mu} \mathbf{u}(\mathbf{x}, t) = \frac{d\delta_0(t)}{dt} \mathbf{F}(\mathbf{x}), \quad (5.52)$$

and

$$\frac{\partial^2 \mathbf{u}_a}{\partial t^2}(\mathbf{x}, t) - \mathcal{L}_{\lambda, \mu} \mathbf{u}_a(\mathbf{x}, t) - \frac{\partial}{\partial t} \mathcal{L}_{\eta, \lambda, \eta, \mu} \mathbf{u}_a(\mathbf{x}, t) = \frac{d\delta_0(t)}{dt} \mathbf{F}(\mathbf{x}), \quad (5.53)$$

with the initial conditions

$$\mathbf{u}(\mathbf{x}, t) = \mathbf{u}_a(\mathbf{x}, t) = \mathbf{0}, \quad \frac{\partial \mathbf{u}}{\partial t}(\mathbf{x}, t) = \frac{\partial \mathbf{u}_a}{\partial t}(\mathbf{x}, t) = \mathbf{0}, \quad t \ll 0. \quad (5.54)$$

We decompose \mathbf{u} and \mathbf{u}_a as

$$\begin{cases} \mathbf{u} = \mathbf{u}^s + \mathbf{u}^p = \mathcal{H}^s[\mathbf{u}] + \mathcal{H}^p[\mathbf{u}] \\ \mathbf{u}_a = \mathbf{u}_a^s + \mathbf{u}_a^p = \mathcal{H}^s[\mathbf{u}_a] + \mathcal{H}^p[\mathbf{u}_a]. \end{cases} \quad (5.55)$$

The Fourier transforms \mathbf{u}_ω^α and $\mathbf{u}_{a,\omega}^\alpha$ of the vector functions \mathbf{u}^α and \mathbf{u}_a^α are respectively solutions of

$$\left(\omega^2 + \mathcal{L}_{\lambda, \mu}^\alpha\right) \mathbf{u}_\omega^\alpha = i\omega \mathcal{H}^\alpha[\mathbf{F}] \quad \text{and} \quad \left(\kappa^\alpha(\omega)^2 + \mathcal{L}_{\lambda, \mu}^\alpha\right) \mathbf{u}_{a,\omega}^\alpha = i \frac{\kappa^\alpha(\omega)^2}{\omega} \mathcal{H}^\alpha[\mathbf{F}], \quad (5.56)$$

where

$$\kappa^\alpha(\omega) = \frac{\omega}{\sqrt{1 - i\omega v_a^2 / c_a^2}}, \quad \alpha = p, s. \quad (5.57)$$

In particular, it implies that

$$\mathbf{u}_a^s = \mathcal{A}_{v_s^2/c_s^2}[\mathbf{u}^s] \quad \text{and} \quad \mathbf{u}_a^p = \mathcal{A}_{v_p^2/c_p^2}[\mathbf{u}^p], \quad (5.58)$$

where \mathcal{A}_a , for $a > 0$, is the attenuation operator

$$\mathcal{A}_a[\phi](t) = \frac{1}{2\pi} \int_{\mathbb{R}} \frac{\kappa_a(\omega)}{\omega} \left\{ \int_{\mathbb{R}} \phi(s) \exp\{i\kappa_a(\omega)s\} ds \right\} \exp\{-i\omega t\} d\omega, \quad (5.59)$$

with $\kappa_a(\omega) = \frac{\omega}{\sqrt{1 - i\omega a}}$.

We also define the operator $\mathcal{A}_{-a,\rho}$ by

$$\mathcal{A}_{-a,\rho}[\phi](t) = \frac{1}{2\pi} \int_{\mathbb{R}^+} \phi(s) \left\{ \int_{|\omega| \leq \rho} \frac{\kappa_{-a}(\omega)}{\omega} \exp\{i\kappa_{-a}(\omega)s\} \exp\{-i\omega t\} d\omega \right\} ds, \quad (5.60)$$

which is associated with $\kappa_{-a}(\omega) = \frac{\omega}{\sqrt{1 + i\omega a}}$. Moreover, its adjoint operator $\mathcal{A}_{-a,\rho}^*$ reads

$$\mathcal{A}_{-a,\rho}^*[\phi](t) = \frac{1}{2\pi} \int_{|\omega| \leq \rho} \frac{\kappa_{-a}(\omega)}{\omega} \exp\{i\kappa_{-a}(\omega)t\} \left\{ \int_{\mathbb{R}^+} \phi(s) \exp\{-i\omega s\} ds \right\} d\omega. \quad (5.61)$$

Then, we have following results from Chapters 1 and 2.

PROPOSITION 5.3.2.

- Let $\phi(t) \in \mathcal{S}([0, \infty))$, \mathcal{S} being the Schwartz space. Then

$$\mathcal{A}_a[\phi](t) = \phi(t) + \frac{a}{2}(t\phi)'(t) + o(a) \quad \text{as } a \rightarrow 0. \quad (5.62)$$

- Let $\phi(t) \in \mathcal{D}([0, \infty))$, where $\mathcal{D}([0, \infty))$ is the space of \mathcal{C}^∞ -functions of compact support on $[0, \infty)$. Then, for all ρ ,

$$\mathcal{A}_{-a,\rho}^*[\phi](t) = S_\rho[\phi](t) - \frac{a}{2}S_\rho[(t\phi)'](t) + o(a) \quad \text{as } a \rightarrow 0. \quad (5.63)$$

- Let $\phi(t) \in \mathcal{D}([0, \infty))$. Then, for all ρ ,

$$\mathcal{A}_{-a,\rho}^*\mathcal{A}_a[\phi](t) = S_\rho[\phi](t) + o(a) \quad \text{as } a \rightarrow 0. \quad (5.64)$$

We extend the operators \mathcal{A}_a , $\mathcal{A}_{-a,\rho}$ and $\mathcal{A}_{-a,\rho}^*$ to tensors \mathbb{G} , that is, for all vectors $\mathbf{p} \in \mathbb{R}^d$,

$$\mathcal{A}_a[\mathbb{G}\mathbf{p}] = \mathcal{A}_a[\mathbb{G}]\mathbf{p}, \quad \mathcal{A}_{-a,\rho}[\mathbb{G}\mathbf{p}] = \mathcal{A}_{-a,\rho}[\mathbb{G}]\mathbf{p}, \quad \text{and} \quad \mathcal{A}_{-a,\rho}^*[\mathbb{G}\mathbf{p}] = \mathcal{A}_{-a,\rho}^*[\mathbb{G}]\mathbf{p}.$$

By the definition of the operators \mathcal{A}_a and $\mathcal{A}_{-a,\rho}$, we have for $\alpha = p, s$:

$$\frac{\partial \mathbb{G}_a^\alpha}{\partial t}(\mathbf{x}, \mathbf{y}, t) = \mathcal{A}_{v_a^2/c_a^2} \left[\frac{\partial \mathbb{G}^\alpha}{\partial t}(\mathbf{x}, \mathbf{y}, \cdot) \right](t), \quad (5.65)$$

$$\frac{\partial \mathbb{G}_{-a,\rho}^\alpha}{\partial t}(\mathbf{x}, \mathbf{y}, t) = \mathcal{A}_{-v_a^2/c_{a,\rho}^2} \left[\frac{\partial \mathbb{G}^\alpha}{\partial t}(\mathbf{x}, \mathbf{y}, \cdot) \right](t). \quad (5.66)$$

Recall that $\mathbf{g} = \mathbf{u}$ and $\mathbf{g}_a = \mathbf{u}_a$ on $\partial\Omega \times \mathbb{R}$. It then follows from (5.58) for $\alpha = p, s$, that:

$$\mathcal{A}_{-v_a^2/c_{a,\rho}^2}^* \mathcal{A}_{v_a^2/c_a^2} [\mathbf{g}_a^\alpha] = S_\rho[\mathbf{g}^\alpha] + o\left(\frac{v_a^2}{c_a^2}\right), \quad (5.67)$$

where

$$\mathbf{g}_a^\alpha = \mathcal{H}^\alpha[\mathbf{g}_a], \quad \mathbf{g}^\alpha = \mathcal{H}^\alpha[\mathbf{g}]. \quad (5.68)$$

Identity (5.67) proves that $\mathcal{A}_{-v_a^2/c_{a,\rho}^2}^*$ is an approximate inverse of $\mathcal{A}_{v_a^2/c_a^2}$. Moreover, it plays a key role in showing that the regularized time reversal algorithm provides a first order correction to the attenuation effect.

5.3.3 HELMHOLTZ-KIRCHHOFF IDENTITY IN VISCOELASTIC MEDIA

In this subsection, we derive a new Helmholtz-Kirchhoff identity in elastic attenuating media. For doing so, let us introduce the conormal derivatives $\frac{\partial \mathbf{u}}{\partial v_a}$

and $\frac{\partial \mathbf{u}}{\partial v_{-a}}$ as follows:

$$\frac{\partial \mathbf{u}}{\partial v_{\pm a}} := \left(\lambda(\nabla \cdot \mathbf{u})\mathbf{n} + \mu(\nabla \mathbf{u}^T + (\nabla \mathbf{u}^T)^T)\mathbf{n} \right) \mp i\omega \left[\eta_\lambda(\nabla \cdot \mathbf{u})\mathbf{n} + \eta_\mu(\nabla \mathbf{u}^T + (\nabla \mathbf{u}^T)^T)\mathbf{n} \right]. \quad (5.69)$$

Note also that for a tensor \mathbb{G} the conormal derivative $\frac{\partial \mathbb{G}}{\partial \nu_{\pm a}}$ means that for all constant vectors \mathbf{p} ,

$$\left[\frac{\partial \mathbb{G}}{\partial \nu_{\pm a}} \right] \mathbf{p} := \frac{\partial [\mathbb{G} \mathbf{p}]}{\partial \nu_{\pm a}}. \quad (5.70)$$

The following properties hold.

PROPOSITION 5.3.3. *For all $\mathbf{x}, \mathbf{z} \in \Omega$, we have*

$$\int_{\partial \Omega} \left[\frac{\partial \mathbb{G}_{-a,\omega}^s(\mathbf{x}, \mathbf{y})}{\partial \nu_{-a}} \overline{\mathbb{G}_{a,\omega}^p(\mathbf{y}, \mathbf{z})} - \mathbb{G}_{-a,\omega}^s(\mathbf{x}, \mathbf{y}) \frac{\partial \overline{\mathbb{G}_{a,\omega}^p(\mathbf{y}, \mathbf{z})}}{\partial \nu_a} \right] d\sigma(\mathbf{y}) = 0. \quad (5.71)$$

Proof. Note that

$$\begin{aligned} \mathcal{J} &:= \int_{\partial \Omega} \left[\frac{\partial \mathbb{G}_{-a,\omega}^s(\mathbf{x}, \mathbf{y})}{\partial \nu_{-a}} \overline{\mathbb{G}_{a,\omega}^p(\mathbf{y}, \mathbf{z})} - \mathbb{G}_{-a,\omega}^s(\mathbf{x}, \mathbf{y}) \frac{\partial \overline{\mathbb{G}_{a,\omega}^p(\mathbf{y}, \mathbf{z})}}{\partial \nu_a} \right] d\sigma(\mathbf{y}) \\ &= \int_{\partial \Omega} \left[\frac{\partial \mathbb{G}_{-a,\omega}^s(\mathbf{x}, \mathbf{y})}{\partial \nu_{-a}} \overline{\mathbb{G}_{a,\omega}^p(\mathbf{y}, \mathbf{z})} - \mathbb{G}_{-a,\omega}^s(\mathbf{x}, \mathbf{y}) \frac{\partial \overline{\mathbb{G}_{a,\omega}^p(\mathbf{y}, \mathbf{z})}}{\partial \nu_{-a}} \right] d\sigma(\mathbf{y}) \\ &= \int_{\Omega} \left[\mathcal{L}_{\lambda,\mu} \mathbb{G}_{-a,\omega}^s(\mathbf{x}, \mathbf{y}) + i\omega \mathcal{L}_{\eta\lambda,\eta\mu} \mathbb{G}_{-a,\omega}^s(\mathbf{x}, \mathbf{y}) \right] \overline{\mathbb{G}_{a,\omega}^p(\mathbf{y}, \mathbf{z})} d\mathbf{y} \\ &\quad - \int_{\Omega} \mathbb{G}_{-a,\omega}^s(\mathbf{x}, \mathbf{y}) \left[\mathcal{L}_{\lambda,\mu} \overline{\mathbb{G}_{a,\omega}^p(\mathbf{y}, \mathbf{z})} + i\omega \mathcal{L}_{\eta\lambda,\eta\mu} \overline{\mathbb{G}_{a,\omega}^p(\mathbf{y}, \mathbf{z})} \right] d\mathbf{y}, \\ &= \int_{\Omega} \left[\mathcal{L}_{\lambda,\mu} \mathbb{G}_{-a,\omega}^s(\mathbf{x}, \mathbf{y}) + i\omega \mathcal{L}_{\eta\lambda,\eta\mu} \mathbb{G}_{-a,\omega}^s(\mathbf{x}, \mathbf{y}) \right] \overline{\mathbb{G}_{a,\omega}^p(\mathbf{y}, \mathbf{z})} d\mathbf{y} \\ &\quad - \int_{\Omega} \mathbb{G}_{-a,\omega}^s(\mathbf{x}, \mathbf{y}) \left[\mathcal{L}_{\lambda,\mu} \mathbb{G}_{a,\omega}^p(\mathbf{y}, \mathbf{z}) - i\omega \mathcal{L}_{\eta\lambda,\eta\mu} \mathbb{G}_{a,\omega}^p(\mathbf{y}, \mathbf{z}) \right] d\mathbf{y}. \end{aligned}$$

Since $\mathbb{G}_{a,\omega}^p(\mathbf{x}, \mathbf{y})$ and $\mathbb{G}_{-a,\omega}^s(\mathbf{x}, \mathbf{y})$ are solutions of equations (5.44) with $\alpha = p, s$, respectively, it follows that

$$\mathcal{J} = \left[\mathcal{H}^s[-\delta_{\mathbf{0}}] * \overline{\mathbb{G}_{a,\omega}^p(\cdot, \mathbf{z})} \right] (\mathbf{x}) - \left[\mathbb{G}_{-a,\omega}^s(\mathbf{x}, \cdot) * \mathcal{H}^p[-\delta_{\mathbf{0}}] \right] (\mathbf{z}).$$

As in the proof of Proposition 5.2.2 one can show that

$$\left[\mathcal{H}^s[-\delta_{\mathbf{0}}] * \overline{\mathbb{G}_{a,\omega}^p(\cdot, \mathbf{z})} \right] (\mathbf{x}) = 0 \quad \text{and} \quad \left[\mathbb{G}_{-a,\omega}^s(\mathbf{x}, \cdot) * \mathcal{H}^p[-\delta_{\mathbf{0}}] \right] (\mathbf{z}) = 0,$$

which completes the proof of the proposition. \square

We now give an approximation of the attenuating co-normal derivative.

PROPOSITION 5.3.4. *If $\mathbf{n} = \widehat{\mathbf{y} - \mathbf{x}}$, then for $\alpha = p, s$, we have*

$$\frac{\partial \mathbb{G}_{\pm a, \omega}^{\alpha}(\mathbf{x}, \mathbf{y})}{\partial v_{\pm a}} \simeq \frac{i c_{\alpha} \omega^2}{\kappa_{\mp}^{\alpha}(\omega)} \mathbb{G}_{\pm a, \omega}^{\alpha}(\mathbf{x}, \mathbf{y}), \quad (5.72)$$

where

$$\kappa_{\mp}^{\alpha}(\omega) = \frac{\omega}{\sqrt{1 \mp i \omega v_{\alpha}^2 / c_{\alpha}^2}}. \quad (5.73)$$

Proof. Indeed, notice that

$$\mathbb{G}_{\pm a, \omega}^{\alpha}(\mathbf{x}, \mathbf{y}) = \left[\frac{\kappa_{\mp}^{\alpha}(\omega)}{\omega} \right]^2 \mathbb{G}_{\kappa_{\mp}^{\alpha}(\omega)}^{\alpha}(\mathbf{x}, \mathbf{y}), \quad \alpha = p, s, \quad (5.74)$$

where $\mathbb{G}_{\omega}^{\alpha}$ are the ideal Green functions. Then, from Proposition 5.2.4, we obtain

$$\begin{aligned} \frac{\partial \mathbb{G}_{\pm a, \omega}^{\alpha}(\mathbf{x}, \mathbf{y})}{\partial v_{\pm a}} &\simeq \left[\frac{\kappa_{\mp}^{\alpha}(\omega)}{\omega} \right]^2 \left(\left(i c_{\alpha}^2 \frac{\kappa_{\mp}^{\alpha}(\omega)}{c_{\alpha}} \mathbb{G}_{\kappa_{\mp}^{\alpha}(\omega)}^{\alpha}(\mathbf{x}, \mathbf{y}) \right) \mp i \omega \left(i v_{\alpha}^2 \frac{\kappa_{\mp}^{\alpha}(\omega)}{c_{\alpha}} \mathbb{G}_{\kappa_{\mp}^{\alpha}(\omega)}^{\alpha}(\mathbf{x}, \mathbf{y}) \right) \right) \\ &\simeq \left[i c_{\alpha} \kappa_{\mp}^{\alpha}(\omega) \left(1 \mp i \omega \frac{v_{\alpha}^2}{c_{\alpha}^2} \right) \right] \mathbb{G}_{\pm a, \omega}^{\alpha}(\mathbf{x}, \mathbf{y}) \\ &\simeq \frac{i c_{\alpha} \omega^2}{\kappa_{\mp}^{\alpha}(\omega)} \mathbb{G}_{\pm a, \omega}^{\alpha}(\mathbf{x}, \mathbf{y}). \end{aligned}$$

□

In particular, the following estimate holds as a direct consequence of Propositions 5.3.3 and 5.3.4.

PROPOSITION 5.3.5. *Let $\Omega \subset \mathbb{R}^d$ be a ball with large (with respect to wavelength) radius. Then for all $\mathbf{x}, \mathbf{z} \in \Omega$ sufficiently far from boundary $\partial\Omega$, we have*

$$\begin{cases} \Re e \left\{ \int_{\partial\Omega} \mathbb{G}_{-a, \omega}^s(\mathbf{x}, \mathbf{y}) \overline{\mathbb{G}_{a, \omega}^p(\mathbf{y}, \mathbf{z})} d\sigma(\mathbf{y}) \right\} \simeq 0, \\ \Re e \left\{ \int_{\partial\Omega} \mathbb{G}_{-a, \omega}^p(\mathbf{x}, \mathbf{y}) \overline{\mathbb{G}_{a, \omega}^s(\mathbf{y}, \mathbf{z})} d\sigma(\mathbf{y}) \right\} \simeq 0. \end{cases} \quad (5.75)$$

5.3.4 ANALYSIS OF THE REGULARIZED TIME REVERSAL IMAGING ALGORITHM

The aim of this subsection is to justify that the regularized time-reversal imaging functional $\tilde{\mathcal{I}}_{a, \rho}$ provides a correction of the attenuation effect.

THEOREM 5.3.6. *The regularized time-reversal imaging functional $\tilde{\mathcal{I}}_{a, \rho}$ satisfies*

$$\tilde{\mathcal{I}}_{a, \rho}(\mathbf{x}) = \tilde{\mathcal{I}}_{\rho}(\mathbf{x}) + o\left(v_s^2 / c_s^2 + v_p^2 / c_p^2\right), \quad (5.76)$$

$$\tilde{\mathcal{I}}_{\rho}(\mathbf{x}) := \int_{\partial\Omega} \int_0^T \left[c_s \frac{\partial}{\partial t} \mathbb{G}^s(\mathbf{x}, \mathbf{y}, s) + c_p \frac{\partial}{\partial t} \mathbb{G}^p(\mathbf{x}, \mathbf{y}, s) \right] S_{\rho}[\mathbf{g}(\mathbf{y}, \cdot)](s) ds d\sigma(\mathbf{y}), \quad (5.77)$$

where S_{ρ} is defined by (5.41).

Proof. We can decompose the functional $\tilde{\mathcal{F}}_{a,\rho}$ as follows:

$$\begin{aligned}\tilde{\mathcal{F}}_{a,\rho}(\mathbf{x}) &= \int_{\partial\Omega} \int_0^T \frac{\partial}{\partial t} \left[c_p \mathbb{G}_{-a,\rho}^p(\mathbf{x}, \mathbf{y}, T-s) + c_s \mathbb{G}_{-a,\rho}^s(\mathbf{x}, \mathbf{y}, T-s) \right] \mathbf{g}_a(\mathbf{y}, T-s) ds d\sigma(\mathbf{y}) \\ &= \int_{\partial\Omega} \int_0^T \frac{\partial}{\partial t} \left[c_p \mathbb{G}_{-a,\rho}^p(\mathbf{x}, \mathbf{y}, s) + c_s \mathbb{G}_{-a,\rho}^s(\mathbf{x}, \mathbf{y}, s) \right] \left(\mathbf{g}_a^s(\mathbf{y}, s) + \mathbf{g}_a^p(\mathbf{y}, s) \right) ds d\sigma(\mathbf{y}) \\ &= \mathcal{J}_{a,\rho}^{ss}(\mathbf{x}) + \mathcal{J}_{a,\rho}^{sp}(\mathbf{x}) + \mathcal{J}_{a,\rho}^{ps}(\mathbf{x}) + \mathcal{J}_{a,\rho}^{pp}(\mathbf{x}),\end{aligned}$$

where

$$\mathcal{J}_{a,\rho}^{\alpha\beta}(\mathbf{x}) = \int_{\partial\Omega} \int_0^T \frac{\partial}{\partial t} \left[c_\alpha \mathbb{G}_{-a,\rho}^\alpha(\mathbf{x}, \mathbf{y}, s) \right] \mathbf{g}_a^\beta(\mathbf{y}, s) ds d\sigma(\mathbf{y}), \quad \alpha, \beta \in \{p, s\}.$$

Similarly we can decompose the functional $\tilde{\mathcal{F}}_\rho$ as

$$\tilde{\mathcal{F}}_\rho(\mathbf{x}) = \mathcal{J}_\rho^{ss}(\mathbf{x}) + \mathcal{J}_\rho^{sp}(\mathbf{x}) + \mathcal{J}_\rho^{ps}(\mathbf{x}) + \mathcal{J}_\rho^{pp}(\mathbf{x}),$$

with

$$\mathcal{J}_\rho^{\alpha\beta}(\mathbf{x}) = \int_{\partial\Omega} \int_0^T \frac{\partial}{\partial t} \left[c_\alpha \mathbb{G}^\alpha(\mathbf{x}, \mathbf{y}, s) \right] S_\rho \left[\mathbf{g}^\beta(\mathbf{y}, \cdot) \right] (s) ds d\sigma(\mathbf{y}), \quad \alpha, \beta \in \{p, s\}.$$

The first term $\mathcal{J}_{a,\rho}^{ss}(\mathbf{x})$ satisfies

$$\begin{aligned}\mathcal{J}_{a,\rho}^{ss}(\mathbf{x}) &= \int_{\partial\Omega} \int_0^T \mathcal{A}_{-v_s^2/c_s^2, \rho} \left[\frac{\partial}{\partial t} \left(c_s \mathbb{G}^s(\mathbf{x}, \mathbf{y}, s) \right) \right] \mathcal{A}_{v_s^2/c_s^2} \left[\mathbf{g}^s(\mathbf{y}, \cdot) \right] (s) ds d\sigma(\mathbf{y}) \\ &= \int_{\partial\Omega} \int_0^T \frac{\partial}{\partial t} \left(c_s \mathbb{G}^s(\mathbf{x}, \mathbf{y}, s) \right) \mathcal{A}_{-v_s^2/c_s^2, \rho}^* \left[\mathcal{A}_{v_s^2/c_s^2} \left[\mathbf{g}^s(\mathbf{y}, \cdot) \right] \right] (s) ds d\sigma(\mathbf{y}) \\ &= \int_{\partial\Omega} \int_0^T \frac{\partial}{\partial t} \left[c_s \mathbb{G}^s(\mathbf{x}, \mathbf{y}, s) \right] S_\rho \left[\mathbf{g}^s(\mathbf{y}, \cdot) \right] (s) ds d\sigma(\mathbf{y}) + o(v_s^2/c_s^2) \\ &= \mathcal{J}_\rho^{ss}(\mathbf{x}) + o(v_s^2/c_s^2),\end{aligned}$$

by using Proposition 5.3.2. Similarly, we get

$$\mathcal{J}_{a,\rho}^{pp}(\mathbf{x}) = \mathcal{J}_\rho^{pp}(\mathbf{x}) + o(v_p^2/c_p^2).$$

Moreover, the coupling terms $\mathcal{J}_{a,\rho}^{sp}$ and $\mathcal{J}_{a,\rho}^{ps}$ vanish. Indeed, due to Proposition 5.3.5, we have

$$\begin{aligned}\mathcal{J}_{a,\rho}^{sp}(\mathbf{x}) &= \frac{1}{2\pi} \int_{\mathbb{R}^d} \int_{|\omega| < \rho} \omega^2 \left[\int_{\partial\Omega} \left[c_s \mathbb{G}_{-a,\omega}^s(\mathbf{x}, \mathbf{y}) \right] \overline{\mathbb{G}_{a,\omega}^p(\mathbf{y}, \mathbf{z})} d\sigma(\mathbf{y}) \right] d\omega \mathbf{F}(\mathbf{z}) d\mathbf{z} \simeq 0, \\ \mathcal{J}_{a,\rho}^{ps}(\mathbf{x}) &= \frac{1}{2\pi} \int_{\mathbb{R}^d} \int_{|\omega| < \rho} \omega^2 \left[\int_{\partial\Omega} \left[c_p \mathbb{G}_{-a,\omega}^p(\mathbf{x}, \mathbf{y}) \right] \overline{\mathbb{G}_{a,\omega}^s(\mathbf{y}, \mathbf{z})} d\sigma(\mathbf{y}) \right] d\omega \mathbf{F}(\mathbf{z}) d\mathbf{z} \simeq 0.\end{aligned}$$

Proposition 5.2.5 shows that we also have

$$\begin{aligned}\mathcal{F}_\rho^{sp}(\mathbf{x}) &= \frac{1}{2\pi} \int_{\mathbb{R}^d} \int_{|\omega| < \rho} \omega^2 \left[\int_{\partial\Omega} [c_s \mathbb{G}_\omega^s(\mathbf{x}, \mathbf{y})] \overline{\mathbb{G}_\omega^p(\mathbf{y}, \mathbf{z})} d\sigma(\mathbf{y}) \right] d\omega \mathbf{F}(\mathbf{z}) d\mathbf{z} \simeq 0, \\ \mathcal{F}_\rho^{ps}(\mathbf{x}) &= \frac{1}{2\pi} \int_{\mathbb{R}^d} \int_{|\omega| < \rho} \omega^2 \left[\int_{\partial\Omega} [c_p \mathbb{G}_\omega^p(\mathbf{x}, \mathbf{y})] \overline{\mathbb{G}_\omega^s(\mathbf{y}, \mathbf{z})} d\sigma(\mathbf{y}) \right] d\omega \mathbf{F}(\mathbf{z}) d\mathbf{z} \simeq 0,\end{aligned}$$

which concludes the proof. \square

It is straightforward to check that

$$\tilde{\mathcal{F}}_\rho(\mathbf{x}) \xrightarrow{\rho \rightarrow \infty} \tilde{\mathcal{F}}(\mathbf{x}) \simeq \mathbf{F}(\mathbf{x}), \quad (5.78)$$

by Theorem 5.2.6. Therefore, $\tilde{\mathcal{F}}_{a,\rho}$ provides a first-order correction in terms of $v_s^2/c_s^2 + v_p^2/c_p^2$ of the attenuation effect. Moreover, the imaging functional $\tilde{\mathcal{F}}_{a,\rho}$ can be seen as the time-reversal functional $\tilde{\mathcal{F}}$ defined by (5.7) applied to $\mathcal{A}_{-v_a^2/c_a^2, \rho}^*[\mathbf{g}_a^\alpha]$, $\alpha = p, s$. As shown in (5.64), the regularized operators $\mathcal{A}_{-v_a^2/c_a^2, \rho}^*$ give a first-order approximation of the inverse of \mathcal{A}_a for $a = v_a^2/c_a^2$. It would be very interesting to construct higher-order reconstructions in terms of the attenuation effect using higher-order approximations of the inverse of the operator \mathcal{A}_a . The problem is more challenging than the one discussed in Chapter 2 for the scalar case because of the coupling between the shear and pressure components. Note finally that, if one applies the time-reversal functional $\tilde{\mathcal{F}}$ to the data \mathbf{g}_a directly, then one finds

$$\begin{aligned}\tilde{\mathcal{F}}(\mathbf{x}) &= \int_{\partial\Omega} \int_0^T \frac{\partial}{\partial t} [c_p \mathbb{G}^p(\mathbf{x}, \mathbf{y}, s) + c_s \mathbb{G}^s(\mathbf{x}, \mathbf{y}, s)] \mathbf{g}_a(\mathbf{y}, s) ds d\sigma(\mathbf{y}) \\ &= \frac{1}{2\pi} \int_{\mathbb{R}^d} \int_{\mathbb{R}} \omega^2 \left[\int_{\partial\Omega} [c_p \mathbb{G}_\omega^p(\mathbf{x}, \mathbf{y}) + c_s \mathbb{G}_\omega^s(\mathbf{x}, \mathbf{y})] \overline{\mathbb{G}_{a,\omega}(\mathbf{y}, \mathbf{z})} d\sigma(\mathbf{y}) \right] d\omega \mathbf{F}(\mathbf{z}) d\mathbf{z}, \quad (5.79)\end{aligned}$$

which gives an error of the order of $v_s^2/c_s^2 + v_p^2/c_p^2$ as can be seen from the expansion (5.62).

As discussed in Chapter 2, the choice of the cut-off parameter ρ is based on the trade off between image resolution and stability. On one hand, ρ must be selected large enough for good resolution. On the other hand, for the stability of the reconstruction, it is required not to be too large. In acoustic case $(a \text{ diam}(\Omega))^{-1/2}$ serves as a threshold for ρ in order to ensure stability, where diam is the diameter (cf. Remark 2.3.6). A reasonable threshold cut-off frequency ρ in elastic case can accordingly be $(\max(v_s^2/c_s^2, v_p^2/c_p^2) \text{ diam}(\Omega))^{-1/2}$.

5.3.5 NUMERICAL SIMULATIONS

In this section we present numerical illustrations and describe our algorithms for numerical resolution of the source problem to show that $\tilde{\mathcal{F}}_{a,\rho}$ provides a better reconstruction than $\tilde{\mathcal{F}}$, where the attenuation effect is not taken into account.

5.3.5.1 DESCRIPTION OF THE ALGORITHM

In the expression of $\tilde{\mathcal{F}}_{a,\rho}$, the solution $\mathbf{v}_{s,a,\rho}(\mathbf{x}, t)$ is very difficult to obtain numerically. Therefore, we prefer to regularize the problem by truncating high-frequency components in space instead of time, in contrast with our theoretical analysis. This can be seen as an approximation $\tilde{\mathbf{v}}_{s,a,\rho}(\mathbf{x}, t)$ of $\mathbf{v}_{s,a,\rho}(\mathbf{x}, t)$ defined as the solution of

$$\frac{\partial^2 \tilde{\mathbf{v}}_{s,a,\rho}}{\partial t^2}(\mathbf{x}, t) - \mathcal{L}_{\lambda,\mu} \tilde{\mathbf{v}}_{s,a,\rho}(\mathbf{x}, t) + \frac{\partial}{\partial t} \mathcal{L}_{\eta_\lambda, \eta_\mu} \tilde{\mathbf{v}}_{s,a,\rho}(\mathbf{x}, t) = \frac{\partial \delta_s(t)}{\partial t} \mathcal{X}_\rho \left[\mathbf{g}_a(\cdot, T-s) \delta_{\partial\Omega} \right](\mathbf{x}),$$

where the operator \mathcal{X}_ρ is defined by

$$\mathcal{X}_\rho \left[\mathbf{g}_a(\cdot, T-s) \delta_{\partial\Omega} \right](\mathbf{x}) = \int_{|\mathbf{k}| \leq \rho} \left[\int_{\partial\Omega} \mathbf{g}_a(\mathbf{y}, T-s) e^{-2i\pi \mathbf{k} \cdot \mathbf{y}} d\sigma(\mathbf{y}) \right] e^{2i\pi \mathbf{k} \cdot \mathbf{x}} d\mathbf{k}.$$

The operator \mathcal{X}_ρ , as the operator S_ρ , truncates high frequencies but in the space variable.

To compute the solution of the viscoelastic wave equation in two dimensions

$$\frac{\partial^2 \mathbf{u}_a}{\partial t^2}(\mathbf{x}, t) - \mathcal{L}_{\lambda,\mu} \mathbf{u}_a(\mathbf{x}, t) \pm \mathcal{L}_{\eta_\lambda, \eta_\mu} \mathbf{u}_a(\mathbf{x}, t) = \mathbf{0},$$

we use the same algorithm as for the non-attenuated case, that is, we use a large box $\Omega \subset Q = [-L/2, L/2]^2$ with periodic boundary condition and again a *splitting spectral Fourier* approach coupled with a PML technique to simulate a free outgoing interface on ∂Q .

5.3.5.2 EXPERIMENTS

In the sequel, for numerical illustrations, Ω is taken to be a unit disk centered at origin. Its boundary is discretized by 2^{11} sensors. Each solution of elastic wave equation is computed over $(\mathbf{x}, t) \in [-L/2, L/2]^2 \times [0, T]$ with $L = 4$ and $T = 2$. We use a step of discretization given by $dt = T/2^{13}$ and $dx = L/2^9$.

Figure 5.4 presents a first experiment with Lamé parameters $(\lambda, \mu) = (1, 1)$ and attenuation coefficients $(\eta_\lambda, \eta_\mu) = (0.0002, 0.0002)$. The first line corresponds to the two components of the initial source \mathbf{F} . The second line corresponds to the reconstruction of \mathbf{F} without taking into account the attenuation effect. The imaging functional $\tilde{\mathcal{F}}(\mathbf{x})$ appears to be blurred due to the coupling effects. The last three lines correspond to reconstructions of \mathbf{F} using the imaging functional $\tilde{\mathcal{F}}_{a,\rho}$ with different values of ρ . We clearly observe a better reconstruction of the source \mathbf{F} than by using the functional $\tilde{\mathcal{F}}$ provided that the regularization parameter ρ is chosen appropriately large in order to ensure the good resolution of the reconstruction.

Figures 5.5 and 5.6 present two other examples of reconstruction using $\tilde{\mathcal{F}}_{a,\rho}$. The same observation holds.

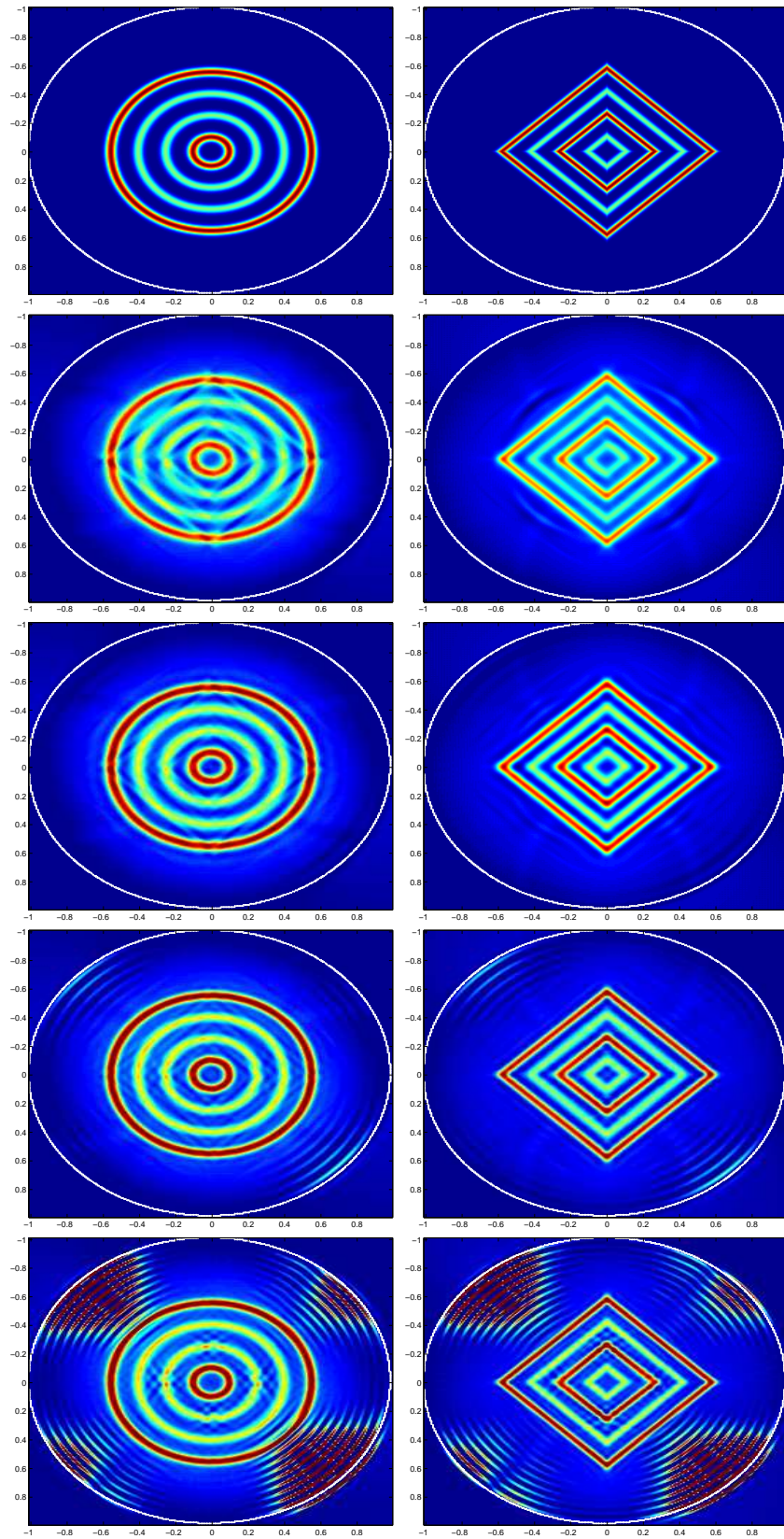


FIGURE 5.4. Comparison between $\tilde{\mathcal{F}}$ and $\tilde{\mathcal{F}}_{a,\rho}$ in a viscoelastic medium; The parameters are $(\lambda, \mu) = (1, 1)$ and $(v_s^2/c_s^2, v_p^2/c_p^2) = (0.0002, 0.0002)$; First line: initial condition; Second line: without correction of attenuation; Last lines: using $\tilde{\mathcal{F}}_{a,\rho}$ with respectively: $\rho = 15, 20, 25$.

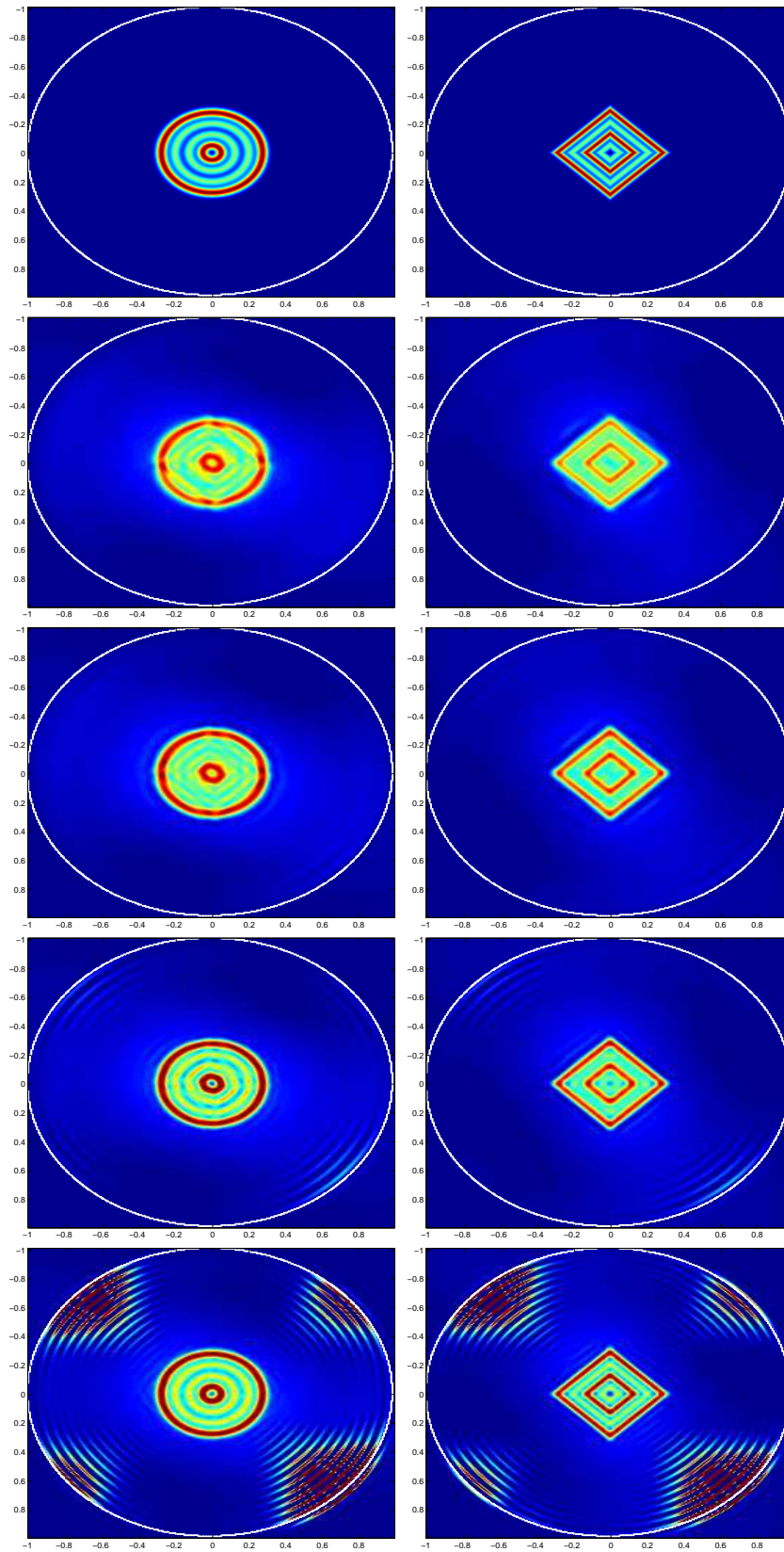


FIGURE 5.5. Comparison between $\tilde{\mathcal{F}}$ and $\tilde{\mathcal{F}}_{a,\rho}$ in a viscoelastic medium; The parameters are $(\lambda, \mu) = (1, 1)$ and $(v_s^2/c_s^2, v_p^2/c_p^2) = (0.00005, 0.00005)$; First line: initial condition; Second line: without correction of attenuation; Last lines: using $\tilde{\mathcal{F}}_{a,\rho}$ with respectively: $\rho = 15, 20, 25$.

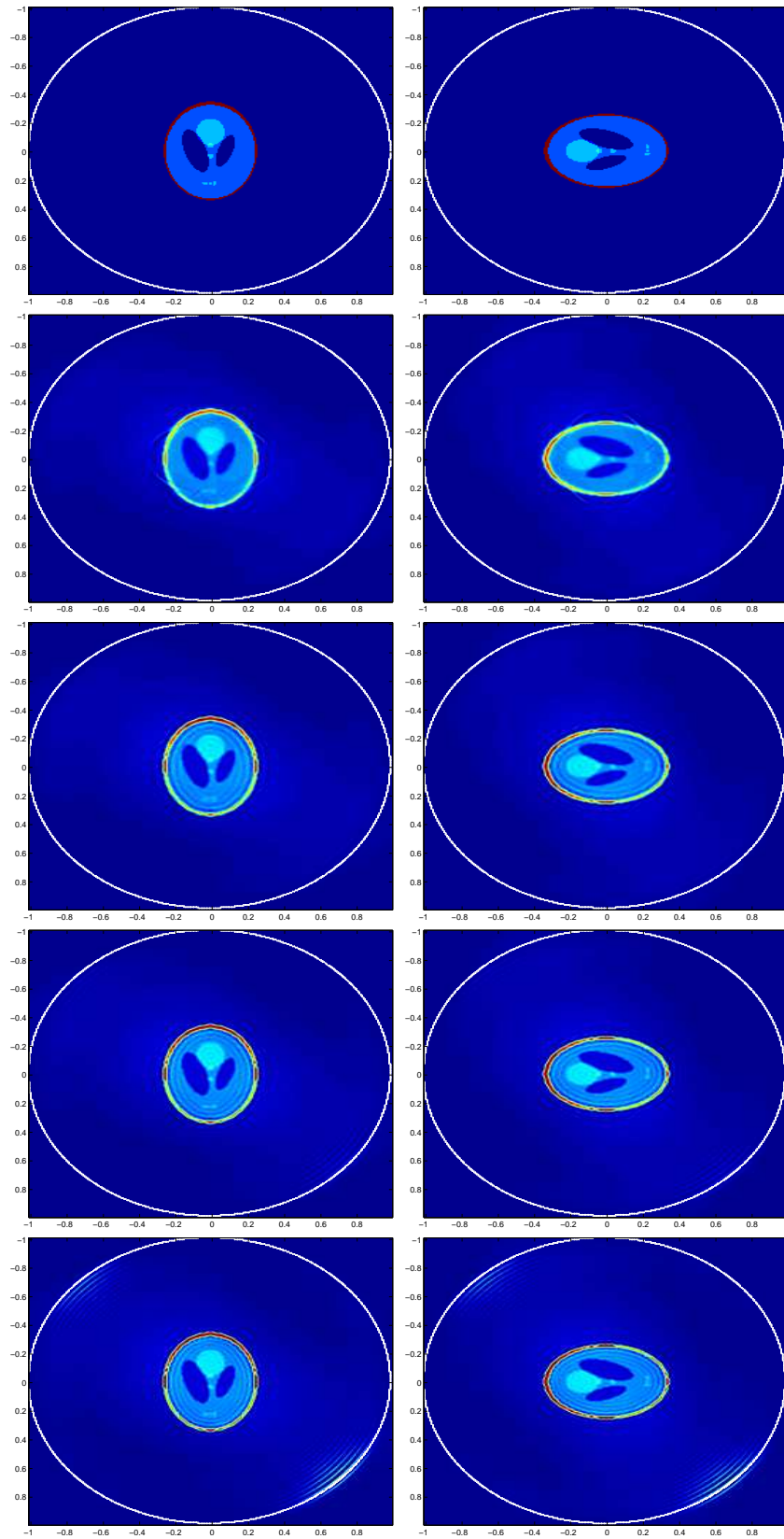


FIGURE 5.6. Comparison between $\tilde{\mathcal{F}}$ and $\tilde{\mathcal{F}}_{a,\rho}$ in a viscoelastic medium; The parameters are $(\lambda, \mu) = (1, 1)$ and $(\eta_\lambda, \eta_\mu) = (0.00005, 0.00005)$; First line: initial source \mathbf{F} ; Second line: reconstruction of \mathbf{F} using $\tilde{\mathcal{F}}$; Three last lines: reconstruction of source \mathbf{F} by using $\tilde{\mathcal{F}}_{a,\rho}$ with respectively: $\rho = 25, 30, 35$.

SOME ANISOTROPIC VISCOELASTIC GREEN FUNCTIONS

6.1 INTRODUCTION

Numerous applications in biomedical imaging [7, 28], seismology [3, 45], exploration geophysics [76, 77], material sciences [5, 27] and engineering sciences [2, 35, 88] have fueled research and development in theory of elasticity. Elastic properties and attributes have gained interest in the recent decades as a diagnostic tool for non-invasive imaging [71, 113]. Their high correlation with the pathology and the underlying structure of soft tissues has inspired many investigations in biomedical imaging and led to many interesting mathematical problems [18, 21, 22, 23, 24, 36, 118, 119].

Biological materials are often assumed to be isotropic and inviscid with respect to elastic deformation. However, several recent studies indicate that many soft tissues exhibit anisotropic and viscoelastic behavior [70, 97, 102, 118, 119, 148]. Sinkus *et al.* have inferred in [118] that breast tumor tends to be anisotropic, while Weaver *et al.* [143] have provided an evidence that even non cancerous breast tissue is anisotropic. White matter in brain [97] and cortical bones [148] also exhibit similar behavior. Moreover, it has been observed that the shear velocities parallel and orthogonal to the fiber direction in forearm [102] and biceps [70] are different. This indicates that the skeletal muscles with directional structure are actually anisotropic. Thus, an assumption of isotropy can lead to erroneous forward-modeled wave synthetics, while an estimation of viscosity can be very useful in characterization and identification of anomaly [36].

A possible approach to handle viscosity effects on image reconstruction has been proposed in Chapter 4, using stationary phase theorem. It is shown that the ideal Green function (in an inviscid regime) can be approximated from the viscous one by solving an ordinary differential equation. Once the ideal Green function is known one can identify a possible anomaly using imaging algorithms such as time reversal, back-propagation, Kirchhoff migration or MUSIC [7, 18, 25, 28]. One can also find the elastic moduli of the anomaly using the

asymptotic formalism and reconstructing a certain polarization tensor in the far field [23, 25, 26, 27].

The importance of Green function stems from its role as a tool for the numerical and asymptotic techniques in biomedical imaging. Many inverse problems involving the estimation and acquisition of elastic parameters become tractable once the associated Green function is computed [6, 18, 25]. Several attempts have been made to compute Green functions in purely elastic and/or isotropic regime. (See, for instance, [36, 42, 45, 105, 136, 137, 138] and references therein). However, it is not possible to give a closed form expression of the elastic Green function for general anisotropic media without imposing certain restrictions. In this chapter, we provide anisotropic viscoelastic Green function in closed form for three particular anisotropic media.

The elastodynamic Green function in isotropic media is calculated by separating wave modes using Helmholtz decomposition of the elastic wavefield [3, 36, 39]. Unfortunately, this simple approach does not work in anisotropic media, where three different waves propagate with different phase velocities and polarization directions [35, 45, 48]. A polarization direction of quasi-longitudinal wave that differs from that of wave vector, impedes Helmholtz decomposition to completely separate wave modes [57].

The phase velocities and polarization vectors are the eigenvalues and eigenvectors of the Christoffel tensor $\underline{\Gamma}$ associated with the medium. So, the wavefield can always be decomposed using the spectral basis of $\underline{\Gamma}$. Based on this observation, Burridge *et al.* [42] proposed a new approach to calculate elastodynamic Green functions. Their approach consists of finding the eigenvalues and eigenvectors of the Christoffel tensor $\underline{\Gamma}(\nabla_x)$ using the duality between algebraic and differential objects. Then, it is possible to express the Green function $\underline{\mathbf{G}}$ in terms of three scalar functions ϕ_i satisfying partial differential equations with constant coefficients. Consequently, the problem of computing $\underline{\mathbf{G}}$ reduces to the resolution of three differential equations for ϕ_i and of three subsequent equations (which may or may not be differential equations) with ϕ_i as source terms. (cf. Section 6.2.3)

Finding the closed form expressions of the eigenvalues of the Christoffel tensor $\underline{\Gamma}$ is usually not so trivial because its characteristic equation is a polynomial of degree six in the components of its argument vector. However, with some restrictions on the material, roots of the characteristic equation can be given [105]. In this chapter, we consider three different media for which not only the explicit expressions of the eigenvalues of $\underline{\Gamma}$ are known [42, 138], but they are also quadratic homogeneous forms, in the components of the argument vector. As a consequence, equations satisfied by ϕ_i become scalar wave equations. Following Burridge *et al.* [42], we find the viscoelastic Green functions for each medium. It is important to note that the elastodynamic Green function

in a purely elastic regime, for the media under consideration, are well known [42, 138]. Also, the expression of the Green function for viscoelastic isotropic medium, which is computed as a special case, matches the one provided in Chapter 4.

In this work, we consider the general model proposed by Szabo and Wu in [128], to describe the viscosity response of soft tissues to low frequency excitations. We present some mathematical notions, theme and the outlines of the chapter in the next section.

6.2 MATHEMATICAL CONTEXT AND CHAPTER OUTLINES

6.2.1 VISCOELASTIC WAVE EQUATION

Consider an open subset Ω of \mathbb{R}^3 , filled with a homogeneous anisotropic viscoelastic material. Let

$$\mathbf{u}(\mathbf{x}, t) : \Omega \times \mathbb{R}^+ \rightarrow \mathbb{R}^3$$

be the displacement field at time t of the material particle at position $\mathbf{x} \in \Omega$ and $\nabla_x \mathbf{u}(\mathbf{x}, t)$ be its gradient.

Under the assumptions of linearity and small perturbations, we define the order two strain tensor by

$$\underline{\underline{\varepsilon}} : (\mathbf{x}, t) \in \Omega \times \mathbb{R}^+ \mapsto \frac{1}{2} (\nabla_x \mathbf{u} + \nabla_x \mathbf{u}^T) (\mathbf{x}, t), \quad (6.1)$$

where the superscript T indicates a transpose operation.

Let $\underline{\underline{\mathbf{C}}} \in \mathcal{L}_s^2(\mathbb{R}^3)$ and $\underline{\underline{\mathbf{V}}} \in \mathcal{L}_s^2(\mathbb{R}^3)$ be the stiffness and viscosity tensors of the material respectively. Here $\mathcal{L}_s^2(\mathbb{R}^3)$ is the space of symmetric tensors of order four. These tensors are assumed to be positive definite, i.e. there exist constants $\beta_c, \beta_v > 0$ such that

$$(\underline{\underline{\mathbf{C}}} : \underline{\underline{\xi}}) : \underline{\underline{\xi}} \geq \beta_c |\underline{\underline{\xi}}|^2 \quad \text{and} \quad (\underline{\underline{\mathbf{V}}} : \underline{\underline{\xi}}) : \underline{\underline{\xi}} \geq \beta_v |\underline{\underline{\xi}}|^2, \quad \forall \underline{\underline{\xi}} \in \mathcal{L}_s(\mathbb{R}^3),$$

where $\mathcal{L}_s(\mathbb{R}^3)$ denotes the space of symmetric tensors of order two.

The generalized Hooke's Law [128] for the power law media states that the stress distribution

$$\underline{\underline{\sigma}} : \Omega \times \mathbb{R}^+ \rightarrow \mathcal{L}_s(\mathbb{R}^3)$$

produced by deformation $\underline{\underline{\varepsilon}}$, satisfies:

$$\underline{\underline{\sigma}} = \underline{\underline{\mathbf{C}}} : \underline{\underline{\varepsilon}} + \underline{\underline{\mathbf{V}}} : \mathcal{A} [\underline{\underline{\varepsilon}}] \quad (6.2)$$

where \mathcal{A} is an attenuation operator defined as

$$\mathcal{A}[\varphi] = \begin{cases} -(-1)^{\gamma/2} \frac{\partial^{\gamma-1} \varphi}{\partial t^{\gamma-1}} & \gamma \text{ is an even integer,} \\ \frac{2}{\pi} (\gamma-1)! (-1)^{(\gamma+1)/2} \left[\frac{H(t)}{t^\gamma} \right] *_t \varphi & \gamma \text{ is an odd integer,} \\ -\frac{2}{\pi} \Gamma(\gamma) \sin\left(\frac{\gamma\pi}{2}\right) \left[\frac{H(t)}{|t|^\gamma} \right] *_t \varphi & \gamma \text{ is a non integer.} \end{cases} \quad (6.3)$$

Note that by convention,

$$\mathcal{A}[\mathbf{u}]_i = \mathcal{A}[u_i] \quad \text{and} \quad \mathcal{A}[\underline{\varepsilon}]_{ij} = \mathcal{A}[\varepsilon_{ij}] \quad 1 \leq i, j \leq 3.$$

Here $H(t)$ is the Heaviside function, Γ is the gamma function and $*_t$ represents convolution with respect to variable t . See [4, 44, 82, 127, 128, 131] for comprehensive details and discussion on fractional attenuation models, causality and the loss operator \mathcal{A} .

The viscoelastic wave equation satisfied by the displacement field $\mathbf{u}(\mathbf{x}, t)$ reads now

$$\rho \frac{\partial^2 \mathbf{u}}{\partial t^2} - \mathbf{F} = \nabla_x \cdot \underline{\underline{\sigma}} = \nabla_x \cdot \left(\underline{\underline{\mathbf{C}}} : \underline{\underline{\varepsilon}} + \underline{\underline{\mathbf{V}}} : \mathcal{A}[\underline{\underline{\varepsilon}}] \right),$$

where $\mathbf{F}(\mathbf{x}, t)$ is the applied force and ρ is the density (supposed to be constant) of the material.

REMARK 6.2.1. For quadratic frequency losses, i.e. when $\gamma = 2$, operator \mathcal{A} reduces to a first order time derivative. Therefore, power-law attenuation model (6.2) turns out to be the Voigt model in this case.

6.2.2 SPECTRAL DECOMPOSITION USING CHRISTOFFEL TENSORS

We introduce now the Christoffel tensors $\underline{\underline{\Gamma}}^c, \underline{\underline{\Gamma}}^v : \mathbb{R}^3 \rightarrow \mathcal{L}_s(\mathbb{R}^3)$ associated respectively with $\underline{\underline{\mathbf{C}}}$ and $\underline{\underline{\mathbf{V}}}$ defined by:

$$\Gamma_{ij}^c(\mathbf{n}) = \sum_{k,l=1}^3 C_{kijl} n_k n_l, \quad \Gamma_{ij}^v(\mathbf{n}) = \sum_{k,l=1}^3 V_{kijl} n_k n_l, \quad \forall \mathbf{n} \in \mathbb{R}^3, \quad 1 \leq i, j \leq 3.$$

Remark that the viscoelastic wave equation can be rewritten in terms of the Christoffel tensors as :

$$\rho \frac{\partial^2 \mathbf{u}}{\partial t^2} - \mathbf{F} = \underline{\underline{\Gamma}}^c[\nabla_x] \mathbf{u} + \underline{\underline{\Gamma}}^v[\nabla_x] \mathcal{A}[\mathbf{u}]. \quad (6.4)$$

Note also that $\underline{\underline{\Gamma}}^c$ and $\underline{\underline{\Gamma}}^v$ are symmetric and positive definite, indeed, as $\underline{\underline{\mathbf{C}}}$ and $\underline{\underline{\mathbf{V}}}$ are already symmetric positive definite.

Let L_i^c be the eigenvalues and \mathbf{D}_i^c be the associated eigenvectors of $\underline{\Gamma}^c$ for $i = 1, 2, 3$. We define the quantities M_i^c and $\underline{\mathbf{E}}_i^c$ by

$$M_i^c = \mathbf{D}_i^c \cdot \mathbf{D}_i^c, \quad \text{and} \quad \underline{\mathbf{E}}_i^c = (M_i^c)^{-1} \mathbf{D}_i^c \otimes \mathbf{D}_i^c. \quad (6.5)$$

As $\underline{\Gamma}^c$ is symmetric, the eigenvectors \mathbf{D}_i^c are orthogonal and the spectral decomposition of the Christoffel tensor $\underline{\Gamma}^c$ can be given as:

$$\underline{\Gamma}^c = \sum_{i=1}^3 L_i^c \underline{\mathbf{E}}_i^c \quad \text{with} \quad \underline{\mathbf{I}} = \sum_{i=1}^3 \underline{\mathbf{E}}_i^c \quad (6.6)$$

where $\underline{\mathbf{I}} \in \mathcal{L}_s(\mathbb{R}^3)$ is the identity tensor.

Similarly, consider $\underline{\Gamma}^v$ the Christoffel tensor associated with $\underline{\mathbf{V}}$ and define the quantities L_i^v , \mathbf{D}_i^v , M_i^v and $\underline{\mathbf{E}}_i^v$ analogously such that

$$\underline{\Gamma}^v = \sum_{i=1}^3 L_i^v \underline{\mathbf{E}}_i^v \quad \text{with} \quad \underline{\mathbf{I}} = \sum_{i=1}^3 \underline{\mathbf{E}}_i^v. \quad (6.7)$$

We assume that the tensors $\underline{\Gamma}^c$ and $\underline{\Gamma}^v$ have the same structure in the sense that the eigenvectors \mathbf{D}_i^c and \mathbf{D}_i^v are equal (see Remark 6.3.3). In the sequel, we use \mathbf{D} instead of \mathbf{D}^c or \mathbf{D}^v and similar for $\underline{\mathbf{E}}$ and M , by abuse of notation.

6.2.3 CHAPTER OUTLINE

The aim of this work is to compute the elastodynamic Green function $\underline{\mathbf{G}}$ associated to viscoelastic wave equation (6.4). More precisely, $\underline{\mathbf{G}}$ is the solution of the equation

$$\left(\underline{\Gamma}^c [\nabla_x] \underline{\mathbf{G}}(\mathbf{x}, t) + \underline{\Gamma}^v [\nabla_x] \mathcal{A}[\underline{\mathbf{G}}](\mathbf{x}, t) \right) - \rho \frac{\partial^2 \underline{\mathbf{G}}(\mathbf{x}, t)}{\partial t^2} = \delta(t) \delta(\mathbf{x}) \underline{\mathbf{I}}, \quad (6.8)$$

The idea is to use the spectral decomposition of $\underline{\mathbf{G}}$ of the form

$$\underline{\mathbf{G}} = \sum_{i=1}^3 \underline{\mathbf{E}}_i (\nabla_x) \phi_i = \sum_{i=1}^3 (\mathbf{D}_i \otimes \mathbf{D}_i) M_i^{-1} \phi_i, \quad (6.9)$$

where ϕ_i are three scalar functions satisfying

$$\left(L_i^c (\nabla_x) \phi_i + L_i^v (\nabla_x) \mathcal{A}[\phi_i] \right) - \rho \frac{\partial^2 \phi_i}{\partial t^2} = \delta(t) \delta(\mathbf{x}). \quad (6.10)$$

We refer to Appendix 6.A for a brief description of this decomposition and [42] for a complete analysis.

Therefore, to obtain an expression of $\underline{\mathbf{G}}$, we need to

- 1- solve three partial differential equations (6.10) in ϕ_i
- 2- solve subsequent equations

$$\psi_i = M_i^{-1} \phi_i \quad (6.11)$$

3- calculate second order derivatives of ψ_i in order to compute

$$(\mathbf{D}_i \otimes \mathbf{D}_i)\psi_i$$

In the following section, we give simple examples of anisotropic media which satisfy some restrictive properties (including $\mathbf{D}^c = \mathbf{D}^v$) and assumptions (see Subsection 6.3.4.2) defining the limits of our approach. In Section 6.4, we derive the solutions ϕ_i of equations (6.10). In Section 6.5, we give an explicit resolution of $\psi_i = M_i^{-1}\phi_i$ and $(\mathbf{D}_i \otimes \mathbf{D}_i)\psi_i$. Finally, in the last section, we compute the Green functions for three simple anisotropic media.

6.3 SOME SIMPLE ANISOTROPIC VISCOELASTIC MEDIA

In this section, we present three viscoelastic media with simple type of anisotropy. We also describe some important properties of the media and our basic assumptions in this chapter.

DEFINITION 6.3.1. We will call a tensor $\underline{\mathbf{c}} = (c_{mn}) \in \mathcal{L}_s(\mathbb{R}^6)$ the Voigt representation of an order four tensor $\underline{\underline{\mathbf{C}}} \in \mathcal{L}_s^2(\mathbb{R}^3)$ if

$$c_{mn} = c_{p(i,j)p(k,l)} = C_{ijkl} \quad 1 \leq i, j, k, l \leq 3$$

where

$$p(i, i) = i, \quad p(i, j) = p(j, i), \quad p(2, 3) = 4, \quad p(1, 3) = 5, \quad p(1, 2) = 6.$$

We will use $\underline{\mathbf{c}}$ and $\underline{\mathbf{v}}$ for the Voigt representations of stiffness tensor $\underline{\underline{\mathbf{C}}}$ and viscosity tensor $\underline{\underline{\mathbf{V}}}$ respectively and let $\underline{\mathbf{c}}$ and $\underline{\mathbf{v}}$ to have a same structure. For each media, the expressions for $\underline{\Gamma}^c$, $L_i^c(\nabla_x)$, $\mathbf{D}_i^c(\nabla_x)$ and $M_i^c(\nabla_x)$ are provided [42, 138]. Throughout this section, μ_{pq} will assume the value c_{pq} for $\underline{\mathbf{c}}$ and v_{pq} for $\underline{\mathbf{v}}$ where the subscripts $p, q \in \{1, 2, \dots, 6\}$. Moreover, we assume that the axes of the material are identical with the Cartesian coordinate axes $\mathbf{e}_1, \mathbf{e}_2$ and \mathbf{e}_3 and $\partial_i = \frac{\partial}{\partial x_i}$.

6.3.1 MEDIUM I

First medium for which we present a closed form elastodynamic Green function is an orthorhombic medium with the tensors $\underline{\mathbf{c}}$ and $\underline{\mathbf{v}}$ of the form:

$$\begin{pmatrix} \mu_{11} & -\mu_{66} & -\mu_{55} & 0 & 0 & 0 \\ -\mu_{66} & \mu_{22} & -\mu_{44} & 0 & 0 & 0 \\ -\mu_{55} & -\mu_{44} & \mu_{33} & 0 & 0 & 0 \\ 0 & 0 & 0 & \mu_{44} & 0 & 0 \\ 0 & 0 & 0 & 0 & \mu_{55} & 0 \\ 0 & 0 & 0 & 0 & 0 & \mu_{66} \end{pmatrix}$$

The Christoffel tensor is given by

$$\underline{\Gamma}^c = \begin{pmatrix} c_{11}\partial_1^2 + c_{66}\partial_2^2 + c_{55}\partial_3^2 & 0 & 0 \\ 0 & c_{66}\partial_1^2 + c_{22}\partial_2^2 + c_{44}\partial_3^2 & 0 \\ 0 & 0 & c_{55}\partial_1^2 + c_{44}\partial_2^2 + c_{33}\partial_3^2 \end{pmatrix}$$

Its eigenvalues $L_i^c(\nabla_x)$ and the associated eigenvectors $\mathbf{D}_i^c(\nabla_x)$ are:

$$L_1^c(\nabla_x) = c_{11}\partial_1^2 + c_{66}\partial_2^2 + c_{55}\partial_3^2$$

$$L_2^c(\nabla_x) = c_{66}\partial_1^2 + c_{22}\partial_2^2 + c_{44}\partial_3^2$$

$$L_3^c(\nabla_x) = c_{55}\partial_1^2 + c_{44}\partial_2^2 + c_{33}\partial_3^2$$

$$\mathbf{D}_i^c = \mathbf{e}_i \quad \text{with} \quad M_i^c = 1 \quad \forall i = 1, 2, 3$$

6.3.2 MEDIUM II

Second medium which we consider is a transversely isotropic medium having symmetry axis along \mathbf{e}_3 and defined by the stiffness and the viscosity tensors $\underline{\mathbf{c}}$ and $\underline{\mathbf{v}}$ of the form:

$$\begin{pmatrix} \mu_{11} & \mu_{12} & -\mu_{44} & 0 & 0 & 0 \\ \mu_{12} & \mu_{11} & -\mu_{44} & 0 & 0 & 0 \\ -\mu_{44} & -\mu_{44} & \mu_{33} & 0 & 0 & 0 \\ 0 & 0 & 0 & \mu_{44} & 0 & 0 \\ 0 & 0 & 0 & 0 & \mu_{44} & 0 \\ 0 & 0 & 0 & 0 & 0 & \mu_{66} \end{pmatrix}$$

with $\mu_{66} = (\mu_{11} - \mu_{12})/2$. Here

$$\underline{\Gamma}^c = \begin{pmatrix} c_{11}\partial_1^2 + c_{66}\partial_2^2 + c_{44}\partial_3^2 & (c_{11} - c_{66})\partial_1\partial_2 & 0 \\ (c_{11} - c_{66})\partial_1\partial_2 & c_{66}\partial_1^2 + c_{11}\partial_2^2 + c_{44}\partial_3^2 & 0 \\ 0 & 0 & c_{44}\partial_1^2 + c_{44}\partial_2^2 + c_{33}\partial_3^2 \end{pmatrix}$$

The eigenvalues $L_i^c(\nabla_x)$ of $\underline{\Gamma}^c(\nabla_x)$ in this case are

$$L_1^c(\nabla_x) = c_{44}\partial_1^2 + c_{44}\partial_2^2 + c_{33}\partial_3^2$$

$$L_2^c(\nabla_x) = c_{11}\partial_1^2 + c_{11}\partial_2^2 + c_{44}\partial_3^2$$

$$L_3^c(\nabla_x) = c_{66}\partial_1^2 + c_{66}\partial_2^2 + c_{44}\partial_3^2$$

and the associated eigenvectors $\mathbf{D}_i^c(\nabla_x)$ are:

$$\mathbf{D}_1^c = \begin{pmatrix} 0 \\ 0 \\ 1 \end{pmatrix}, \quad \mathbf{D}_2^c = \begin{pmatrix} \partial_1 \\ \partial_2 \\ 0 \end{pmatrix}, \quad \mathbf{D}_3^c = \begin{pmatrix} \partial_2 \\ -\partial_1 \\ 0 \end{pmatrix}.$$

Thus $M_1^c = 1$, and $M_2^c = M_3^c = \partial_1^2 + \partial_2^2$

6.3.3 MEDIUM III

Finally, we will present the elastodynamic Green function for another transversely isotropic media with the axis of symmetry along \mathbf{e}_3 and having $\underline{\mathbf{c}}$ and $\underline{\mathbf{v}}$ of the form:

$$\begin{pmatrix} \mu_{11} & \mu_{11} - 2\mu_{66} & \mu_{11} - 2\mu_{44} & 0 & 0 & 0 \\ \mu_{11} - 2\mu_{66} & \mu_{11} & \mu_{11} - 2\mu_{44} & 0 & 0 & 0 \\ \mu_{11} - 2\mu_{44} & \mu_{11} - 2\mu_{44} & \mu_{11} & 0 & 0 & 0 \\ 0 & 0 & 0 & \mu_{44} & 0 & 0 \\ 0 & 0 & 0 & 0 & \mu_{44} & 0 \\ 0 & 0 & 0 & 0 & 0 & \mu_{66} \end{pmatrix}$$

The Christoffel tensor in this case is

$$\underline{\Gamma}^c = \begin{pmatrix} c_{11}\partial_1^2 + c_{66}\partial_2^2 + c_{44}\partial_3^2 & (c_{11} - c_{66})\partial_1\partial_2 & (c_{11} - c_{44})\partial_1\partial_3 \\ (c_{11} - c_{66})\partial_1\partial_2 & c_{66}\partial_1^2 + c_{11}\partial_2^2 + c_{44}\partial_3^2 & (c_{11} - c_{44})\partial_2\partial_3 \\ (c_{11} - c_{44})\partial_1\partial_3 & (c_{11} - c_{44})\partial_2\partial_3 & c_{44}\partial_1^2 + c_{44}\partial_2^2 + c_{11}\partial_3^2 \end{pmatrix}$$

Its eigenvalues $L_i^c(\nabla_x)$ are:

$$\begin{aligned} L_1^c(\nabla_x) &= c_{11}\partial_1^2 + c_{11}\partial_2^2 + c_{11}\partial_3^2 = c_{11}\Delta_x \\ L_2^c(\nabla_x) &= c_{66}\partial_1^2 + c_{66}\partial_2^2 + c_{44}\partial_3^2 \\ L_3^c(\nabla_x) &= c_{44}\partial_1^2 + c_{44}\partial_2^2 + c_{44}\partial_3^2 = c_{44}\Delta_x \end{aligned}$$

and the eigenvectors $\mathbf{D}_i^c(\nabla_x)$ are:

$$\mathbf{D}_1^c = \begin{pmatrix} \partial_1 \\ \partial_2 \\ \partial_3 \end{pmatrix}, \quad \mathbf{D}_2^c = \begin{pmatrix} \partial_2 \\ -\partial_1 \\ 0 \end{pmatrix}, \quad \mathbf{D}_3^c = \begin{pmatrix} -\partial_1\partial_3 \\ -\partial_2\partial_3 \\ \partial_1^2 + \partial_2^2 \end{pmatrix} \quad (6.12)$$

In this case, $M_1^c = \Delta_x$, $M_2^c = \partial_1^2 + \partial_2^2$ and $M_3^c = (\partial_1^2 + \partial_2^2)\Delta_x$

6.3.4 PROPERTIES OF THE MEDIA AND MAIN ASSUMPTIONS

6.3.4.1 PROPERTIES

In all anisotropic media discussed above, it holds that

- The Christoffel tensors $\underline{\Gamma}^c$ and $\underline{\Gamma}^v$ have the same structure in the sense that

$$\mathbf{D}_i^c = \mathbf{D}_i^v, \quad \forall i = 1, 2, 3.$$

- The eigenvalues $L_i^c(\nabla_x)$ are homogeneous quadratic forms in the components of the argument vector ∇_x *i.e.*

$$L_i^c[\nabla_x] = \sum_j^3 a_{ij}^2 \frac{\partial^2}{\partial x_j^2},$$

and therefore equations (6.10) are actually scalar wave equations.

- In all the concerning cases (see Remark 6.3.2), the operator $M_i^c(\nabla_x)$ is either constant or has a homogeneous quadratic form

$$M_i^c = \sum_j^3 m_{ij}^2 \frac{\partial^2}{\partial x_j^2}.$$

6.3.4.2 ASSUMPTIONS

In addition, we assume that

- the eigenvalues of $\underline{\Gamma}^c$ and $\underline{\Gamma}^v$ satisfy

$$L_i^v(\nabla_x) = \beta_i L_i^c(\nabla_x). \quad (6.13)$$

- and the loss per wavelength is small, i.e.

$$\beta_i \ll 1, \quad \forall i = 1, 2, 3. \quad (6.14)$$

REMARK 6.3.2. The expression $M_3^c = (\partial_1^2 + \partial_2^2)\Delta_x$ will be avoided in the construction of the Green function by using the expression

$$\underline{\mathbf{G}} = \phi_3 \underline{\mathbf{I}} + \underline{\mathbf{E}}_1(\nabla_x)(\phi_1 - \phi_3) + \underline{\mathbf{E}}_2(\nabla_x)(\phi_2 - \phi_3).$$

REMARK 6.3.3. In general, \mathbf{D}_i^c and \mathbf{D}_i^v are dependent on the parameters c_{pq} and v_{pq} . Consequently, $\underline{\Gamma}^c$ and $\underline{\Gamma}^v$ cannot be diagonalized simultaneously. However, in certain restrictive cases where the polarization directions of different wave modes (i.e. quasi longitudinal (qP) and quasi shear waves (qSH and qSV)) are independent of the stiffness or viscosity parameters, it is possible to diagonalize both $\underline{\Gamma}^c$ and $\underline{\Gamma}^v$ simultaneously. In fact, it is the case for each one of the media presented above.

The assumption on the eigenvalues L_i^v and L_i^c , implies that for a given wave mode, its velocity decays uniformly in all direction (i.e. velocity dissipation is isotropic), but for different wave modes (qP, qSH and qSV) the decay rates are different.

6.4 RESOLUTION OF THE MODEL WAVE PROBLEM

Let us now study the scalar wave problems (6.10). We consider a model problem and drop the subscript for brevity in this section as well as in the next section. Consider

$$\left(L^c[\nabla_x]\phi + L^v[\nabla_x]\mathcal{A}[\phi] \right) - \rho \frac{\partial^2 \phi}{\partial t^2} = \delta(t)\delta(\mathbf{x}). \quad (6.15)$$

Our assumptions on the media imply that L^c and L^v have the following form;

$$L^c[\nabla_x] = \sum_{j=1}^3 a_j^2 \frac{\partial^2}{\partial x_j^2} \quad \text{and} \quad L^v[\nabla_x] = \beta L^c[\nabla_x] = \sum_{j=1}^3 \beta a_j^2 \frac{\partial^2}{\partial x_j^2}$$

Therefore, the model equation (6.15) can be rewritten as:

$$\sum_{j=1}^3 \left(a_j^2 \frac{\partial^2 \phi}{\partial x_j^2} + \beta a_j^2 \mathcal{A} \left[\frac{\partial^2 \phi}{\partial x_j^2} \right] \right) - \rho \frac{\partial^2 \phi}{\partial t^2} = \delta(t) \delta(\mathbf{x}),$$

By a change of variables $x_j = \frac{a_j}{\sqrt{\rho}} \xi_j$, we obtain in function $\tilde{\phi}(\xi) = \phi(\mathbf{x})$ the following transformed equation :

$$\Delta_\xi \tilde{\phi} + \beta \mathcal{A} [\Delta_\xi \tilde{\phi}] - \frac{\partial^2 \tilde{\phi}}{\partial t^2} = \frac{\sqrt{\rho}}{a} \delta(t) \delta(\xi). \quad (6.16)$$

where the constant $a = |a_1 a_2 a_3|$.

Now, we apply \mathcal{A} on both sides of the equation (6.16), and replace the resulting expression for $\mathcal{A} [\Delta_\xi \tilde{\phi}]$ back into the equation (6.16). This yields:

$$\Delta_\xi \tilde{\phi} + \beta \mathcal{A} \left[\frac{\partial^2 \tilde{\phi}}{\partial t^2} \right] - \beta^2 \mathcal{A}^2 [\Delta_\xi \tilde{\phi}] - \frac{\partial^2 \tilde{\phi}}{\partial t^2} = \frac{\sqrt{\rho}}{a} \delta(\xi) \{ \delta(t) - \beta \mathcal{A} [\delta(t)] \}.$$

Recall that $\beta \ll 1$ and the term in β^2 is negligible; see Subsection 6.3.4.2. Therefore, it holds

$$\Delta_\xi \tilde{\phi} + \beta \mathcal{A} \left[\frac{\partial^2 \tilde{\phi}}{\partial t^2} \right] - \frac{\partial^2 \tilde{\phi}}{\partial t^2} \simeq \frac{\sqrt{\rho}}{a} \delta(\xi) \{ \delta(t) - \beta \mathcal{A} [\delta(t)] \}. \quad (6.17)$$

Finally, taking temporal Fourier transform on both sides of (6.17), we obtain the corresponding Helmholtz equation:

$$\Delta_\xi \tilde{\Phi} + \omega^2 (1 - \beta \widehat{\mathcal{A}}(\omega)) \tilde{\Phi} = (1 - \beta \widehat{\mathcal{A}}(\omega)) \frac{\sqrt{\rho}}{a} \delta(\xi) \quad (6.18)$$

where $\tilde{\Phi}(\xi, \omega)$ and $\widehat{\mathcal{A}}(\omega)$ are the Fourier transforms of $\tilde{\phi}(\xi, t)$ and the kernel of the convolution operator \mathcal{A} respectively. Let

$$\kappa(\omega) = \sqrt{\omega^2 (1 - \beta \widehat{\mathcal{A}}(\omega))}.$$

Then the solution of the Helmholtz equation (6.18) (see for instance [53, 98]) is expressed as

$$\Phi(\mathbf{x}, \omega) = \sqrt{\rho} (1 - \beta \widehat{\mathcal{A}}(\omega)) \frac{\exp \{ \sqrt{-1} \kappa(\omega) \tau(\mathbf{x}) \}}{4 a \pi \tau(\mathbf{x})}.$$

where

$$\tau(\mathbf{x}) = \sqrt{\rho} \sqrt{\frac{x_1^2}{a_1^2} + \frac{x_2^2}{a_2^2} + \frac{x_3^2}{a_3^2}}$$

Using density normalized constants $b_j = \frac{a_j}{\sqrt{\rho}}$, we have

$$\Phi(\mathbf{x}, \omega) = (1 - \beta \widehat{\mathcal{A}}(\omega)) \frac{\exp \{ \sqrt{-1} \kappa(\omega) \tau(\mathbf{x}) \}}{4 b \rho \pi \tau(\mathbf{x})}. \quad (6.19)$$

where constant $b = |b_1 b_2 b_3|$ and

$$\tau(\mathbf{x}) = \sqrt{\frac{x_1^2}{b_1^2} + \frac{x_2^2}{b_2^2} + \frac{x_3^2}{b_3^2}}$$

6.5 RESOLUTION OF THE MODEL POTENTIAL PROBLEM

In this section, we find the solution of equation (6.11). We once again proceed with a model problem. Once the solution is obtained, we will aim to calculate its second order derivatives in order to evaluate $\mathbf{D} \otimes \mathbf{D}\psi$.

6.5.1 THE POTENTIAL PROBLEM

Let $\psi(\mathbf{x}, t)$, be the solution of equation (6.11) and $\Psi(\mathbf{x}, \omega)$ be its Fourier transform. Then $\Psi(\mathbf{x}, \omega)$ satisfies,

$$M\Psi(\mathbf{x}, \omega) = \Phi(\mathbf{x}, \omega) = \left(1 - \beta\widehat{\mathcal{A}}(\omega)\right) \frac{\exp\{\sqrt{-1}\kappa(\omega)\tau(\mathbf{x})\}}{4b\rho\pi\tau(\mathbf{x})}. \quad (6.20)$$

When M is constant, the solution of this equation is directly calculated. As $M = (\partial_1^2 + \partial_2^2)\Delta_x$ will not be used in the construction of Green function (see Remark 6.3.4.2), we are only interested in the case where M is a homogeneous quadratic form in the component of ∇_x , that is

$$M = \sum_{j=1}^3 m_j^2 \frac{\partial^2}{\partial x_j^2}.$$

So, the model equation (6.20) can be rewritten as:

$$\sum_{j=1}^3 m_j^2 \frac{\partial^2 \Psi}{\partial x_j^2} = \left(1 - \beta\widehat{\mathcal{A}}(\omega)\right) \frac{\exp\{\sqrt{-1}\kappa(\omega)\tau(\mathbf{x})\}}{4b\rho\pi\tau(\mathbf{x})} \quad m_j \neq 0, \quad \forall j \quad (6.21)$$

By a change of variables $x_j = m_j \eta_j$, equation (6.21) becomes Poisson equation in $\bar{\Psi}(\eta, \omega) = \Psi(\mathbf{x}, \omega)$ *i.e.*

$$\Delta_\eta \bar{\Psi} = \left(1 - \beta\widehat{\mathcal{A}}(\omega)\right) \frac{\exp\{\sqrt{-1}\kappa(\omega)\bar{\tau}(\eta)\}}{4b\rho\pi\bar{\tau}(\eta)} = \bar{\Phi}(\eta, \omega) \quad (6.22)$$

where,

$$\bar{\tau}(\eta) = \sqrt{\frac{m_1^2 \eta_1^2}{b_1^2} + \frac{m_2^2 \eta_2^2}{b_2^2} + \frac{m_3^2 \eta_3^2}{b_3^2}} = \tau(\mathbf{x}) \quad \text{and} \quad \bar{\Phi}(\eta, \omega) = \Phi(\mathbf{x}, \omega)$$

Notice that the source $\bar{\Phi}(\eta, \omega)$ is symmetric with respect to ellipsoid $\bar{\tau}$, *i.e.*

$$\bar{\Phi}(\eta, \omega) = \bar{\Phi}(\bar{\tau}, \omega).$$

Therefore, the solution $\bar{\Psi}$ of the Poisson equation (6.22) is the potential field of a uniformly charged ellipsoid due to a charge density $\bar{\Phi}(\bar{\tau}, \omega)$. The potential field $\bar{\Psi}$ can be calculated with a classical approach using ellipsoidal coordinates. See, for instance, [50, 80] for the theory of potential problems in ellipsoidal coordinates.

For the solution of the Poisson equation (6.22) we recall following result from [80, Ch. 7, Sec.6].

PROPOSITION 6.5.1. *Let*

$$f(z) = \sum_{j=1}^3 \frac{\zeta_j^2}{(\alpha_j h)^2 + z} - 1 \quad \text{and} \quad g(z) = \prod_{j=1}^3 [(\alpha_j h)^2 + z]$$

and let $Z(h, \zeta)$ be the largest algebraic root of $f(z)g(z) = 0$. Then the solution of the Poisson equation

$$\Delta^2 Y(\zeta) = 4\pi\chi \left(\frac{\zeta_1^2}{\alpha_1^2} + \frac{\zeta_2^2}{\alpha_2^2} + \frac{\zeta_3^2}{\alpha_3^2} \right) \quad \zeta \in \mathbb{R}^3, \quad \alpha_1, \alpha_2, \alpha_3 > 0,$$

is given by

$$Y(\zeta) = 2\pi\alpha_1\alpha_2\alpha_3 \int_0^\infty \chi(h)I(h, \zeta)dh.$$

with kernel $I(h, \zeta)$ given by

$$I(h, \zeta) = \begin{cases} h^2 \int_{Z(h, \zeta)}^\infty \frac{1}{\sqrt{g(z)}} dz, & Z > 0 \\ h^2 \int_0^\infty \frac{1}{\sqrt{g(z)}} dz, & Z < 0 \end{cases}$$

Hence, the solution of equation (6.22) can be given as

$$\bar{\Psi}(\eta, \omega) = \frac{2\pi b}{m} \left(1 - \beta \widehat{\mathcal{A}}(\omega)\right) \frac{1}{4\pi} \int_0^\infty \frac{\exp\{\sqrt{-1}\kappa(\omega)h\}}{4b\rho\pi h} I(h, \eta)dh$$

or equivalently,

$$\Psi(\mathbf{x}, \omega) = \frac{1}{8\rho\pi m} \left(1 - \beta \widehat{\mathcal{A}}(\omega)\right) \int_0^\infty \frac{\exp\{\sqrt{-1}\kappa(\omega)h\}}{h} I(h, \mathbf{x})dh, \quad m = m_1 m_2 m_3. \quad (6.23)$$

By the change of variable $s = h^{-2}z$, we can write $I(h, \mathbf{x})$ as:

$$I(h, \mathbf{x}) = \begin{cases} mh \int_{S(h, \mathbf{x})}^\infty \frac{1}{\sqrt{G(s)}} ds, & h < \tau \\ mh \int_0^\infty \frac{1}{\sqrt{G(s)}} ds, & h > \tau \end{cases} \quad (6.24)$$

with $S(h, \mathbf{x}) = h^{-2}Z(h, \mathbf{x})$ being the largest algebraic root of the equation

$$F(s)G(s) = 0$$

where

$$\begin{cases} F(s) = h^2 f(h^2 s) = \sum_{j=1}^3 \{V_j(s)\}^{-1} x_j^2 - h^2 \\ G(s) = \frac{m^2}{h^6} g(h^2 s) = \prod_{j=1}^3 \{V_j(s)\} \\ \text{with } V_j(s) = b_j^2 + m_j^2 s \end{cases} \quad (6.25)$$

REMARK 6.5.2. Note that, $F(s) \equiv 0$ corresponds to a set of confocal ellipsoids

$$s \mapsto h^2(s) = \sum_{j=1}^3 \{V_j(s)\}^{-1} x_j^2 \quad (6.26)$$

such that $\tau(\mathbf{x}) = h(0)$ i.e. $S(\tau) = 0$. Moreover, $S > 0$ if the ellipsoid h lies inside τ and $S < 0$ if the ellipsoid h lies outside τ .

6.5.2 DERIVATIVES OF THE POTENTIAL FIELD

In this subsection, we compute the derivatives of the potential Ψ . We note that $I(h, \mathbf{x})$ is constant with respect to \mathbf{x} when $h > \tau$. So,

$$\frac{\partial I(h, \mathbf{x})}{\partial x_k} = \begin{cases} -mh \frac{\partial S(h, \mathbf{x})}{\partial x_k} \frac{1}{\sqrt{G(S(h, \mathbf{x}))}}, & h < \tau \\ 0, & h > \tau \end{cases}$$

for $k = 1, 2, 3$ and by consequence,

$$\frac{\partial \Psi}{\partial x_k} = -\frac{1}{8\rho\pi m} (1 - \beta \widehat{\mathcal{A}}(\omega)) \int_0^\infty \frac{\exp\{\sqrt{-1}\kappa(\omega)h\}}{h} \frac{\partial I(h, \mathbf{x})}{\partial x_k} dh$$

or

$$\frac{\partial \Psi}{\partial x_k} = -\frac{1}{8\rho\pi} (1 - \beta \widehat{\mathcal{A}}(\omega)) \int_0^\tau \left[\exp\{\sqrt{-1}\kappa(\omega)h\} \right] \frac{\partial S(h, \mathbf{x})}{\partial x_k} \frac{1}{\sqrt{G(S(h, \mathbf{x}))}} dh. \quad (6.27)$$

Now, we apply $\frac{\partial}{\partial x_l}$ for $l = 1, 2, 3$ on (6.27) to obtain the second order derivatives of Ψ :

$$\begin{aligned} -8\rho\pi \frac{\partial^2 \Psi}{\partial x_k \partial x_l} &= (1 - \beta \widehat{\mathcal{A}}(\omega)) \frac{\partial}{\partial x_l} \left[\int_0^\tau \left[\exp\{\sqrt{-1}\kappa(\omega)h\} \right] \frac{\partial S}{\partial x_k} \frac{1}{\sqrt{G(S)}} dh \right] \\ &= (1 - \beta \widehat{\mathcal{A}}(\omega)) \frac{\partial \tau}{\partial x_l} \left\{ \left[\exp\{\sqrt{-1}\kappa(\omega)\tau\} \right] \frac{\partial S(\tau)}{\partial x_k} \frac{1}{\sqrt{G(S(\tau))}} \right\} \\ &\quad + (1 - \beta \widehat{\mathcal{A}}(\omega)) \int_0^\tau \left[\exp\{\sqrt{-1}\kappa(\omega)h\} \right] \\ &\quad \times \frac{1}{\sqrt{G(S)}} \left\{ \frac{\partial^2 S}{\partial x_k \partial x_l} - \frac{1}{2} \frac{\partial S}{\partial x_k} \frac{\partial S}{\partial x_l} \frac{G'(S)}{G(S)} \right\} dh \end{aligned}$$

As $F(S)G(S) = 0$ and $G(s)$ is normally non-zero on S , by differentiating $F(S) = 0$, we obtain [42, Eq.s (5.21)-(5.23)]

$$\frac{\partial S}{\partial x_k} = -\frac{2x_k}{V_k(S)F'(S)} \quad (6.28)$$

$$\frac{\partial^2 S}{\partial x_k \partial x_l} = -\frac{4x_k x_l}{V_k(S)V_l(S)[F'(S)]^2} \left\{ \frac{F''(S)}{F'(S)} + \frac{m_k^2}{V_k(S)} + \frac{m_l^2}{V_l(S)} \right\} - \frac{2\delta_{kl}}{V_k(S)F'(S)} \quad (6.29)$$

where,

$$F'(s) = -\sum_{j=1}^3 \frac{m_j^2 x_j^2}{V_j^2(s)}, \quad F''(s) = \sum_{j=1}^3 \frac{2m_j^4 x_j^2}{V_j^3(s)}, \quad G'(s) = G(s) \sum_{j=1}^3 \frac{m_j^2}{V_j(s)} \quad (6.30)$$

and prime represents a derivative with respect to variable s .

Substituting the values from (6.28) and (6.29), the second order derivative of Ψ becomes:

$$\begin{aligned} 4\rho\pi \frac{\partial^2 \Psi}{\partial x_k \partial x_l} &= \left(1 - \beta \widehat{\mathcal{A}}(\omega)\right) \int_0^\tau \left[\exp\{\sqrt{-1}\kappa(\omega)h\} \right] \frac{1}{F'(S)\sqrt{G(S)}} \\ &\times \left[\frac{2x_k x_l}{V_k(S)V_l(S)F'(S)} \left\{ \frac{F''(S)}{F'(S)} + \frac{m_k^2}{V_k(S)} + \frac{m_l^2}{V_l(S)} + \frac{1}{2} \frac{G'(S)}{G(S)} \right\} + \frac{\delta_{kl}}{V_k(S)} \right] dh \\ &- \frac{x_k x_l \left(1 - \beta \widehat{\mathcal{A}}(\omega)\right)}{aa_k^2 a_l^2 F'(0)} \left\{ \frac{\exp\{\sqrt{-1}\kappa(\omega)\tau\}}{\tau} \right\}. \end{aligned} \quad (6.31)$$

REMARK 6.5.3. *If for some $i \in \{1, 2, 3\}$, $m_i \rightarrow 0$ one semi axis of the ellipsoid τ tends to infinity but no singularity occurs and the results of this section stay valid in that case [42].*

6.6 ELASTODYNAMIC GREEN FUNCTION

In this section we present the expressions for the elastodynamic Green functions for the media presented in Section 6.3. Throughout this section $c_p = \sqrt{\frac{c_{pp}}{\rho}}$ with $p \in \{1, 2, \dots, 6\}$. We recall that $\kappa_i(\omega) = \sqrt{\omega^2 \left(1 - \beta_i \widehat{\mathcal{A}}(\omega)\right)}$.

6.6.1 MEDIUM I

All the eigenvectors of $\underline{\Gamma}$ are constants in this case *i.e.* $\mathbf{D}_i = \mathbf{e}_i$, therefore $M_i = 1$ and $\underline{\mathbf{E}}_i = \mathbf{e}_i \otimes \mathbf{e}_i$. If $\widehat{\mathbf{G}}$ is the Fourier transform of the viscoelastic Green function $\underline{\mathbf{G}}$

with respect to variable t , then:

$$\begin{aligned}\widehat{\mathbf{G}}(\mathbf{x}, \omega) &= \sum_{i=1}^3 \Phi_i(x, \omega) \mathbf{e}_i \otimes \mathbf{e}_i \\ &= \frac{1}{4\pi\rho} \sum_{i=1}^3 \left[\frac{c_{i+3} (1 - \beta_i \widehat{\mathcal{A}}(\omega))}{c_i c_4 c_5 c_6 \tau_i} \exp(\sqrt{-1} \kappa_i(\omega) \tau_i) \right] \mathbf{e}_i \otimes \mathbf{e}_i\end{aligned}\quad (6.32)$$

where

$$\tau_1 = \sqrt{\frac{x_1^2}{c_1^2} + \frac{x_2^2}{c_6^2} + \frac{x_3^2}{c_5^2}}, \quad \tau_2 = \sqrt{\frac{x_1^2}{c_6^2} + \frac{x_2^2}{c_2^2} + \frac{x_3^2}{c_4^2}}, \quad \tau_3 = \sqrt{\frac{x_1^2}{c_5^2} + \frac{x_2^2}{c_4^2} + \frac{x_3^2}{c_3^2}}.$$

6.6.2 MEDIUM II

According to Section 6.4, the functions Φ_i , $i = 1, 2, 3$ have following expressions:

$$\Phi_1(\mathbf{x}, \omega) = (1 - \beta_1 \widehat{\mathcal{A}}(\omega)) \frac{\exp\{\sqrt{-1} \kappa_1(\omega) \tau_1(\mathbf{x})\}}{4c_4^2 c_3 \rho \pi \tau_1(\mathbf{x})}$$

$$\Phi_2(\mathbf{x}, \omega) = (1 - \beta_2 \widehat{\mathcal{A}}(\omega)) \frac{\exp\{\sqrt{-1} \kappa_2(\omega) \tau_2(\mathbf{x})\}}{4c_1^2 c_4 \rho \pi \tau_2(\mathbf{x})}$$

$$\Phi_3(\mathbf{x}, \omega) = (1 - \beta_3 \widehat{\mathcal{A}}(\omega)) \frac{\exp\{\sqrt{-1} \kappa_3(\omega) \tau_3(\mathbf{x})\}}{4c_6^2 c_4 \rho \pi \tau_3(\mathbf{x})}$$

where

$$\tau_1(\mathbf{x}) = \sqrt{\frac{x_1^2}{c_4^2} + \frac{x_2^2}{c_4^2} + \frac{x_3^2}{c_3^2}}, \quad \tau_2(\mathbf{x}) = \sqrt{\frac{x_1^2}{c_1^2} + \frac{x_2^2}{c_1^2} + \frac{x_3^2}{c_4^2}}, \quad \tau_3(\mathbf{x}) = \sqrt{\frac{x_1^2}{c_6^2} + \frac{x_2^2}{c_6^2} + \frac{x_3^2}{c_4^2}}.$$

Medium	b_1	b_2	b_3	m_1	m_2	m_3	M_i
I	c_1	c_6	c_5	1	0	0	M_1
	c_6	c_2	c_4	0	1	0	M_2
	c_5	c_4	c_3	0	0	1	M_3
II	c_4	c_4	c_3	0	0	1	M_1
	c_1	c_1	c_4	1	1	0	M_2
	c_6	c_6	c_4	*	*	*	M_3
III	c_1	c_1	c_1	1	1	1	M_1
	c_6	c_6	c_4	1	1	0	M_2
	c_4	c_4	c_4	*	*	*	M_3

TABLE 6.1: Values of b_i and m_i for different media. Here * represents a value which is not used for reconstructing Green function.

In order to calculate Green function, we use the expression

$$\widehat{\mathbf{G}}(\mathbf{x}, \omega) = \Phi_3 \mathbf{I} + \mathbf{D}_1 \otimes \mathbf{D}_1 M_1^{-1} (\Phi_1 - \Phi_3) + \mathbf{D}_2 \otimes \mathbf{D}_2 M_2^{-1} (\Phi_2 - \Phi_3).$$

$\mathbf{D}_1 = \mathbf{e}_3$ and $M_1 = 1$, yield

$$\mathbf{D}_1 \otimes \mathbf{D}_1 M_1^{-1} (\Phi_1 - \Phi_3) = (\Phi_1 - \Phi_3) \mathbf{e}_3 \otimes \mathbf{e}_3.$$

In order to compute $\mathbf{D}_2 \otimes \mathbf{D}_2 M_2^{-1} (\Phi_2 - \Phi_3)$, suppose

$$\Psi_2 = M_2^{-1} \Phi_2 \quad \text{and} \quad \Psi_3 = M_2^{-1} \Phi_3,$$

and notice that $m_1 = m_2 = 1$ and $m_3 = 0$. Moreover for Φ_2 and Φ_3 , $b_1 = b_2$; see Table 6.1. Thus, we have

$$\begin{aligned} \frac{4\rho\pi}{(1-\beta_2\widehat{\mathcal{A}}(\omega))} \frac{\partial^2 \Psi_2}{\partial x_k \partial x_l} &= \widehat{\mathbf{R}}_k \widehat{\mathbf{R}}_l \left\{ \frac{\exp\{\sqrt{-1}\kappa_2(\omega)\tau_2\}}{c_1^2 c_4 \tau_2} \right\} \\ &\quad - \frac{1}{c_4 R^2} (\delta_{kl} - 2\widehat{\mathbf{R}}_k \widehat{\mathbf{R}}_l) \int_0^{\tau_2} \left[\exp\{\sqrt{-1}\kappa_2(\omega)h\} \right] dh \\ \frac{4\rho\pi}{(1-\beta_3\widehat{\mathcal{A}}(\omega))} \frac{\partial^2 \Psi_3}{\partial x_k \partial x_l} &= \widehat{\mathbf{R}}_k \widehat{\mathbf{R}}_l \left\{ \frac{\exp\{\sqrt{-1}\kappa_3(\omega)\tau_3\}}{c_6^2 c_4 \tau_3} \right\} \\ &\quad - \frac{1}{c_4 R^2} (\delta_{kl} - 2\widehat{\mathbf{R}}_k \widehat{\mathbf{R}}_l) \int_0^{\tau_3} \left[\exp\{\sqrt{-1}\kappa_3(\omega)h\} \right] dh \end{aligned}$$

where $\widehat{\mathbf{R}}_k = \frac{x_k}{R}$ for $k = 1, 2$. We refer to Appendix 6.C for the derivation of this result.

By using the second derivatives of Ψ_2 and Ψ_3 and the expression

$$\mathbf{D}_2 \otimes \mathbf{D}_2 M_2^{-1} (\Phi_2 - \Phi_3) = \sum_{k,l=1}^2 \partial_k \partial_l (\Psi_2 - \Psi_3) \mathbf{e}_k \otimes \mathbf{e}_l,$$

we finally arrive at

$$\begin{aligned} \widehat{\mathbf{G}}(\mathbf{x}, \omega) &= (1 - \beta_3 \widehat{\mathcal{A}}(\omega)) \frac{\exp\{\sqrt{-1}\kappa_3(\omega)\tau_3(\mathbf{x})\}}{4c_6^2 c_4 \rho \pi \tau_3(\mathbf{x})} \mathbf{I} \\ &\quad + (1 - \beta_1 \widehat{\mathcal{A}}(\omega)) \frac{\exp\{\sqrt{-1}\kappa_1(\omega)\tau_1(\mathbf{x})\}}{4c_4^2 c_3 \rho \pi \tau_1(\mathbf{x})} \mathbf{e}_3 \otimes \mathbf{e}_3 \\ &\quad + \left[(1 - \beta_2 \widehat{\mathcal{A}}(\omega)) \frac{\exp\{\sqrt{-1}\kappa_2(\omega)\tau_2(\mathbf{x})\}}{4c_1^2 c_4 \rho \pi \tau_2(\mathbf{x})} \right. \\ &\quad \quad \left. - (1 - \beta_3 \widehat{\mathcal{A}}(\omega)) \frac{\exp\{\sqrt{-1}\kappa_3(\omega)\tau_3(\mathbf{x})\}}{4c_6^2 c_4 \rho \pi \tau_3(\mathbf{x})} \right] \widehat{\mathbf{R}} \otimes \widehat{\mathbf{R}} \\ &\quad - \frac{1}{4\rho\pi c_4 R^2} \left[(1 - \beta_2 \widehat{\mathcal{A}}(\omega)) \int_0^{\tau_2} \left[\exp\{\sqrt{-1}\kappa_2(\omega)h\} \right] dh \right. \\ &\quad \quad \left. - (1 - \beta_3 \widehat{\mathcal{A}}(\omega)) \int_0^{\tau_3} \left[\exp\{\sqrt{-1}\kappa_3(\omega)h\} \right] dh \right] (\mathbf{I} - 2\widehat{\mathbf{R}} \otimes \widehat{\mathbf{R}}). \end{aligned}$$

Or equivalently,

$$\begin{aligned}\widehat{\mathbf{G}}(\mathbf{x}, \omega) &= \Phi_1 \mathbf{e}_3 \otimes \mathbf{e}_3 + \Phi_2 \widehat{\mathbf{R}} \otimes \widehat{\mathbf{R}} + \Phi_3 (\mathbf{J} - \widehat{\mathbf{R}} \otimes \widehat{\mathbf{R}}) \\ &\quad - \frac{1}{R^2} \left[c_1^2 \int_0^{\tau_2} h \Phi_2(h, \omega) dh - c_6^2 \int_0^{\tau_3} h \Phi_3(h, \omega) dh \right] (\mathbf{J} - 2\widehat{\mathbf{R}} \otimes \widehat{\mathbf{R}}).\end{aligned}$$

Here $\mathbf{J} = \mathbf{I} - \mathbf{e}_3 \otimes \mathbf{e}_3$ and $\widehat{\mathbf{R}} = \widehat{\mathbf{R}}_1 \mathbf{e}_1 + \widehat{\mathbf{R}}_2 \mathbf{e}_2$.

6.6.3 MEDIUM III

The solutions of the wave equation Φ_i , $i = 1, 2, 3$ for Medium III are

$$\begin{aligned}\Phi_1(\mathbf{x}, \omega) &= \left(1 - \beta_1 \widehat{\mathcal{A}}(\omega)\right) \frac{\exp\{\sqrt{-1}\kappa_1(\omega)\tau_1(\mathbf{x})\}}{4c_1^3 \rho \pi \tau_1(\mathbf{x})} \\ \Phi_2(\mathbf{x}, \omega) &= \left(1 - \beta_2 \widehat{\mathcal{A}}(\omega)\right) \frac{\exp\{\sqrt{-1}\kappa_2(\omega)\tau_2(\mathbf{x})\}}{4c_6^2 c_4 \rho \pi \tau_2(\mathbf{x})} \\ \Phi_3(\mathbf{x}, \omega) &= \left(1 - \beta_3 \widehat{\mathcal{A}}(\omega)\right) \frac{\exp\{\sqrt{-1}\kappa_3(\omega)\tau_3(\mathbf{x})\}}{4c_4^3 \rho \pi \tau_3(\mathbf{x})}.\end{aligned}$$

where

$$\tau_1(\mathbf{x}) = \frac{1}{c_1} \sqrt{x_1^2 + x_2^2 + x_3^2} = \frac{r}{c_1}, \quad \tau_2(\mathbf{x}) = \sqrt{\frac{x_1^2}{c_6^2} + \frac{x_2^2}{c_6^2} + \frac{x_3^2}{c_4^2}}, \quad \tau_3(\mathbf{x}) = \frac{r}{c_4}$$

Once again, we use the expression

$$\widehat{\mathbf{G}}(\mathbf{x}, t) = \Phi_3 \mathbf{I} + \mathbf{D}_1 \otimes \mathbf{D}_1 M_1^{-1} (\Phi_1 - \Phi_3) + \mathbf{D}_2 \otimes \mathbf{D}_2 M_2^{-1} (\Phi_2 - \Phi_3).$$

Suppose

$$\Psi_1 = M_1^{-1} \Phi_1 \quad \text{and} \quad \Psi_3 = M_1^{-1} \Phi_3.$$

Notice that $m_1 = m_2 = m_3 = 1$ for M_1 and $b_1 = b_2 = b_3$ for Φ_1 as well as Φ_3 (see Table 6.1). Thus,

$$\begin{aligned}\frac{4\rho\pi}{(1 - \beta_1 \widehat{\mathcal{A}}(\omega))} \frac{\partial^2 \Psi_1}{\partial x_k \partial x_l} &= \widehat{\mathbf{r}}_k \widehat{\mathbf{r}}_l \left\{ \frac{\exp\{\sqrt{-1}\kappa_1(\omega)\tau_1\}}{c_1^3 \tau_1} \right\} \\ &\quad - \frac{1}{r^3} (\delta_{kl} - 3\widehat{\mathbf{r}}_i \widehat{\mathbf{r}}_j) \int_0^{\tau_1} [h \exp\{\sqrt{-1}\kappa_1(\omega)h\}] dh \\ \frac{4\rho\pi}{(1 - \beta_3 \widehat{\mathcal{A}}(\omega))} \frac{\partial^2 \Psi_3}{\partial x_k \partial x_l} &= \widehat{\mathbf{r}}_k \widehat{\mathbf{r}}_l \left\{ \frac{\exp\{\sqrt{-1}\kappa_3(\omega)\tau_1\}}{c_1^3 \tau_3} \right\} \\ &\quad - \frac{1}{r^3} (\delta_{kl} - 3\widehat{\mathbf{r}}_i \widehat{\mathbf{r}}_j) \int_0^{\tau_3} [h \exp\{\sqrt{-1}\kappa_3(\omega)h\}] dh.\end{aligned}$$

We refer to Appendix 6.B for the derivation of this result. It yields

$$\begin{aligned}
\mathbf{D}_1 \otimes \mathbf{D}_1 M_1^{-1} (\Phi_1 - \Phi_3) &= \frac{\hat{\mathbf{r}} \otimes \hat{\mathbf{r}}}{4\rho\pi} \left[\left(1 - \beta_1 \widehat{\mathcal{A}}(\omega)\right) \frac{\exp\{\sqrt{-1}\kappa_1(\omega)\tau_1(\mathbf{x})\}}{c_1^3 \tau_1(\mathbf{x})} \right. \\
&\quad \left. + \left(1 - \beta_3 \widehat{\mathcal{A}}(\omega)\right) \frac{\exp\{\sqrt{-1}\kappa_3(\omega)\tau_3(\mathbf{x})\}}{c_4^3 \tau_3(\mathbf{x})} \right] \\
&\quad - \frac{(\mathbf{I} - 3\hat{\mathbf{r}} \otimes \hat{\mathbf{r}})}{4\rho\pi r^3} \left[\left(1 - \beta_1 \widehat{\mathcal{A}}(\omega)\right) \int_0^{\tau_1} \left[h \exp\{\sqrt{-1}\kappa_1(\omega)h\} \right] dh \right. \\
&\quad \left. - \left(1 - \beta_3 \widehat{\mathcal{A}}(\omega)\right) \int_0^{\tau_3} \left[h \exp\{\sqrt{-1}\kappa_3(\omega)h\} \right] dh \right] \\
&= \hat{\mathbf{r}} \otimes \hat{\mathbf{r}} \left[\Phi_1(\mathbf{x}, \omega) - \Phi_3(\mathbf{x}, \omega) \right] \\
&\quad - \frac{1}{r^3} \left[\int_0^{\tau_1} h^2 \Phi_1(h, \omega) dh - \int_0^{\tau_3} h^2 \Phi_3(h, \omega) dh \right] (\mathbf{I} - 3\hat{\mathbf{r}} \otimes \hat{\mathbf{r}}),
\end{aligned}$$

where $\hat{\mathbf{r}} = \hat{\mathbf{r}}_1 \mathbf{e}_1 + \hat{\mathbf{r}}_2 \mathbf{e}_2 + \hat{\mathbf{r}}_3 \mathbf{e}_3$ with $\hat{\mathbf{r}}_i = \frac{x_i}{r}$ for all $i = 1, 2, 3$.

In order to compute, $\mathbf{D}_2 \otimes \mathbf{D}_2 M_2^{-1} (\Phi_2 - \Phi_3)$, suppose

$$\Psi_2 = M_2^{-1} \Phi_2 \quad \text{and} \quad \Psi_4 = M_2^{-1} \Phi_3.$$

By using formula (6.40) with $m_1 = m_2 = 1$ and $m_3 = 0$, we obtain:

$$\begin{aligned}
\frac{4\rho\pi}{(1 - \beta_2 \widehat{\mathcal{A}}(\omega))} \frac{\partial^2 \Psi_2}{\partial x_k \partial x_l} &= \hat{\mathbf{R}}_k \hat{\mathbf{R}}_l \left\{ \frac{\exp\{\sqrt{-1}\kappa_2(\omega)\tau_2\}}{c_6^2 c_4 \tau_2} \right\} \\
&\quad - \frac{1}{c_4 R^2} (\delta_{kl} - 2\hat{\mathbf{R}}_k \hat{\mathbf{R}}_l) \int_0^{\tau_2} \left[\exp\{\sqrt{-1}\kappa_2(\omega)h\} \right] dh \\
\frac{4\rho\pi}{(1 - \beta_3 \widehat{\mathcal{A}}(\omega))} \frac{\partial^2 \Psi_4}{\partial x_k \partial x_l} &= \hat{\mathbf{R}}_k \hat{\mathbf{R}}_l \left\{ \frac{\exp\{\sqrt{-1}\kappa_3(\omega)\tau_3\}}{c_4^3 \tau_3} \right\} \\
&\quad - \frac{1}{c_4 R^2} (\delta_{kl} - 2\hat{\mathbf{R}}_k \hat{\mathbf{R}}_l) \int_0^{\tau_3} \left[\exp\{\sqrt{-1}\kappa_3(\omega)h\} \right] dh
\end{aligned}$$

with $\widehat{\mathbf{R}}_k = \frac{x_k}{R}$ and $k, l \in \{1, 2\}$. This allows us to write

$$\begin{aligned}
\mathbf{D}_2 \otimes \mathbf{D}_2 M_2^{-1}(\Phi_2 - \Phi_3) &= \frac{1}{4\rho\pi} \left(\widehat{\mathbf{R}}_2^2 \mathbf{e}_1 \otimes \mathbf{e}_1 - \widehat{\mathbf{R}}_1 \widehat{\mathbf{R}}_2 \left[\mathbf{e}_1 \otimes \mathbf{e}_2 + \mathbf{e}_2 \otimes \mathbf{e}_1 \right] + \widehat{\mathbf{R}}_1^2 \mathbf{e}_2 \otimes \mathbf{e}_2 \right) \\
&\quad \times \left[\left(1 - \beta_2 \widehat{\mathcal{A}}(\omega) \right) \frac{\exp \{ \sqrt{-1} \kappa_2(\omega) \tau_2(\mathbf{x}) \}}{c_1^3 \tau_2(\mathbf{x})} \right. \\
&\quad \left. + \left(1 - \beta_3 \widehat{\mathcal{A}}(\omega) \right) \frac{\exp \{ \sqrt{-1} \kappa_3(\omega) \tau_3(\mathbf{x}) \}}{c_4^3 \tau_3(\mathbf{x})} \right] \\
&\quad - \frac{1}{4c_4 \rho \pi R^2} \left((1 - 2\widehat{\mathbf{R}}_2^2) \mathbf{e}_1 \otimes \mathbf{e}_1 \right. \\
&\quad \left. - 2\widehat{\mathbf{R}}_1 \widehat{\mathbf{R}}_2 \left[\mathbf{e}_1 \otimes \mathbf{e}_2 + \mathbf{e}_2 \otimes \mathbf{e}_1 \right] + (1 - 2\widehat{\mathbf{R}}_1^2) \mathbf{e}_2 \otimes \mathbf{e}_2 \right) \\
&\quad \times \left[\left(1 - \beta_2 \widehat{\mathcal{A}}(\omega) \right) \int_0^{\tau_2} \left[\exp \{ \sqrt{-1} \kappa_2(\omega) h \} \right] dh \right. \\
&\quad \left. - \left(1 - \beta_3 \widehat{\mathcal{A}}(\omega) \right) \int_0^{\tau_3} \left[\exp \{ \sqrt{-1} \kappa_3(\omega) h \} \right] dh \right] \\
&= -\frac{1}{R^2} \left[c_6^2 \int_0^{\tau_2} h \Phi_2(h, \omega) dh \right. \\
&\quad \left. - c_4^2 \int_0^{\tau_3} h \Phi_3(h, \omega) dh \right] (\underline{\mathbf{J}} - 2\widehat{\mathbf{R}}^\perp \otimes \widehat{\mathbf{R}}^\perp) \\
&\quad + \left[\Phi_2(\mathbf{x}, \omega) - \Phi_3(\mathbf{x}, \omega) \right] \widehat{\mathbf{R}}^\perp \otimes \widehat{\mathbf{R}}^\perp,
\end{aligned}$$

where $\widehat{\mathbf{R}}^\perp = \widehat{\mathbf{R}}_2 \mathbf{e}_1 - \widehat{\mathbf{R}}_1 \mathbf{e}_2$ and $\underline{\mathbf{J}} = \underline{\mathbf{I}} - \mathbf{e}_3 \otimes \mathbf{e}_3$.

Finally, we arrive at

$$\begin{aligned}
\underline{\widehat{\mathbf{G}}}(\mathbf{x}, \omega) &= \Phi_3 \underline{\mathbf{I}} + \mathbf{D}_1 \otimes \mathbf{D}_1 M_1^{-1}(\Phi_1 - \Phi_3) + \mathbf{D}_2 \otimes \mathbf{D}_2 M_2^{-1}(\Phi_2 - \Phi_3), \\
&= \Phi_1 \widehat{\mathbf{r}} \otimes \widehat{\mathbf{r}} + \Phi_2 \widehat{\mathbf{R}}^\perp \otimes \widehat{\mathbf{R}}^\perp + \Phi_3 \left(\underline{\mathbf{I}} - \widehat{\mathbf{r}} \otimes \widehat{\mathbf{r}} - \widehat{\mathbf{R}}^\perp \otimes \widehat{\mathbf{R}}^\perp \right) \\
&\quad - \frac{1}{r^3} \left[\int_0^{\tau_1} h^2 \Phi_1(h, \omega) dh - \int_0^{\tau_3} h^2 \Phi_3(h, \omega) dh \right] (\underline{\mathbf{I}} - 3\widehat{\mathbf{r}} \otimes \widehat{\mathbf{r}}) \\
&\quad - \frac{1}{R^2} \left[c_1^2 \int_0^{\tau_2} h \Phi_2(h, \omega) dh - c_6^2 \int_0^{\tau_3} h \Phi_3(h, \omega) dh \right] (\underline{\mathbf{J}} - 2\widehat{\mathbf{R}}^\perp \otimes \widehat{\mathbf{R}}^\perp).
\end{aligned}$$

6.6.4 ISOTROPIC MEDIUM

When $c_{66} = c_{44}$, medium III becomes isotropic. In this case

$$\Phi_2(\mathbf{x}, \omega) = \Phi_3(\mathbf{x}, \omega), \quad \beta_2 = \beta_3, \quad \tau_1(\mathbf{x}) = \frac{r}{c_1}, \quad \text{and} \quad \tau_2(\mathbf{x}) = \frac{r}{c_4} = \tau_3(\mathbf{x})$$

Thus, the Green function in an isotropic medium with independent elastic parameters c_{11} and c_{44} can be given in frequency domain as:

$$\begin{aligned}\widehat{\mathbf{G}}(\mathbf{x}, \omega) &= \Phi_2 \mathbf{I} + \mathbf{D}_1 \otimes \mathbf{D}_1 M_1^{-1} (\Phi_1 - \Phi_2) \\ &= -\frac{1}{r^3} \left[\int_0^{\frac{r}{c_1}} h^2 \Phi_1(h, \omega) dh - \int_0^{\frac{r}{c_4}} h^2 \Phi_2(h, \omega) dh \right] (\mathbf{I} - 3\hat{\mathbf{r}} \otimes \hat{\mathbf{r}}) \\ &\quad + \Phi_1 \hat{\mathbf{r}} \otimes \hat{\mathbf{r}} + \Phi_2 (\mathbf{I} - \hat{\mathbf{r}} \otimes \hat{\mathbf{r}}),\end{aligned}$$

where Φ_1 and Φ_2 are the same as in Subsection 6.6.3. This expression of the Green function has already been reported in Chapter 4.

6.A DECOMPOSITION OF THE GREEN FUNCTION

Consider the elastodynamics equation satisfied by \mathbf{G} :

$$\left(\underline{\Gamma}^c(\nabla_x) \underline{\mathbf{G}}(\mathbf{x}, t) + \underline{\Gamma}^v(\nabla_x) \mathcal{A}[\underline{\mathbf{G}}](\mathbf{x}, t) \right) - \rho \frac{\partial^2 \underline{\mathbf{G}}(\mathbf{x}, t)}{\partial t^2} = \delta(t) \delta(\mathbf{x}) \mathbf{I}. \quad (6.33)$$

If $\underline{\mathbf{G}}(\mathbf{x}, t)$ is given in the form

$$\underline{\mathbf{G}}(\mathbf{x}, t) = \sum_{i=1}^3 \underline{\mathbf{E}}_i(\nabla_x) \phi_i, \quad (6.34)$$

then substituting (6.34) in (6.33) yields:

$$\begin{aligned}\delta(t) \delta(\mathbf{x}) \mathbf{I} &= \left(\underline{\Gamma}^c(\nabla_x) \underline{\mathbf{G}}(\mathbf{x}, t) + \underline{\Gamma}^v(\nabla_x) \mathcal{A}[\underline{\mathbf{G}}](\mathbf{x}, t) \right) - \rho \frac{\partial^2 \underline{\mathbf{G}}(\mathbf{x}, t)}{\partial t^2} \\ &= \sum_{i,j=1}^3 \left(L_j^c(\nabla_x) \phi_i + L_j^v(\nabla_x) \mathcal{A}[\phi_i] \right) \underline{\mathbf{E}}_j(\nabla_x) \underline{\mathbf{E}}_i(\nabla_x) - \rho \sum_{i=1}^3 \underline{\mathbf{E}}_i(\nabla_x) \frac{\partial^2 \phi_i(\mathbf{x}, t)}{\partial t^2}\end{aligned}$$

By definition $\underline{\mathbf{E}}_i(\nabla_x)$ is a projection operator which satisfies

$$\underline{\mathbf{E}}_i(\nabla_x) \underline{\mathbf{E}}_j(\nabla_x) = \delta_{ij} \underline{\mathbf{E}}_j(\nabla_x)$$

Consequently, we can have

$$\begin{aligned}\delta(t) \delta(\mathbf{x}) \mathbf{I} &= \sum_{i,j=1}^3 \underline{\mathbf{E}}_j(\nabla_x) \delta_{ij} \rho^{-1} \left(L_j^c(\nabla_x) \phi_i + L_j^v(\nabla_x) \mathcal{A}[\phi_i] \right) - \rho \sum_{i=1}^3 \underline{\mathbf{E}}_i(\nabla_x) \frac{\partial^2 \phi_i(\mathbf{x}, t)}{\partial t^2} \\ &= \sum_{i=1}^3 \underline{\mathbf{E}}_i(\nabla_x) \left(\left(L_i^c(\nabla_x) \phi_i + L_i^v(\nabla_x) \mathcal{A}[\phi_i] \right) - \rho \frac{\partial^2 \phi_i(\mathbf{x}, t)}{\partial t^2} \right).\end{aligned}$$

Moreover, $\mathbf{I} = \sum_{i=1}^3 \underline{\mathbf{E}}_i(\nabla_x)$, therefore

$$\sum_{i=1}^3 \underline{\mathbf{E}}_i(\nabla_x) \left(\left(L_i^c(\nabla_x) \phi_i + L_i^v(\nabla_x) \mathcal{A}[\phi_i] \right) - \rho \frac{\partial^2 \phi_i(\mathbf{x}, t)}{\partial t^2} - \delta(t) \delta(\mathbf{x}) \right) = 0$$

Hence, (6.10) is the sufficient conditions for the functions ϕ_i in order to express $\underline{\mathbf{G}}$ in the form (6.8).

6.B DERIVATIVE OF POTENTIAL: CASE I

If $b_1 = b_2 = b_3$ and $m_1 = m_2 = m_3$, we have

$$\left\{ \begin{array}{l} V_1(s) = V_2(s) = V_3(s) = b_1^2 + m_1^2 s \\ F(s) = \sum_{j=1}^3 \left[\frac{x_j^2}{V_1(s)} - h^2 \right] = \left[\frac{r^2}{V_1(s)} - h^2 \right] \\ F'(s) = \sum_{j=1}^3 \left\{ -\frac{m_1^2 x_j^2}{V_1^2(s)} \right\} = \left\{ -\frac{m_1^2 r^2}{V_1^2(s)} \right\} \quad \text{and} \\ F'(0) = \left\{ -\frac{m_1^2 r^2}{b_1^4} \right\} \\ F''(s) = \sum_{j=1}^3 \left[\frac{2m_1^4 x_j^2}{V_1^3(s)} \right] = \left[\frac{2m_1^4 r^2}{V_1^3(s)} \right] \\ G(s) = \{V_1(s)\}^3 \\ G'(s) = G(s) \left[\frac{3m_1^2}{V_1(s)} \right] \end{array} \right. \quad (6.35)$$

with $r = \sqrt{x_1^2 + x_2^2 + x_3^2}$. When $F(S) = 0$, we have

$$\left\{ \begin{array}{l} V_1(S) = \left[\frac{r^2}{h^2} \right], \\ \left[\frac{1}{V_k(S)V_l(S)F'(S)} \right] = \left[-\frac{1}{m_1^2 r^2} \right], \\ \left\{ \frac{1}{F'(S)\sqrt{G(S)}} \right\} = \left\{ -\frac{1}{m_1^2 r h} \right\}, \\ \left[\frac{F''(S)}{F'(S)} + \frac{m_k^2}{V_k(S)} + \frac{m_l^2}{V_l(S)} + \frac{1}{2} \frac{G'(S)}{G(S)} \right] = \left[\frac{3}{2} \frac{m_1^2}{V_1(S)} \right] = \left[\frac{3}{2} \frac{m_1^2 h^2}{r^2} \right]. \end{array} \right. \quad (6.36)$$

Substituting (6.35) and (6.36) in (6.31) we finally arrive at:

$$\frac{4\rho m_1^2 \pi}{(1 - \beta \widehat{\mathcal{A}}(\omega))} \frac{\partial^2 \Psi}{\partial x_k \partial x_l} = \widehat{\mathbf{r}}_k \widehat{\mathbf{r}}_l \left\{ \frac{\exp\{\sqrt{-1}\kappa(\omega)\tau\}}{b\tau} \right\} - \frac{1}{r^3} (\delta_{kl} - 3\widehat{\mathbf{r}}_i \widehat{\mathbf{r}}_j) \int_0^\tau \left[h \exp\{\sqrt{-1}\kappa(\omega)h\} \right] dh \quad (6.37)$$

where $\widehat{\mathbf{r}}_j = \frac{x_j}{r}$ for all $j = 1, 2, 3$.

6.C DERIVATIVE OF POTENTIAL: CASE II

If $b_1 = b_2$, $m_1 = m_2$ and $m_3 = 0$, we have

$$\left\{ \begin{array}{l} V_1(s) = V_2(s) = b_1^2 + m_1^2 s \quad \text{and} \quad V_3(s) = b_3^2 \\ F'(s) = \left[-\sum_{j=1}^2 \frac{m_1^2 x_j^2}{V_1^2(s)} \right] = \left[-\frac{m_1^2 R^2}{V_1^2(s)} \right] \quad \text{and} \\ F'(0) = \left[-\frac{m_1^2 R^2}{b_1^4} \right] \\ F''(s) = \left\{ \sum_{j=1}^2 \frac{2m_1^4 x_j^2}{V_1^3(s)} \right\} = \left\{ \frac{2m_1^4 R^2}{V_1^3(s)} \right\} \\ G(s) = b_3^2 [V_1(s)]^2 \quad \text{and} \\ G'(s) = G(s) \left[\frac{2m_1^2}{V_1(s)} \right] \end{array} \right. \quad (6.38)$$

with $R = \sqrt{x_1^2 + x_2^2}$. For all $l, k \in \{1, 2\}$, we have

$$\left\{ \begin{array}{l} \left[\frac{1}{V_k(S)V_l(S)F'(S)} \right] = \left[-\frac{1}{m_1^2 R^2} \right], \\ \left\{ \frac{1}{F'(S)\sqrt{G(S)}} \right\} = \left[-\frac{V(S)}{m_1^2 b_3 R^2} \right], \\ \left[\frac{F''(S)}{F'(S)} + \frac{m_k^2}{V_k(S)} + \frac{m_l^2}{V_l(S)} + \frac{1}{2} \frac{G'(S)}{G(S)} \right] = \left[\frac{m_1^2}{V_1(S)} \right]. \end{array} \right. \quad (6.39)$$

Substituting (6.38) and (6.39) in (6.31) and after simple calculations, we finally arrive at:

$$\begin{aligned} \frac{4\rho m_1^2 \pi}{(1 - \beta \widehat{\mathcal{A}}(\omega))} \frac{\partial^2 \Psi}{\partial x_k \partial x_l} &= \widehat{\mathbf{R}}_k \widehat{\mathbf{R}}_l \left\{ \frac{\exp\{\sqrt{-1}\kappa(\omega)\tau\}}{b\tau} \right\} \\ &\quad - \frac{1}{b_3 R^2} (\delta_{kl} - 2\widehat{\mathbf{R}}_k \widehat{\mathbf{R}}_l) \int_0^\tau \left[\exp\{\sqrt{-1}\kappa(\omega)h\} \right] dh \quad (6.40) \end{aligned}$$

where $\widehat{\mathbf{R}}_k = \frac{x_k}{R}$ for $k = 1, 2$.

CONCLUSION AND PERSPECTIVES

Source localization problems have been of significant interest in recent years due to a variety of associated applications in diverse domains. If the sources are temporally localized, these problems are equivalent to find *initial state* of a system governed by differential equations from the observations over a finite interval of time. In this work, we concentrate on the inverse problems related to acoustic and elastic source localization in attenuating media from wavefield measurements. We successfully handle attenuation effect in both acoustic and elastic media and present efficient and stable algorithms to compensate for these effects on image resolution.

In a first attempt, we recover initial pressure distribution in an attenuating medium with and without imposed boundary conditions. We retrieve the non-attenuated boundary data from measured data by using the asymptotically obtained iterative pseudo-inverse of an ill-conditioned attenuation operator. Subsequently, we use the retro-projected inverse Radon transform formulae to reconstruct initial condition on the pressure distribution. We compare this approach with a singular value decomposition (SVD) approach, our results are clearly more stable and accurate than the SVD approach. In order to address incomplete data problems, we use *TV-Tikhonov* regularization methods, wherein we present special *preconditioning weights*, which significantly improve convergence speed of the iterative algorithm. For a medium with imposed boundary conditions, we use a duality approach followed by the pseudo-inverse attenuation correction technique, to recover ideal Radon transform of the initial conditions.

For more efficient and robust reconstructions of temporally localized acoustic sources, we study time reversal methods for both non-attenuating and attenuating media. As the attenuated waves are not time reversible, we use the strategy of back-propagating adjoint attenuated waves and aim to reconstruct

sources stably. To do so, we truncate the high frequency components; thereby controlling the *anti-damping term* inducing instability. By using the asymptotic development of the attenuation operator with respect to a small attenuation coefficient, we prove that this technique compensates for attenuation effects up to first order. We then present an original strategy to compensate for attenuation effects up to higher orders by pre-processing measured data using pseudo-inverse of the attenuation operator and subsequently using ideal time-reversal techniques. Numerical results indicate the stability of the pre-processing approach.

Further, we introduce efficient weighted imaging algorithms for locating noise sources by cross correlation techniques, wherein we use the regularized back-propagator to correct the effects of acoustic attenuation. We successfully address the impact of spatial correlation in the noise source localization problem by designing appropriate imaging functionals. Our functionals are capable of first locating the noise sources and then estimating the correlation structure between them. Numerical results show the viability of the proposed imaging techniques.

In order to extend elastic anomaly detection algorithms to viscoelastic media, we first derive a closed form expression for an isotropic viscoelastic Green function. Then, we propose an attenuation correction technique for a quasi-incompressible medium based on stationary phase analysis of the attenuation operator. We prove that one can access, approximately, the ideal (inviscid) Green function from the viscoelastic one by inverting an ordinary differential operator. This consequently allows one to use ideal anomaly detection algorithms for viscoelastic media.

In a general elastic setting, we revisit elastic time reversal techniques and propose a modified imaging functional based on the weighted Helmholtz decomposition. We justify mathematically that it provides a better approximation of the sources than by simply back-propagating the time reverted displacement field. Then we consider the problem of reconstructing sources in a homogeneous viscoelastic medium from wavefield measurements. We provide a regularized time reversal imaging functional based on the adjoint attenuated wave. We prove that it corrects attenuation effect on image resolution up to first order in terms of viscosity parameters.

Finally, we provide some anisotropic viscoelastic Green functions, with an aim to extend our results to anisotropic media. We use spectral decomposition of the Christoffel tensor associated with the medium to write Green function in terms of the derivatives of three scalar functions following wave equations. Then, the Green function is obtained by solving the wave equations and the subsequent potential equations. The potential equations are resolved using an argument of potential theory in ellipsoidal coordinates.

FUTURE DIRECTIONS AND OPEN QUESTIONS

The algorithms proposed in this thesis for imaging and to compensate for wave signal attenuation require further attention to be adopted for more realistic propagation models, for example, by taking into account non-linearity, anisotropy and heterogeneity. Moreover, in view of their applications for non-destructive testing, underwater acoustics and data communication, the low frequency electromagnetic waves in dissipative regime need due attention.

The question of a spatially variable attenuation correction is still open. The adjoint wave time reversal algorithms presented for attenuating media seem to be the only available option at present. However, inhomogeneity in elastic media can create some troubles due to mode conversion between waves [111].

Recovery of the attenuation map $a(x)$ can provide additional information to practitioners [36]. An interesting problem is to retrieve this attenuation map from far field measurements of the pressure wave generated by an unknown extended source distribution.

In the time reversal techniques, most often, full boundary measurements are considered or a very dense array of transducers completely surrounding the object of interest is used in order to obtain a stable reconstruction. However, when we have partial measurements or only a few transducers in place on the boundary, which is usually the case in practical situations, the time reversal techniques do not provide *ideal results* [33, 37]. Using a geometric control technique, Bardos *et al.* [33] have actually addressed the limited-view problem. For the case of few transducers on the boundary, it would be very challenging to find the lower bounds on the number of transducers in order to get a stable reconstruction. The compressive sensing techniques would be quite useful in this analysis. In this regard we refer to [64, 103].

The problem of ambient noise source localization in elastic media, finds applications in biomedical imaging. The passive *in vivo* elastography experiments have already been successfully conducted, in which *skeletal muscle noise* has been used for imaging [29, 112]. The noise source localization algorithms for general isotropic elastic and viscoelastic media will be the subject of further investigations. We expect that an additional difficulty in elastic media would be involved due to the conversion between different wave modes (that is, pressure and shear waves) [111]. A transversally isotropic medium would be a realistic choice for passive elastography.

BIBLIOGRAPHY

- [1] M. Abramowitz and I. Stegun, *Handbook of Mathematical Functions*, Dover Publications, New York, 1965. [cited at p. 61]
- [2] J. D. Achenbach, *Wave Propagation in Elastic Solids*, North-Holland Publishing Company, Amsterdam, 1973. [cited at p. 133]
- [3] K. Aki and P. G. Richards, *Quantitative Seismology*, W. H. Freeman and Co., San Francisco, second edition, 1980. [cited at p. 89, 105, 133, 134]
- [4] V. N. Alekseev and S. A. Rybak, Equations of state for viscoelastic biological media. *Acoustical Physics*, 48(5): (2002), pp 511–517. [cited at p. 85, 136]
- [5] G. Allaire, *Shape Optimization by the Homogenization Method*, Applied Mathematical Sciences, vol. 146, Springer-Verlag, 2002. [cited at p. 133]
- [6] C. Alves and H. Ammari, Boundary integral formulae for the reconstruction of imperfections of small diameter in an elastic medium, *SIAM Journal on Applied Mathematics*, 62(1): (2001), pp 94–106. [cited at p. 134]
- [7] H. Ammari, *An introduction to Mathematics of Emerging Biomedical Imaging*, Mathematics & Applications, vol. 62, Springer-Verlag, Berlin, 2008. [cited at p. 1, 39, 42, 58, 63, 83, 91, 96, 99, 133]
- [8] H. Ammari (ed.) *Mathematical Modeling in Biomedical Imaging I*, Lecture Notes in Mathematics, vol. 1983, Springer-Verlag, Berlin, 2009. [cited at p. 1, 83, 91, 96, 99]
- [9] H. Ammari (ed.) *Mathematical Modeling in Biomedical Imaging II*, Lecture Notes in Mathematics, vol. 2035, Springer-Verlag, Berlin, 2011. [cited at p. 1]
- [10] H. Ammari, M. Asch, L. Guadarrama Bustos, V. Jugnon and H. Kang, Transient wave imaging with limited-view data, *SIAM Journal on Imaging Sciences*, 4:(2011), pp 1097-1121. [cited at p. 11, 27, 39]

- [11] H. Ammari, E. Bossy, V. Jugnon and H. Kang, Mathematical modelling in photo-acoustic imaging of small absorbers, *SIAM Review*, 52:(2010), pp 677-695. [cited at p. 2, 5, 11, 27, 39, 40, 103]
- [12] H. Ammari, E. Bossy, V. Jugnon and H. Kang, Reconstruction of the Optical Absorption Coefficient of a Small Absorber from the Absorbed Energy Density, *SIAM Journal on Applied Mathematics*, 71:(2011), pp 676-693. [cited at p. 11, 34, 39]
- [13] H. Ammari, E. Bretin, J. Garnier and V. Jugnon, Coherent interferometric strategy for photo-acoustic imaging, *SIAM Journal on Numerical Analysis*, to appear. [cited at p. 34]
- [14] H. Ammari, E. Bretin, J. Garnier and A. Wahab, Noise source localization in an attenuating medium, *SIAM Journal on Applied Mathematics*, to appear. [cited at p. 7]
- [15] H. Ammari, E. Bretin, J. Garnier, and A. Wahab, Time reversal in attenuating acoustic media, In *Mathematical and Statistical Methods for Imaging*, Contemporary Mathematics, vol 548, pp 151-163, American Mathematical Society, Providence, 2011. [cited at p. 7]
- [16] H. Ammari, E. Bretin, J. Garnier and A. Wahab, Time reversal in viscoelastic media, , preprint. [cited at p. 7]
- [17] H. Ammari, E. Bretin, V. Jugnon and A. Wahab, Photoacoustic imaging for attenuating acoustic media, In *Mathematical Modeling in Biomedical Imaging II*, vol 2035, pp 57-84, Lecture Notes in Mathematics, Springer-Verlag, Berlin, 2011. [cited at p. 7]
- [18] H. Ammari, P. Calmon and E. Iakovleva, Direct elastic imaging of a small inclusion, *SIAM Journal on Imaging Science*, 1:(2008), pp 169-187. [cited at p. 83, 133, 134]
- [19] H. Ammari, Y. Capdeboscq, H. Kang and A. Kozhemyak, Mathematical models and reconstruction methods in magneto-acoustic imaging, *Euro. J. Appl. Math.*, 20:(2009), pp 303-317. [cited at p. 2, 39, 83, 91, 96, 103]
- [20] H. Ammari, P. Garapon, L. Guadarrama Bustos and H. Kang, Transient anomaly imaging by the acoustic radiation force, *Journal of Differential Equations*, 249:(2010), pp 1579-1595. [cited at p. 2, 39, 103]
- [21] H. Ammari, P. Garapon and F. Jouve, Separation of scales in elasticity imaging: A numerical study, *Journal of Computational Mathematics*, 28:(2010), pp 354-370. [cited at p. 133]
- [22] H. Ammari, P. Garapon, F. Jouve, H Kang and H. Lee, A new optimal control approach towards reconstruction of acoustic and elastic inclusions, *SIAM Journal on Control and Optimization*, to appear. [cited at p. 133]
- [23] H. Ammari, P. Garapon, H. Kang and H. Lee, A method if biological tissues elasticity reconstruction using magnetic resonance elastography measurements, *Quarterly in Applied Mathematics*, 66(1):(2008), pp 139-176. [cited at p. 83, 99, 103, 133, 134]

- [24] H. Ammari, P. Garapon, H. Kang and H. Lee, Effective viscosity properties of dilute suspensions of arbitrarily shaped particles, *Asymptotic Analysis*, to appear. [cited at p. 83, 133]
- [25] H. Ammari, L. Guadarrama-Bustos, H. Kang and H. Lee, Transient elasticity imaging and time reversal, *Proceedings of the Royal Society of Edinburgh: Section A Mathematics*, 141:(2011), pp 1121-1140. [cited at p. 39, 83, 91, 96, 99, 103, 133, 134]
- [26] H. Ammari and H. Kang, Expansion methods, In *Handbook of Mathematical Methods in Imaging*, pp 447–499, Springer-Verlag, New York, 2011. [cited at p. 83, 99, 134]
- [27] H. Ammari and H. Kang, *Polarization and Moment Tensors: with Applications to Inverse Problems and Effective Medium Theory*, Applied Mathematical Sciences, vol. 162, Springer-Verlag, New York, 2007. [cited at p. 96, 99, 105, 133, 134]
- [28] H. Ammari and H. Kang, *Reconstruction of Small Inhomogeneities from Boundary Measurements*, Lecture Notes in Mathematics, vol. 1846, Springer-Verlag, Berlin, 2004. [cited at p. 96, 133]
- [29] A. Archer and K. G. Sabra, Two dimensional spatial coherence of the natural vibrations of the biceps brachii muscle generated during voluntary contractions, *32nd Annual International Conference of the IEEE EMBS*, Buenos Aires, Argentina, Sep. 2010, pp 170–173. [cited at p. 2, 157]
- [30] C. Bardos, A mathematical and deterministic analysis of the time-reversal mirror, In *Inside out: Inverse Problems.*, MSRI Publ., 47: (2008), pp 381–400. [cited at p. 39]
- [31] C. Bardos and M. Fink, Mathematical foundations of the time reversal mirror, *Asymptot. Anal.*, 29:(2002), pp 157–182. [cited at p. 39]
- [32] C. Bardos, J. Garnier, and G. Papanicolaou, Identification of Green’s functions singularities by cross correlation of noisy signals, *Inverse Problems*, 24: (2008), 015011. [cited at p. 55]
- [33] C. Bardos, G. Lebeau, and J. Rauch, Sharp sufficient conditions for the observation, control, and stabilization of waves from the boundary, *SIAM J. Control Optim.*, 30:(1992), pp 1024–1065. [cited at p. 157]
- [34] A. Beck and M. Teboulle, A fast iterative shrinkage-thresholding algorithm for linear inverse problems, *SIAM Journal on Imaging Sciences*, 2:(2009), pp 183–202. [cited at p. 15]
- [35] A. Ben-Menahem and S. J. Singh, *Seismic waves and sources*, Springer-Verlag, 1981. [cited at p. 133, 134]
- [36] J. Bercoff, M. Tanter, M. Muller and M. Fink, The role of viscosity in the impulse diffraction field of elastic waves induced by the acoustic radiation force, *IEEE Transactions on Ultrasonics, Ferroelectrics and Frequency Control*, 51(11):(2004), pp 1523–1535. [cited at p. 1, 83, 96, 103, 133, 134, 157]

- [37] M. Bergounioux, X. Bonnefond and P. Maréchal, Optimal control techniques for thermo-acoustic tomography, *preprint(HAL-00530719, V2)*, 2011. [cited at p. 3, 157]
- [38] L. Borcea; G. C. Papanicolaou, C. Tsogka and J. G. Berrymann, Imaging and time reversal in random media, *Inverse Problems*, 18:(2002), pp 1247–1279. [cited at p. 39]
- [39] E. Bretin, L. Guadarrama Bustos and A. Wahab, On the Green function in viscoelastic media obeying a frequency power law, *Mathematical Methods in the Applied Sciences*, 34(7): (2011), pp 819–830. [cited at p. 7, 134]
- [40] E. Bretin and A. Wahab, Some anisotropic viscoelastic Green functions, In *Mathematical and Statistical Methods in Imaging*, Contemporary Mathematics, vol 548, pp 129-149, American Mathematical Society, Providence, 2011. [cited at p. 7]
- [41] P. Burgholzer, H. Grun, M. Haltmeier, R. Nuster and G. Paltauf, Compensation of acoustic attenuation for high resolution photoacoustic imaging with line detectors, *Proc. of SPIE*, 6437: (2007), 643724. [cited at p. 1, 5, 11, 39]
- [42] R. Burridge, P. Chadwick and A. N. Norris, Fundamental elastodynamic solutions for anisotropic media with ellipsoidal slowness surfaces, *Proceedings of Royal Society of London*, 440(1910):(1993), pp 655–681. [cited at p. 6, 134, 135, 137, 138, 146]
- [43] C. Canuto, M. Y. Hussaini, A. Quarteroni, and T. A. Zang, *Spectral Methods in Fluid Dynamics*, Springer-Verlag, New York-Heidelberg-Berlin, 1987. [cited at p. 114]
- [44] M. Caputo, Linear models of dissipation whose Q is almost frequency independent-II, *Geophys J. R. Astron. Soc.*, 13:(1967), pp 529–539. [cited at p. 85, 136]
- [45] J. M. Carcione, *Wave Field in the Real Media: Wave Propagation in Anisotropic, Anelastic, Porous and Electromagnetic Media*. Elsevier Science, second edition, 2007. [cited at p. 133, 134]
- [46] S. Catheline, N. Bencech, J. Brum, and C. Negreira, Time-reversal of elastic waves in soft solids, *Phys. Rev. Lett.*, 100:(2008), 064301. [cited at p. 5, 103, 104]
- [47] S. Catheline, J. L. Gennisson, G. Delon, R. Sinkus, M. Fink, S. Abdouelkaram and J. Culioli, Measurement of viscoelastic properties of solid using transient elastography: an inverse problem approach, *Journal of Acoustical Society of America*, 116: (2004), pp 3734–3741. [cited at p. 83, 103]
- [48] V. Červený, *Seismic Ray Theory*, Cambridge University Press, 2001. [cited at p. 134]
- [49] A. Chambolle, An algorithm for total variation minimization and applications, *J. Math. Imag. Vis.*, 20:(2004), pp 89–97. [cited at p. 15]
- [50] S. Chandrasekhar, *Ellipsoidal Figures of Equilibrium*, Yale University Press, 1969. [cited at p. 6, 144]

- [51] Y. Colin de Verdière, Semi classical analysis and passive imaging, *Nonlinearity*, 22:(2009), pp R45–75. [cited at p. 55]
- [52] P. Combettes and V. Wajs, Signal recovery by proximal forward-backward splitting, *Mult. Model. Simul.*, 4:(2005), pp 1168–1200. [cited at p. 15]
- [53] R. Courant and D. Hilbert, *Methods of Mathematical Physics*, vol. 2, Wiley-Interscience, 1989. [cited at p. 142]
- [54] B. T. Cox, J. G. Laufer and P. C. Beard, The challenges for quantitative photoacoustic imaging, *Proceedings of SPIE*, 7177:(2009), 717713. [cited at p. 34]
- [55] I. Daubechies, M. Defrise and C. De Mol, An iterative thresholding algorithm for linear inverse problems with a sparsity constraint *Comm. Pure Appl. Math.*, 57:(2004), pp 1413–1457. [cited at p. 15]
- [56] J. de Rosny, G. Lerosey, A. Tourin and M. Fink, Time reversal of electromagnetic waves, In *Lecture Notes in Comput. Sci. Eng.*, vol. 59, pp. 187–202, Springer-Verlag, Berlin 2008. [cited at p. 39]
- [57] J. Dellinger, *Anisotropic Seismic Wave Propagation*, PhD thesis, Stanford University, USA, 1991. [cited at p. 134]
- [58] F. A. Duck, *Physical Properties of Tissue. A Comprehensive Review*, Academic Press, London, 1990. [cited at p. 84]
- [59] C. L. Epstein, *Introduction to the Mathematics of Medical Imaging*, second edition, SIAM, 2007. [cited at p. 1]
- [60] D. Finch, M. Haltmeier and Rakesh, Inversion of spherical means and the wave equation in even dimensions, *SIAM Journal on Applied Mathematics*, 68:(2007), pp 392–412. [cited at p. 3, 5, 13]
- [61] D. Finch, S. Patch and Rakesh, Determining a function from its mean-values over a family of spheres, *SIAM Journal on Mathematical Analysis*, 35:(2004), pp 1213–1240. [cited at p. 3, 5, 13]
- [62] M. Fink, Time reversed acoustics, *Physics Today*, 50:(1997), pp 34. [cited at p. 5, 39, 103]
- [63] M. Fink and C. Prada, Acoustic time-reversal mirrors. *Inverse Problems*, 17:(2001), pp R1–R38. [cited at p. 39, 103]
- [64] M. Fornasier, H. Rauhut, Compressive Sensing, In *Handbook of Mathematical Methods in Imaging*, pp 187–228, Springer-Verlag, New York, 2011. [cited at p. 157]
- [65] J.-P. Fouque, J. Garnier, G. Papanicolaou and K. Sølna, *Wave Propagation and Time Reversal in Randomly Layered Media*, Stochastic Modelling and Applied Probability, vol. 56, Springer-Verlag, New York, 2007. [cited at p. 39, 63]
- [66] J. G. Fujimoto, D. L. Farkas (eds.), *Biomedical Optical Imaging*, Oxford University Press, 2009. [cited at p. 1]

- [67] J. Garnier and G. Papanicolaou, Passive sensor imaging using cross correlations of noisy signals in a scattering medium, *SIAM Journal on Imaging Sciences*, 2:(2009), pp 396–437. [cited at p. 2, 55, 57]
- [68] J. Garnier and G. Papanicolaou, Resolution analysis for imaging with noise, *Inverse Problems*, 26:(2010), 074001. [cited at p. 2, 55]
- [69] J. Garnier and K. Sølna, Filtered Kirchhoff migration of cross correlations of ambient noise signals, *Inverse Problems and Imaging*, vol. 5:(2011), pp. 371–390. [cited at p. 2, 55]
- [70] J. L. Gennisson, S. Catheline, S. Chaffai and M. Fink, Transient elastography in anisotropic medium: Application to the measurement of slow and fast shear wave speeds in muscles, *Journal of Acoustical Society of America*, 114(1):(2003), pp 536–541. [cited at p. 133]
- [71] J. F. Greenleaf, M. Fatemi and M. Insana, Selected methods for imaging elastic properties of biological tissues, *Annu. Rev. Biomed. Eng.*, 5: (2003), pp 57–78. [cited at p. 1, 2, 83, 103, 133]
- [72] M. Haltmeier, R. Kowar, A. Leitao, O. Scherzer and Kaczmarz, Methods for regularizing nonlinear ill-posed equations II, *Applications, Inverse Problems and Imaging*, 1:(2007), 507–523. [cited at p. 5, 14]
- [73] M. Haltmeier, O. Scherzer, P. Burgholzer, R. Nuster and G. Paltauf, Thermoacoustic tomography and the circular Radon transform: exact inversion formula, *Math. Model. Meth. Appl. Sci.*, 17(4):(2007), pp 635–655. [cited at p. 3, 11]
- [74] M. Haltmeier, T. Schuster and O. Scherzer, Filtered back-projection for thermoacoustic computed tomography in spherical geometry, *Mathematical Methods in the Applied Sciences*, 28:(2005), pp 1919–1937. [cited at p. 3, 11]
- [75] F. Hastings, J. B. Schneider, and S. L. Brochat, Application of the perfectly matched layer (PML) absorbing boundary condition to elastic wave propagation, *J. Acoust. Soc. Am.*, 100:(1996), pp 3061–3069. [cited at p. 114]
- [76] K. Helbig. *Foundations of Anisotropy for Exploration Seismics*, Pergamon, New York, 1994. [cited at p. 133]
- [77] K. Helbig and L. Thomsen, 75-plus years of anisotropy in exploration and reservoir seismics: A historical review of concepts and methods, *Geophysics*, 70:(2005). [cited at p. 133]
- [78] L. Hormander, *The Analysis of the Linear Partial Differential Operators I: Distribution Theory and Fourier Analysis*, Classics in Mathematics, Springer-Verlag, Berlin, 2003. [cited at p. 34, 45, 99, 120]
- [79] J. Huang, N. Ohnishi, and N. Sugie, Building ears for robots: sound localization and separation, *Artificial Life and Robotics*, 1:(2007), pp 157–163. [cited at p. 2, 55]
- [80] O. D. Kellogg, *Foundations of Potential Theory*, Frederick Unger Publishing Company, New York, 1929. [cited at p. 6, 87, 144]

- [81] R. Kowar, Integral equation models for thermo-acoustic imaging of dissipative tissue, *Inverse Problems*, 26(9):(2010), 095005. [cited at p. 11]
- [82] R. Kowar and O. Scherzer, Photoacoustic imaging taking into account attenuation, In *Mathematical Modeling in Biomedical Imaging II*, vol 2035, pp 85–130, Lecture Notes in Mathematics, Springer-Verlag, Berlin, 2011. [cited at p. 1, 5, 18, 39, 85, 103, 136]
- [83] R. Kowar, O. Scherzer and X. Bonnefond, Causality analysis of frequency dependent wave attenuation, *Mathematical Methods in the Applied Sciences*, 34(1):(2011), pp 108–124. [cited at p. 11, 18, 83, 103]
- [84] P. Kuchment and L. Kunyansky, Mathematics of photoacoustic and thermoacoustic tomography, In *Handbook of Mathematical Methods in Imaging*, pp 817–865, Springer-Verlag, New York, 2011. [cited at p. 11]
- [85] L. Kunyansky, Explicit inversion formulas for the spherical mean Radon transform, *Inverse Problems*, 23:(2007), pp 373–383. [cited at p. 3, 13]
- [86] P. J. La Rivière, J. Zhang and M. A. Anastasio, Image reconstruction in optoacoustic tomography for dispersive acoustic media, *Opt. Lett.*, 31:(2006); pp 781–783. [cited at p. 1, 5, 11, 12, 19, 39]
- [87] C. Larmat, J. P. Montagner, M. Fink, Y. Capdeville, A. Tourin, E. Clévéde, Time-reversal imaging of seismic sources and application to the great Sumatra earthquake, *Geophysical Research Letters*, 33:(2006), L19312. [cited at p. 103]
- [88] S. G. Lekhnitskii, *Theory of Elasticity of an Anisotropic Body*, Mir Publishers, Moscow, 1981. [cited at p. 133]
- [89] G. Lerosey, J. de Rosny, A. Tourin, A. Derode, G. Montaldo and M. Fink, Time-reversal of electromagnetic waves and telecommunication, *Radio Sci.* 40:(2005), RS612. [cited at p. 103]
- [90] E. Martinson, Hiding the acoustic signature of a mobile robot, In *intelligent Robots and Systems*, IEEE/RSJ International Conference, pp 985–990, San Diego, 2007. [cited at p. 55]
- [91] E. Martinson and A. Schultz, Discovery of sound sources by an autonomous mobile robot, *J. Autonomous Robots*, 27:(2009), pp 221–237. [cited at p. 55]
- [92] K. Maslov, H. F. Zhang and L. V. Wang, Effects of wavelength-dependent fluence attenuation on the noninvasive photoacoustic imaging of hemoglobin oxygen saturation in subcutaneous vasculature in vivo, *Inverse Problems*, 23:(2007), pp S113–S122. [cited at p. 11]
- [93] P. Milanfar (ed.), *Super Resolution Imaging*, CRC Press, USA, 2011. [cited at p. 1]
- [94] G. W. Milton, D. J. Eyre and V. J. Mantese, Finite frequency range Kramers-Krönig relations: Bounds on the dispersion, *Physical Review Letters*, 79:(1997), pp 3062–3075. [cited at p. 87]

- [95] D. Modgil and P. J. La Rivière, Photoacoustic image reconstruction in an attenuating medium using singular value decomposition, *IEEE Nuclear Science Symposium Conf. Record*, (2008), pp 4489–4493. [cited at p. 5]
- [96] K. Nakadai, D. Matsuura, H. G. Okuno and H. Kitano, Applying scattering theory to robot audition system: robust sound source localization and extraction, In *Proceedings of IEEE/RSJ Intl. Conference on Intelligent Robots and Systems*, pp 1147–1152, Las Vegas, 2003. [cited at p. 55, 77]
- [97] R. Namani and P. V. Bayly, Shear wave propagation in anisotropic soft tissues and gels, *31st Annual International Conference of IEEE EMBS*, Minneapolis, Minnesota USA, 2009. [cited at p. 133]
- [98] J. C. Nedelec, *Acoustic and Electromagnetic Equations: Integral Representations for Harmonic Problems*, Applied Mathematical Sciences, Vol. 144, Springer Verlag, 2001. [cited at p. 88, 142]
- [99] L.V. Nguyen, A family of inversion formulas in thermo-acoustic tomography, *Inverse Problems and Imaging*, 3:(2009), pp 649–675. [cited at p. 3, 13]
- [100] A. F. Nikiforov and V. B. Uvarov, *Special Functions of Mathematical Physics: A Unified Introduction with Applications*, Birkhäuser, Basel, 1988. [cited at p. 61]
- [101] P. D. Norville, W. R. Scott, Time-reversal focusing of elastic surface waves, *Acoustical Society of America*, 118(2):(2005), pp 735-744. [cited at p. 103, 104]
- [102] T. Oida, Y. Kang, T. Azuma, J. Okamoto, A. Amano, L. Axel, O. Takizawa, S. Tsutsumi and T. Matsuda, The measurement of anisotropic elasticity in skeletal muscle using MR elastography, *Proc. Intl. Soc. Mag. Reson. Med.*, 13:(2005), pp 2020–2020. [cited at p. 133]
- [103] J. M. Parot, Localizing impulse sources in an open space by time reversal with very few transducers, *Applied Acoustics*, 69(4):(2008), pp 311–324. [cited at p. 157]
- [104] K. Patch and M. Haltmeier, Thermoacoustic tomography - ultrasound attenuation artifacts, *IEEE Nuclear Science Symposium Conference*, 4:(2006), pp 2604–2606. [cited at p. 1, 11]
- [105] R. G. Payton, *Elastic Wave Propagation in Transversely Isotropic Media*, Martinus Nijhoff Publishers, 1983. [cited at p. 134]
- [106] K. D. Phung and X. Zhang, Time reversal focusing of the initial state for Kirchhoff plate, *SIAM Journal on Applied Mathematics*, 68:(2008), pp 1535-1556. [cited at p. 2, 103, 104]
- [107] C. Prada, E. Kerbrat, D. Cassereau and M. Fink, Time reversal techniques in ultrasonic nondestructive testing of scattering media, *Inverse Problems*, 18:(2002), pp 1761-1773. [cited at p. 103]
- [108] J. Pujol, *Elastic Wave Propagation and Generation in Seismology*. Cambridge University Press, United Kingdom, 2003. [cited at p. 88]

- [109] H. Roitner and P. Burgholzer, Efficient modeling and compensation of ultrasound attenuation losses in photoacoustic imaging, *Inverse Problems*, 27:(2011), 015003 [cited at p. 1, 39]
- [110] T. D. Rossing, *Springer Handbook of Acoustics*, Springer-Verlag, New York, 2007. [cited at p. 83]
- [111] L. Ryzhik, G. Papanicolaou and J. B. Keller, Transport equations for elastic and other waves in random media, *Wave Motion* 24(4):(1996), pp 327–370. [cited at p. 157]
- [112] K. G. Sabra, S. Conti, P. Roux and W. A. Kuperman, Passive in vivo elastography from skeletal muscle noise, *Applied Physics Letters*, 90:(2007), 194101. [cited at p. 2, 157]
- [113] A. P. Sarvazyan, O. V. Rudenko, S. C. Swanson, J. B. Fowlkers and S. V. Emelianovs, Shear wave elasticity imaging: a new ultrasonic technology of medical diagnostics; *Ultrasound in Med. & Biol.*, 24(9):(1998), pp 1419–1435. [cited at p. 1, 2, 83, 103, 133]
- [114] O. Scherzer (ed.), *Handbook of Mathematical Methods in Imaging*, Springer-Verlag, New York, 2011. [cited at p. 1]
- [115] O. Scherzer (ed.), *Mathematical Models for Registration and Applications to Medical Imaging*, Mathematics in Industry, vol. 10, Springer-Verlag, Berlin, 2006. [cited at p. 1]
- [116] O. Scherzer, M. Grasmair, H. Grossauer, M. Haltmeier and F. Lenzen, *Variational Methods in Imaging*, Applied Mathematical Sciences, vol. 167, Springer-Verlag, New York, 2009. [cited at p. 1]
- [117] N. M. Shapiro, M. Campillo, L. Stehly and M. H. Ritzwoller, High-resolution surface wave tomography from ambient noise, *Science*, 307:(2005), pp 1615–1618. [cited at p. 2, 55]
- [118] R. Sinkus, J. Lorenzn, D. Schrader, M. Lorenzen, M. Dargatz and D. Holz. High resolution tensor MR elastography for breast tumor detection, *Phys. Med. Biol.*, 45(6):(2000), pp 1649–1664. [cited at p. 133]
- [119] R. Sinkus, M. Tanter, S. Catheline, J. Lorenzen, C. Kuhl, E. Sondermann and M. Fink, Imaging anisotropic and viscous properties of breast tissue by magnetic resonance-elastography, *Magnetic Resonance in Medicine*, 53:(2005), pp 372–387. [cited at p. 133]
- [120] N. B. Smith and A. Webb, *Introduction to Medical Imaging: Physics, Engineering and Clinical Applications*, Cambridge University Press, New York, 2011. [cited at p. 1]
- [121] R. Snieder, Extracting the Green’s function of attenuating heterogeneous acoustic media from uncorrelated waves, *Journal of Acoustical Society of America*, 121:(2007), pp 2637–2643. [cited at p. 54, 55]

- [122] L. Stehly, M. Campillo and N. M. Shapiro, A study of the seismic noise from its long-range correlation properties, *Journal Geophys. Res.*, 111:(2006), (B10306). [cited at p. 2, 55]
- [123] G. Strang, On the construction and comparison of difference schemes, *SIAM J. Numer. Anal.*, 5:(1968), pp 506–517. [cited at p. 115]
- [124] N. V. Sushilov and R. S. C. Cobbold, Frequency-domain wave equation and its time-domain solutions in attenuating media, *Journal of Acoustical Society of America*, 115:(2004), pp 1431–1436. [cited at p. 11]
- [125] T. L. Szabo, Causal theories and data for acoustic attenuation obeying a frequency power law, *Journal of Acoustical Society of America*, 97:(1995), pp 14–24. [cited at p. 18, 83, 84]
- [126] T. L. Szabo, *Diagnostic Ultrasound Imaging: Inside out*, Elsevier Academic Press, 2004. [cited at p. 1]
- [127] T. L. Szabo, Time domain wave equations for lossy media obeying a frequency power law, *Journal of Acoustical Society of America*, 96(1):(1994), pp 491–500. [cited at p. 5, 85, 136]
- [128] T. L. Szabo and J. Wu, A model for longitudinal and shear wave propagation in viscoelastic media *Journal of Acoustical Society of America*, 107(5):(2000), pp 2437–2446. [cited at p. 83, 84, 85, 103, 135, 136]
- [129] M. Tanter and M. Fink, Time reversing waves for biomedical applications, In *Mathematical Modeling in Biomedical Imaging I*, Lecture Notes in Mathematics, vol. 1983, pp 73–97, Springer-Verlag, Berlin, 2009. [cited at p. 39]
- [130] J. J. Teng, G. Zhang and S. X. Huang, Some theoretical problems on variational data assimilation, *Appl. Math. Mech.*, 28:(2007), pp 581-591. [cited at p. 2, 103]
- [131] E. C. Titchmarsh, *Introduction to the Theory of Fourier Integrals*, Clarendon Press, Oxford, 1948. [cited at p. 85, 136]
- [132] B. E. Treeby and B. T. Cox, Fast, tissue-realistic models of photoacoustic wave propagation for homogeneous attenuating media, *Proc. of SPIE*, 7177:(2009), 717716. [cited at p. 1, 11, 39]
- [133] B. E. Treeby and B. T. Cox, Modeling power law absorption and dispersion for acoustic propagation using the fractional Laplacian *Journal of Acoustical Society of America*, 127(5):(2009), pp 2741–2748. [cited at p. 1]
- [134] B. E. Treeby, E. Z. Zhang and B. T. Cox, Photoacoustic tomography in absorbing acoustic media using time reversal, *Inverse Problems*, 26(11):(2010), 115003. [cited at p. 1, 5, 39]
- [135] J. M. Valin, F. Michaud, J. Rouat and D. Létourneau, Robust sound source localization using a microphone array on a mobile robot, In *Intelligent Robots and Systems IEEE/RSJ International Conference*, pp 1228–1233, 2003. [cited at p. 55]

- [136] V. Vavryčuk, Asymptotic Green's function in homogeneous anisotropic viscoelastic media, *Proc. Royal Soc. A*, 463:(1993), pp 2689–2707. [cited at p. 134]
- [137] V. Vavryčuk, Elastodynamic and elastostatic Green tensors for homogeneous weak transversely isotropy media, *Geophysics J. Int.*, 130:(1997), pp 786–800. [cited at p. 134]
- [138] V. Vavryčuk, Exact elastodynamic Green functions for simple types of anisotropy derived from higher-order ray theory, *Studia Geophysica et Geodaetica*, 45(1):(2001), pp 67–84. [cited at p. 134, 135, 138]
- [139] L. V. Wang (ed.), *Photoacoustic Imaging and Spectroscopy*, Optical science and engineering, vol 144, CRC Press, 2009. [cited at p. 1]
- [140] L.V. Wang and X. Yang, Boundary conditions in photoacoustic tomography and image reconstruction, *J. Biomed. Optics.*, 12:(2007), pp 14–27. [cited at p. 25]
- [141] K. Wapenaar, Retrieving the elastodynamic Green's function of an arbitrary inhomogeneous medium by cross correlation, *Phys. Rev. Lett.*, 93:(2004), 254301. [cited at p. 107]
- [142] K. Wapenaar and J. Fokkema, Green's function representations for seismic interferometry, *Geophysics*, 71:(2006), pp SI33–SI46. [cited at p. 107, 109]
- [143] J. Weaver, M. Dooley, E. Van Houten, M. Hood, X. C. Qin, F. Kennedy, S. Poplack and K. Paulsen. Evidence of the anisotropic nature of the mechanical properties of breast tissue, *Med. Phys.*, 29:(2002), pp 1291–1291. [cited at p. 133]
- [144] A. Wiegmann, Fast Poisson, fast Helmholtz and fast linear elastostatic solvers on rectangular parallelepipeds, *Technical Report LBNL-43565*, Lawrence Berkeley National Laboratory, MS 50A-1148, One Cyclotron Rd, Berkeley CA 94720, June 1999. [cited at p. 115]
- [145] M. Xu and L.V. Wang, Photoacoustic imaging in biomedicine, *Rev. Scient. Instrum.*, 77:(2006), pp 041–101. [cited at p. 11]
- [146] Y. Xu and L.V. Wang, Reconstructions in limited-view thermoacoustic tomography, *Medical Physics*, 31:(2004), pp 724–733. [cited at p. 14]
- [147] Y. Xu and L. V. Wang, Time reversal and its application to tomography with diffraction sources, *Physical Review Letters*, 92(3):(2004), 033902. [cited at p. 39]
- [148] H. S. Yoon and J. L. Katz, Ultrasonic wave propagation in human cortical bone I: theoretical considerations for hexagonal symmetry, *J. Biomech.*, 9:(1976), pp 407–412. [cited at p. 133]
- [149] G. L. Zeng, *Medical Image Reconstruction: A Conceptual Tutorial*, Springer Verlag & Higher Education Press, 2010. [cited at p. 1]

INDEX

- acoustic source problem, 4
- acoustic time reversal, 39
- adjoint attenuated acoustic wave, 44
- anisotropic media, 133
- approximate inverse attenuation filter, 48
- asymptotics of attenuation operator, 20, 35, 36
- attenuated acoustic Helmholtz-Kirchhoff identity, 68
- attenuated acoustic time reversal, 43, 47
- attenuated Radon transform, 18, 25
- attenuation, 1, 3, 11, 30, 46, 87
- attenuation coefficient, 5, 20, 50
- attenuation operator, 5, 19, 32, 45, 46

- correlated point sources, 76
- correlation matrix, 77, 78
- cut off parameter, 44, 69, 70

- data pre-processing approach, 48, 56, 72
- dispersion, 87
- duality approach, 27
- duality TV algorithm, 15

- elastic Helmholtz-Kirchhoff identity, 107, 123
- elastic source problem, 4
- elastic time reversal, 103, 104, 116
- empirical cross correlation, 57
- extended sources, 75

- filtered back-projection, 32
- fractional Laplacian, 24

- Green function, 133

- ideal acoustic Helmholtz-Kirchhoff identity, 42, 58
- ideal acoustic time reversal, 40, 41, 63
- instability, 20, 44, 58, 69, 70

- limited-view data, 14, 27

- modified ideal acoustic time reversal, 41

- noise source problem, 6, 55, 56

- photo-acoustic imaging, 11, 40
- power spectral density, 59
- power-law model, 18, 24
- preconditioning weights, 15

- Radon transform, 3, 11, 13, 28
- retro-projection formulae, 13

- shear velocity, 133
- shrinkage thresholding algorithm, 15, 25
- spatially correlated sources, 74, 77
- stability, 22, 50
- stationary phase theorem, 12, 31, 32, 34, 46, 133
- statistical cross correlation, 57, 62, 65, 68
- SVD approach, 19

- thermo-viscous model, 18, 20, 30, 39, 66
- Tikhonov regularization, 14, 25
- time reversal, 104
- total variation, 14

- viscoelastic media, 133
- viscosity, 133